ADVANCED RECEIVERS FOR WIDEBAND CDMA SYSTEMS

MATTI LATVA-AHO

Department of Electrical Engineering

OULU 1998

MATTI LATVA-AHO

ADVANCED RECEIVERS FOR WIDEBAND CDMA SYSTEMS

Academic Dissertation to be presented with the assent of the Faculty of Technology, University of Oulu, for public discussion in Raahensali (Auditorium L10), Linnanmaa, on October 16th, 1998, at 12 noon.

OULUN YLIOPISTO, OULU 1999

Manuscript received 3.9.1998
Accepted 7.9.1998

Communicated by
Professor Michael Honig
Doctor Peter Jung

ISBN 951-42-5039-7
(URL: http://herkules.oulu.fi/isbn9514250397/)

ALSO AVAILABLE IN PRINTED FORMAT

ISBN 951-42-5031-1
ISSN 0355-3213 (URL: http://herkules.oulu.fi/issn03553213/)

OULU UNIVERSITY LIBRARY
OULU 1999

Latva-aho, Matti, Advanced receivers for wideband CDMA systems
Department of Electrical Engineering University of Oulu, P.O.Box 5000, FIN-90401, Finland
1999
Oulu, Finland
(Manuscript received 3.9.1998)

Abstract

Advanced receiver structures capable of suppressing multiple-access interference in code-division multiple-access (CDMA) systems operating in frequency-selective fading channels are considered in this thesis. The aim of the thesis is to develop and validate novel receiver concepts suitable for future wideband cellular CDMA systems. Data detection and synchronization both for downlink and uplink receivers are studied.

The linear minimum mean squared error (LMMSE) receivers are derived and analyzed in frequency-selective fading channels. Different versions of the LMMSE receivers are shown to be suitable for different data rates. The precombining LMMSE receiver, whichis also suitable for relatively fast fading channels, is shown to improve the performance of the conventional RAKE receivers signicantly in the FRAMES wideband CDMA concept. It is observed that the performance of the conventional RAKE receivers is degraded signicantly with highest data rates due to multiple-access interference (MAI) as well as due to inter-path interference.

Based on a general convergence analysis, it is observed that the postcombining LMMSE receivers are mainly suited to the high data rate indoor systems. The blind adaptive LMMSE-RAKE receiverdeveloped for relatively fast fading frequency-selective channels gives superior rate of convergence and bit error rate (BER) performance in comparison to other blind adaptive receivers based on least mean squares algorithms.

The minimum variance method based delay estimation in blind adaptive receivers is shown to result in improved delay acquisition performance in comparison to the conventional matched filter and subspace based acquisition schemes. A novel delay tracking algorithm suitable to blind least squares receivers is also proposed. The analysis shows improved tracking performance in comparison to the standard delay-locked loops.

Parallel interference cancellation (PIC) receivers are developed for the uplink. Data detection, channel estimation, delay acquisition, delay tracking, inter-cell interference suppression, and array processing in PIC receivers are considered. A multistage data detector with the tentative data decision and the channel estimate feedback from the last stage is developed. Adaptive channel estimation filters are used to improve the channel estimation accuracy. The PIC method is also applied to the timing synchronization of the receiver. It is shown that the PIC based delay acquisition and tracking methods can be used to improve the performance of the conventional synchronization schemes.

Although the overall performance of the PIC receiver is relatively good in the single-cell case, its performance is signicantly degraded in a multi-cell environment due to unknown signal components which degrade the MAI estimates and subsequently the cancellation efficiency. The blind receiver concepts developed for the downlink are integrated into the PIC receivers for inter-cell interference suppression. The resulting LMMSE-PIC receiver is capable of suppressing residual interference and results in good BER performance in the presence of unknown signal components.

Keywords: blind adaption, channel estimation, interference cancellation, lmmse receivers

To my family

Preface

The research related to this thesis has been carried out at the University of Oulu in the spread spectrum research group of the Telecommunication Laboratory and the Centre for Wireless Communications (CWC). I became involved with CDMA research at Nokia Mobile Phones in 1992 whilst working towards a master's theses with the topic "Digital code tracking loop for CDMA receiver". Returning to university in the end of 1993 gave me the opportunity to concentrate more on academic research. I finished my licentiate thesis in early 1996 on the topic of "Channel estimation in multiuser CDMA receivers". I was fortunate to have Dr. Jorma Lilleberg from Nokia Mobile Phones as my licentiate thesis supervisor. Encouraged by him I started to work with Dr. Markku Juntti on multiuser detection, which lead me to the path towards this thesis also supervised by Dr. Jorma Lilleberg.

I have had the pleasure to work in various CDMA related research projects during these years. A start at Nokia Mobile Phones in a CDMA test-bed project taught me a great deal of innovative thinking. The university projects with Nokia and the European Space Agency taught me serious working habbits. The cooperation between different Nokia units has proven to be fruitful. Working the last two and half years in the European FRAMES project gave me the opportunity to be involved with something of real importance. Thanks to all partners in the project, I was allowed to continue multiuser detection studies in the project. Without that possibility I would not have finished this thesis.

I would like to thank Professor Pentti Leppänen for his constant support during these years at the university. Without his flexibility and understanding on various issues, my journey towards this thesis would have been even more difficult. I was very lucky to have the opportunity to work with Dr. Markku Juntti. We have made such a great team that I sincerely hope we can work together in the future. The discussions I have had with Dr. Ian Oppermann stimulated many of the ideas presented in this thesis.

I would like to thank all persons working at the Telecommunication Laboratory and CWC both in the past and present. Some of you were really important in convincing me to carry on with my thesis. For our great computer resources during these years I wish to thank Pekka Nissinaho and Jari Sillanpää. I had the

pleasure to instruct the master's thesis of Jari Vallström, Markku Heikkilä and Kimmo Kansanen who have influenced the contents of my thesis either directly or indirectly.

I am grateful to the reviewers of the thesis; Professor Michael Honig from Northwestern University, Evanston, IL, USA, and Dr. -Ing. habil. Peter Jung of Siemens AG Semiconductors, Munich, Germany. I wish to thank Dr. Jari Iinatti, Dr. Markku Juntti, Mr. Pertti Järvensivu, Dr. Jorma Lilleberg, Dr. Ian Oppermann and Mr. Harri Saarnisaari for reading and commenting on the manuscript.

The financial support for the thesis has been provided by the University of Oulu, the European Comission, the Technology Development Centre of Finland, Nokia Mobile Phones, Ltd., and Nokia Telecommunications, Ltd. The support of the foundations: Jenny ja Antti Wihurin Rahasto, Telecom Finland Oy:n tutkimus- ja koulutussäätiö, Oy Nokia Ab:n säätiö, Kaupallisten ja teknillisten tieteiden tukisäätiö and Tekniikan Edistämissäätiö is gratefully acknowledged.

I want to thank my parents and parents-in-law for taking care of my family especially during the process of writing the thesis. I dedicate this thesis to my wife Kirsi who spent so many lonely moments due to my work during these years, as well as to our lovely daughters Maiju and Jenni who bring sunshine and joy to our lives.

Oulu, September 7, 1998 Matti Latva-aho

List of Contributions

Most of the results presented in this thesis have been published or have been submitted for publication in international conferences and journals. For the sake of clarity and uniformity, the thesis is presented in form of a monograph. The publications have been prepared in co-operation with colleagues at the University of Oulu. All listed papers except Papers XVIII and XIX have been written by the author. The simulation results presented in Papers VIII, IX, XII, XV, XVIII and XXV have been produced by other authors either partially or completely. In the case of Papers VIII, IX, XVIII and XXIV the author supervised the master's theses research where the simulations were carried out. All other analysis and simulation results presented in publications, submitted material or this thesis have been produced solely by the author. During the research which has lead to this thesis the following publicactions have been prepared.

I Latva-aho M & Lilleberg J (1995) Adaptive channel estimator for multiuser CDMA receivers. In: Proc. of the International Symposium on Synchronization, Saalbau, Essen, Germany, 127–131.

II Latva-aho M (1996) Method and arrangement for controlling a loop filter. U.S. patent No. 5,589,795, Nokia Mobile Phones Ltd. Salo, Finland.

III Latva-aho M & Lilleberg J (1996) Parallel interference cancellation in multiuser detection. In: Proc. IEEE International Symposium on Spread Spectrum Techniques and Applications (ISSSTA), Mainz, Germany, 3: 1151–1155.

IV Latva-aho M & Lilleberg J (1996) Parallel interference cancellation based delay tracker for CDMA receivers. In: Proc. Conference on Information Sciences and Systems (CISS), Princeton, NJ, USA, 2: 852–857.

V Latva-aho M & Lilleberg J (1996) Delay trackers for multiuser CDMA receivers. In: Proc. IEEE International Conference on Universal Personal Communications (ICUPC), Boston, MA, USA, 1: 326–330.

VI Latva-aho M & Lilleberg J Parallel interference cancellation - a multiuser detection framework. In: Proc. Interference Rejection and Signal Separa-

tion in Wireless Communications (IRSS'96) Symposium, March 19, 1996, New Jersey Institute of Technology, NJ, USA, 127–146.

VII Latva-aho M & Lilleberg J (1998) Parallel interference cancellation in multiuser CDMA channel estimation. Kluwer Academic Publishers 7(2/3): 171–195.

VIII Latva-aho M & Vallström J (1996) Quasi-coherent delay-locked loops for fading channels. In: Proc. IEEE International Symposium on Spread Spectrum Techniques and Applications (ISSSTA), Mainz, Germany, 1: 455–459.

IX Latva-aho M, Juntti M & Heikkilä M (1997) Parallel interference cancellation receiver for DS-CDMA systems in fading channels. In: Proc. IEEE International Symposium on Personal, Indoor, and Mobile Radio Communications (PIMRC), Helsinki, Finland, 2: 559–564.

X Latva-aho M & Juntti M (1997) Modified adaptive LMMSE receiver for DS-CDMA systems in fading channels. In: Proc. IEEE International Symposium on Personal, Indoor, and Mobile Radio Communications, Helsinki, Finland, 2: 554–558.

XI Latva-aho M & Juntti M (199x) LMMSE detection for DS-CDMA systems in fading channels. IEEE Transactions on Communications, submitted.

XII Oppermann I & Latva-aho M (1997) Adaptive LMMSE receiver for wideband CDMA systems. In: Proc. Communication Theory Mini-Conference (CTMC) in conjunction with IEEE Global Telecommunication Conference (GLOBECOM), Phoenix, AZ, USA, 133–138.

XIII Latva-aho M, Juntti M & Oppermann I (1998) Reconfigurable adaptive RAKE receiver for wideband CDMA systems. In: Proc. IEEE Vehicular Technology Conference (VTC), Ottawa, Canada, 3: 1740–1744.

XIV Latva-aho M (1998) Bit error probability analysis for FRAMES W-CDMA downlink receivers. IEEE Transactions on Vehicular Technology, to appear.

XV Latva-aho M & Oppermann I (199x) A packetized wideband CDMA system based on adaptive LMMSE receivers with antenna diversity. IEEE Transactions on Vehicular Technology, submitted.

XVI Latva-aho M & Juntti M (1998) Modified LMMSE receiver for DS-CDMA – Part I: Performance analysis and adaptive implementations. In: Proc. IEEE International Symposium on Spread Spectrum Techniques and Applications (ISSSTA), Sun City, South Africa, 2: 652–657.

XVII Latva-aho M (1998) Modified LMMSE receiver for DS-CDMA – Part II: Performance in FMA2 downlink. In: Proc. IEEE International Symposium on Spread Spectrum Techniques and Applications (ISSSTA), Sun City, South Africa, 2: 658–662.

XVIII Juntti M, Latva-aho M, Kansanen K & Kaurahalme O (1998) Perfor-

mance of parallel interference cancellation for CDMA in estimated fading channels with delay mismatch. In: Proc. IEEE International Symposium on Spread Spectrum Techniques and Applications (ISSSTA), Sun City, South Africa, 3: 936–940.

XIX Juntti M & Latva-aho M (199x) Bit error probability analysis of linear receivers for CDMA systems. IEEE Transactions on Communications, accepted for publication.

XX Latva-aho M (1998) FMA2 downlink performance analysis. In: Proc. ACTS Mobile Communication Summit, Rhodes, Greece, 343–348.

XXI Latva-aho M (1998) Blind adaptive single-user receivers for DS-CDMA systems in frequency-selective fading channels. In: Proc. IEEE Global Telecommunication Conference (GLOBECOM), Sydney, Australia.

XXII Latva-aho M (1998) Blind least-squares single-user receiver for CDMA systems. In: Proc. IEEE International Symposium on Wireless Communications (ISWC'98), Montreal, Canada, p 33.

XXIII Latva-aho M, Lilleberg J, Iinatti J & Juntti M (1998) CDMA downlink code acquisition performance in frequency-selective fading channels. In: Proc. IEEE International Symposium on Personal, Indoor, and Mobile Radio Communications (PIMRC), Boston, MA, USA.

XXIV Latva-aho M, Juntti M & Kansanen K (1999) Residual interference suppression in parallel interference cancellation receivers. International Conference on Communications (ICC), Vancouver, Canada, submitted.

XXV Latva-aho M (1998) LMMSE receivers for DS-CDMA systems in frequency-selective fading channels. In: Swarts F, van Rooyen P, Oppermann I & Lötter M (eds), CDMA Techniques for 3rd Generation Mobile Systems, Kluwer Academic Publishers, Chapter 13.

Contents

1. Introduction

Explosive growth in wireless communications, in conjuction with emerging new applications, has increased the demand for bandwidth efficient multiple-access schemes. Traditional wireline networks have already been extended to high-speed data applications. The inevitable trend also in wireless communications is in high data rate services. Higher data rates require larger frequency bands for the evolving wireless communication systems. The lack of spectrum availability is already a problem in metropolitan areas and the competition for frequencies amongst operators is becoming more significant. Thus, the worldwide spectrum adminstration has become one important factor in determing the evolution of the future wireless communication systems. As the demand for new improved services increases, traditional receiver techniques become insufficient faced with finite frequency band availability. For the aforementioned reasons, there is a need for advanced receiver concepts which are able to increase the capacity of wireless networks. In this thesis, some of the new receiver techniques are studied, specifically, receivers based on multiuser interference suppression and cancellation suitable to emerging wideband code-division multiple-access (CDMA) systems.

1.1. Code-division multiple-access techniques

There are several ways to allocate frequency spectrum to users [1]. The traditional approach has been to separate users either in frequency (frequency-division multiple-access, FDMA) or time (time-division multiple-access, TDMA). Both of these schemes rely on orthogonal user partitioning in the time-frequency plane and thus the number of users that can be served is determined by the number of orthogonal time or frequency slots available. In CDMA systems, all users share the same frequency band at all times, unlike the FDMA and TDMA systems. In CDMA, the separation of the users is carried out by assigning each user with a user specific signature sequence upon which the transmitted data is overlayed. The separation in the code domain rather than in frequency or time allows us to stretch the capacity given that there are enough signature sequences for user separation.

CDMA technology is based on spread specrum (SS) techniques which were first used in military applications [2]. Their salient features of suppressing intentional jamming and separating different signals gave the starting point for applying them to personal communications. The two most common spreading methods for spread-spectrum communication systems are direct-sequence (DS) and frequency hopping (FH). In a frequency hopping system, the transmission frequency is changed regularly according to a pseudo-random noise (PN) sequence. The hopping patterns of the users are selected in such a way that different users are not likely to transmit simultaneously on the same frequency. While frequency hopping has become very popular in military applications, direct-sequence has gained more interest in commercial systems. In a DS system, a high rate pseudo-random spreading sequence modulates the data. Due to the high frequency of the sequence, the DS modulated signal has a much broader bandwidth than the data signal. Hence, the name spread-spectrum.

A PN sequence for CDMA systems should have an impulse-like autocorrelation and low cross-correlations with the other users' codes. Impulse-like autocorrelation of the sequence allows to resolve the multipath signal components and to combine them in the RAKE receiver [3]; this is especially beneficial in frequency-selective fading channels. The low cross-correlations would limit the interference from the other users. A low interference level can be maintained only by accurate transmission power control of all users. Power control is the most vital requirement for the conventional DS-CDMA receivers. Inaccurate power control causes the phenomenon referred to as the near-far problem (NFB), which means that a weak user's signal is buried by the multiple-access interference (MAI) caused by stronger users' signals. Even a small amount of MAI can drastically degrade the performance of conventional single-user receivers [4]. The shortcomings of the conventional receivers have given rise to efforts to enhance receiver performance in the presence of multiple-access interference. The so-called multiuser interference suppression or cancellation receivers [4, 5, 6] utilize the interference structure in order to improve receiver performance and system capacity.

1.2. Evolving CDMA systems

The third generation worldwide system for wireless land-mobile communications is being standardized by the International Telecommunication Union (ITU). The standardization process in Europe has been co-ordinated by the European Telecommunications Standards Insitute (ETSI), where the Special Mobile Group 2 (SMG2) was set up to validate different proposals in order to specify the ETSI UMTS (Universal Mobile Telephone System) Terrestrial Radio Access (UTRA) system. The following options [7] were considered for the UTRA concept: wideband CDMA (WCDMA), OFDM (orthogonal frequency-division multiplex), wideband TDMA, hybrid TDMA-CDMA and ODMA (opportunity driven multiple-access). Extensive evaluations were followed by a final selection. The wideband CDMA concept was selected as the third generation standard in Europe [7] for the frequency bands

allocated to frequency-division duplex (FDD) services, whereas the TDMA-CDMA hybrid concept was chosen for time-division duplex (TDD) services. In this thesis, only the WCDMA related issues are studied.

The WCDMA concept has mainly been influenced by the European FRAMES (Future Radio Wideband Multiple Access Systems) project and the wideband CDMA concept (FRAMES multiple access mode 2, FMA2)[1] developed therein [8], as well as the WCDMA proposal by NTT DoCoMo [9]. FMA2 [8, 10] is a wideband CDMA radio-access concept that has been designed on the basis of the UMTS requirements and the flexibility needs of third generation cellular services. The main features of the FMA2 concept may be summarized as follows.

- Variable data rates from 16 kbit/s to 2 Mbit/s are supported.
- Possibility for packet access.
- High initial capacity and coverage with support for future capacity and coverage enhancing technologies, such as smart antennas and multiuser receivers.
- Asynchronous network topology.
- Fast power control for both uplink and downlink.
- Coherent receivers both at base stations and mobile terminals.

The FMA2 concept has been designed to faciliate advanced receiver techniques, such as smart antennas and multiuser detection, both in the uplink and in the downlink. This is possible due to the relatively short spreading sequences (256 chips) used. One of the main differences between the WCDMA proposal and the FMA2 concept is the long spreading sequences (40960 chips) and pilot symbols instead of the pilot channel in the downlink of the WCDMA system. Fast power control is used in both the uplink and downlink in both systems. The power control may cause a near-far problem in the downlink, whereas it is used to counteract the near-far problem in the uplink. The use of mixed data rate services with different quality-of-service (QoS) requirements also causes a near-far problem for low data rate users. In order to avoid performance degradation due to downlink power control and mixed services, near-far resistant receivers can be used. Different receiver techniques for CDMA systems are briefly reviewed in the following section.

1.3. Review of earlier work

Communications in fading channels has been studied intensively since the sixties [11]. Channel modelling [12], optimal single-user communication receivers [13], optimal [14, 15] and sub-optimal multiuser communication receivers [16], diversity techniques [11], receiver synchronization [17], advanced signal detection and

[1]Hereafter the wideband CDMA component in the UTRA concept is denoted by WCDMA and the FRAMES wideband CDMA proposal by FMA2. See Appendix 1 for other definitions.

estimation schemes [18, 19], interference rejection [20], adaptive signal processing methods [21], multiple-access schemes [1], spread-spectrum techniques [2], modulation schemes [22], coding methods [23], network protocols [24] and many other aspects are well documented in existing literature. The emerging CDMA systems require advanced receiver concepts, most of which have been developed in recent years. In this section, the most relevant topics in the area of receiver algorithms for CDMA communications are briefly reviewed. More comprehensive surveys can be found in [4, 5, 6, 25, 26, 27] for multiuser CDMA receivers and [28] for fading channel communications in general.

The optimal receiver for single-user communications in multipath channels causing inter-symbol interference (ISI) is the maximum likelihood sequence detector (MLSD) [22], which requires that the channel is known. In practice, the channel must be estimated, and hence the MLSD receiver is decoupled into an estimator which estimates the received noiseless signal and a correlator, which correlates the received signal with this estimate [13, 19, 28, 29].

The simplest *suboptimal single-user receivers* for DS systems are the correlation receivers [2]. The most widely used receiver in CDMA systems is the RAKE receiver, which consists of a bank of correlators to receive several multipath components [3]. Coherent, differentially coherent, or non-coherent RAKE receiver structures can be used depending on the bit error rate requirements and signaling formats. Usually maximal ratio combining (MRC) is used with coherent RAKE receivers, whereas equal gain combining (EGC) is more favourable with differentially coherent and noncoherent RAKE receivers. The third generation CDMA systems support coherent RAKE receivers both for uplink and downlink [30], whereas, either noncoherent or differentially coherent RAKE receivers are used in second generation CDMA systems [31] at base station receivers.

Channel estimation is one of the most important issues with coherent RAKE receivers. Channel estimation includes delay estimation and channel complex coefficient estimation [17]. Several synchronization schemes for initial spreading code timing acquisition have been reported, see [2, 32, 33, 34] and references therein. The spreading code timing tracking has been studied for additive white Gaussian noise (AWGN) channels in [2, 35], for multipath channels in [36, 37], for fading channels in [36, 38], and for multiuser communications in [39]. The channel complex coefficient estimation [17] in RAKE receivers has been studied for single-user communications in [28] and for multiuser communications in [25, 40]. Different methods for carrier frequency synchronization, which is important with mobile-satellite systems based on low earth orbit (LEO) satellites, have been presented in [17, 41].

Verdu derived the optimal *MLSD receiver for multiuser CDMA* communications [14]. Due to its high complexity, several suboptimal receivers have been proposed (see the literature reviews [4, 5, 6, 42] and references therein). The suboptimal receivers can be categorized in several ways, but the most suitable for the purposes of this thesis is to divide them into linear equalizer type receivers and interference cancellation type receivers.

The *linear multiuser interference suppression receivers* are based on general equalization techniques [22, 43]. The conceptually simplest linear multiuser re-

ceiver is the zero-forcing equalizer (often called decorrelator) both for multiuser and inter-symbol interference, which has been studied for AWGN channels in [44, 45, 46, 47, 48, 49], for fading channels in [25, 26, 44, 50, 51, 52], with adaptive antennas in [53, 54, 55, 56, 57, 58, 59], with multiple data rates in [60, 61], with delay estimation errors in [62, 63, 64], with finite length equalizer effects in [25, 46, 65, 66, 67], and decorrelators for the hybrid TDMA-CDMA third generation system in [26, 55, 56].

Another popular linear multiuser receiver is based on linear minimum mean squared error (LMMSE) equalizers [22]. The LMMSE receiver is equal to the linear receiver maximizing the signal-to-interference-plus-noise ratio (SINR) [68]. Centralized LMMSE receivers have been proposed for AWGN channels in [69], for fading channels in [26, 70, 71], and for antenna array receivers [55, 56, 72, 73]. Bounds for the near-far ratio and SINR of the LMMSE receiver in AWGN channels have been derived in [74], and the bit error probability (BEP) has been analyzed in [75] for AWGN channels and in [76, 77] for fading channels. The LMMSE receivers with power control are studied in [78], and the LMMSE receivers with the pre-RAKE idea [79] in [80]. The LMMSE receivers have attracted most interest due to their applicability to adaptive implementations and single-user receivers. Adaptive LMMSE receivers for AWGN channels have been considered in [68, 81, 82, 80]. The convergence of the adaptive least mean squares (LMS) algorithm used for the LMMSE receivers has been considered in [83, 84, 85, 86]. Adaptive LMMSE receivers in fading channels have been studied in [76, 77, 87, 88, 89, 90, 91]. Coding with the adaptive LMMSE receivers has been addressed in [85, 92]. Adaptive LMMSE receivers for packet data communications have been studied in [90, 93]. An improved LMMSE receiver, less sensitive to the time delay estimation errors, has been proposed in [94]. It is well known [68] that mean squared error and minimum output energy (MOE) criteria lead to the same receivers in AWGN channels. Receivers suitable for blind adaptation utilizing the MOE criterion have been studied for AWGN channels in [95, 96, 97, 98, 99, 100], for flat fading channels in [101], for non-fading multipath channels in [102] and for frequency-selective fading channels in [103]. Blind adaptive least squares receivers have been studied in [101, 104, 105, 106]. A blind receiver performing both the MOE filtering and timing estimation has been studied in [107]. Adaptive LMMSE and MOE receivers with differential coding have been studied in [54, 108].

The idea of *interference cancellation* (IC) receivers is to estimate the multiple-access and multipath induced interference and then subtract the interference estimate from the received signal. There are several principles of estimating the interference leading to different IC techniques. The interference can be cancelled simultaneously from all users leading to parallel interference cancellation (PIC), or on a user-by-user basis leading to successive (or serial) interference cancellation (SIC). The interference cancellation utilizing tentative data decisions is called hard decision (HD) interference cancellation and it requires explicit channel estimation. The soft decision (SD) interference cancellation utilizes only the composite signal of the data and the channel coefficient and no explicit channel estimation is needed. Usually the interference is estimated iteratively in several receiver stages, which leads to the so-called multistage receivers.

The multistage HD-PIC receiver has been proposed and analyzed for AWGN channels in [109, 110, 111, 112, 113, 114, 115], for slowly fading channels in [116, 117, 118, 119, 120, 121, 122], and for relatively fast fading channels in [40, 123, 124, 125]. The HD-PIC receivers for transmissions with diversity encoding has been analyzed in [126], for systems with multiple data rates in [127], and with trellis-coded CDMA systems in AWGN channels in [128]. The application of the HD-PIC to multiuser delay estimation in relatively fast fading channels has been considered in [39, 40, 131], and the effect of delay estimation errors on the performance of the HD-PIC receiver in [132], and to the SD-PIC receiver in [133, 134]. The SD-PIC receivers with linear data-amplitude product estimation for slowly fading channels have been considered in [133, 135], and for multi-cellular systems in [136]. The SD-PIC receivers with soft nonlinearity have been considered for AWGN channels in [137, 138, 139]. In [140] it was shown that the SD-PIC receiver with an infinite number of stages is actually a decorrelating receiver. A PIC receiver cancelling interference partially has been proposed in [141, 142]. In [143, 144, 145, 146] the expectation maximization (EM) [147] and the space alternating generalized EM (SAGE) algorithms [148] have been used in deriving different forms of IC receivers.

SD-SIC has been considered in [135, 149, 150], and HD-SIC in [151, 152, 153, 154, 155, 156]. The SIC for multirate CDMA communications has been studied in [157, 158]. The effect of delay estimation errors to the SD-SIC has been considered in [134, 159] and to the HD-SIC in [160]. The combination of the PIC and the SIC receivers has been studied in [161]. Interference cancellation based on user grouping has been considered for serial interference cancellation in [162], for parallel interference cancellation in [163, 164], groupwise SIC for multiple data rates in [165, 166], and for generic multiuser receivers in [167, 168].

Although the research on advanced receiver techniques suitable for CDMA communications is somewhat mature, there are still open problems some of which are studied in this thesis. The relation between the topics studied in this thesis and other existing results is discussed in the next section.

1.4. Parallel work and the scope of the thesis

The LMMSE receivers and the HD-PIC receivers are studied in this thesis. The LMMSE receivers are studied due to their applicability to the downlink receivers. Receivers suitable to FMA2 downlink and to more general CDMA systems operating in frequency-selective fading channels are considered. The HD-PIC receivers are studied due to their applicability to FMA2 and WCDMA base station receivers, as well as due to previous experience on their performance in fading channels [25].

The precombining LMMSE criterion used to derive downlink receivers results in robust adaptive interference suppression schemes for relatively fast fading channels. Related work has been reported in [76, 97]. The approach in [76] has been rather heuristic, whereas, a theoretical treatment to LMMSE detection in multipath fading channels with rigorous performance analysis is given in this thesis. Also the receiver structure is different from the one presented in [76]. In [108] adaptive

single-user receivers based on differential encoding have been studied both in flat fading and frequency-selective fading channels. However, since the future mobile communication systems [7] support the use of coherent rather than differentially coherent receivers, the schemes presented in [108] are not considered in this thesis.

By using the minimum output energy (MOE) criterion in a constrained optimization problem, blind adaptive receivers are obtained [96]. The main difference between the precombining LMMSE receivers and the blind adaptive receivers [95, 96, 97, 98, 99, 100, 101, 102, 103, 104, 105, 106] is the optimization criterion used. The MOE criterion leads to significantly different adaptive implementations than the modified mean squared error (MSE) criterion used in this thesis. The blind adaptive receivers have not been studied extensively in fading channels before.

The bit error probability analysis developed for the precombining LMMSE receivers has not been presented before in frequency-selective fading channels. The FMA2 concept downlink performance analysis and the problems related to the RAKE receivers in the WCDMA system have not been presented earlier.

Synchronization schemes for the precombining LMMSE receivers have been addressed in [107]. However, no analysis on code acquisition times was given. Furthemore the research was carried out only in AWGN channels. The mean acquisition times in fading channels are analyzed in this thesis. The delay tracking method for the precombining LMMSE receivers studied in this thesis has not been applied before to multiuser CDMA communications.

Combination of the decorrelating receivers with antenna arrays in multipath channels was studied in [54]. In this thesis, similar structures are derived for the LMMSE receivers. Other related work has been reported in [55, 56, 72, 73].

The uplink receivers studied in this thesis are of the HD-PIC type. A great deal of similar work for SD-PIC receivers in AWGN channels has been reported in [133, 135, 141, 142, 169]. Research for the HD-PIC receivers in AWGN channels has been reported in [143, 144, 146]. Studies for the HD-PIC receivers in fading channels have been reported in [25, 39, 40, 125, 129, 130, 131] and some of those results are presented in this thesis. During the time of publishing the results of HD-PIC receivers, other similar results in frequency-selective fading channels were not available.

The channel estimator structure used in the HD-PIC receiver studied in this thesis has been used in single-user receivers in [170] and is modified for the HD-PIC receiver [40]. The adaptive FIR channel estimation filters were originally developed for single-user RAKE receiver in [28]. The adaptive IIR filters [171] have not been used in channel estimation before. The multistage data detection scheme has been modified from the original version [114].

Delay acquisition with the HD-PIC receivers in fading channels has not been previously addressed. The PIC based delay tracker is developed in the course of this work, but the EM algorithm leads to very similar delay estimator [143, 146]. Practical PIC based delay trackers for multiuser receivers have not been studied before.

The combination of the blind interference suppression schemes and the PIC receivers, i.e., the hybrid LMMSE-PIC receiver has not been studied earlier. The

blind interference suppression is used to make the biased MAI estimate due to unknown signal components smaller. Some methods for bias reduction have been reported in [141, 142]. The previously known methods are based on some form of partial interference cancellation [142] where only a fraction of the MAI estimate is subtracted at each cancellation stage.

The PIC based direction-of-arrival estimator for antenna array receivers is developed in the course of this work, but the SAGE algorithm leads to a similar scheme [144].

1.5. Outline of the thesis

Novel receiver techniques to increase overall system capacity have been investigated. The main emphasis has been in validation of the novel receiver concepts in evolving CDMA systems and the development of the receiver algorithms for frequency-selective fading channels. Both the downlink and the uplink receivers are considered. The Roman numerals below refer to the list of contributions.

In Chapter 2, general linear system model is developed for the purposes of this thesis. The limitations of the conventional RAKE receivers in WCDMA type systems will also be discussed as a motivation to the rest of the thesis.

Chapter 3, results of which have been presented in Papers X, XI, XIV, XVI, XVII, XIX, XX and XXV, presents the principles of the pre and the postcombining LMMSE receivers. Bit error probability analysis for both receivers will be developed. The performance of the conventional RAKE and the modifed LMMSE receivers will be compared in the FMA2 downlink. The LMMSE receiver principles are also augmented to the spatial domain.

Chapter 4, results of which have been documented in Papers X - XIII, XXI and XXV, presents a novel adaptive LMMSE-RAKE receiver. The performance of the receiver is compared to the performance of other blind adaptive receivers. The issues related to the adaptive postcombining LMMSE receivers in fading channels are also considered.

Chapter 5, results of which are presented in Papers XXII, XXIII and XXV considers timing synchronization issues in LMMSE receivers. Delay acquisition based on the minimum variance method will be studied in the precombining LMMSE receivers. An improved delay tracking algorithm will be also developed for the blind adaptive LS receivers.

Chapter 6, results of which are in part included in Papers I - IX, XVIII, XXIV and XXV, is devoted to uplink receivers based on parallel interference cancellation. Multistage data detection, channel estimation, delay acquisition, delay tracking, inter-cell interference suppression and array processing in PIC receivers are considered.

Chapter 7 concludes the thesis. The main results and contributions are summarized. Open problems are highlighted for future research.

2. Preliminaries

The CDMA system model for the purposes of this thesis is developed in Section 2.1 and the channel models in Section 2.2. The third generation WCDMA mobile communication system is primarily based on the conventional RAKE receivers. However, there are some fundamental limitations associated with the conventional RAKE receivers. These are briefly reviewed in Section 2.3.

2.1. System model

A standard model for an asynchronous DS-CDMA system with K users and L propagation paths will be considered. The kth user data bits are modulated by using binary phase shift keying (BPSK) and spread by multiplying the data modulated signal by a binary pseudo-random noise sequence given by

$$s_k(t) = \sum_{j=0}^{G-1} s_k(j)p(t - jT_c), \tag{2.1}$$

where G is the number of chips per symbol, i.e., processing gain or spreading factor, $s_k(j) \in \{-1, 1\}$ is the jth chip of the kth user $p(t)$ is the chip waveform, T_c is the chip interval, and t is the continuous-time index. It will be assumed that the length of the PN sequence equals one symbol interval[1]. Now, the complex envelope of the received signal can be expressed as

$$r(t) = \sum_{n=0}^{N_b-1} \sum_{k=1}^{K} A_k b_k^{(n)} s_k(t - nT) * c_k(t) + n(t), \tag{2.2}$$

[1]In the FMA2 system the data of the kth user is spread by multiplying the data modulated signal by a binary pseudo-random noise sequence which consists of the Walsh code ($s_{[w]k}$) used for orthogonal channelization and the scrambling code ($s_{[s]}$) used for the Walsh code scrambling. The combination of these two codes results in a spreading sequence $s_k(t) = \sum_{g=1}^{P/G} \sum_{j=0}^{G-1} s_{[w]k}(j)s_{[s]}(j + (g-1)G)p(t - jT_c)$, where G is the actual spreading factor used (the length of the Walsh code), P is the length of the scrambling code, $s_{[w]k}(j), s_{[s]}(j) \in \{-1, 1\}$ is the jth chip of codes, and $p(t)$ is the chip waveform.

where N_b is the number of received symbols, K is the number of users, $A_k = \sqrt{E_k/T}$ is the received amplitude, E_k/T is the energy per symbol, $b_k^{(n)}$ is the nth transmitted data symbol, $s_k(t)$ is the kth user's signature signal (in the sequel $\int_0^{\mathrm{T}} |s_k(t)|^2 dt = 1$ and the spreading waveform is real valued), T denotes the symbol interval, $n(t)$ is a complex zero mean additive white Gaussian noise process with two-sided power spectral density σ^2, $*$ denotes convolution and

$$c_k(t) = \sum_{l=1}^{L_k} c_{k,l}^{(n)} \delta(t - \tau_{k,l}) \tag{2.3}$$

is the impulse response of the kth user's radio channel, where L_k is the number of propagation paths (here $L_k = L$, $\forall\, k$, for notational simplicity), $c_{k,l}^{(n)}$ is the complex gain of the kth user's lth path during the nth symbol interval (contains also carrier phases), $\tau_{k,l}$ is the propagation delay and $\delta(t)$ is the Dirac's delta function. The received signal has the form

$$r(t) = \sum_{n=0}^{N_b-1} \sum_{k=1}^{K} \sum_{l=1}^{L} A_k b_k^{(n)} c_{k,l}^{(n)} s_k(t - nT - \tau_{k,l}) + n(t). \tag{2.4}$$

The received signal is time-discretized by anti-alias filtering and sampling $r(t)$ at the rate $T_s^{-1} = \frac{SG}{T}$, where S is the number of samples per chip. The received discrete-time signal over a data block of N_b symbols is

$$\mathbf{r} = \mathbf{SCAb} + \mathbf{n} \in \mathbb{C}^{SGN_b}, \tag{2.5}$$

where

$$\mathbf{r} = \left[\mathbf{r}^{\mathrm{T}(0)}, \ldots, \mathbf{r}^{\mathrm{T}(N_b-1)}\right]^{\mathrm{T}} \in \mathbb{C}^{SGN_b} \tag{2.6}$$

is the input sample vector with

$$\mathbf{r}^{\mathrm{T}(n)} = \left[r(T_s\,(nSG+1)), \ldots, r(T_s\,(n+1)SG)\right] \in \mathbb{C}^{SG}, \tag{2.7}$$

$$\begin{aligned} \mathbf{S} &= \left[\mathbf{S}^{(0)}, \mathbf{S}^{(1)}, \ldots, \mathbf{S}^{(N_b-1)}\right] \in \mathbb{R}^{SGN_b \times KLN_b} \\ &= \begin{pmatrix} \mathbf{S}^{(0)}(0) & \mathbf{0} & \cdots & \mathbf{0} \\ \vdots & \mathbf{S}^{(1)}(0) & \ddots & \vdots \\ \mathbf{S}^{(0)}(D) & \vdots & \ddots & \mathbf{0} \\ \mathbf{0} & \mathbf{S}^{(1)}(D) & \ddots & \mathbf{S}^{(N_b-1)}(0) \\ \vdots & \ddots & \ddots & \vdots \\ \mathbf{0} & \cdots & \mathbf{0} & \mathbf{S}^{(N_b-1)}(D) \end{pmatrix} \end{aligned} \tag{2.8}$$

is the sampled spreading sequence matrix, $D = \lceil \frac{T+T_m}{T} \rceil$ [2], T_m is the maximum delay spread,

$$\mathbf{S}^{(n)} = \left[\mathbf{s}_{1,1}^{(n)}, \ldots, \mathbf{s}_{1,L}^{(n)}, \ldots, \mathbf{s}_{K,L}^{(n)}\right] \in \mathbb{R}^{SGN_b \times KL}, \tag{2.9}$$

[2] $\lceil \cdot \rceil$ denotes the ceiling function. In a single-path channel, $D = 1$ due to the asynchronity of users. In multipath channels, $D \geq 2$ due to the multipath spread. The code matrix is defined with several components $(\mathbf{S}^{(n)}(0), \ldots, \mathbf{S}^{(n)}(D))$ for each symbol interval to simplify the presentation of the cross-correlation matrix components.

where

$$\mathbf{s}_{k,l}^{(n)} = \begin{cases} \mathbf{0}_{SGN_b\times 1}^{\mathrm{T}} & n=0,\ \tau_{k,l}=0 \\ \Big[\big[s_k(T_s(SG-\tau_{k,l}+1)),\ldots,s_k(T_sSG)\big]^{\mathrm{T}},\ \mathbf{0}_{(SGN_b-\tau_{k,l})\times 1}^{\mathrm{T}}\Big]^{\mathrm{T}}, & n=0,\ \tau_{k,l}>0 \\ \big[\mathbf{0}_{((n-1)SG+\tau_{k,l})\times 1}^{\mathrm{T}},\ \mathbf{s}_k^{\mathrm{T}}, \mathbf{0}_{(SG(N_b-n)-\tau_{k,l})\times 1}^{\mathrm{T}}\big]^{\mathrm{T}}, & 0<n<N_b-1 \\ \big[\mathbf{0}_{(SG(N_b-1)+\tau_{k,l})\times 1}^{\mathrm{T}},\ \big[s_k(Ts),\ldots,s_k(T_s(SG-\tau_{k,l}))\big]\big]^{\mathrm{T}}, & n=N_b-1 \end{cases} \tag{2.10}$$

where $\tau_{k,l}$ is time-discretized delay in sample intervals and

$$\mathbf{s}_k = \big[s_k(T_s),\ldots,s_k(T_s\,SG)\big]^{\mathrm{T}} \in \mathbb{R}^{SG} \tag{2.11}$$

is the sampled signature sequence of the kth user,

$$\mathbf{C} = \mathrm{diag}\big[\mathbf{C}^{(0)},\ldots,\mathbf{C}^{(N_b-1)}\big] \in \mathbb{C}^{KLN_b\times KN_b} \tag{2.12}$$

is the channel coefficient matrix with

$$\mathbf{C}^{(n)} = \mathrm{diag}\big[\mathbf{c}_1^{(n)},\ldots,\mathbf{c}_K^{(n)}\big] \in \mathbb{C}^{KL\times K}, \tag{2.13}$$

and

$$\mathbf{c}_k^{(n)} = \big[c_{k,1}^{(n)},\ldots,c_{k,L}^{(n)}\big]^{\mathrm{T}} \in \mathbb{C}^{L}, \tag{2.14}$$

$$\mathbf{A} = \mathrm{diag}\big[\mathbf{A}^{(0)},\ldots,\mathbf{A}^{(N_b-1)}\big] \in \mathbb{R}^{KN_b\times KN_b} \tag{2.15}$$

is the matrix of total received average amplitudes with

$$\mathbf{A}^{(n)} = \mathrm{diag}\big[A_1,\ldots,A_K\big] \in \mathbb{R}^{K\times K}, \tag{2.16}$$

$$\mathbf{b} = \big[\mathbf{b}^{\mathrm{T}(0)},\ldots,\mathbf{b}^{\mathrm{T}(N_b-1)}\big]^{\mathrm{T}} \in \Xi^{KN_b} \tag{2.17}$$

is the data vector with the modulation symbol alphabet Ξ (with BPSK $\Xi = \{-1,1\}$) and

$$\mathbf{b}^{(n)} = \big[b_1^{(n)},\ldots,b_K^{(n)}\big] \in \Xi^{K}, \tag{2.18}$$

and $\mathbf{n} \in \mathbb{C}^{SGN_b}$ is the channel noise vector. It is assumed that the data bits are independent identically distributed (i.i.d.) random variables independent from the channel coefficients and the noise process.

The cross-correlation matrix for the spreading sequences can be formed as

$$\mathbf{R} = \mathbf{S}^{\mathrm{T}}\mathbf{S} \in \mathbb{R}^{KLN_b\times KLN_b} \tag{2.19}$$

$$= \begin{pmatrix} \mathbf{R}^{(0,0)} & \cdots & \mathbf{R}^{(0,D)} & \mathbf{0}_{KL}\cdots & \mathbf{0}_{KL} \\ \vdots & \ddots & \ddots & \ddots & \vdots \\ \mathbf{R}^{(D,0)} & \ddots & \ddots & \ddots & \mathbf{0}_{KL} \\ \mathbf{0}_{KL} & \ddots & \ddots & \ddots & \mathbf{R}^{(N_b-D,N_b-1)} \\ \vdots & \ddots & \ddots & \ddots & \vdots \\ \mathbf{0}_{KL} & \cdots & \mathbf{0}_{KL} & \cdots & \mathbf{R}^{(N_b-1,N_b-1)} \end{pmatrix},$$

where

$$\mathbf{R}^{(n,n-j)} = \sum_{i=0}^{D-j} \mathbf{S}^{\mathrm{T}(n)}(i)\mathbf{S}^{(n-j)}(i+j), \quad j \in \{0,\ldots,D\}, \tag{2.20}$$

and $\mathbf{R}^{(n-j,n)} = \mathbf{R}^{\mathrm{T}(n,n-j)}$. The elements of the correlation matrix can be written as

$$\mathbf{R}^{(n,n')} = \begin{pmatrix} \mathbf{R}_{1,1}^{(n,n')} & \cdots & \mathbf{R}_{1,K}^{(n,n')} \\ \vdots & \ddots & \vdots \\ \mathbf{R}_{K,1}^{(n,n')} & \cdots & \mathbf{R}_{K,K}^{(n,n')} \end{pmatrix} \in \mathbb{R}^{KL\times KL}, \tag{2.21}$$

and

$$\mathbf{R}_{k,k'}^{(n,n')} = \begin{pmatrix} R_{k1,k'1}^{(n,n')} & \cdots & R_{k1,k'L}^{(n,n')} \\ \vdots & \ddots & \vdots \\ R_{kL,k'1}^{(n,n')} & \cdots & R_{kL,k'L}^{(n,n')} \end{pmatrix} \in \mathbb{R}^{L\times L}, \tag{2.22}$$

where

$$R_{kl,k'l'}^{(n,n')} = \sum_{j=\tau_{k,l}}^{SG-1+\tau_{k,l}} s_k(T_s(j-\tau_{k,l}))s_{k'}(T_s(j-\tau_{k'l'}+(n'-n)SG)) = \mathbf{s}_{k,l}^{\mathrm{T}(n)}\mathbf{s}_{k',l'}^{(n')} \tag{2.23}$$

represents the correlation between users k and k', lth and l'th paths, between their nth and n'th symbol intervals.

2.2. Channel model

The channel coefficient vector

$$\mathbf{c} = \left[\mathbf{c}^{\mathrm{T}(0)}, \mathbf{c}^{\mathrm{T}(1)}, \ldots, \mathbf{c}^{\mathrm{T}(N_b-1)}\right]^{\mathrm{T}} \in \mathbb{C}^{KLN_b}, \tag{2.24}$$

where $\mathbf{c}^{(n)} = \left[\mathbf{c}_1^{\mathrm{T}(n)}, \ldots, \mathbf{c}_K^{\mathrm{T}(n)}\right]^{\mathrm{T}} \in \mathbb{C}^{KL}$ and $\mathbf{c}_k^{(n)} = \left[c_{k,1}^{(n)}, \ldots, c_{k,L}^{(n)}\right]^{\mathrm{T}} \in \mathbb{C}^{L}$, is assumed to be a complex Gaussian random vector with zero mean and covariance matrix $\mathbf{\Sigma_c}$. It is assumed that the fading channel coefficients have a zero mean and variance normalized for convenience so that

$$\sum_{l=1}^{L} \mathrm{E}\left[|c_{k,l}^{(n)}|^2\right] = 1, \ \forall\, k. \tag{2.25}$$

The channel coefficients are assumed to be independent, i.e., $\mathrm{E}\left[c_{k,l}^{(n)}, c_{k',l'}^{*(n)}\right] = \mathrm{E}\left[|c_{k,l}|^2\right]\delta_{k,k'}\delta_{l,l'}$, where $\delta_{k,k'}$ is the discrete Kronecker delta function[3], and $\mathrm{E}\left[|c_{k,l}|^2\right]$

[3] $\delta_{n,m} = \begin{cases} 1, & n = m \\ 0, & n \neq m \end{cases}$

is the power of the lth path of user k. The assumption is equivalent to the common uncorrelated scattering (US) model [22]. The channels are assumed to be stationary over the observation interval so that the channel autocorrelation function $\varphi_{k,l}(n,n') = \mathrm{E}\left(c_{k,l}^{(n)} c_{k,l}^{*(n')}\right)$ is a function of the time difference $n'-n$ only. The assumption is equivalent to the common wide-sense stationary (WSS) model [172]. In other words, the channel autocorrelation becomes

$$\varphi_{k,l}(i) = \mathrm{E}\left[c_{k,l}^{(n)} c_{k,l}^{*(n+i)}\right]. \tag{2.26}$$

The stationarity assumption is valid if the vehicle speed does not change during the transmission. The Doppler power spectrum is assumed to be the classical Jakes's spectrum [172, Sec. 5.4], which results in the Clarke's channel autocorrelation function

$$\varphi_{k,l}(i) = \mathrm{E}\left[|c_{k,l}|^2\right] \mathcal{J}_0\left(2\pi f_d \frac{i}{T}\right), \tag{2.27}$$

where $\mathcal{J}_0$ is the zero-order Bessel function of the first kind,

$$f_d = \frac{v}{c_{light}} f_c \tag{2.28}$$

is the maximum Doppler spread, v is the speed of the vehicle, c_{light} is the speed of light, and f_c is the carrier frequency. The width of the channel autocorrelation function is called channel coherence time, denoted by T_{coh}. The coherence time satisfies $T_{coh} \approx 1/f_d$. The channel is said to be slowly fading if $T_{coh} \gg T$ or $f_d T \ll 1$, and fast fading if $T_{coh} < T$ or $f_d T > 1$. In the intermediate case $T_{coh} > T$ or $f_d T < 1$, the channel will be termed *relatively fast fading*. This is often the case in mobile communication systems with high vehicle speeds and speech services. With higher data rates, the channels are slowly fading, e.g., in an indoor environment.

The covariance matrix of the channel can be partitioned as ($\mathbf{\Sigma_c} = \mathrm{E}\left[\mathbf{c}\mathbf{c}^{\mathrm{H}}\right]$)

$$\mathbf{\Sigma_c} = \begin{pmatrix} \mathbf{\Sigma}_{\mathbf{c}^{(0)}} & \mathbf{\Sigma}_{\mathbf{c}^{(0)},\mathbf{c}^{(1)}} & \cdots & \mathbf{\Sigma}_{\mathbf{c}^{(0)},\mathbf{c}^{(N_b-1)}} \\ \mathbf{\Sigma}^{\mathrm{H}}_{\mathbf{c}^{(0)},\mathbf{c}^{(1)}} & \mathbf{\Sigma}_{\mathbf{c}^{(1)}} & \cdots & \mathbf{\Sigma}_{\mathbf{c}^{(1)},\mathbf{c}^{(N_b-1)}} \\ \vdots & \vdots & \ddots & \vdots \\ \mathbf{\Sigma}^{\mathrm{H}}_{\mathbf{c}^{(0)},\mathbf{c}^{(N_b-1)}} & \mathbf{\Sigma}^{\mathrm{H}}_{\mathbf{c}^{(1)},\mathbf{c}^{(N_b-1)}} & \cdots & \mathbf{\Sigma}_{\mathbf{c}^{(N_b-1)}} \end{pmatrix} \in \mathbb{C}^{KLN_b \times KLN_b}. \tag{2.29}$$

With the WSSUS channel model, the blocks in (2.29) for the uplink channel can be expressed as

$$\mathbf{\Sigma}_{\mathbf{c}^{(n)},\mathbf{c}^{(n+i)}} = \begin{pmatrix} \mathbf{\Sigma}_{\mathbf{c}_1^{(n)},\mathbf{c}_1^{(n+i)}} & \mathbf{0}_L & \cdots & \mathbf{0}_L \\ \mathbf{0}_L & \mathbf{\Sigma}_{\mathbf{c}_2^{(n)},\mathbf{c}_2^{(n+i)}} & \cdots & \mathbf{0}_L \\ \vdots & \vdots & \ddots & \vdots \\ \mathbf{0}_L & \mathbf{0}_L & \cdots & \mathbf{\Sigma}_{\mathbf{c}_K^{(n)},\mathbf{c}_K^{(n+i)}} \end{pmatrix} \in \mathbb{C}^{KL \times KL}, \tag{2.30}$$

and

$$\mathbf{\Sigma}_{\mathbf{c}_k^{(n)},\mathbf{c}_k^{(n+i)}} = \begin{pmatrix} \varphi_{k,1}(i) & 0 & \cdots & 0 \\ 0 & \varphi_{k,2}(i) & \cdots & 0 \\ \vdots & \vdots & \ddots & \vdots \\ 0 & 0 & \cdots & \varphi_{k,L}(i) \end{pmatrix} \in \mathbb{C}^{L\times L}. \tag{2.31}$$

The downlink channels are same for all users at a certain reception point, e.g., for the user $k = 1$. Hence for the downlink the covariance matrix elements are

$$\mathbf{\Sigma}_{\mathbf{c}^{(n)},\mathbf{c}^{(n+i)}} = \begin{pmatrix} \mathbf{\Sigma}_{\mathbf{c}_1^{(n)},\mathbf{c}_1^{(n+i)}} & \mathbf{\Sigma}_{\mathbf{c}_1^{(n)},\mathbf{c}_1^{(n+i)}} & \cdots & \mathbf{\Sigma}_{\mathbf{c}_1^{(n)},\mathbf{c}_1^{(n+i)}} \\ \mathbf{\Sigma}_{\mathbf{c}_1^{(n)},\mathbf{c}_1^{(n+i)}} & \mathbf{\Sigma}_{\mathbf{c}_1^{(n)},\mathbf{c}_1^{(n+i)}} & \cdots & \mathbf{\Sigma}_{\mathbf{c}_1^{(n)},\mathbf{c}_1^{(n+i)}} \\ \vdots & \vdots & \ddots & \vdots \\ \mathbf{\Sigma}_{\mathbf{c}_1^{(n)},\mathbf{c}_1^{(n+i)}} & \mathbf{\Sigma}_{\mathbf{c}_1^{(n)},\mathbf{c}_1^{(n+i)}} & \cdots & \mathbf{\Sigma}_{\mathbf{c}_1^{(n)},\mathbf{c}_1^{(n+i)}} \end{pmatrix} \in \mathbb{C}^{KL\times KL}, \tag{2.32}$$

and

$$\mathbf{\Sigma}_{\mathbf{c}_1^{(n)},\mathbf{c}_1^{(n+i)}} = \begin{pmatrix} \varphi_{1,1}(i) & 0 & \cdots & 0 \\ 0 & \varphi_{1,2}(i) & \cdots & 0 \\ \vdots & \vdots & \ddots & \vdots \\ 0 & 0 & \cdots & \varphi_{1,L}(i) \end{pmatrix} \in \mathbb{C}^{L\times L}. \tag{2.33}$$

2.3. Limitations of the conventional RAKE receivers

One of the most important requirements for the UMTS is high and variable data rate. In FMA2 and WCDMA systems it is possible to increase the data rate without bandwidth expansion by reducing the spreading factor. This is referred to as a *variable spreading factor* (VSF) technique. Alternatively the spreading factor may remain fixed and the data rate is increased by allocating several parallel spreading codes, i.e., data channels for the same service. This is referred to as a *multicode* (MC) technique. The combination of these two techniques is also supported, which results in hybrid VSF-MC techniques.

In the first phase of the third generation CDMA systems, the receivers will be based on the conventional RAKE receivers. From the RAKE receiver perspective, the multirate techniques are quite different. First, separate despreading devices, i.e., correlators are needed for each data channel. Hence, the MC technique is more hardware intensive than the VSF technique. Secondly, the mechanism generating interference is quite different.

In the VSF approach, the spreading factor can be as small as four in FMA2 concept. In multipath channels, the small spreading factor will cause so-called *inter-path interference* (IPI) due to imperfect spreading sequence autocorrelations. Due to IPI, multipath components are correlated and some diversity is lost, even if the ISI was rather small. E.g., if two multipath components are merged to one propagation path resulting in a single-path channel, there is IPI but no ISI and diversity gain is lost. Hence, although ISI may be negligible IPI can be quite

large. The smaller the spreading factor is, the larger the loss due to IPI will be. This phenomenom is illustrated in Figure 2.1. The bit error probability curves were generated by using the characteristic function method described in Section 3.1.1. Random spreading sequences and one chip delay between the multipath components was used. As we can see, the performance loss is significant already at the signal-to-noise ratio (SNR) of 10 dB. RAKE receivers have traditionally been used [3] in spread-spectrum systems, i.e., in systems with large spreading factors. The future CDMA systems with relatively small spreading factors result in significant performance losses in RAKE receivers due to IPI.

With the MC technique, IPI is rather small due to the higher spreading factor. Instead of IPI, *inter-channel interference* (ICI) causes performance degradation in the RAKE receivers in the same way as the multiple-access or multiuser interference in any CDMA system. The bit error probability degradation as a function of the number of parallel data channels is illustrated in Figure 2.2. The parameters and the analysis method used are the same as in Figure 2.1. The results of Figure 2.2 reveal that although the mechanism for generating interference in VSF and MC techniques are quite different, the performance is almost the same with both of them with the same data rate. This can be seen, e.g., by examining the BEPs with different spreading factors at the level of 10^{-2}. When the spreading factor is divided in half, the number of parallel codes channels is also halved to obtain the same BEP.

The performance is also similar in a near-far situation. The bit error probabilities for different near-far ratios[4] are presented for a two-user case in Figure 2.3. The near-far resistance is improved approximately by 3 dB when doubling the spreading factor. The performance will therefore be equal with both MC and VSF techniques assuming the same energy per information bit.

Based on the bit error performance results of both multirate techniques it can be concluded that the performance of the conventional RAKE receivers is interference limited. With the variable spreading factor approach the inter-path interference limits the performance. With the multicode technique, the inter-channel interference is the limiting factor and both techniques are sensitive to the near-far problem when the RAKE receivers are used. Clearly the major problem with the conventional RAKE receivers is that the performance is degraded as the data rate increases. The performance degradation can be avoided by using some near-far resistant receivers.

In the reminder of the thesis, advanced receivers that take into account the structure of the interference and enhance both the receiver peformance and the system capacity by suppressing or cancelling the interference will be studied. Receiver techniques suitable for downlink receivers will be addressed in Chapters 3 - 5 and for uplink receivers in Chapter 6.

[4]The near-far ratio is the difference between the power of the desired user and an interfering user.

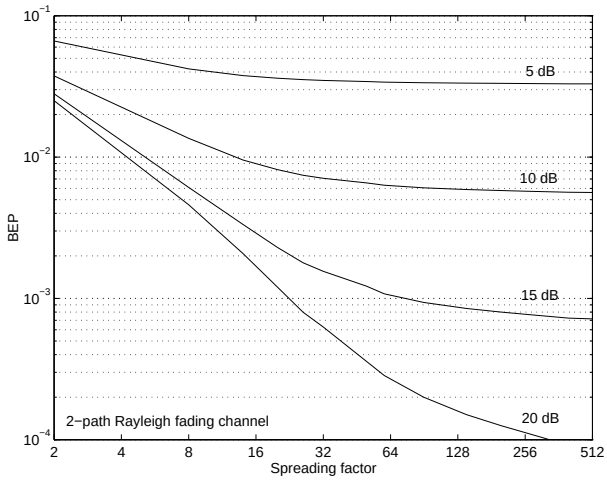

Fig. 2.1. The bit error probability degradation of the conventional RAKE receiver due to inter-path interference in a Rayleigh fading channel with two paths of the same power as a function of the spreading factor of random sequences in a single-user system using BPSK modulation with different SNRs.

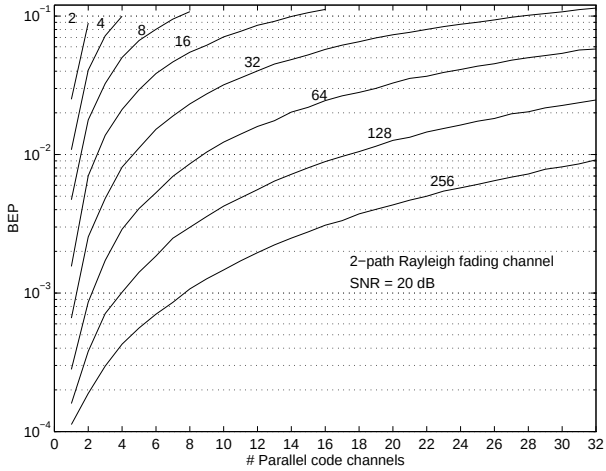

Fig. 2.2. The bit error probability degradation of the conventional RAKE receiver due to inter-channel interference in a Rayleigh fading channel with two paths of the same power as a function of the number of parallel data channels in a single-user system using BPSK modulation with different spreading factors (2 - 256) at the SNR of 20 dB.

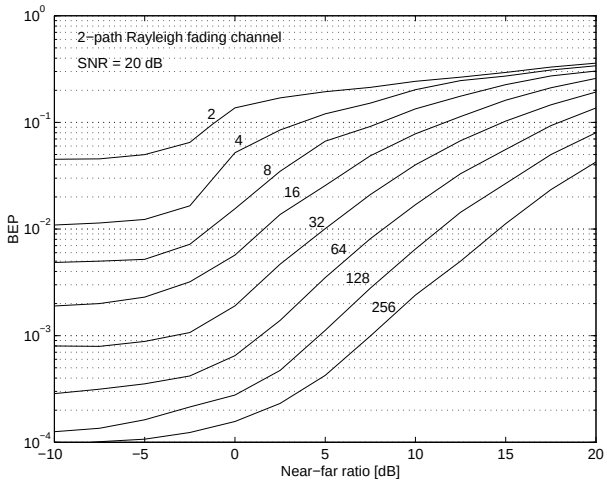

Fig. 2.3. The bit error probability degradation of the conventional RAKE receiver due to the near-far problem in a Rayleigh fading channel with two paths of the same power as a function of the near-far ratio for different spreading factors (2 - 256) in a two-user system using BPSK modulation at the SNR of 20 dB for the desired user.

3. LMMSE receivers in multipath fading channels

The conventional approach to reception in CDMA systems is to neglect multiple-access interference and the near-far problem. This poses tight limits to the system capacity due to interference even if strict power control is used. Another more efficient way to detect different users in CDMA systems is based on multiuser receivers. An optimal maximum likelihood multiuser receiver requires joint estimation of channel parameters and data symbols [25, 129, 173]. Optimal receivers are far too complex for practical implementations and hence several suboptimal receivers [4, 5, 6] have been proposed. Most near-far resistant receivers are centralized, i.e., all user signals are processed jointly in the receiver. When considering downlink receivers, only the desired user signal should be demodulated while suppressing the interference due to other users. The linear minimum mean squared error single-user receivers [68, 81, 82] are one option for the downlink receivers. The adaptive versions of the LMMSE receivers are usually defined in such a way that only one user is demodulated, as desired in the downlink. The standard LMMSE receiver, called *postcombining LMMSE receiver* in the sequel, [68, 81, 82] minimizes the mean squared error between the receiver output and the true transmitted data sequence. The LMMSE receivers are capable of handling both inter-path and inter-channel interference under severe near-far situations. The coefficients of the postcombining LMMSE receiver [68] depend on the channel coefficients of all users, and hence it must be adapted as the channel changes. If the fade rate of the channel is fast enough, the standard adaptive LMMSE receivers need to be updated continuously. Thus, the postcombining LMMSE receivers will have severe convergence problems in relatively fast fading channels. Nevertheless, they can be applied if the rate of fading is sufficiently low with respect to the data rate as will be demonstrated in Section 4.2.

The optimization criterion can be modified to overcome the convergence problems[1] of the postcombining LMMSE receiver. The modified optimization criterion, which leads to the *precombining LMMSE receiver*, minimizes the MSE between the receiver output and the channel coefficient data symbol product for each path.

[1] Although the term *tracking* is used to denote the convergence of a time-variant filter, the term *convergence* will be used in this thesis.

Hence it assumes that the channel parameters of the desired user are known or estimated, as is the case in the conventional coherent RAKE receiver. The precombining LMMSE receiver depends only on the normalized signature sequence cross-correlations and the average channel profiles of the users. Since the delays and the average channel profiles change rather slowly, the adaptation requirements of the precombining LMMSE receiver are significantly less stringent than those of the adaptive postcombining LMMSE receivers [82]. What is more, the complexity of the conventional coherent RAKE receiver is increased only moderately. The adaptive implementations of the precombining LMMSE receiver do not necessarily require training sequences, since the decisions made by the conventional RAKE receiver can often be used to train the adaptive receiver. Thus, the precombining LMMSE receiver can be viewed as an add-on feature in the conventional coherent RAKE receivers.

In this chapter, the precombining LMMSE receiver is derived and its performance in fading multipath channels is analyzed. The bit error probability (BEP) of the precombining LMMSE detector is compared to the BEP of the postcombining LMMSE detector both in AWGN and Rayleigh fading channels. To obtain more concrete performance figures for the precombining LMMSE receivers, their performance in the FMA2 downlink will be evaluated.

The rest of this chapter is organized as follows. The principles of the LMMSE receivers in fading multipath channels are presented in Section 3.1. Bit error probability analysis for the precombining LMMSE receivers in fading channels will be developed in Section 3.1.1 and for the postcombining LMMSE receiver in Section 3.1.2. Numerical results for the LMMSE detectors operating in the downlink of CDMA systems are presented in Section 3.1.3. The performance of the conventional RAKE and the modifed LMMSE receivers will be compared in FMA2 downlink in Section 3.2. The LMMSE receiver principles are extended to the spatial domain in Section 3.3. Results on LMMSE receivers in fading channels are summarized in Section 3.4.

3.1. Pre and postcombining LMMSE receivers in fading channels

There are two approaches which may be employed for linear multiuser detection in multipath channels. Multiuser filtering can take place either after multipath combining or prior to it. In other words, the multiuser receiver can be either a *postcombining interference suppression* type of receiver (Figure 3.1(a)), or a *precombining interference suppression* type of receiver (Figure 3.1(b)). Performance differences of the two structures for the decorrelating detector in known fixed channels have been compared in [54]. The results show that the order of multipath combining and interference suppression does not have a significant impact on the bit error probability of the decorrelator when the product of the number of users and the number of multipath components (KL) is relatively low. As the product KL becomes large, the cross-correlation matrix of users' signature sequences

becomes ill-conditioned. In such a case, multipath combining prior to interference suppression usually yields stable matrix inversion and robust performance. However, multipath combining prior to interference suppression makes channel estimation more difficult since the multiuser detector depends on the channel estimates, which cannot be estimated at the output of the detector in that case. Therefore, the practical implementations of the multiuser receivers first perform interference suppression, and subsequently, channel estimation [25, 26, 54, 174]. Such receivers also have the advantage that the detector does not depend on the fading channel state.

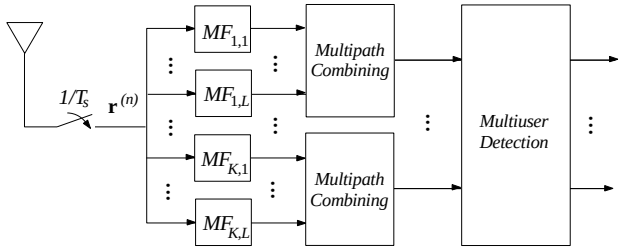

(a) Postcombining interference suppression receiver.

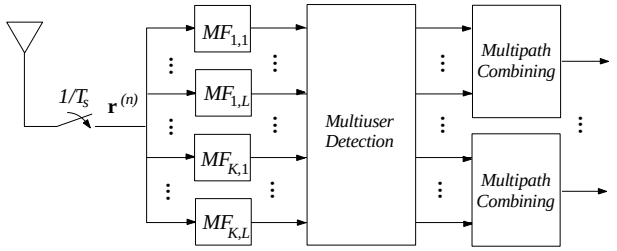

(b) Precombining interference suppression receiver.

Fig. 3.1. Multiuser receiver structures.

A postcombining LMMSE receiver minimizes the cost function $\mathrm{E}\{|\mathbf{b} - \hat{\mathbf{b}}|^2\}$ elementwise, where $\hat{\mathbf{b}} = \mathbf{L}_{[post]}^{\mathrm{H}}\mathbf{r}$, and $|\mathbf{x}|$ is the vector of absolute values of the elements of the vector $\mathbf{x}$. It is easy to show [175, p. 391] that the postcombining LMMSE receiver for all users is

$$\mathbf{L}_{[post]} = \mathbf{SCA}\left(\mathbf{AC}^{\mathrm{H}}\mathbf{RCA} + \sigma^2\mathbf{I}\right)^{-1} \in \mathbb{C}^{SGN_b \times KN_b}, \tag{3.1}$$

where $\mathbf{R} = \mathbf{S}^{\mathrm{T}}\mathbf{S}$ is the signature sequence cross-correlation matrix. The output of the postcombining LMMSE receiver is

$$\mathbf{y}_{[post]} = \left(\mathbf{A}\mathbf{C}^{\mathrm{H}}\mathbf{R}\mathbf{C}\mathbf{A} + \sigma^2\mathbf{I}\right)^{-1}(\mathbf{S}\mathbf{C}\mathbf{A})^{\mathrm{H}}\mathbf{r} \in \mathbb{C}^K, \tag{3.2}$$

where $(\mathbf{S}\mathbf{C}\mathbf{A})^{\mathrm{H}}\mathbf{r}$ is the multipath combined matched filter bank output. Thus, the postcombining LMMSE detector clearly leads to a postcombining interference suppression type of receiver (Figure 3.1(a)). If the channel is a non-fading AWGN channel, i.e., all non-zero elements in $\mathbf{C}$ are equal to 1, the detector can be written in the standard form [68]: $\mathbf{L}_{[post]} = \mathbf{S}\left(\mathbf{R} + \sigma^2(\mathbf{A}^{\mathrm{H}}\mathbf{A})^{-1}\right)^{-1}$. It can be seen from (3.1) that the postcombining LMMSE receiver in fading channels depends on the channel complex coefficients of all users and paths. If the channel is changing rapidly, the optimal LMMSE receiver changes continuously. Thus, the adaptive versions of the LMMSE receivers have increasing convergence problems as the fading rate increases.

The dependence on the fading channel state can be removed by applying a precombining interference suppression type of receiver (Figure 3.1(b)). This can be accomplished by minimizing each element of $\mathrm{E}\{|\mathbf{h} - \hat{\mathbf{h}}|^2\}$, where $\mathbf{h} = \mathbf{C}\mathbf{A}\mathbf{b}$ is the product between the channel coefficients, user amplitudes and data, and $\hat{\mathbf{h}} = \mathbf{L}_{[pre]}^{\mathrm{T}}\mathbf{r}$ its estimate. This leads to the precombining LMMSE receiver (see Appendix 2):

$$\mathbf{L}_{[pre]} = \mathbf{S}\left(\mathbf{R} + \sigma^2\mathbf{\Sigma}_{\mathbf{h}}^{-1}\right)^{-1} \in \mathbb{R}^{SGN_b \times KLN_b}, \tag{3.3}$$

where $\mathbf{\Sigma}_{\mathbf{h}} = \mathrm{diag}\left[A_1^2\mathbf{\Sigma}_{\mathbf{c}_1}, \ldots, A_K^2\mathbf{\Sigma}_{\mathbf{c}_K}\right] \in \mathbb{R}^{KLN_b \times KLN_b}$ is the covariance matrix of $\mathbf{h}$ and it consists of user powers and the average channel tap powers, with $\mathbf{\Sigma}_{\mathbf{c}_k} = \mathrm{diag}\left[\mathrm{E}[|c_{k,1}|^2], \ldots, \mathrm{E}[|c_{k,L}|^2]\right] \in \mathbb{R}^{L \times L}$ where $\mathrm{E}[|c_{k,l}|^2]$ is the average power of the kth user's lth propagation path. The output of the precombining LMMSE receiver is

$$\mathbf{y}_{[pre]} = \left(\mathbf{R} + \sigma^2\mathbf{\Sigma}_{\mathbf{h}}^{-1}\right)^{-1}\mathbf{S}^{\mathrm{T}}\mathbf{r} \in \mathbb{C}^{KL}, \tag{3.4}$$

where $\mathbf{S}^{\mathrm{T}}\mathbf{r}$ is the matched filter bank output vector without multipath combining. Thus, the precombining LMMSE receiver leads to a receiver structure as shown in Figure 3.1(b). As can be seen from (3.3), the precombining receiver no longer depends on the instantaneous values of the channel complex coefficients but on the average power profiles of the channels. The receiver is of the exact same form as the postcombining LMMSE receiver in a non-fading AWGN channel. The adaptation requirements are now significantly milder and the receiver can be made adaptive even in relatively fast fading channels. Since interference is separately suppressed in each multipath component before multipath combining, the precombining LMMSE receiver has the same structure as the conventional RAKE receiver. Hence, the precombining LMMSE receiver is called an *LMMSE-RAKE receiver.*

3.1.1. Performance analysis for the precombining LMMSE receiver

The performance of the precombining LMMSE receiver is analyzed in a known channel to obtain an expression for the average bit error probability. The analysis is based on the characteristic function method presented in [176]. The characteristic function is solved via eigen-analysis for the matrix formed from the decision variable. The same analysis has been previously applied to the conventional RAKE receivers [28] and decorrelating receivers [25, 129, 177].

The decision variable of the precombining LMMSE receiver ($M = 1$) for user k after maximal ratio combining can be expressed in the form

$$y^{(n)}_{[pre,MRC]k} = \mathbf{c}^{\mathrm{H}(n)}_k \mathbf{y}^{(n)}_{[pre]k}, \tag{3.5}$$

where

$$\mathbf{c}^{(n)}_k = \left[c^{(n)}_{k,1}, \ldots, c^{(n)}_{k,L}\right]^{\mathrm{T}} \in \mathbb{C}^L \tag{3.6}$$

is the combining vector, and

$$\mathbf{y}^{(n)}_{[pre]} = \mathbf{L}^{\mathrm{T}}_{[pre]} \bar{\mathbf{r}}^{(n)} = \left[\mathbf{y}^{\mathrm{T}(n)}_{[pre]1}, \ldots, \mathbf{y}^{\mathrm{T}(n)}_{[pre]K}\right]^{\mathrm{T}}, \tag{3.7}$$

where

$$\mathbf{y}^{(n)}_{[pre]k} = \left[y^{(n)}_{[pre]k,1}, \ldots, y^{(n)}_{[pre]k,L}\right]^{\mathrm{T}} \in \mathbb{C}^L \tag{3.8}$$

includes the LMMSE receiver output vector for user k. Let

$$\mathbf{Q} = \frac{1}{2}\begin{pmatrix} \mathbf{0}_L & \mathbf{I}_L \\ \mathbf{I}_L & \mathbf{0}_L \end{pmatrix} \in \{0, \frac{1}{2}\}^{2L \times 2L}, \tag{3.9}$$

and

$$\boldsymbol{\nu} = \left[\mathbf{c}^{\mathrm{T}(n)}_k, \mathbf{y}^{\mathrm{T}(n)}_{[pre]k}\right]^{\mathrm{T}} \in \mathbb{C}^{2L}. \tag{3.10}$$

By rewriting (3.5), the decision variable can be expressed in the form

$$y^{(n)}_{[pre,MRC]k} = \boldsymbol{\nu}^{\mathrm{H}} \mathbf{Q} \boldsymbol{\nu}. \tag{3.11}$$

The LMMSE receiver output vector $\mathbf{y}^{(n)}_{[pre]k}$ conditioned on the data vector $\bar{\mathbf{b}}^{(n)}$ $\left(\bar{\mathbf{b}}^{(n)} = \left[\bar{\mathbf{b}}^{\mathrm{T}(n)}_1, \ldots, \bar{\mathbf{b}}^{\mathrm{T}(n)}_K\right]^{\mathrm{T}}, \ \bar{\mathbf{b}}^{\mathrm{T}(n)}_k = \left[b^{(n-D)}_k, \ldots, b^{(n)}_k, \ldots, b^{(n+D)}_k\right]^T\right)$ is a complex Gaussian random vector. Since the weight vector $\mathbf{c}^{(n)}_k$ is also Gaussian, the probability of bit error for user k conditioned on $\bar{\mathbf{b}}^{(n)}$ can be expressed in the case of the BPSK modulation as [176]

$$Pr\{\text{error}|\bar{\mathbf{b}}^{(n)}\} = \sum_{\substack{i=1 \\ \lambda_i < 0}}^{2L} \prod_{\substack{j=1 \\ j \neq i}}^{2L} \frac{1}{1 - \frac{\lambda_j}{\lambda_i}}, \tag{3.12}$$

where $\lambda_i, i = 1, 2, \ldots, 2L$ are the eigen-values of the matrix $\mathbf{\Sigma}_{\boldsymbol{\nu}|\bar{\mathbf{b}}^{(n)}}\mathbf{Q}$, and

$$\mathbf{\Sigma}_{\boldsymbol{\nu}|\bar{\mathbf{b}}^{(n)}} = \begin{pmatrix} \mathbf{\Sigma}_{\mathbf{c}_k^{(n)}} & \mathbf{\Sigma}_{\mathbf{c}_k^{(n)},\mathbf{y}_{[pre]k}^{(n)}|\bar{\mathbf{b}}^{(n)}} \\ \mathbf{\Sigma}^{\mathrm{H}}_{\mathbf{c}_k^{(n)},\mathbf{y}_{[pre]k}^{(n)}|\bar{\mathbf{b}}^{(n)}} & \mathbf{\Sigma}_{\mathbf{y}_{[pre]k}^{(n)}|\bar{\mathbf{b}}^{(n)}} \end{pmatrix} \in \mathbb{R}^{2L\times 2L} \tag{3.13}$$

is the covariance matrix of the vector $\boldsymbol{\nu}$. Finally, the bit error probability for the kth user is expressed as

$$P_k = \frac{1}{2^{MK-1}} \sum_{\substack{\bar{\mathbf{b}}^{(n)}\in\{-1,1\}^{MK-1} \\ b_k=1}} Pr\{\text{error}|\bar{\mathbf{b}}^{(n)}\}. \tag{3.14}$$

In the following, the elements of the covariance matrix are elaborated in more detail for the receiver span of one symbol interval ($M = 1$) for simplicity. The combining vector covariance matrix is

$$\mathbf{\Sigma}_{\mathbf{c}_k^{(n)}} = \begin{pmatrix} \mathrm{E}[|c_{k,1}^{(n)}|^2] & & \mathbf{0} \\ & \ddots & \\ \mathbf{0} & & \mathrm{E}[|c_{k,L}^{(n)}|^2] \end{pmatrix} \in \mathbb{R}^{L\times L}, \tag{3.15}$$

the covariance matrix between the combining vector and the interference suppression filter output vector becomes

$$\mathbf{\Sigma}_{\mathbf{c}_k^{(n)},\mathbf{y}_{[pre]k}^{(n)}|\bar{\mathbf{b}}^{(n)}} = \begin{pmatrix} \mathbf{\Sigma}_{c_{k,1}^{(n)},y_{[pre]k,1}^{(n)}|\bar{\mathbf{b}}^{(n)}} & & \mathbf{0} \\ & \ddots & \\ \mathbf{0} & & \mathbf{\Sigma}_{c_{k,L}^{(n)},y_{[pre]k,L}^{(n)}|\bar{\mathbf{b}}^{(n)}} \end{pmatrix} \in \mathbb{R}^{L\times L}, \tag{3.16}$$

and the covariance matrix of the interference suppression filter output vector has the form

$$\mathbf{\Sigma}_{\mathbf{y}_{[pre]k}^{(n)}|\bar{\mathbf{b}}^{(n)}} = \begin{pmatrix} \mathbf{\Sigma}_{y_{[pre]k,1}^{(n)},y_{[pre]k,1}^{(n)}|\bar{\mathbf{b}}^{(n)}} & \cdots & \mathbf{\Sigma}_{y_{[pre]k,1}^{(n)},y_{[pre]k,L}^{(n)}|\bar{\mathbf{b}}^{(n)}} \\ \vdots & \ddots & \vdots \\ \mathbf{\Sigma}_{y_{[pre]k,L}^{(n)},y_{[pre]k,1}^{(n)}|\bar{\mathbf{b}}^{(n)}} & \cdots & \mathbf{\Sigma}_{y_{[pre]k,L}^{(n)},y_{[pre]k,L}^{(n)}|\bar{\mathbf{b}}^{(n)}} \end{pmatrix} \in \mathbb{R}^{L\times L}, \tag{3.17}$$

where

$$\mathbf{\Sigma}_{c_{k,l}^{(n)},y_{[pre]k,l}^{(n)}|\bar{\mathbf{b}}^{(n)}} = A_k\mathrm{E}[|c_{k,l}^{(n)}|^2]\bar{\mathbf{s}}_{k,l}^{\mathrm{T}}\mathbf{w}_{k,l} + \sum_{k'=1,k'\neq k}^{K} A_k b_k^{(n)}\mathrm{E}[|c_{k,l}^{(n)}|^2]\bar{\mathbf{s}}_{k',l}^{\mathrm{T}}\mathbf{w}_{k,l}, \tag{3.18}$$

and

$$\mathbf{\Sigma}_{y_{[pre]k,l}^{(n)},y_{[pre]k,l'}^{(n)}|\bar{\mathbf{b}}^{(n)}} = A_k^2\sum_{l'=1}^{L}\mathrm{E}[|c_{k,l'}^{(n)}|^2]\mathbf{w}_{k,l}^{\mathrm{T}}\bar{\mathbf{s}}_{k,l'}\bar{\mathbf{s}}_{k,l'}^{\mathrm{T}}\mathbf{w}_{k,l}$$

$$+ \quad \mathbf{w}_{k,l}^{\mathrm{T}} \sum_{k'=1,k'\neq k}^{K} A_{k'}^2 \sum_{l'=1}^{L} \mathrm{E}[|c_{k,l'}^{(n)}|^2] \bar{\mathbf{s}}_{k',l'} \bar{\mathbf{s}}_{k',l'}^{\mathrm{T}} \mathbf{w}_{k,l}$$

$$+ \quad \Big(A_k \mathbf{w}_{k,l}^{\mathrm{T}} \sum_{k'=1,k'\neq k}^{K} b_k^{(n)} b_{k'}^{*(n)} A_{k'} \sum_{l'=1}^{L} \mathrm{E}[|c_{k,l'}^{(n)}|^2]$$

$$\cdot \bar{\mathbf{s}}_{k,l'} \bar{\mathbf{s}}_{k',l'}^{\mathrm{T}} \mathbf{w}_{k,l} \Big) + \sigma^2 \mathbf{w}_{k,l}^{\mathrm{T}} \mathbf{w}_{k,l}, \tag{3.19}$$

where $\mathbf{w}_{k,l}$ is the middle block column of $\mathbf{L}_{[pre]}$ and $\bar{\mathbf{s}}_{k,l}$ is the windowed signature sequence for the kth user's lth path (see Section 4.1 for more details). The covariance matrix elements were derived for a synchronous downlink channel, i.e., $c_{k,l}^{(n)} = c_l^{(n)} \forall k$. The analysis can be easily extended to a more general asynchronous case with longer LMMSE filters. Incorporation of the impact of the channel estimation errors is also possible, as is shown in [25, 129, 177].

Although the bit error probability expression in (3.12) is not very intuitive, it is extremely useful in computing numerical examples. It can be simplified by using a Gaussian approximation for the residual interference, which has been shown [75] to be accurate in evaluating the BEP of the LMMSE detectors in AWGN channels. In the Gaussian approximation, the contribution of the interfering user bits is approximated as random variables from a discrete uniform distribution. As a result, the elements in the last summations in (3.18) and (3.19) become zero valued ($\mathrm{E}[b_k] = 0$), and the BEP evaluation is simplified. The verification of the Gaussian approximation for the precombining LMMSE receivers in multipath fading channels will be provided through some comparisons, which are presented in Section 3.1.3.

3.1.2. Performance analysis for the postcombining LMMSE receiver

The decision variable for the postcombining LMMSE receiver for the kth user can be expressed as [14]

$$y_{[post]k} = (\mathbf{L}_{[post]})_k^{\mathrm{H}} \mathbf{r} = (\mathbf{L}_{[post]})_k^{\mathrm{H}} \mathbf{SCAb} + (\mathbf{L}_{[post]})_k^{\mathrm{H}} \mathbf{n}. \tag{3.20}$$

where $(\cdot)_k$ denotes the middle element of the middle block for the kth user of the matrix. The bit error probability in a fixed Gaussian channel for a processing window of N_b symbols can be expressed as

$$P_{k|\mathbf{C}} = \frac{1}{2^{N_b K - 1}} \sum_{\substack{\mathbf{b}\in\{-1,1\}^{N_b K-1} \\ b_k = 1}} \mathrm{Q}\left(\frac{\mathrm{Re}\Big\{ (\mathbf{L}_{[post]}^{\mathrm{H}} \mathbf{SCAb})_k \Big\}}{\sqrt{\mathrm{Re}\Big\{ \sigma^2 (\mathbf{L}_{[post]}^{\mathrm{H}} \mathbf{L}_{[post]})_k \Big\}}} \right), \tag{3.21}$$

The bit error probability in Rayleigh fading channels is obtained by integrating $P_{k|\mathbf{C}}$ over the channel envelope distributions of all users and paths:

$$P_k = \underbrace{\int_0^\infty \cdots \int_0^\infty}_{KL} p(|c_{1,1}|) \cdots p(|c_{K,L}|) P_{k|\mathbf{C}} \quad d|c_{1,1}| \cdots d|c_{K,L}|. \tag{3.22}$$

The evaluation of this equation would be very intensive, since the argument of (3.21) depends on the channel coefficients $\mathbf{C}$ and the data bits $\mathbf{b}$ of all users. Furthermore, the bit error probability should be averaged over all possible phase and delay differences between the users and multipath components. It is possible to simplify the bit error probability equation by using the Gaussian approximation [75], but still the multiple integral equation should be computed over the distributions of channel envelopes $\left(p(|c_{k,l}|) = \frac{|c_{k,l}|}{\mathrm{E}[|c_{k,l}|^2]/2} \cdot \exp(-\frac{|c_{k,l}|^2}{\mathrm{E}[|c_{k,l}|^2]})\right)$ of all users and paths. For this reason, the performance of the postcombining LMMSE receiver in fading channels will only be evaluated by simulations in this section. Some analytic performance results will be presented based on the Gaussian approximation in fixed multipath channels.

By invoking the Gaussian approximation presented in [75], the bit error probability in fixed multipath channels with components of equal energy for the postcombining LMMSE detector can be approximated as

$$P_k \approx \mathrm{Q}\left(\sqrt{\mathrm{Re}\left\{\frac{A_k^2 \left(\mathbf{L}_{[post]}^{\mathrm{H}} \mathbf{S}\right)_k^2}{\sigma^2 \left(\mathbf{L}_{[post]}^{\mathrm{H}} \mathbf{L}_{[post]}\right)_k + \frac{1}{A_k^2} \sum\limits_{\substack{k'=1 \\ k' \neq k}}^{K} A_{k'}^2 \left(\mathbf{L}_{[post]}^{\mathrm{H}} \mathbf{S}\right)_{k'}^2}\right\}}\right). \tag{3.23}$$

The Gaussian approximation can be used for the precombining LMMSE detector as well. The decision variable for the precombining LMMSE detector ($M = 1$) is $y_{[pre]k}^{(n)} = \sum_{l=1}^{L} \left(\mathbf{L}_{[pre]}^{\mathrm{T}}\right)_{k,l} \mathbf{r}$, and hence the bit error probability in fixed channels, where the multipath components are of equal energy can be approximated as

$$P_k \approx \mathrm{Q}\left(\sqrt{\sum_{l=1}^{L} \frac{A_k^2 \left(\mathbf{L}_{[pre]}^{\mathrm{T}} \mathbf{S}\right)_{k,l}^2}{\sigma^2 \left(\mathbf{L}_{[pre]}^{\mathrm{T}} \mathbf{L}_{[pre]}\right)_{k,l} + \frac{1}{A_k^2} \sum\limits_{\substack{k'=1 \\ k' \neq k}}^{K} A_{k'}^2 \sum\limits_{l'=1}^{L} \left(\mathbf{L}_{[pre]}^{\mathrm{T}} \mathbf{S}\right)_{k',l'}^2}}\right). \tag{3.24}$$

3.1.3. Numerical examples

Both computer simulations and numerical analysis were carried out to investigate the performance of the two versions of the LMMSE receivers. The main parameters

used are the following: carrier frequency 2.0 GHz, symbol rate 16 kbits/s, 31 chip Gold code, and rectangular chip shape. Synchronous downlink with equal energy two-path ($L = 2$) Rayleigh fading channel with vehicle speeds 40 km/h was studied (which results in the maximum normalized Doppler shift of $4.63 \cdot 10^{-3}$) and a maximum delay spread of 10 chip intervals was used. The number of users considered was 1 – 30. Perfect channel estimation and ideal truncated precombining LMMSE receivers were used both in the analysis and the simulations. The receiver processing window length was three symbols ($M = 3$, $D = 1$) unless otherwise stated. The simulation results were obtained by averaging the BEPs of randomly selected users with different delay spreads. The exact analysis was perfomed by using 10000 different bit patterns, and the multipath delays were changed after every 100 bit patterns. In the Gaussian approximation case, the BEPs were averaged over all possible multipath delay combinations discretized at the sample rate for randomly selected users. First, the performance results of the precombining LMMSE receivers are presented. After that, the results for the postcombining LMMSE receiver will be discussed.

The validity of the Gaussian approximation [75] in frequency-selective fading channels was studied in order to further simplify the analysis. The results for both the conventional RAKE receiver and the precombining LMMSE receiver are presented in Figure 3.2. The approximation is accurate for the precombining LMMSE receiver in multipath fading channels, whereas slightly optimistic for the conventional RAKE receiver, as was expected. Also the simulation results indicate that the Gaussian approximation is accurate for the precombining LMMSE receiver (Figure 3.3). It is worth noting that the accuracy of the Gaussian approximation depends on the powers of the interfering users with the conventional RAKE receivers and also with the precombining LMMSE receivers with large amount of users in a multipath channel.

According to the analysis results of Figure 3.2, the precombining LMMSE receiver can significantly improve the performance of the conventional RAKE receiver. Using the raw BEP of 10^{-2} as a target value,[2] we can see that the capacity of the conventional RAKE is less than 40 % of the processing gain. The precombining LMMSE receiver has double the capacity (80 % of the processing gain in these examples) in comparison to the conventional RAKE receiver.

In Figure 3.4 the required average SNRs to obtain a certain BEP for a given number of users for both the conventional RAKE and the precombining LMMSE receivers are plotted. From this figure the advantages of using the precombining LMMSE receivers can be clearly seen. The conventional RAKE receiver supports only 12 users to obtain the BEP of 10^{-2}, whereas the precombining LMMSE receiver supports 25 users at a 10 dB lower power. Furthermore, the conventional RAKE receiver is sensitive to the near-far problem, indicating that the potential gains are much higher. The inter-path interference problem (Section 2.3) can also be seen from the figure. The conventional RAKE cannot achieve the BEP of 10^{-4} even in the single-user case due to the IPI induced BEP saturation.

Due to the difficult BEP analysis of the postcombining LMMSE receiver in

[2]Usually the practical channel codes require this raw BEP level for the satisfactory performance [23].

fading multipath channels, the BEP was analyzed by using the Gaussian approximations (3.23) and (3.24) in fixed two-path channels. The results are presented in Figure 3.5. The detector lengths were 11 symbol intervals for both receivers in asynchronous two-path channels with maximum delay spreads of 10 chip intervals. The postcombining LMMSE receiver has always better performance than the precombining LMMSE receiver, as was expected. However, the difference is negligible at SNR values less than 10 dB. At high SNRs, the postcombining LMMSE receiver has very good performance when compared to the precombining LMMSE receiver. The superior performance of the postcombining LMMSE receivers can also be seen in fading channel simulation results which are shown in Figure 3.6.

By comparing the results of Figures 3.6 and 3.3, we can see that the effective number of users with the precombining LMMSE receivers is approximately KL, since the BER of the postcombining LMMSE receiver with 20 users is roughly the same as the BER with the precombining LMMSE receiver with 10 users. This was the case also with 30 and 15 users, although not shown in the figures. Hence, the postcombining LMMSE receivers have potentially L times larger capacity than the precombining LMMSE receivers in multipath channels with L paths of equal energy.

The coefficients of the optimum precombining LMMSE receiver (3.3) depend on the average channel tap powers $\mathrm{E}[|c_{k,l}|^2]$. The coefficients of the postcombining LMMSE receiver (3.1), on the other hand, depend on the instantaneous channel coefficient values. Instead of using the true average channel tap powers in determining the precombining LMMSE receiver it is possible to calculate the receiver coefficients by using a short-term average of the channel tap powers. In that way, the precombining LMMSE receiver would track the channel envelope variations. The robustness against fading is sacrificed, but the performance can be improved as is shown in Figure 3.7. The short-term averaging intervals have been 100, 300 and 500 symbol intervals. The averaging was achieved by averaging the instantaneous channel tap powers with a recursive integrator with feedforward coefficient $2/N$ and feedback coefficient $1-2/N$ [3]. The precombining LMMSE receiver coefficients were updated once in 10 symbol intervals by using the short-term average power instead of the true long-term average.

The results indicate that the performance can be improved when using the short-term average rather than the long-term average ($N \to \infty$) in determining the precombining LMMSE receiver coefficients. With the vehicle speed of 40 km/h the performance improvement is significant only when $N \leq 300$. In practice, this type of receiver must be able to track the short-term average channel envelope variations. However, the convergence rate of the most practical adaptive implementations of the precombining LMMSE receiver is insufficient to track the channel tap power variations. Also, the BER of the postcombining LMMSE receiver is shown in the same figure. The performance of the postcombining LMMSE receiver is still much better than the performance of the precombining LMMSE receivers using short-term channel tap powers.

[3] A moving average filter of length N can be approximated by a first order recursive integrator with feedforward coefficient $2/N$ and feedback coefficient $1-2/N$ [171, p. 64].

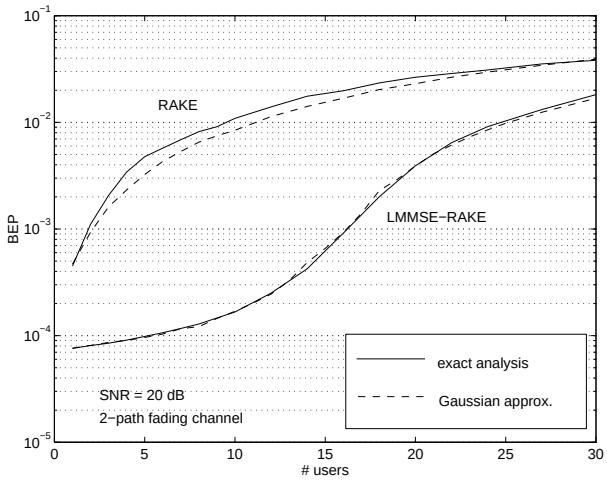

Fig. 3.2. Bit error probabilities (BEP) as a function of the number of users for the conventional RAKE and the precombining LMMSE (LMMSE-RAKE) receivers with the exact analysis and the Gaussian approximation in two path fading channels at vehicle speeds of 40 km/h and average SNRs of 20 dB.

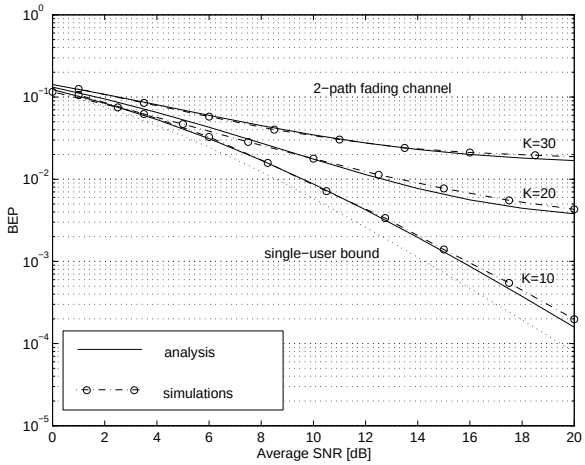

Fig. 3.3. Simulated and analytical bit error probabilities as a function of the average signal-to-noise ratio for the precombining LMMSE receiver in two-path fading channels at vehicle speeds of 40 km/h with different numbers of users.

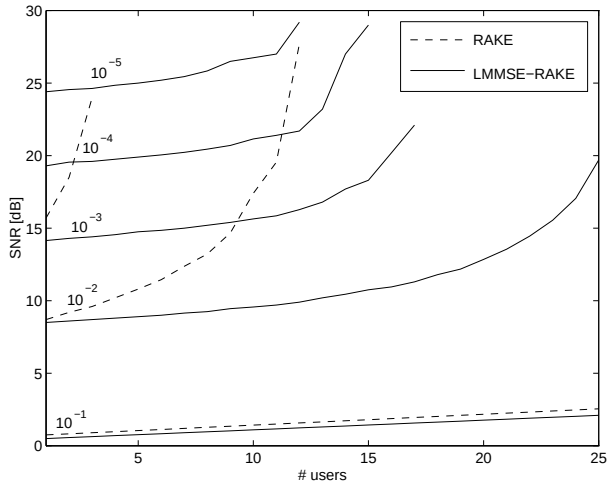

Fig. 3.4. Required average SNR versus the number of users to obtain a certain BEP ($10^{-5} - 10^{-1}$) for both the conventional RAKE and the precombining LMMSE receivers at vehicle speeds of 40 km/h.

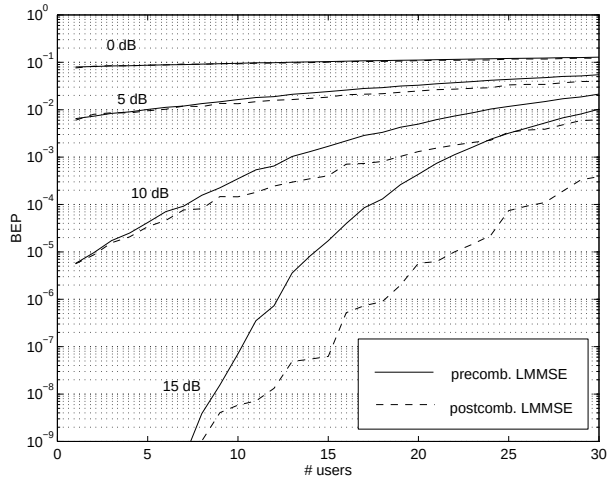

Fig. 3.5. Bit error probabilities as a function of the number of users for the postcombining and the precombining LMMSE detectors in an asynchronous two-path fixed channel with different SNRs.

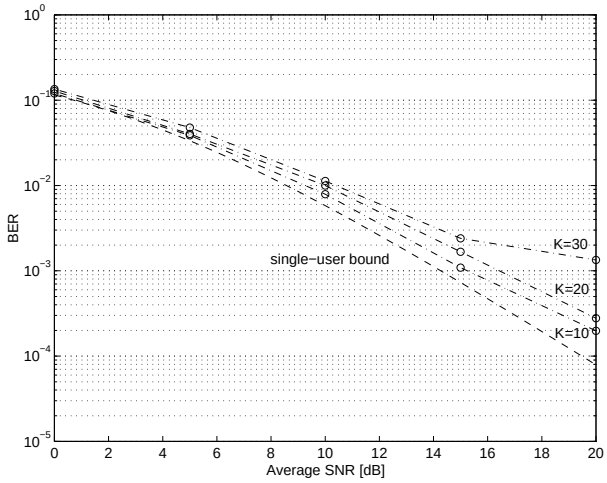

Fig. 3.6. Simulated bit error rates as a function of the average SNR for the postcombining LMMSE receiver in a two-path fading channel at vehicle speeds of 40 km/h with different numbers of users.

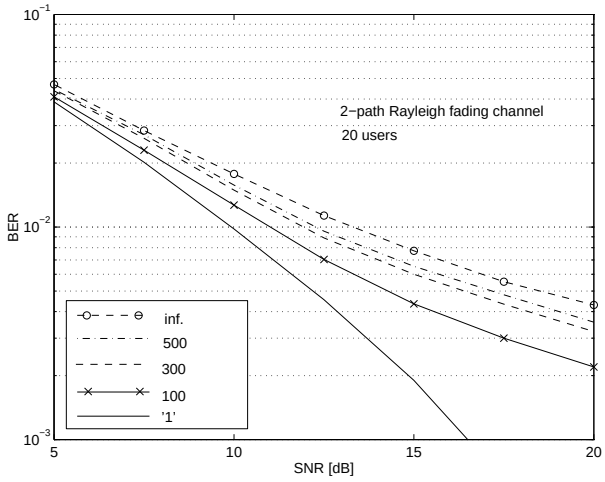

Fig. 3.7. BERs as a function of the average SNR in a two-path fading channel for vehicle speeds of 40 km/h in a 20-user case for the precombining LMMSE receiver with different short-term channel tap power averaging intervals (N = 100, 300, 500, ∞) and the postcombining LMMSE receiver ('1').

3.1.4. Discussion

The performance of the LMMSE receivers for DS-CDMA systems in fading channels was studied in this section. Both numerical analysis and computer simulations were used to evaluate the performance and the capacity of the LMMSE receivers in fading channels. The two receivers studied were the postcombining LMMSE and the precombining LMMSE receiver. Based on the results, it can be concluded that the postcombining LMMSE receiver has potentially higher capacity than the precombining LMMSE receiver. Due to obvious convergence problems (see Section 4.2), the postcombining LMMSE receivers are useful only with highest data rates when the normalized rate of fading is very small. The precombining LMMSE receivers do not have such convergence requirements and there are in principle no constraints for their use in fading channels. The precombining LMMSE receivers treat each multipath component as an independent interferer. The interference suppression capability is therefore degraded in radio channels with many distinct multipath components.

The comparisons between the precombining LMMSE and the conventional RAKE receivers revealed significant performance improvements when using the precombining LMMSE receivers. Hence, the precombining LMMSE receiver structure can be used to enhance the performance of the conventional RAKE receiver.

Instead of using the long-term average channel tap powers in determining the coefficients for the precombining LMMSE receiver, the short-term average values can also be used. It was shown by some numerical examples that this type of precombining LMMSE receiver results in improved BER performance in comparison to the receiver based on the long-term average channel tap powers. However, this performance improvement is probably lost in practical adaptive implementations.

3.2. Bit error probability analysis for FMA2 downlink receivers

In this section, the bit error probability of the precombining LMMSE receiver is compared to the BEP of the conventional RAKE receiver in frequency-selective Rayleigh fading channels using the FMA2 downlink signal structure [10]. The basic features of the FMA2 system are reviewed in Section 3.2.1. The principles and restrictions in applying interference suppression in third generation WCDMA system are discussed in Section 3.2.2. The assumptions used in the analysis are presented in Section 3.2.3. The numerical results are presented in Section 3.2.4. Some conclusions on the FMA2 downlink performance are drawn in Section 3.2.5.

3.2.1. Basic features of the FMA2 system

FMA2 [8, 10] is a wideband CDMA radio-access concept that has been designed on the basis of the UMTS requirements and the flexibility needs of third generation cellular services. The main features of the FMA2 concept include [10]:

- Support for high data rate transmission; more than 384 kbit/s with wide-area coverage and up to 2 Mbit/s for indoor and local outdoor coverage.
- High service flexibility with support of multiple parallel variable rate services for each active user, also with packetized transmission.
- High initial capacity and coverage with built-in support for future capacity and coverage enhancing technologies, such as smart antennas, multiuser receivers and base station diversity.
- Support for soft handover as well as inter-frequency handover for operation with hierarchical cell structures.
- Backward combatibility to GSM; handover between GSM and FMA2 supported.

The FMA2 concept clearly satisfies the UMTS requirements [7]. Some of the more detailed technical parameters for the FMA2 air interface are listed below.

- Basic chip rate 4.096 MHz; expandable to 8.192 and 16.384 MHz.
- Spreading modulation dual-channel QPSK (with complex scrambling in the uplink).
- Data modulation BPSK for each data channel[4].
- Spreading factor may vary from 4 to 256.

[4]By definition, a physical data channel is one BPSK modulated and spread I or Q branch signal. Hence, one I-Q pair carries two physical channels and is actually QPSK modulated.

- Variable length Walsh codes are used for channel separation. The scrambling codes in the uplink are the extended very-large Kasami codes of length 256 unique to each mobile terminal, extended Gold codes of length 256 are used for the downlink. The optional long scrambling code (40960 chips) for the uplink is derived from a Gold code of length $2^{41} - 1$.
- The coded bit rate of each data channel may vary from 16 kbit/s to 1.024 Mbit/s.
- 200 kHz carrier raster with a basic carrier spacing from 4.4 MHz to 5 MHz for the basic chip rate of 4.096 MHz; root raised cosine filtering with roll-off 0.22 is used for band limitation.
- 10 ms frame length; a super-frame consists of 60 frames.
- Asynchronous operation, i.e., no need for accurate base station synchronization.
- Both variable spreading factor and multi-code techniques to support multi-rate transmission.
- Rate matching with either unequal repetition or puncturing [178].
- Convolutional codes of constraint length 9 with rates 1/2 and 1/3 used for BER $= 10^{-3}$ services. An additional Reed-Solomon code is used as an outer code for BER $= 10^{-6}$ services.
- Flexible interleaving with variable interleaving depths to support ARQ with packet data and to support service multiplexing.
- Fast power control for both the uplink and the downlink with dynamic ranges of 80 dB and 20 dB, respectively. The power control command rate and the step-size are cell-specific parameters in the range of 400 – 1600 Hz and 0.5 – 2 dB, respectively.
- Flexible support of variable-rate services; data rate is allowed to vary frame-by-frame.
- Pilot symbols in the uplink to assist coherent demodulation; a pilot channel is used in the downlink. Optionally, pilot symbols can be used to support downlink beamforming. The pilot symbol rate is a cell-specific parameter in the range of 400 – 1600 Hz.

A more detailed introduction to the FMA2 concept can be found in [8, 10].

3.2.2. Interference suppression in WCDMA

The two main classes for near-far resistant receivers are interference cancellation type receivers and linear equalizer based interference suppression receivers [4, 6, 5].

Interference cancellation based receivers require that the data symbols and the channel coefficients of all users are estimated to create the multiple-access interference estimate. Clearly, this kind of detectors are well suited for the uplink, since all user signals are demodulated by the base station. Interference cancellation type detectors do not require short spreading sequences, since the cancellation can be performed for the sampled wideband signal. On the other hand, linear equalizer type detectors require short spreading sequences in order to retain MAI cyclo-stationarity over sufficiently short cycles. Since the equalizers do not necessarily need any information on the interfering users, they are also well suited to down-link receivers. In particular, the precombining LMMSE receiver is an attractive alternative for the WCDMA downlink receivers.

Equalizers require cyclo-stationary interference, and therefore, the equalizer taps need to be changed if the spreading code is changing from one symbol interval to another. In such a case, cyclically shifted filter bank [68] type equalizers can be used. Altogether, P/G sets of equalizer taps are needed, where P is the scrambling code length and G is the actual spreading factor used. Hence, with a scrambling code length of 256 chips, 8 sets of taps are needed for $G = 32$. If a 40960 chip length scrambling code is used, as in the WCDMA proposal, 1280 tap sets would be required. If the mobile speed is 120 km/h, the path delay changes 0.1 chips in 0.22 seconds[5]. Within 0.22 seconds, the same scrambling code section has been repeated only 22 times ($\frac{0.22s}{10ms}$) with the scrambling code length of 40960 chips. The adaptive equalizers would need several hundreds or even thousands of iterations to converge. So, it is clear that linear interference suppression schemes cannot be applied with these long scrambling codes. Hence, the linear interference suppression receivers studied in this section are well suited for the FMA2 downlink, but cannot be applied in the WCDMA proposal [179][6]. The performance of the FMA2 downlink with the conventional RAKE and the precombining LMMSE receivers is analyzed in the next section.

3.2.3. Parameters and assumptions used in the analysis

Perfect channel estimation and ideal truncated precombining LMMSE receivers are used to obtain the lower bounds of bit error probability. Random (long) scrambling codes are used to simplify the practical numerical analysis.

The spreading factors used correspond to the highest data rates using the variable spreading factor approach. The channel model used is a two-path fading channel (equal energies) with maximum delay spread of 2 μs and velocity of 5 km/h for the spreading factors $G = 2$ and 4; delay spread of 7 μs and velocity of 50 km/h for $G = 8$, 16, 32. The actual delay values were randomly selected. The smallest spreading factors are only used with low vehicle speeds and small delay spreads.

In order to cover approximately the same time span with the equalizers in the

[5]Delay errors larger than 0.1 chips cause significant performance losses to linear receivers [63].
[6]The European WCDMA proposal is subject to changes.

two channels used, the LMMSE receiver lengths were different for each spreading factor. The LMMSE receiver length in symbol intervals was 17 symbols for $G = 2$; 9 symbols for $G = 4$, 8; 5 symbols for $G = 16$; and 3 symbols for $G = 32$. It should be noted that since the length of the optimum LMMSE detector is infinite, longer detectors would yield slightly better performance.

The analysis is carried out both with and without the near-far problem. The near-far cases studied were: 50% of users have 6 dB higher power; or there is one interferer of 20 dB higher power. The latter figure is based on downlink power control with a limited dynamic range (20 dB), which means that in the worst case there can be users that have 20 dB higher power. The BEP is also analyzed as a function of the near-far-ratio in a two-user case.

Root raised cosine filtering with a roll-off factor of 0.22 was used and the number of samples per chip was 4. The analysis was perfomed by using 10000 different bit patterns of length 3 – 17 bits depending on the detector length. The carrier phase for the second multipath component was randomly selected for each bit pattern. The multipath delays were changed after every 100 bit patterns. The data channel (the Walsh code) was randomly selected for each bit pattern.

The control channels [10] were not included in the analysis, which means that the data modulation for the single data channel case was BPSK. In the multicode case, the data modulation is QPSK. The bit error probability for QPSK modulation is approximately the same as for BPSK, and hence, the results for BPSK can also be used for the QPSK case. The channel bit rates studied were 2.048 Mbit/s – 128 kbit/s ($G = 2 - 32$) for a single code channel. The source symbol rates for the case of three parallel data channels (two I-Q pairs) are then 2.048 Mbit/s – 128 kbit/s ($G = 2 - 32$) if the channel code rate is assumed to be 1/3 (no coding was used in the analysis; only the raw BEP is analyzed). The key parameters used in the analysis are summarized in Table 3.1.

The conclusions to be drawn from the analysis are based on the raw BEP target value of 10^{-2} and a two-path Rayleigh channel with equal energies and maximum delay spreads of 2 or 7 μs (Table 3.1). In practical systems, the target raw BEP can be higher (up to 10^{-1}), depending on the channel code being used. It should also be noted that the channel multipath profile as well as the fast power control loop used to compensate for the fast fading have significant impact on the BEP results. Therefore, the analysis results presented in this Section can be considered only indicative when considering the practical WCDMA system. Nevertheless, the comparisons between the conventional RAKE receiver and the precombining LMMSE receiver are still justified.

3.2.4. Numerical examples

The bit error probabilities as a function of the number of users for different spreading factors in the single data channel case are given in Figure 3.8 for the conventional RAKE receiver, and in Figure 3.9 for the precombining LMMSE receiver, respectively. If the target raw bit error rate is 10^{-2} at 20 dB, the conventional

RAKE can support roughly 50 % fewer users than the precombining LMMSE receiver. The same results for the case when each user has three parallel data channels are given in Figures 3.10 and 3.11. Again in this case the LMMSE receiver has two times higher capacity. We can also observe that the minimum spreading factor used with the conventional RAKE should be eight rather than four. However, the precombining LMMSE receiver can also provide acceptable performance with a spreading factor of two.

In Figures 3.8 and 3.9, only one I-Q pair is used and in Figures 3.10 and 3.11 two are used simultaneously. By comparing the BEPs, e.g., with three users for spreading factors 8 – 32 of Figures 3.10 and 3.11 with the results obtained with three users for spreading factors 4 – 16 in Figures 3.8 and 3.9, we see that the performances with two data channels per user are roughly equal to the case when the spreading factor is decreased and only one data channel is used. Hence the performance with the VSF and MC techniques is approximately equal in the FMA2 downlink.

The bit error probabilities as a function of the average SNR for different numbers of active users in single data channel case are presented in Figures 3.12 – 3.15 for the spreading factors 4 – 32. The Gaussian approximation [75] of MAI was used in this analysis. The Gaussian approximation is very accurate for the LMMSE receivers, whereas, it is slightly optimistic for the conventional RAKE. However, by comparing the BEPs at 20 dB to the earlier results (Figure 3.8), we can see that the difference is rather small. In the single-user case, the BEP of the conventional RAKE saturates with small spreading factors due to the bad average autocorrelation properties of the combined Walsh code and the scrambling code. If the number of users is half of the spreading factor, the BEP of the conventional RAKE is the same regardless of the spreading factor. If the target raw BEP at 20 dB is 10^{-2}, the capacity with the conventional RAKE is half of the spreading factor in the case with no near-far problem. The capacity with the precombining LMMSE detector is approximately 100 % of the spreading factor. Alternatively if the target BEP is 10^{-2} with a half load ($K = G/2$), the conventional RAKE receivers would require 20 dB SNR whereas the precombining LMMSE receiver needs only 10 dB. This is valid for all spreading factors studied.

In near-far situations, the BEP of the conventional RAKE receiver collapses completely. Under rather mild near-far conditions, where 50 % of users have 6 dB higher power (Figure 3.16), only the spreading factor 32 results in acceptable performance. The absolute minimum spreading factor which may be used in this case is 16 for the conventional RAKE to achieve the BEP of 10^{-2}. The bit error performance for the precombining LMMSE detector is the same with the near-far cases at high SNRs, and hence, the results for the precombining LMMSE receiver can be read from the Figure 3.9. In a more severe near-far situation, such as when there is one interferer of 20 dB higher power (Figure 3.17), the BEP of the conventional RAKE is unacceptably high. The precombining LMMSE detector, on the other hand, gives excellent results in this case. The maximum number of users which may be supported whilst maintaining a BEP of 10^{-2} at the SNR of 20 dB in the different cases studied are summarized in Table 3.2.

The BEPs as a function of the near-far ratio with different SNRs are given

in Figure 3.18. The precombining LMMSE receiver has similar performance regardless of the near-far ratio at large SNRs. The conventional RAKE receiver is sensitive to the near-far problem and has relatively high BEP with the lowest spreading factors even with small near-far ratios. With mixed data rate services with different QoS requirements, the high data rate channels require higher power, which causes a near-far problem for the low data rate users. E.g., a data channel with a spreading factor of $G = 8$ will be seen at a 15 dB higher power for the data channels with the spreading factor of $G = 256$. Based on this observation, the maximum dynamic range for the downlink power control should be reduced in a mixed data rate system since the average near-far ratio is a combination of the power control and the data rate caused power difference between the users. In Table 3.3 the maximum allowable downlink power control dynamic ranges are calculated based on the BEP results of Figure 3.18 and the raw BEP requirement of 10^{-2}. Based on the BEP curves of Figure 3.18 and the results of Table 3.3, an approximate formula for calculating the maximum power control dynamic can be given as: $\Delta\mathcal{P} \approx 10log(G_{min} \cdot 3/8)$, where G_{min} is the lowest spreading factor used. It is obvious that the power control dynamic range must be reduced when using small spreading factors with the conventional RAKE receiver. In theory, there are no constraints for the power control dynamic range when using the precombining LMMSE receivers, as can be seen from Figure 3.18.

Large near-far ratios can be avoided by reducing the power control dynamic range and by allocating different data rate groups to different cells or different carrier frequencies. By extrapolating the numerical result of Figure 3.18 to the largest spreading factors (64 – 256), it can be estimated that the maximum power control dynamic range is 20 dB for the spreading factor of 256 in a two-user case. Assuming that there are the data rate groups A (spreading factors 8 – 32, 4 is not used) and B (spreading factors 64 – 256), the maximum allowable power control dynamic range would be approximately 5 dB in the group A and 15 dB in the group B. Although this result is deduced starting from a simple two-user two-path case, the message is clear: service mix per carrier should be reduced when using conventional RAKE receivers.

3.2.5. Discussion

The downlink performance for the FMA2 concept utilizing either the conventional RAKE or the precombining LMMSE receivers was studied in this section. The analysis results revealed that the performance of the conventional RAKE receiver is tolerable without the near-far problem if the number of users is less than half of the spreading factor. Due to the downlink power control and mixed data rate service induced near-far problem, the performance of the conventional RAKE receiver collapses. Large near-far ratios can be avoided by reducing the power control dynamic range and by allocating different data rate groups to different cells or different carrier frequencies.

By using adaptive equalizers, satisfactory performance would be obtained under

various channel conditions and data rates without strict limits for the service mix or power control dynamic range. Both the general results of Section 3.1.3 and the FMA2 specific results of this section show significant system capacity and receiver performance improvements when using the LMMSE receivers instead of the conventional RAKE receivers.

The results clearly show the inter-path interference problem with small spreading factors. One possibility to reduce the problem is to decorrelate the propagation paths of the desired user. In other words IPI is forced to zero and diversity gain is increased. The BEP improvements at high SNRs[7] can be estimated in the single-user case by comparing Figures 3.8 and 3.9. Implementation of the decorrelating detector for the desired user's propagation paths would require computation of the inverse of the cross-correlation matrix of size $ML \times ML$, where L is the number of propagation paths and M is the length of the detector in symbol intervals. In [180] it was shown that decorrelators can be realized even in long code systems, and hence the decorrelation of the propagation paths is one possibility to enhance the performance and the capacity of the WCDMA downlink. However, the problems related to the robustness of the decorrelator in the presence of timing errors [63] would demand for high-resolution timing estimators for such receivers. In [181] a timing estimator suitable to iterative decorrelating receivers has been studied.

Another possible solution to suppress IPI would be to use adaptive channel impulse response matched filters prior to signal despreading. After such a channel matched filter the channel caused distortion is compensated and only one correlator is needed for despreading. Effectively, the adaptive channel matched filter equalizes the chip waveform. In synchronous downlink with orthogonal channel separation MAI is zero with the optimum sampling instant from the channel matched filter. Since the channel matched filter is the same for all users at a mobile terminal, the filter can be adapted by using the pilot channel bits as a training sequence. Another possibility is to use also the signals of other users to increase the training signal energy. Data detection for those users would be required unless only the pilot symbols are utilized. This approach fails at base station receivers and also in the case when downlink beamforming is used. The adaptive channel matched filter can be applied also in a long code system since the filter depends only on the channel impulse response. The drawback of this approach is that the filter weights depend on the channel phases, which causes convergence problems in fading channels as will be discussed in Section 4.2.

[7]LMMSE and decorrelating receivers are asymptotically equal.

Table 3.1. Parameters used in the analysis with different data rates.

Data rate [kbit/s]	Spreading factor (G)	Processing window (M)	Delay spread [μs]	Velocity [km/h]
2048	2	17	2	5
1024	4	9	2	5
512	8	9	7	50
256	16	5	7	50
128	32	3	7	50

Table 3.2. The maximum number of users which may be supported whilst maintaining a bit error probabilty of 10^{-2} at the SNR of 20 dB for the conventional RAKE and the precombining LMMSE receiver with equal energy users and near-far situation (50 % of users have 6 dB higher power). A single data channel per user is used.

	Equal energies		Near-far prob.	
G	RAKE	LMMSE	RAKE	LMMSE
2	-	2	-	2
4	1	3	-	3
8	4	7	-	7
16	6	12	-	12
32	14	28	4	28

Table 3.3. The maximum power control dynamic range in a two-user case with different data rates to obtain a BEP of 10^{-2}.

Spreading factor (G_{max})	Spreading factor ratio (G_{max}/G_{min})	Maximum power control dynamic range $\Delta\mathcal{P}$ (dB)
32	1 (G_{min}=32)	11
	2 (G_{min}=16)	8
	4 (G_{min}=8)	5
	8 (G_{min}=4)	2
16	1 (G_{min}=16)	8
	2 (G_{min}=8)	5
	4 (G_{min}=4)	2
8	1 (G_{min}=8)	5
	2 (G_{min}=4)	2
4	-	-

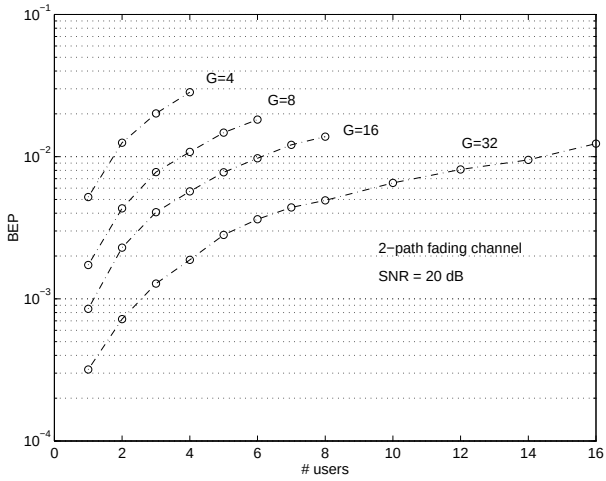

Fig. 3.8. Bit error probabilities as a function of the number of users for the conventional RAKE receiver with different spreading factors (G) in a two-path Rayleigh fading channel with maximum delay spreads of 2 μs for $G = 4$, and 7 μs for other spreading factors. The average signal-to-noise ratio is 20 dB, the data modulation is BPSK and the energy of all users is equal. Data rates vary from 128 kbit/s to 1.024 Mbit/s; no coding is assumed.

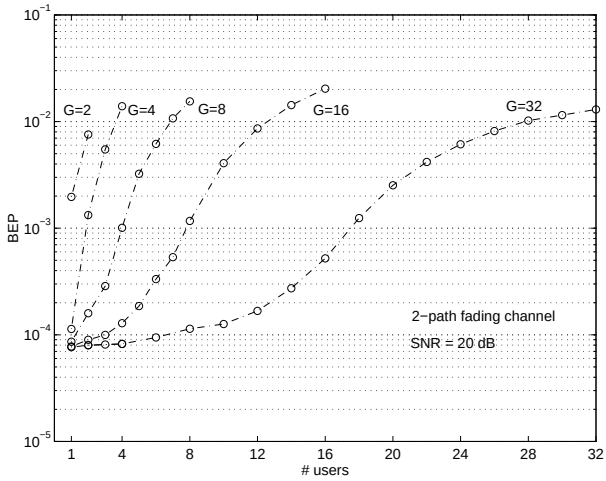

Fig. 3.9. Bit error probabilities as a function of the number of users for the precombining LMMSE (LMMSE-RAKE) receiver with different spreading factors (G) in a two-path Rayleigh fading channel with maximum delay spreads of 2 μs for $G = 2$, 4; and 7 μs for other spreading factors. The average signal-to-noise ratio is 20 dB, the data modulation is BPSK and the energy of all users is equal. Data rates vary from 128 kbit/s to 2.048 Mbit/s; no coding is assumed.

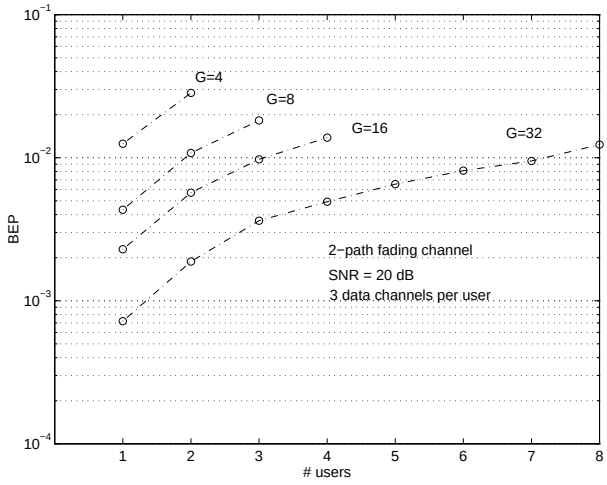

Fig. 3.10. Bit error probabilities as a function of the number of users for the conventional RAKE receiver with different spreading factors (G) in a two-path Rayleigh fading channel with maximum delay spreads of 2 μs for $G = 4$, and 7 μs for other spreading factors. The average signal-to-noise ratio is 20 dB, the data modulation is QPSK and the energy of all users is equal. Data rates vary from 128 kbit/s to 1.024 Mbit/s; the channel code rate is assumed to be 1/3.

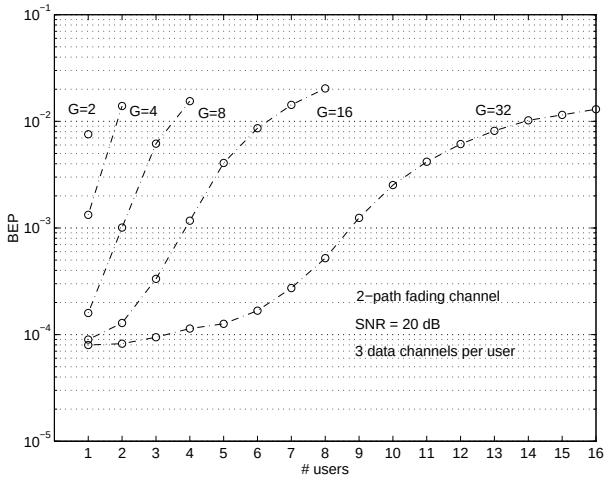

Fig. 3.11. Bit error probabilities as a function of the number of users for the precombining LMMSE (LMMSE-RAKE) receiver with different spreading factors (G) in a two-path Rayleigh fading channel with maximum delay spreads of 2 μs for $G = 2$, 4; and 7 μs for other spreading factors. The average signal-to-noise ratio is 20 dB, the data modulation is QPSK and the energy of all users is equal. Data rates vary from 128 kbit/s to 2.048 Mbit/s; the channel code rate is assumed to be 1/3.

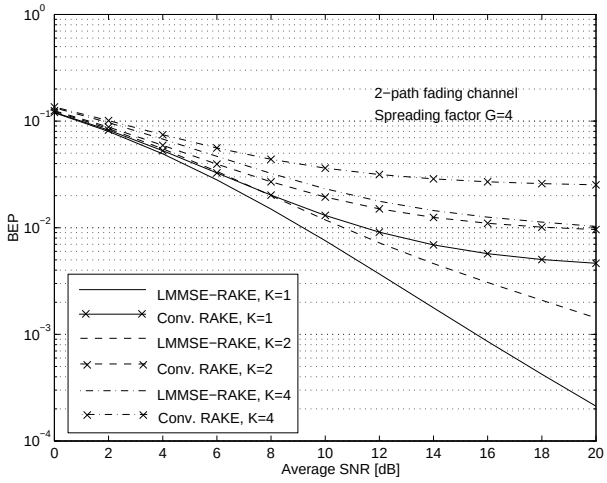

Fig. 3.12. Bit error probabilities as a function of the average SNR for the conventional RAKE receiver and the precombining LMMSE (LMMSE-RAKE) receiver with different number of users ($K = 1, 2, 4$) in a two-path Rayleigh fading channel with a maximum delay spread of 2 μs. The data modulation is BPSK at 1.024 Mbit/s ($G = 4$), the energy of all users is equal, no channel coding is assumed.

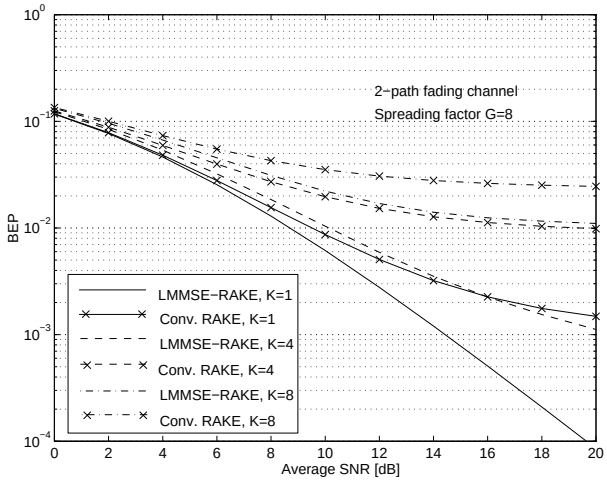

Fig. 3.13. Bit error probabilities as a function of the average SNR for the conventional RAKE receiver and the precombining LMMSE (LMMSE-RAKE) receiver with different number of users ($K = 1, 4, 8$) in a two-path Rayleigh fading channel with a maximum delay spread of 7 μs. The data modulation is BPSK at 512 kbit/s ($G = 8$), the energy of all users is equal, no channel coding is assumed.

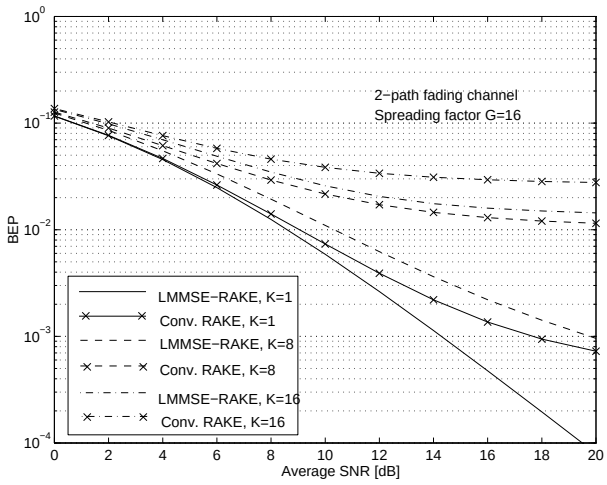

Fig. 3.14. Bit error probabilities as a function of the average SNR for the conventional RAKE receiver and the precombining LMMSE (LMMSE-RAKE) receiver with different number of users ($K = 1, 8, 16$) in a two-path Rayleigh fading channel with a maximum delay spread of 7 μs. The data modulation is BPSK at 256 kbit/s ($G = 16$), the energy of all users is equal, no channel coding is assumed.

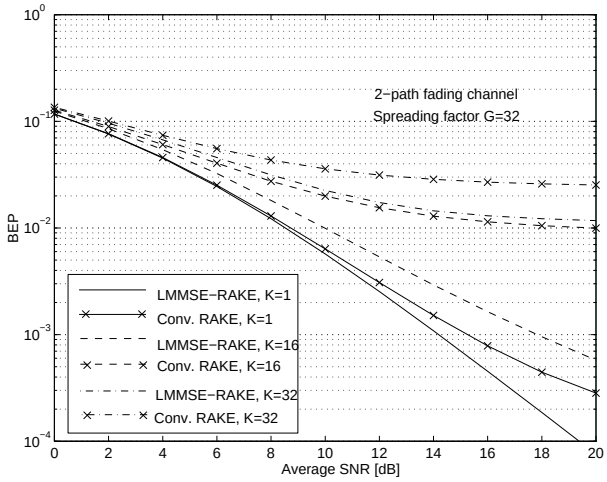

Fig. 3.15. Bit error probabilities as a function of the average SNR for the conventional RAKE receiver and the precombining LMMSE (LMMSE-RAKE) receiver with different number of users ($K = 1, 16, 32$) in a two-path Rayleigh fading channel with a maximum delay spread of 7 μs. The data modulation is BPSK at 128 kbit/s ($G = 32$), the energy of all users is equal, no channel coding is assumed.

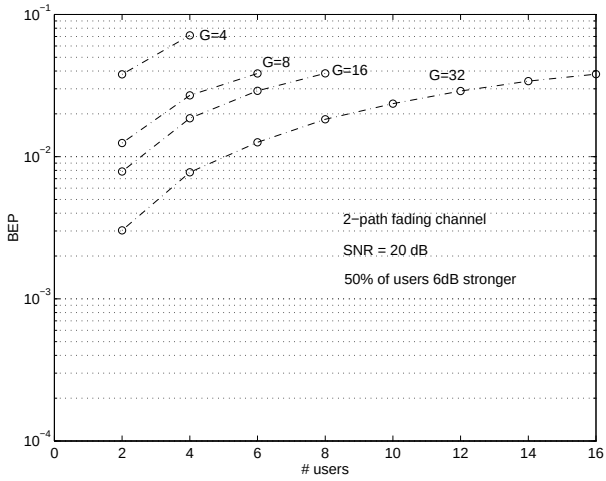

Fig. 3.16. Bit error probabilities as a function of the number of users for the conventional RAKE receiver with different spreading factors (G) in a two-path Rayleigh fading channel with maximum delay spreads of 2 μs for $G = 4$, and 7 μs for other spreading factors. The average signal-to-noise ratio is 20 dB, the data modulation is BPSK and 50 % of users have 6 dB higher power. Data rates vary from 128 kbit/s to 1.024 Mbit/s; no coding is assumed.

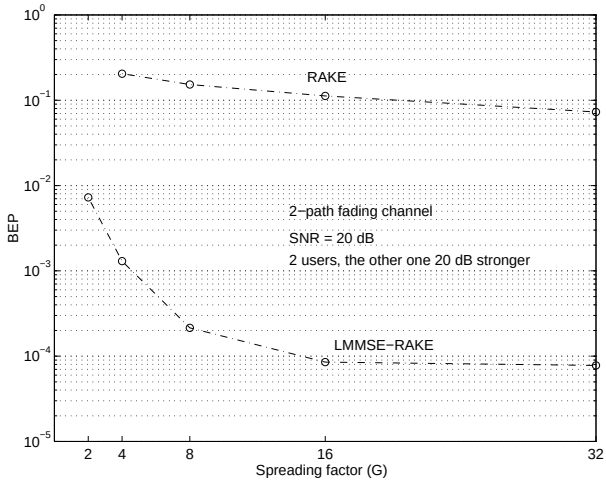

Fig. 3.17. Bit error probabilities as a function of the spreading factor for the conventional RAKE and the precombining LMMSE (LMMSE-RAKE) receiver with different spreading factors (G) in a two-path Rayleigh fading channel with maximum delay spreads of 2 μs for $G = 4$, and 7 μs for other spreading factors. The average signal-to-noise ratio is 20 dB, the data modulation is BPSK, the number of users is 2, the other user has 20 dB higher power. Data rates vary from 128 kbit/s to 2.048 Mbit/s; no coding is assumed.

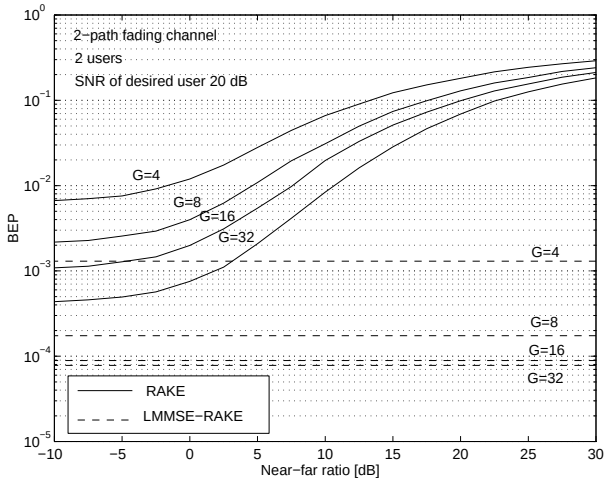

Fig. 3.18. Bit error probabilities as a function of the near-far ratio for the conventional RAKE and the precombining LMMSE (LMMSE-RAKE) receiver with different spreading factors (G) in a two-path Rayleigh fading channel with maximum delay spreads of 2 μs for $G = 4$, and 7 μs for other spreading factors. The average signal-to-noise ratio is 20 dB for the user of interest, the data modulation is BPSK and the number of users is 2. Data rates vary from 128 kbit/s to 2.048 Mbit/s; no coding is assumed.

3.3. Extensions to the spatial domain

Spatial signal processing techniques [182] can be used to improve the performance and the capacity of radio systems [183]. Spatial signal processing provides additional means for diversity in CDMA systems in cases when the signals received at different sensors or from different directions are uncorrelated. The basic RAKE receivers utilize only the delay spread, i.e., the frequency-selectivity of the channel. The spatial signal processing techniques utilize also the angle spread, i.e., the channel space-selectivity [183]. The amount of the spatial diversity offered by the channel depends on the angle spread of the channel and the accuracy of the spatial domain algorithms. Some spatial domain algorithms require explicit estimation of the direction-of-arrival, whereas, the other techniques rely on adaptively adjusting the steering vector coefficients to satisfy some optimization criterion. With adaptive antenna arrays interference can be suppressed significantly by directing the receiver antenna pattern towards the desired user or by setting nulls towards dominant interferers [183]. By combining multiuser and antenna array receivers, the performance can be enhanced significantly [184]. For extensive surveys on spatial-temporal receivers see [183, 185, 186] and references therein.

At present, the spatial domain processing is better suited to the uplink tranceivers. However, due to the large variety of mobile terminals expected in the future, spatial domain processing will be used at the mobile terminals also. The signal structure of the third generation WCDMA system has pilot symbols in the downlink direction to facilitate the downlink beamforming. For this reason alone spatial domain signal processing at the downlink receivers deserves consideration.

Combined spatial and temporal signal processing in decorrelating receivers were studied in [54, 57, 58]. The same principles can be applied to the LMMSE receivers. The following combinations of the spatial-temporal LMMSE receivers are possible: the *spatial-temporal-multiuser (STM) receiver*, the *spatial-multiuser-temporal (SMT) receiver*, the *temporal-multiuser-spatial (TMS)* receiver and the *multiuser-spatial-temporal (MST) receiver* (Figures 3.19 and 3.20). The multiuser-temporal-spatial (MTS) is equivalent to the MST receiver and the temporal-spatial-multiuser (TSM) corresponds to the STM receiver from the interference suppression point of view.

The principles of the different LMMSE estimators are given in Appendix 2. Applying those principles to the different versions of the spatial-temporal LMMSE receivers of Figures 3.19 and 3.20, the receiver filters of Table 3.4 can be defined (see Appendix 4 for the system model definitions).

It was pointed out in Section 3.1.2 that the BEP analysis for the postcombining LMMSE receiver is not trivial. Hence, the performance comparisons of the spatial-temporal LMMSE receivers is out of the scope of this thesis. However, the BEP could be analyzed in AWGN channels by using the methods outlined in Section 3.1.2. Based on such an evaluation carried out for the decorrelating receiver [54], the best performance is obtained when the multiuser interference suppression takes place as late as possible, i.e., $\mathrm{BER}_{[STM]} < \mathrm{BER}_{[SMT]} < \mathrm{BER}_{[MST]}$.

The TMS configuration leads to the coherent antenna diversity receivers. In [90, 187] the TMS configuration was studied in a packetized CDMA system. A novel

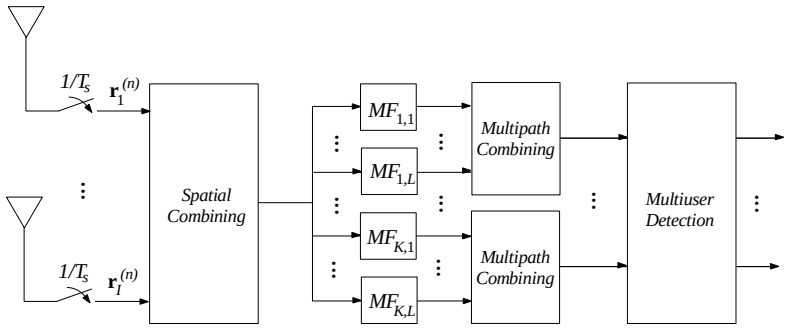

(a) STM receiver.

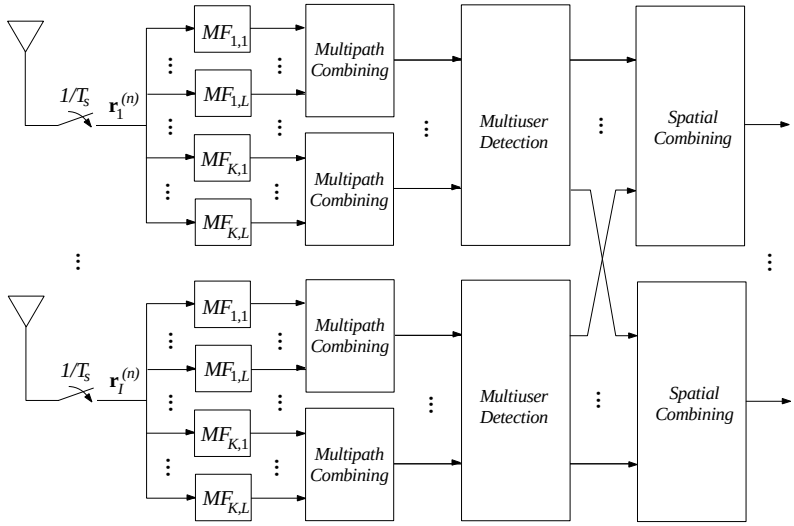

(b) TMS receiver.

Fig. 3.19. Postcombining interference suppression receivers with spatial signal processing.

antenna diversity combining rule based on the final MSE after receiver training was proposed. Without such a combining rule, only selection diversity could be used in adaptive postcombining LMMSE receivers with antenna diversity.

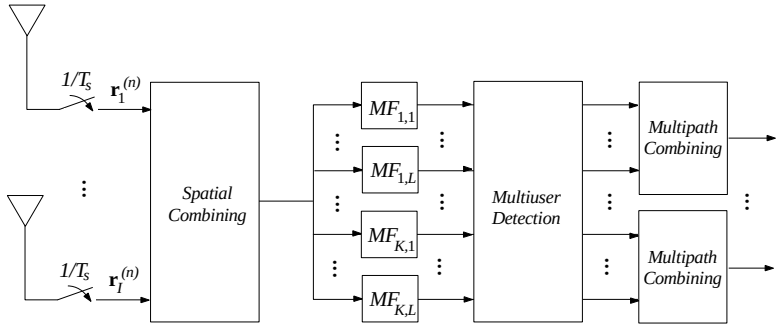

(a) SMT receiver.

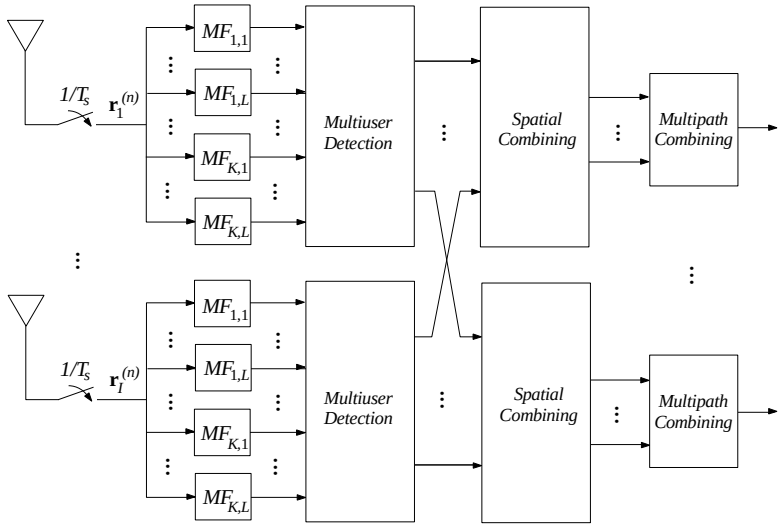

(b) MST receiver.

Fig. 3.20. Precombining interference suppression receivers with spatial signal processing.

Table 3.4. Different spatial-temporal LMMSE receiver configurations.

Config.	LMMSE receiver filter
STM	$\mathbf{L}_{[STM]} = \sum_{i=1}^{I} \mathbf{S}(\mathbf{C} \odot \mathbf{\Phi}_i)$ $\cdot\left(\sum_{i=1}^{I} \mathbf{A}^{\mathrm{H}}(\mathbf{\Phi}_i^{\mathrm{H}} \odot \mathbf{C}^{\mathrm{H}})\mathbf{R}(\mathbf{C} \odot \mathbf{\Phi}_i)\mathbf{A} + \sigma^2\mathbf{I}\right)^{-1}$
SMT	$\mathbf{L}_{[SMT]} = \sum_{i=1}^{I} \mathbf{S}\mathbf{\Phi}_i\left(\sum_{i=1}^{I} \mathbf{\Phi}_i^{\mathrm{H}}\mathbf{R}\mathbf{\Phi}_i + \sigma^2\mathbf{\Sigma}_{\mathbf{h}}^{-1}\right)^{-1}$
MST	$\mathbf{L}_{[MST]i} = \mathbf{S}\left(\mathbf{R} + \sigma^2\mathbf{\Sigma}_{\mathbf{h}}^{-1}\right)^{-1}$
TMS	$\mathbf{L}_{[TMS]i} = \mathbf{SCA}\left(\mathbf{AC}^{\mathrm{H}}\mathbf{RCA} + \sigma^2\mathbf{I}\right)^{-1}$

3.4. Summary

LMMSE detection in frequency-selective fading channels was studied in this section. The bit error probability of the postcombining and the precombining LMMSE receivers was addressed. The postcombining LMMSE receiver has potentially better receiver performance and system capacity but suffers from convergence problems in fading channels.

The comparisons between the conventional RAKE receiver and the precombining LMMSE receiver revealed significant improvements in system capacity when using the precombining LMMSE receivers. The performance of the conventional RAKE receiver is significantly degraded when the data rate is increased. The performance of the precombining LMMSE receiver degrades significantly less when increasing the data rate.

The LMMSE receiver principles were augmented to the spatial domain. Several alternative receiver structures were presented, but neither analysis nor simulations were performed.

The precombining LMMSE receiver is a promising alternative to the conventional RAKE receivers in third generation WCDMA systems. Hence, it is worth elaborating the receiver algorithms in more detail. In the next section, adaptive implementations for the postcombining and the precombining LMMSE receivers are studied.

4. Single-user LMMSE receivers for frequency-selective fading channels

The precombining LMMSE receivers require the knowledge of the spreading codes and the delays of all users. Also a matrix inversion is required as can be seen in (3.3). The spreading codes and the delays for all users may not be known at the mobile terminals and the direct matrix inversion is computationally intensive. For these reasons the LMMSE receivers are usually solved iteratively for each user by using some adaptive algorithm such as the least mean squares algorithm. The adaptive LMMSE receivers require a reference signal used for adaptive filter training. In this chapter, the training based on the decisions produced by the conventional RAKE receiver is studied both with the postcombining and the precombining LMMSE receivers. The motivation behind the RAKE based training is the fact that the third generation WCDMA proposals are based on the conventional RAKE receivers and there are no training sequences available [30]. If the system is primarily based on the conventional RAKE receivers, the raw BER of the RAKE must be at least $10^{-1} - 10^{-2}$, which should be sufficient training.

This chapter is organized as follows. An adaptive algorithm for the precombining LMMSE receiver (LMMSE-RAKE) is derived in Section 4.1. As will be shown, the adaptive LMMSE-RAKE receiver can be implemented using the decisions and the channel estimates of the conventional RAKE receiver. Hence, no training sequences are needed for the adaptation, and the adaptive LMMSE-RAKE receiver can be considered to be blind. Comparisons to other blind adaptive receivers are made in Section 4.1.2. The numerical analysis and the simulation results show that the decisions of the conventional RAKE are in most cases sufficiently reliable for proper training. Depending on the adaptive implementation of the LMMSE-RAKE receivers the performance may sometimes be worse than with the conventional RAKE receivers. To avoid such a situation, the adaptive receiver branch could be switched off during the periods when it would impair the performance. Two different switching criteria are presented in Section 4.1.3. It is shown that decisions made by the conventional RAKE receiver can be used to train the postcombining LMMSE receiver. A general convergence analysis will be developed in Section 4.2.2 for the postcombining LMMSE receiver in order to assess its usefulness in fading channels. The chapter is summarized in Section 4.3.

4.1. Adaptive precombining LMMSE receivers

The modified MSE criterion $\mathrm{E}\{|\mathbf{h}-\hat{\mathbf{h}}|^2\}$ requires that the reference signal $\mathbf{h} = \mathbf{CAb}$ is available in adaptive implementations. Hence, the adaptive versions of the precombining LMMSE receiver need to know spreading sequence timing, data bits, and complex channel coefficients of each desired multipath component of estimates thereof. This side information on channel parameters may not be available in all applications. In the conventional coherent RAKE receiver this information is available. An adaptive least mean squares version of the precombining LMMSE receiver which is based on the structure similar to the conventional RAKE receivers is derived in the sequel. Since we are interested in finding adaptive single-user receivers, the optimization criterion is presented for each path separately, i.e., $J_{k,l} = \mathrm{E}\{|(\mathbf{h})_{k,l} - (\hat{\mathbf{h}})_{k,l}|^2\}$.

The modified cost function results in separate LMMSE receivers for each multipath component, as can be seen in Figure 3.1. The adaptive LMMSE receiver is actually an adaptive RAKE receiver, where each receiver branch is adapted independently to suppress MAI. Hence, this receiver (Figure 4.1) is called the *adaptive LMMSE-RAKE receiver.*

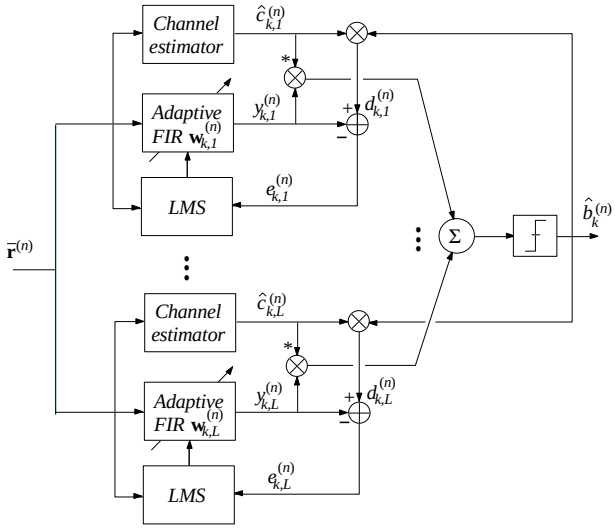

Fig. 4.1. General block diagram of the adaptive LMMSE-RAKE receiver.

The practical linear receivers do not need to process the whole received signal block of N_b symbol intervals at once. It was shown, e.g., in [25, 65] that the finite length FIR versions of linear multiuser receivers of length less than 10 symbol intervals are sufficient in many cases. The received signal is processed in blocks of

M symbols ($M < N_b$). Let the input sample vector during the nth symbol be

$$\bar{\mathbf{r}}^{(n)} = \left[\mathbf{r}^{\mathrm{T}(n-D)}, \ldots, \mathbf{r}^{\mathrm{T}(n)}, \ldots, \mathbf{r}^{\mathrm{T}(n+D)}\right]^{\mathrm{T}} \in \mathbb{C}^{MSG}, \tag{4.1}$$

where $M = (2D+1)$ is the sample vector length in symbol intervals. The received signal vectors are fed to the linear filters with impulse response

$$\mathbf{w}_{k,l}^{(n)} = \left[w_{k,l}^{(n)}(0), \ldots, w_{k,l}^{(n)}(MSG-1)\right]^{\mathrm{T}} \in \mathbb{C}^{MSG}. \tag{4.2}$$

The output of the lth receiver branch can be written as $y_{k,l}^{(n)} = \mathbf{w}_{k,l}^{\mathrm{H}(n)} \bar{\mathbf{r}}^{(n)}$. The decisions in an LMMSE-RAKE receiver are made according to

$$\hat{b}_k^{(n)} = \operatorname{sgn}\left(\sum_{l=1}^{L} \hat{c}_{k,l}^{*(n)} y_{k,l}^{(n)}\right), \tag{4.3}$$

where $\operatorname{sgn}(\cdot)$ is the signum function and $\hat{c}_{k,l}^{(n)}$ is the estimated channel coefficient.

The filter coefficients are derived using the MSE criterion ($\mathrm{E}[|e_{k,l}^{(n)}|^2]$), which leads to the optimal filter coefficients $\mathbf{w}_{[MSE]k,l} = \mathbf{\Sigma}_{\bar{\mathbf{r}}}^{-1} \mathbf{\Sigma}_{\bar{\mathbf{r}} d_{k,l}}$ [21], where $\mathbf{\Sigma}_{\bar{\mathbf{r}} d_{k,l}}$ is the cross-correlation vector between the input vector $\bar{\mathbf{r}}$ and the desired response $d_{k,l}$. Adaptive filtering is based on iteratively solving the optimization problem. The most widely used methods are based on estimating the gradient of the error function and aiming at the negative gradient directions, which provide steepest descent on the error surface. The filter weights are updated according to

$$\mathbf{w}_{k,l}^{(n+1)} = \mathbf{w}_{k,l}^{(n)} - \mu \nabla_{k,l}, \tag{4.4}$$

where μ is a step-size parameter and $\nabla_{k,l}$ is the gradient of the MSE with respect to the filter weights[1]. Let us first assume that the receiver processing window M is only one symbol interval, i.e., $\bar{\mathbf{r}}^{(n)} = \mathbf{r}^{(n)} \hat{=} \mathbf{r}$. The gradient of the MSE ($J_{k,l} = \mathrm{E}\{|c_{k,l} A_k b_k - \mathbf{w}_{k,l}^{\mathrm{H}} \mathbf{r}|^2\}$) with respect to the filter weight vector $\mathbf{w}_{k,l}$ is

$$\begin{aligned} \nabla_{k,l} &= -2\mathrm{E}\left[\mathbf{r}(c_{k,l} A_k b_k)^*\right] + 2\mathrm{E}\left[\mathbf{r}\mathbf{r}^{\mathrm{H}}\right]\mathbf{w}_{k,l} \\ &= -2\mathbf{\Sigma}_{\mathbf{r} d_{k,l}} + 2\mathbf{\Sigma}_{\mathbf{r}} \mathbf{w}_{k,l}, \end{aligned} \tag{4.5}$$

where $d_{k,l} = c_{k,l} A_k b_k$ (In the remainder of this chapter, it will be assumed that $A_k = 1$, $\forall k$.). The resulting iterative algorithm includes the recursions

$$\mathbf{w}_{k,l}^{(n+1)} = \mathbf{w}_{k,l}^{(n)} + 2\mu\left(\mathbf{\Sigma}_{\mathbf{r} d_{k,l}} - \mathbf{\Sigma}_{\mathbf{r}} \mathbf{w}_{k,l}^{(n)}\right) \tag{4.6}$$

and is called the steepest descent algorithm [21]. The widely used approximation of the gradient is the so-called stochastic approximation: $\nabla_{k,l} \approx -2\mathbf{r}(c_{k,l} b_k)^* + 2\mathbf{r}\mathbf{r}^{\mathrm{H}} \mathbf{w}_{k,l}^{(n)} = -2\mathbf{r}(c_{k,l} b_k)^* + 2\mathbf{r} y_{k,l}^*$. Using this as a gradient estimate and assuming now that $M > 1$, the so-called least mean squares (LMS) algorithm has the form

$$\mathbf{w}_{k,l}^{(n+1)} = \mathbf{w}_{k,l}^{(n)} + 2\mu \bar{\mathbf{r}}^{(n)}\left(c_{k,l}^{(n)} b_k^{(n)} - y_{k,l}^{(n)}\right)^* \in \mathbb{C}^{MSG}. \tag{4.7}$$

[1] $\nabla_{k,l} = \frac{\partial J_{k,l}}{\partial \mathrm{Re}\{\mathbf{w}_{k,l}\}} + j\frac{\partial J_{k,l}}{\partial \mathrm{Im}\{\mathbf{w}_{k,l}\}} = 2\frac{\partial J_{k,l}}{\partial \mathbf{w}_{k,l}^*}$ [21, pp. 197, 894].

The receiver vector can be decomposed into adaptive and fixed components such that

$$\mathbf{w}_{k,l}^{(n)} = \bar{\mathbf{s}}_{k,l} + \mathbf{x}_{k,l}^{(n)} \in \mathbb{C}^{MSG}, \tag{4.8}$$

where $\mathbf{x}_{k,l}^{(n)}$ is the adaptive filter component and

$$\bar{\mathbf{s}}_{k,l} = \left[\mathbf{0}^{\mathrm{T}}_{(DSG+\tau_{k,l})\times 1}, \mathbf{s}_k^{\mathrm{T}}, \mathbf{0}^{\mathrm{T}}_{(DSG-\tau_{k,l})\times 1}\right]^{\mathrm{T}} \tag{4.9}$$

is the fixed spreading sequence[2] of the kth user with the delay $\tau_{k,l}$. Hence, the adaptive component can be overlaid on the conventional RAKE receiver, as is shown in Figure 4.2. The updates for the adaptive component can be written as

$$\begin{aligned}\mathbf{x}_{k,l}^{(n+1)} &= \mathbf{x}_{k,l}^{(n)} + 2\mu_{k,l}^{(n)}\left(c_{k,l}^{(n)} b_k^{(n)} - y_{k,l}^{(n)}\right)^{*} \bar{\mathbf{r}}^{(n)} \\ &= \mathbf{x}_{k,l}^{(n)} + 2\mu_{k,l}^{(n)} e_{k,l}^{*(n)} \bar{\mathbf{r}}^{(n)},\end{aligned} \tag{4.10}$$

where $\mu_{k,l}^{(n)}$ is a time-variant step-size parameter, which controls the rate of convergence of the algorithm.

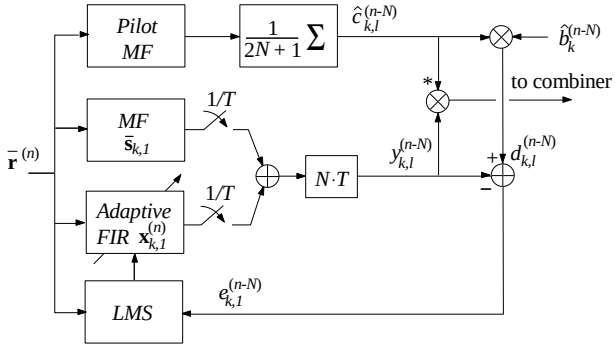

Fig. 4.2. Block diagram of one receiver branch in the adaptive LMMSE-RAKE receiver.

The optimal step-size depends on the eigenvalues of the input vector covariance matrix $\mathbf{\Sigma}_{\bar{\mathbf{r}}}$ [21]. Quite often the step-size is chosen as

$$\mu_{k,l}^{(n)} = \mu/(\bar{\mathbf{r}}^{\mathrm{H}(n)}\bar{\mathbf{r}}^{(n)});\ 0 < \mu < 1. \tag{4.11}$$

[2]With this definition interference is not suppressed symmetrically from past and future samples. With the definition $\bar{\mathbf{s}}_{k,l} = [\mathbf{0}^{\mathrm{T}}_{DSG\times 1}, \mathbf{s}_k^{\mathrm{T}}, \mathbf{0}^{\mathrm{T}}_{DSG\times 1}]^{\mathrm{T}}$ symmetric interference suppression is achieved. In such a case, however, the received signal must be delayed separately for each RAKE branch. It should be noted that with receiver span of one symbol interval ($M = 1$) only the latter definition results in satisfactory performance with large delay spreads. In the numerical examples (Section 4.1.2.3) the receiver with span one symbol interval in a two-path fading channel uses the sequences $\bar{\mathbf{s}}_{k,1} = [\mathbf{s}_k^{\mathrm{T}}, \mathbf{0}^{\mathrm{T}}_{\tau_{[max]}\times 1}]^{\mathrm{T}}$ and $\bar{\mathbf{s}}_{k,2} = [\mathbf{0}^{\mathrm{T}}_{\tau_{[max]}\times 1}, \mathbf{s}_k^{\mathrm{T}}]^{\mathrm{T}}$, where $\tau_{[max]}$ is the maximum delay difference between the multipath components.

An LMS algorithm with this step-size is called the normalized LMS (NLMS) algorithm [21]. The actual value of the step-size is crucial for the adaptive postcombining LMMSE receiver when used in fading channels [91]. Since the precombining LMMSE receiver does not need to track the fading channel coefficients, the step-size can be set more freely. The NLMS algorithm will be used in all numerical examples presented in this thesis.

The error signals, $e_{k,l}^{(n)} = d_{k,l}^{(n)} - y_{k,l}^{(n)}$, produced by the difference between the reference signals and the filter outputs, are used to update the filter weights. Either known or estimated data symbols are used as reference signals in the adaptive postcombining LMMSE receivers. The product of the estimated channel coefficients and data symbols is the reference signal in the adaptive precombining LMMSE receiver ($d_{k,l}^{(n)} = \hat{c}_{k,l}^{(n)} b_k^{(n)}$ or $d_{k,l}^{(n)} = \hat{c}_{k,l}^{(n)} \hat{b}_k^{(n)}$, respectively). The data decisions produced initially by a conventional RAKE receiver are often sufficiently reliable for adapting the receiver as will be demonstrated through numerical examples.

It is clear that the channel estimator performance significantly affects the convergence of the adaptive LMMSE-RAKE receiver. If the system provides an unmodulated pilot channel, the channel can be estimated accurately from the pilot. E.g., the FMA2 concept includes an optional pilot channel for the downlink. The pilot channel may have a higher power than the data channels, which assists channel estimation particularly in heavily loaded situations. The most trivial way to estimate the channel coefficients from the pilot channel is to filter the pilot channel correlator outputs with a moving average filter. Depending on the rate of fading, the averaging can be made over such a long time interval that the zero-mean MAI will be averaged out towards zero. In fast fading channels when the averaging interval must be rather short a near-far resistant channel estimator, e.g., based on the LMMSE criterion could be used to provide reliable channel estimates. This is possible if the channel is estimated from the output of the adaptive receiver branch [97]. In the numerical examples presented in this thesis, a conventional smoothing (see p. 130) based channel estimator utilizing a pilot channel has been used. The channel estimate is given as

$$\hat{c}_{k,l}^{(n)} = \frac{1}{2N+1} \sum_{i=-N}^{N} \bar{\mathbf{s}}_{p,l}^{\mathrm{T}} \bar{\mathbf{r}}^{(n-i)}, \tag{4.12}$$

where $2N+1$ is the smoother length in symbol intervals, N is the smoothing delay (see Figure 4.2) and $\bar{\mathbf{s}}_{p,l}$ denotes the pilot channel code for the lth path.

4.1.1. Approximate BEP analysis with imperfect reference

In the adaptive LMMSE-RAKE receiver, the decisions and the channel estimates made by the conventional RAKE receiver are used in training. Hence, the reference signal used for receiver adaptation contains errors which impair the BEP of the receiver in the steady-state. In this section, an approximate BEP equation is given for the adaptive versions of the precombining LMMSE receivers, which takes into

account the impacts of the imperfect training signal.

The Gaussian approximation has been used to analyze the performance of the adaptive LMMSE detectors [81, 188]. The bit error probability for an adaptive LMMSE detector in fixed channels can be approximated as [81]

$$P_k \approx \mathrm{Q}\left(\sqrt{\sum_{l=1}^{L}\frac{\sigma_d^2 - J_{k,l}^{(\infty)}}{J_{k,l}^{(\infty)}}}\right), \tag{4.13}$$

where σ_d^2 is the variance of the desired response, $J_{k,l}^{(\infty)}$ is the final steady-state mean squared error for the adaptive algorithm, and it is used to estimate the impact of the noise and the residual interference on the receiver performance. This approximation for the BEP will be used to evaluate the BEP of the adaptive precombining LMMSE receiver with imperfect reference signal.

For the LMS algorithm, the mean squared error at iteration n is given by

$$J_{k,l}^{(n)} = J_{[opt]k,l} + J_{[ex]k,l}^{(n)}, \tag{4.14}$$

where $J_{[opt]k,l} = \sigma_d^2 - \mathbf{\Sigma}_{\bar{\mathbf{r}}d_{k,l}}^{\mathrm{H}}\mathbf{\Sigma}_{\bar{\mathbf{r}}}^{-1}\mathbf{\Sigma}_{\bar{\mathbf{r}}d_{k,l}}$ is the MSE of the optimal Wiener filter [21], $d_{k,l}$ is the desired response with power $\sigma_d^2 = \mathrm{E}[|c_{k,l}^{(n)}b_k^{(n)}|^2]$,

$$J_{[ex]k,l}^{(n)} = \mathrm{tr}\big[\mathbf{\Sigma}_{\bar{\mathbf{r}}}\mathbf{\Gamma}^{(n)}\big], \tag{4.15}$$

is the excess MSE, tr[·] is the trace of a matrix, and $\mathbf{\Gamma}^{(n)} = \mathrm{E}\big[(\mathbf{w}_{[MSE]k,l} - \mathbf{w}_{k,l}^{(n)})(\mathbf{w}_{[MSE]k,l} - \mathbf{w}_{k,l}^{(n)})^{\mathrm{H}}\big]$ is the tap weight error covariance matrix at iteration n. The final steady-state MSE achieved is given by [21, 84]

$$J_{k,l}^{(\infty)} = \frac{J_{[opt]k,l}}{1 - \sum_{i=1}^{(2D+1)SG}\mu\lambda_i/(2-\mu\lambda_i)}, \tag{4.16}$$

where λ_i are the eigenvalues of $\mathbf{\Sigma}_{\bar{\mathbf{r}}}$. Assuming that the step-size μ is relatively small, the final steady-state MSE can be approximated as

$$J_{k,l}^{(\infty)} \approx J_{[opt]k,l} = \sigma_d^2 - \mathbf{\Sigma}_{\bar{\mathbf{r}}d_{k,l}}^{\mathrm{H}}\mathbf{\Sigma}_{\bar{\mathbf{r}}}^{-1}\mathbf{\Sigma}_{\bar{\mathbf{r}}d_{k,l}}. \tag{4.17}$$

For notational simplicity, it will be assumed in the sequel that the multipath intensity profile is flat and that the user energy is equal to one ($\sigma_d^2 = E_k/L = 1/L$).

If the reference signal based on estimated channel coefficients and data decisions ($d_{k,l}^{(n)} = \hat{c}_{k,l}^{(n)}\hat{b}_k^{(n)}$) deviates from the real desired reference, the elements of the cross-correlation vector $\mathbf{\Sigma}_{\bar{\mathbf{r}}d_{k,l}}$ get smaller and the final MSE increases. This will increase the BEP as can be seen from (4.13). Let us first assume that the data decisions $\hat{b}_k^{(n)} = b_k^{(n)}$ are correct and that the radio channel is estimated by using a pilot channel and a moving average smoother of length $2N+1$. It is straightforward to show (Appendix 3) that in the synchronous downlink channel with equal energy propagation paths ($\varphi_{k,l}(0) = \frac{1}{L}$), desired user power $A_1^2 = 1$ and pilot channel power $A_p^2 = 1$, the cross-correlation $\mathbf{\Sigma}_{\bar{\mathbf{r}}d_{k,l}}$ can be approximated as

$$\tilde{\mathbf{\Sigma}}_{\bar{\mathbf{r}}d_{k,l}} \approx \frac{1}{(2N+1)}\left(\sum_{i=-N}^{N}\varphi_{k,l}(i)\right)\bar{\mathbf{s}}_{k,l} \tag{4.18}$$

where $\varphi_{k,l}(i) = \mathrm{E}\left[c_{k,l}^{(n)} c_{k,l}^{*(n+i)}\right]$ is the channel autocorrelation coefficient for the delay of i symbols (see Section 2.2). If the channel is not changing significantly during the channel estimation observation interval $(2N+1)$, the channel autocorrelation is approximately constant over $2N+1$ symbols and the cross-correlation with estimated channel can be approximated as $\tilde{\mathbf{\Sigma}}_{\bar{\mathbf{r}}d_{k,l}} \approx \frac{1}{L}\bar{\mathbf{s}}_{k,l}$. Hence, the channel estimation based on the pilot channel degrades the performance of the adaptive LMMSE-RAKE receiver only marginally. If the channel changes significantly within the observation interval, the summation in (4.18) is reduced and the BEP is significantly degraded if the channel estimation interval $(2N+1)$ is not made smaller.

The impact of the incorrect data decisions in the reference signal on the convergence of the adaptive algorithm is significantly more difficult to analyze than the impact of the channel estimation errors. However, a useful insight can be obtained by using the simplified analysis presented below. Its conclusions are verified by Monte-Carlo computer simulations presented in the next section. The decision errors in the reference signal are assumed to be independent from the LMMSE receiver output. This assumption is valid, e.g., if the adaptive filter is trained by using the data decisions made by the conventional RAKE receiver. It is assumed that the channel is known and that the data decisions are completely independent from the adaptive LMMSE-RAKE receiver outputs. Furthermore, the errors are assumed to be i.i.d. uniform random variables that are independent from the input signal vector $\bar{\mathbf{r}}$. These latter two assumptions are not exactly valid, since the RAKE receiver is making the decisions based on $\bar{\mathbf{r}}$ which means that the decision errors depend on the input vector. The exact analysis of the BEP with decision errors is somewhat cumbersome, and this simplified analysis is used only to obtain insight to the problem at hand. The cross-correlation vector with an erroneous training signal in a known channel for BPSK modulated data can be expressed as

$$\begin{aligned} \tilde{\mathbf{\Sigma}}_{\bar{\mathbf{r}}d_{k,l}} &= (1-P_e)\mathbf{\Sigma}_{\bar{\mathbf{r}}d_{k,l}} + P_e(-\mathbf{\Sigma}_{\bar{\mathbf{r}}d_{k,l}}) \\ &= (1-2P_e)\mathbf{\Sigma}_{\bar{\mathbf{r}}d_{k,l}}. \end{aligned} \tag{4.19}$$

If the bit error rate of the reference signal (P_e) is 0, no impairment is caused. For the reference bit error rate 0.5, the cross-correlation will be zero, $J_{k,l}^{(\infty)} = 1/L$, and the bit error rate of the LMMSE-RAKE receiver will be 0.5.

The analysis with imperfect reference signals assumes that the expectation is taken in the cross-correlation $\mathbf{\Sigma}_{\bar{\mathbf{r}}d_{k,l}}$ computation. In practical algorithms the expectation is only approximated and the results are valid for small step-size values only. The impact of the imperfect reference signal with different step-size values will be studied through simulations.

4.1.1.1. Numerical examples

The main parameters used are the following: carrier frequency 2.0 GHz, symbol rate 16 kbits/s, 31 chip Gold code, and rectangular chip waveform. Synchronous downlink with equal energy two-path $(L=2)$ Rayleigh fading channel with vehicle

speeds of 40 km/h (which results in the maximum normalized Doppler shift of $4.63 \cdot 10^{-3}$) and maximum delay spread of 10 chip intervals. The number of users examined was 1 – 30 including the unmodulated pilot channel. The average energy was the same for the pilot channel and user data channels. A simple moving average smoother of length 11 symbols was used in a conventional channel estimator. Perfect channel estimation and ideal truncated precombining LMMSE receivers were used in the analysis to obtain the bit error probability lower bounds. The receiver processing window is three symbols ($M = 3$) unless otherwise stated. The adaptive algorithm used in the simulations was normalized LMS with $\mu_{k,l}^{(n)} = \frac{1}{100 \cdot (2D+1)SG} \left(\bar{\mathbf{r}}_{k,l}^{\mathrm{H}(n)} \bar{\mathbf{r}}_{k,l}^{(n)} \right)^{-1}$. The simulation results were produced by averaging over the BERs of randomly selected users with different delay spreads.

If the proposed adaptive receiver is used to improve the performance of the conventional RAKE receiver, and the system does not provide a training sequence, it is important that the receiver can be adapted using decision direction only. That is, the decisions made by the conventional RAKE receiver could be used in training. In order to determine the impact of decision errors on the performance of the precombining LMMSE receivers, the BEP with imperfect training signal was calculated according to (4.13) and (4.19). The results are presented in Figure 4.3. The results verify that with moderate reference BERs ($< 10^{-2}$) the BEP of the precombining LMMSE receiver is not degraded significantly when the number of users is more than 10. The simplified analysis shows that the precombining LMMSE detector can be trained using an imperfect training signal, and the reference signal BER requirements are moderate.

The impact of imperfect training was also confirmed by fading channel simulations, where the decisions and the channel estimates made by the conventional RAKE receiver were used to train the adaptive LMMSE-RAKE receiver (Figure 4.4). The simulation results also show that if the number of users is not too high ($K < 30$), the adaptive LMMSE-RAKE outperforms the conventional RAKE receiver at high SNRs. Due to imperfect adaptation, the conventional RAKE has better BER performance at low SNRs. If the number of users is 30, the adaptive LMMSE-RAKE receiver always has worse performance than the conventional RAKE receiver. When the BER with the conventional RAKE receiver is larger than $3 \cdot 10^{-2}$ the training based on the conventional RAKE receiver fails and the adaptive LMMSE-RAKE does not improve the performance.

The conclusions to be made from the results presented in this section are that the conventional RAKE receiver can be used to train the LMMSE-RAKE receiver provided that the BER of the conventional RAKE is not very high.

4.1.2. Blind adaptive receivers

In Chapter 3 the postcombining and precombining interference suppression type LMMSE receivers were studied. The discussion is extended to blind receivers of the form $\mathbf{\Sigma}_{\bar{\mathbf{r}}}^{-1} \bar{\mathbf{s}}_{k,l}$ in this section. Each multipath component requires a separate

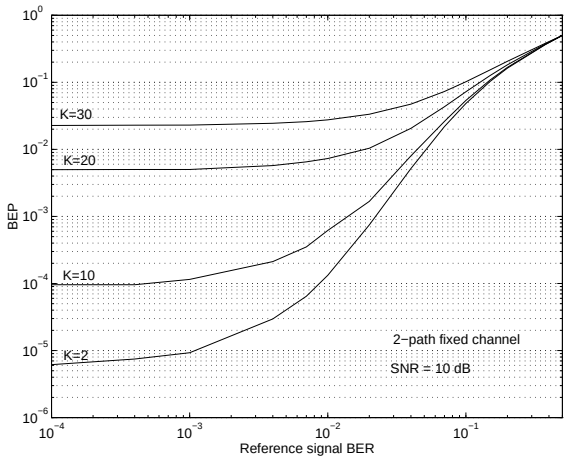

Fig. 4.3. Bit error probabilities as a function of the reference signal bit error rate for the precombining LMMSE receiver in fixed two-path channels at the SNR 10 dB with different numbers of users.

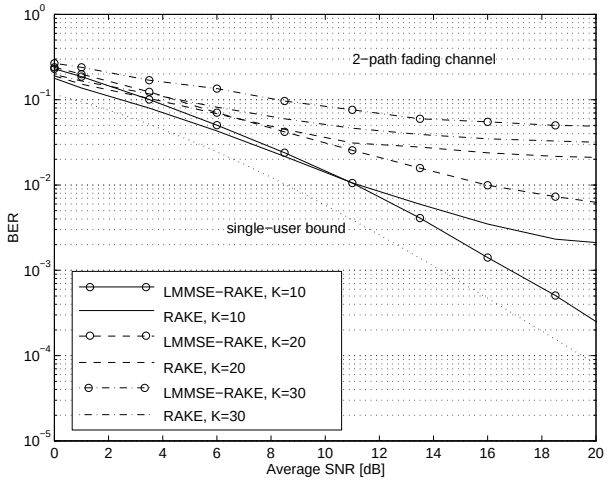

Fig. 4.4. Simulated bit error rates as a function of the average SNR for the conventional RAKE and the adaptive LMMSE-RAKE in a two-path fading channel for vehichle speeds 40 km/h with different numbers of users.

LMMSE filter in precombining LMMSE receivers. Hence, the decision variable is a maximal ratio combined output of all filters expressed as

$$\begin{aligned} z_k^{(n)} &= \sum_{l=1}^{L} \hat{c}_{k,l}^{*(n)} y_{k,l}^{(n)} \\ &= \sum_{l=1}^{L} \hat{c}_{k,l}^{*(n)} \mathbf{w}_{k,l}^{\mathrm{H}(n)} \bar{\mathbf{r}}^{(n)} \\ &= \sum_{l=1}^{L} \hat{c}_{k,l}^{*(n)} \left(\mathbf{\Sigma}_{\bar{\mathbf{r}}}^{-1} \bar{\mathbf{s}}_{k,l} \right)^{\mathrm{H}} \bar{\mathbf{r}}^{(n)} \\ &= \left(\mathbf{\Sigma}_{\bar{\mathbf{r}}}^{-1} \left(\sum_{l=1}^{L} \hat{c}_{k,l}^{(n)} \bar{\mathbf{s}}_{k,l} \right) \right)^{\mathrm{H}} \bar{\mathbf{r}}^{(n)} \\ &= \bar{\mathbf{s}}_{[MRC]k}^{\mathrm{H}(n)} \mathbf{\Sigma}_{\bar{\mathbf{r}}}^{-1} \bar{\mathbf{r}}^{(n)}. \end{aligned} \tag{4.20}$$

The last form reveals that the blind receivers can be presented by using only a single receiver filter similar to the postcombining LMMSE receivers. However, as the derivation above shows, it does not matter whether L or only one receiver filter is used; the receivers are mathematically equal and the performance will be the same. In fact, the blind adaptive receivers cannot be presented in the form of the postcombining LMMSE receivers (3.1). Using only one interference suppression filter instead of L separate filters results in problems in receiver adaptation, since the channel estimates would be needed to determine the maximal ratio combined signature sequence $\bar{\mathbf{s}}_{[MRC]k}^{(n)}$. By using separate filters, the channel estimation can be performed more easily. For that reason, only the solutions based on separate interference suppression filters are considered in the sequel. It must be pointed out that in the adaptive LMMSE-RAKE receiver, where the channel estimation is based on a pilot channel, both receiver structures are possible.

4.1.2.1. Receivers based on LMS algorithms

One possible adaptive implementation of the precombining LMMSE receiver is the adaptive LMMSE-RAKE receiver. Since, the true transmitted bits and channel coefficients required in the receiver adaptation are not available, the estimates provided by the conventional RAKE receiver are used to train the receiver. Hence, the adaptive LMMSE-RAKE receiver is blind in the sense that no training sequences are required. The minimum output energy criterion was used in [96] to derive blind adaptive receivers. It is well known that the MSE and MOE criterion lead to the same receivers up to a scalar and have the same performance under ideal conditions. However, their performance depends on the adaptive implementations which may differ significantly. There are also other known blind adaptive algorithms suitable for single-user precombining LMMSE receivers, such as the unconstrained [103] and constrained constant modulus algorithm [97, 100, 103],

Griffiths' algorithm [100] and the generalized sidelobe canceller [98, 100, 103]. Also the blind adaptive algorithms based on higher order statistics [189] have been proposed [190]. In the sequel, the principles of some blind receivers based on the traditional LMS algorithms are briefly reviewed.

Adaptive LMMSE-RAKE

The adaptive LMMSE-RAKE includes recursions (see Section 4.1)

$$\mathbf{x}_{k,l}^{(n+1)} = \mathbf{x}_{k,l}^{(n)} + 2\mu_{k,l}^{(n)} \left(\hat{c}_{k,l}^{(n)} \hat{b}_k^{(n)} - y_{k,l}^{(n)} \right)^* \bar{\mathbf{r}}^{(n)}. \tag{4.21}$$

It should be observed that although no training sequences are needed in the adaptive LMMSE-RAKE receiver, the adaptation is not blind from the adaptive algorithm perspective, i.e., a reference signal is used to train the interference suppression filter.

Adaptive MOE receiver

The generalized sidelobe canceller (GSC) [191] can be used as a general framework for blind adaptive receivers which decompose the filter into fixed and adaptive parts. The GSC is based on the constrained optimization of the MOE. The GSC algorithm has been applied to blind adaptive single-user receivers in [103, 98, 100]. In the single-user receiver case, only the desired user sequence is used in the constraint matrix and the constraint value is equal to 1. If the constraint matrix contains several constraints, the fixed part decorrelates the desired signal component from those specified as additional constraints [98]. This structure could be beneficial when receiving several parallel data channels, i.e., with the multicode option (see Chapter 2) in the third generation CDMA systems. Also, the multipath decorrelating receiver (see Section 3.2.5) can be presented in the GSC framework by using the desired user sequence L times in the constraint matrix and by using an $L \times L$ identity matrix as a constraint matrix. The GSC algorithm with multiple constraints is not studied further in this thesis.

If only a single constraint is used, the basic blind adaptive MOE receivers [96] are obtained. The MOE ($\mathrm{E}[|y_{k,l}|^2]$) and the MSE criteria lead to the receivers $\mathbf{w}_{[MOE]k,l} = \boldsymbol{\Sigma}_{\bar{\mathbf{r}}}^{-1}\bar{\mathbf{s}}_{k,l}/(\bar{\mathbf{s}}_{k,l}^{\mathrm{T}}\boldsymbol{\Sigma}_{\bar{\mathbf{r}}}^{-1}\bar{\mathbf{s}}_{k,l})$ [96] and $\mathbf{w}_{[MSE]k,l} = \boldsymbol{\Sigma}_{\bar{\mathbf{r}}}^{-1}\boldsymbol{\Sigma}_{\bar{\mathbf{r}}d_{k,l}} = \boldsymbol{\Sigma}_{\bar{\mathbf{r}}}^{-1}\bar{\mathbf{s}}_{k,l}\mathrm{E}[|c_{k,l}|^2]$. Hence the receivers are equal up to a scalar, and they have the same performance in an ideal case. The normalization of the filter weights has an impact on the decomposition of the filter weights as will be shown in Section 4.1.3. The adaptive and non-adaptive components are constrained to satisfy $\bar{\mathbf{s}}_{k,l}^{\mathrm{T}}\mathbf{x}_{k,l}^{(n)} = 0$ in the MOE receivers. The stochastic approximation of the gradient for the MOE criterion is $\nabla_{k,l} = \bar{\mathbf{r}}^{(n)}\bar{\mathbf{r}}^{\mathrm{H}(n)}\mathbf{w}_{k,l}$. The orthogonality condition is maintained at each step of the algorithm by projecting the gradient onto the linear subspace orthogonal to $\bar{\mathbf{s}}_{k,l}$. In practice, this is accomplished by subtracting an estimate of the desired signal component from the received signal vector. Hence, the blind

receiver based on the MOE criterion with receiver span of one symbol interval [96] and with receiver span of three symbol intervals [95] includes recursions

$$\mathbf{x}_{k,l}^{(n+1)} = \mathbf{x}_{k,l}^{(n)} - 2\mu_{k,l}^{(n)} \bar{\mathbf{r}}^{\mathrm{H}(n)} (\bar{\mathbf{s}}_{k,l} + \mathbf{x}_{k,l}^{(n)}) \Big(\bar{\mathbf{r}}^{(n)} - \mathbf{F}_{k,l} \big(\mathbf{F}_{k,l}^{\mathrm{T}} \bar{\mathbf{r}}^{(n)} \big) \Big), \tag{4.22}$$

where

$$\mathbf{F}_{k,l} = \begin{pmatrix} \mathbf{0}_{\tau_{k,l}\times 1}^{\mathrm{T}}, & \mathbf{s}_k^{\mathrm{T}}, & \mathbf{0}_{(2DSG-\tau_{k,l})\times 1}^{\mathrm{T}} \\ \mathbf{0}_{(SG+\tau_{k,l})\times 1}^{\mathrm{T}}, & \mathbf{s}_k^{\mathrm{T}}, & \mathbf{0}_{((2D-1)SG-\tau_{k,l})\times 1}^{\mathrm{T}} \\ & \vdots & \\ \mathbf{0}_{(2DSG+\tau_{k,l})\times 1}^{\mathrm{T}}, & \big[s_k(T_s), \ldots, s_k(T_s(SG-\tau_{k,l})) \big] & \end{pmatrix}^{\mathrm{T}} \in \mathbb{R}^{MSG\times M} \tag{4.23}$$

is a block diagonal matrix of sampled spreading sequence vectors. Effectively M separate filters are adapted in (4.22) as was proposed in [95].

Griffiths' algorithm

In Griffiths' algorithm [192, pp. 85 – 86] it is assumed that the cross-correlation vector $\mathbf{\Sigma}_{\bar{\mathbf{r}}d_{k,l}}$ in (4.5) is known. Furthermore the instantaneous estimate for the covariance is used, i.e., $\mathbf{\Sigma}_{\bar{\mathbf{r}}} \approx \bar{\mathbf{r}}^{(n)} \bar{\mathbf{r}}^{\mathrm{H}(n)}$. In this case the cross-correlation is $\mathbf{\Sigma}_{\bar{\mathbf{r}}d_{k,l}} = \mathrm{E}[|c_{k,l}|^2]\bar{\mathbf{s}}_{k,l}$. Hence, Griffiths' algorithm results in adaptation according to

$$\mathbf{x}_{k,l}^{(n+1)} = \mathbf{x}_{k,l}^{(n)} + 2\mu_{k,l}^{(n)} \Big(\mathrm{E}\big[|c_{k,l}|^2\big] \mathbf{F}_{k,l} \mathbf{1}_M - \bar{\mathbf{r}}_{k,l}^{*(n)} (\bar{\mathbf{s}}_{k,l} + \mathbf{x}_{k,l}^{(n)})^{\mathrm{H}} \bar{\mathbf{r}}^{(n)} \Big). \tag{4.24}$$

In practice, the energy of multipath components ($\mathrm{E}[|c_{k,l}|^2]$) is not known and it must be estimated.

Constant modulus algorithm

The optimization criterion with the constant modulus algorithms [192, Chapt. 6] is $\mathrm{E}\big[(|y_{k,l}|^2 - \omega)^2\big]$, where ω is the so-called constant modulus (CM), which is set according to the received signal power, i.e, $\omega = \mathrm{E}[|c_{k,l}|^2]$ or $\omega^{(n)} = |c_{k,l}^{(n)}|^2$. Using the CM algorithm, it is possible to avoid the use of the data decisions in the reference signal in the adaptive LMMSE-RAKE receiver by taking the absolute value of the estimated channel coefficients ($|\hat{c}_{k,l}^{(n)}|$) in adapting the receiver [97]. In the precombining LMMSE receiver framework, the cost function for the BPSK data modulation is $\mathrm{E}\big[||\hat{\mathbf{h}}|^2 - |\mathbf{h}|^2|^2\big]$. The stochastic approximation of the gradient for the CM criterion is $\nabla_{k,l} = (|y_{k,l}^{(n)}|^2 - |\hat{c}_{k,l}^{(n)}|^2)\bar{\mathbf{r}}^{(n)} \bar{\mathbf{r}}^{\mathrm{H}(n)} \mathbf{w}_{k,l}$. Hence, the constant modulus algorithm can be expressed as

$$\mathbf{x}_{k,l}^{(n+1)} = \mathbf{x}_{k,l}^{(n)} - 2\mu_{k,l}^{(n)} y_{k,l}^{*(n)} (|y_{k,l}^{(n)}|^2 - |\hat{c}_{k,l}^{(n)}|^2) \bar{\mathbf{r}}^{(n)}. \tag{4.25}$$

Constrained LMMSE-RAKE, Griffiths' and constant modulus algorithms

The adaptive LMMSE-RAKE (4.21), the Griffiths' (4.24) and the constant modulus algorithm (4.25) contain no constraints. By applying the orthogonality constraint $\bar{\mathbf{s}}_{k,l}^{\mathrm{T}}\mathbf{x}_{k,l}^{(n)} = 0$ to each of these algorithms, an additional term $\bar{\mathbf{s}}_{k,l}^{\mathrm{T}}\mathbf{x}_{k,l}^{(n)}\bar{\mathbf{s}}_{k,l}$ is subtracted from the new update $\mathbf{x}_{k,l}^{(n+1)}$ at every iteration [97]. The constrained LMMSE-RAKE receiver becomes

$$\mathbf{x}_{k,l}^{(n+1)} = \mathbf{x}_{k,l}^{(n)} + 2\mu_{k,l}^{(n)}\left(\hat{c}_{k,l}^{(n)}\hat{b}_k^{(n)} - y_{k,l}^{(n)}\right)^{*}\bar{\mathbf{r}}^{(n)} - \bar{\mathbf{s}}_{k,l}^{\mathrm{T}}\mathbf{x}_{k,l}^{(n)}\bar{\mathbf{s}}_{k,l}. \tag{4.26}$$

The Griffiths' and the constant modulus algorithms can also be defined in a similar fashion.

4.1.2.2. Blind least squares receivers

All blind adaptive algorithms described in the previous section are based on the gradient of the cost function. In practical adaptive algorithms the gradient is estimated, i.e., the expectation in the optimization criterion is not taken but is replaced in most cases by some stochastic approximation. In fact, the stochastic approximation used in LMS algorithms is accurate only for small step-sizes μ. This results in rather slow convergence, which may be intolerable in practical applications. Another drawback with the blind adaptive receivers presented above is the delay estimation. Those receiver structures as such support only conventional delay estimation based on matched filtering (MF). The MF based delay estimation is sufficient for the downlink receivers in systems with an unmodulated pilot channel since the zero-mean MAI can be averaged out if the rate of fading is low enough. However, all emerging CDMA systems do not have the pilot channel. In those cases it would be beneficial to use some near-far resistant delay estimators.

One possible solution to both the convergence and the synchronization problems is based on blind linear least squares (LS) receivers [105], which are based on minimizing the least squares cost function

$$J_{[LS]k,l} = \sum_{j=n-N+1}^{n}\left(c_{k,l}^{(j)}b_k^{(j)} - \mathbf{w}_{k,l}^{\mathrm{H}(n)}\bar{\mathbf{r}}^{(j)}\right)^2, \tag{4.27}$$

where N is the observation window in symbol intervals. The least squares estimate for the filter weights can be written as

$$\mathbf{w}_{k,l}^{(n)} = \hat{\mathbf{\Sigma}}_{\bar{\mathbf{r}}}^{-1(n)}\bar{\mathbf{s}}_{k,l}, \tag{4.28}$$

where $\hat{\mathbf{\Sigma}}_{\bar{\mathbf{r}}}^{-1(n)}$ denotes the estimated covariance matrix over a finite data block. The estimate for the covariance matrix is called the sample-covariance matrix,

which can be expressed as

$$\hat{\mathbf{\Sigma}}_{\bar{\mathbf{r}}}^{(n)} = \sum_{j=n-N+1}^{n} \bar{\mathbf{r}}^{(j)} \bar{\mathbf{r}}^{\mathrm{H}(j)}. \tag{4.29}$$

Analogous to the MOE criterion, the LS criterion can be modified as

$$J_{[LS']k,l} = \sum_{j=n-N+1}^{n} \left(\mathbf{w}_{k,l}^{\mathrm{H}(n)} \bar{\mathbf{r}}^{(j)} \right)^2, \quad \text{subject to} \quad \mathbf{w}_{k,l}^{\mathrm{T}} \bar{\mathbf{s}}_{k,l} = 1, \tag{4.30}$$

which results in the receiver coefficients [105]

$$\mathbf{w}_{k,l}^{(n)} = \frac{\hat{\mathbf{\Sigma}}_{\bar{\mathbf{r}}}^{-1(n)} \bar{\mathbf{s}}_{k,l}}{\bar{\mathbf{s}}_{k,l}^{\mathrm{T}} \hat{\mathbf{\Sigma}}_{\bar{\mathbf{r}}}^{-1(n)} \bar{\mathbf{s}}_{k,l}}. \tag{4.31}$$

The adaptation of the blind LS receiver means updating the inverse of the sample-covariance. It is clear that the blind adaptive LS receiver is significantly more complex than the stochastic gradient based blind adaptive receivers. Recursive methods, such as the recursive least squares (RLS) algorithm [21], for updating the inverse and iteratively finding the filter weights are known. Also, the methods based on eigen-decomposition of the covariance matrix have been proposed to avoid explicit matrix inversion [102, 193]. In this thesis, only the method based on the matrix inversion lemma [194]

$$(\mathbf{A} + \mathbf{BCD})^{-1} = \mathbf{A}^{-1} - \mathbf{A}^{-1}\mathbf{B}(\mathbf{DA}^{-1}\mathbf{B} + \mathbf{C}^{-1})^{-1}\mathbf{DA}^{-1} \tag{4.32}$$

is considered. Equation (4.32) can be used to update the inverse of the sample-covariance as a new data vector is received:

$$\hat{\mathbf{\Sigma}}_{\bar{\mathbf{r}}}^{-1(n)} = \left(\hat{\mathbf{\Sigma}}_{\bar{\mathbf{r}}}^{(n-1)} + \bar{\mathbf{r}}^{(n)} \bar{\mathbf{r}}^{\mathrm{H}(n)} \right)^{-1} = \mathbf{\Sigma}_{\bar{\mathbf{r}}}^{-1(n-1)} - \frac{\mathbf{\Sigma}_{\bar{\mathbf{r}}}^{-1(n-1)} \bar{\mathbf{r}}^{(n)} \bar{\mathbf{r}}^{\mathrm{H}(n)} \mathbf{\Sigma}_{\bar{\mathbf{r}}}^{-1(n-1)}}{1 + \bar{\mathbf{r}}^{\mathrm{H}(n)} \mathbf{\Sigma}_{\bar{\mathbf{r}}}^{-1(n-1)} \bar{\mathbf{r}}^{(n)}}. \tag{4.33}$$

In time-variant channels, the old values of the inverse must be weighted by the so-called forgetting factor ($0 < \gamma < 1$), which results in the following recursive inverse updating rule [191, p. 407]

$$\hat{\mathbf{\Sigma}}_{\bar{\mathbf{r}}}^{-1(n)} = \frac{1}{\gamma} \left(\hat{\mathbf{\Sigma}}_{\bar{\mathbf{r}}}^{-1(n-1)} - \frac{\hat{\mathbf{\Sigma}}_{\bar{\mathbf{r}}}^{-1(n-1)} \bar{\mathbf{r}}^{(n)} \bar{\mathbf{r}}^{\mathrm{H}(n)} \hat{\mathbf{\Sigma}}_{\bar{\mathbf{r}}}^{-1(n-1)}}{\gamma + \bar{\mathbf{r}}^{\mathrm{H}(n)} \hat{\mathbf{\Sigma}}_{\bar{\mathbf{r}}}^{-1(n-1)} \bar{\mathbf{r}}^{(n)}} \right). \tag{4.34}$$

It will be demonstrated by numerical examples that it is sufficient to initialize the algorithm as $\hat{\mathbf{\Sigma}}_{\bar{\mathbf{r}}}^{-1(0)} = \mathbf{I}$.

Once the inverse for the sample-covariance is obtained, the blind receiver can be solved if the delay for the signal component of interest is known. As was indicated earlier, the blind LS receiver structure can be used for delay estimation as well. Namely, the minimum variance delay estimator developed for beamforming [191] gives the blind MOE receiver for the correct delay. In delay estimation, the power at the estimator output is maximized for the correct delay. Clearly, this property can be used in delay estimation, as will be shown in Chapter 5.

4.1.2.3. Numerical examples

In this section the convergence and the BER performance of the different blind adaptive receivers are studied. The parameters used in the simulations are the same as in Section 4.1.1.1, except the delay difference between the multipath components is 5 chip intervals.

The excess mean squared error[3] (4.15) was simulated as a function of iterations for the blind adaptive receivers in a two-path fading channel with the SNR of 20 dB with 10 and 20 active users. The curves have been obtained by averaging the squared errors from 200 simulations for the adaptive LMMSE-RAKE receiver and 100 times for other receivers. The results for the constant modulus, the Griffiths', the blind MOE, and the LMMSE-RAKE receivers with step-sizes $\mu = 10^{-1}$ and 100^{-1} (the NLMS algorithm was used with $\mu_{k,l}^{(n)} = \mu\big((2D+1)SG\bar{\mathbf{r}}_{k,l}^{\mathrm{H}(n)}\bar{\mathbf{r}}_{k,l}^{(n)}\big)^{-1}$) are presented in Figures 4.5 – 4.8.

Based on these results, all other schemes except the adaptive LMMSE-RAKE require rather small step-size for sufficiently small excess MSE. With decreasing step-size, the excess MSE of all schemes studied approaches zero and their performance is equal. Using a filtered estimate[4] of the received signal power instead of the instantaneous value did not improve the convergence of the constant modulus algorithm significantly. The addition of the constraint on the unconstrained algorithms did not have significant impact to the convergence, and therefore, these results are not shown in the figures. Based on the presented results it may be concluded that the adaptive LMMSE-RAKE converges faster than the other known blind adaptive receivers based on stochastic gradient algorithms. The constant modulus algorithm would require the smallest step-size for the same final MSE and has the slowest convergence for that reason. The Griffiths' algorithm and the blind MOE receivers have roughly the same convergence rate, although the latter is slightly better.

The bit error rates of different schemes were studied in a 30-user and 15-user case with different step-sizes at the SNR of 20 dB. The results are presented in Table 4.1. The performance of different algorithms is very similar with small step-sizes ($\mu = 100^{-1}$). When faster convergence is required and the step-size must be increased ($\mu = 10^{-1}$), only the adaptive LMMSE-RAKE receivers result in significant performance improvements with respect to the conventional RAKE receiver. With 15 users their performance is degraded only marginally when increasing the step-size from $\mu = 100^{-1}$ to $\mu = 10^{-1}$. The basic version of the adaptive LMMSE-RAKE receiver (4.21) has worse performance than the conventional RAKE receivers in the 30-user case. The orthogonalized (or constrained) LMMSE-RAKE receiver does not have such a problem unless the step-size is too large. Since the BERs of all blind adaptive receivers are quite similar with small step-size, the BERs versus SNR for all schemes can be estimated from Figure 4.4 with moderate system loads.

[3]The filter coefficients have been normalized at every iteration when computing the excess MSE such that $\mathbf{w}_{k,l}^{\mathrm{H}(n)}\mathbf{w}_{k,l}^{(n)} = 1$.

[4]A recursive estimator with a forgetting factor of 0.9975 was used to average the absolute values of the channel estimates. See p. 43 for the recursive filter definition.

The BER simulation results for the blind LS receivers in a known two-path fading channel with varying averaging interval in sample-covariance estimation for $K = 10$ and 20 are presented in Figure 4.9. The direct inversion instead of the iterative matrix inversion (4.34) was used. Based on the results, the observation interval in sample-covariance estimation must be relatively long to obtain good performance. The receiver with span one symbol interval ($M = 1$) has better performance with smaller averaging intervals than the receiver with span three symbol intervals ($M = 3$). The reason for this is the dimensions of the matrix that is inverted; in the first case the matrix is of size $(31 + \tau_{[max]}) \times (31 + \tau_{[max]})$[5] and in the second case 93×93. The imperfections in the sample-covariance are emphasized more with larger receiver spans.

The convergence curves (excess MSE) for the blind LS receivers are presented in Figures 4.10 and 4.11 for different forgetting factors. Only 20 simulation runs were averaged to obtain the curves of Fig. 4.10 and 50 runs to obtain the curves of Fig. 4.11. Clearly, the blind LS receiver improves the convergence in comparison to the blind adaptive LMS based receivers. The comparison is not fair, since the LMS algorithms were used in the receivers with span three and their convergence can also be improved with smaller spans.

In practice, the inverse is computed iteratively, e.g., by using the scheme of (4.33). The Frobenius norm[6] was evaluated as a function of time for the scheme by using the identity matrix as the initial value for the inverse. The results (see Figure 4.12) indicate that the iterative algorithm performs well and the convergence of the iterative scheme is fast.

[5]The receiver vector length has been one symbol interval plus the maximum delay difference between the multipath components $\tau_{[max]}$.

[6]$\|\mathbf{A}\|_F = \sqrt{\mathrm{tr}\left[\mathbf{A}^{\mathrm{H}}\mathbf{A}\right]}$

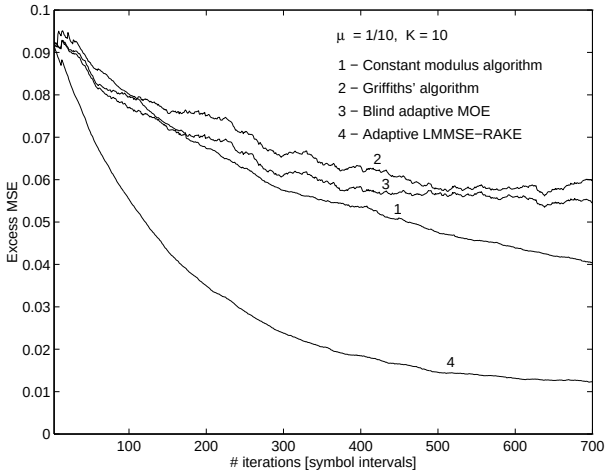

Fig. 4.5. Excess mean squared error as a function of the number of iterations for different blind adaptive receivers in a two-path fading channel with vehicle speeds of 40 km/h, the number of active users $K = 10$, SNR = 20 dB, $\mu = 10^{-1}$.

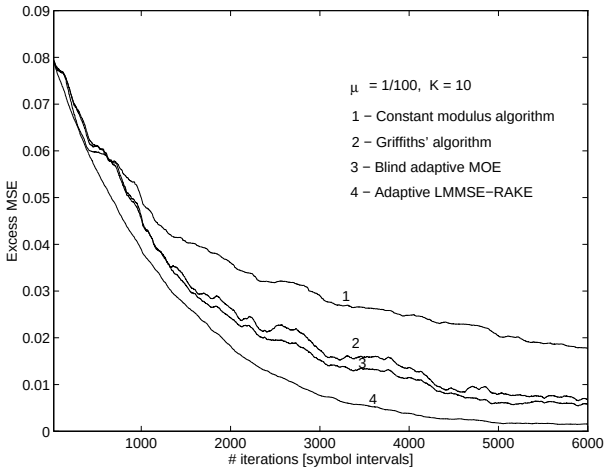

Fig. 4.6. Excess mean squared error as a function of the number of iterations for different blind adaptive receivers in a two-path fading channel with vehicle speeds of 40 km/h, the number of active users $K = 10$, SNR = 20 dB, $\mu = 100^{-1}$.

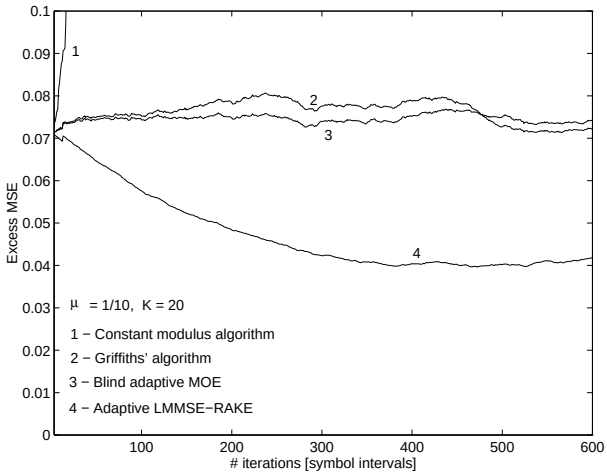

Fig. 4.7. Excess mean squared error as a function of the number of iterations for different blind adaptive receivers in a two-path fading channel with vehicle speeds of 40 km/h, the number of active users $K = 20$, SNR = 20 dB, $\mu = 10^{-1}$.

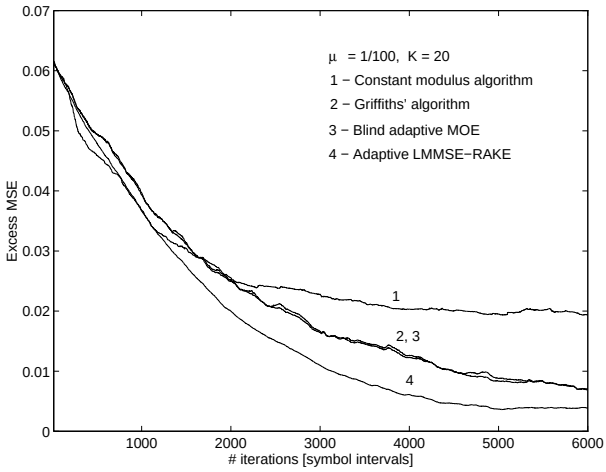

Fig. 4.8. Excess mean squared error as a function of the number of iterations for different blind adaptive receivers in a two-path fading channel with vehicle speeds of 40 km/h, the number of active users $K = 20$, SNR = 20 dB, $\mu = 100^{-1}$.

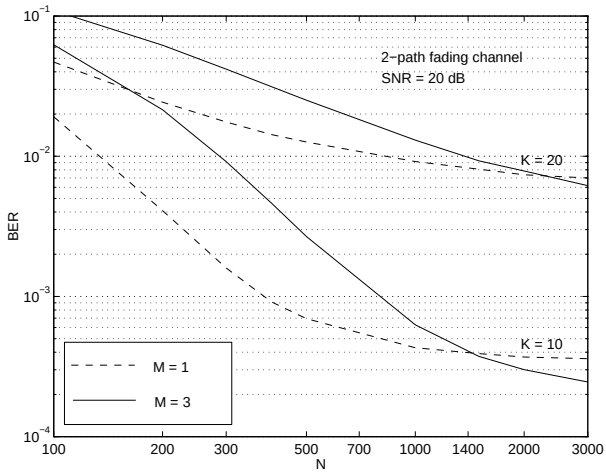

Fig. 4.9. BER as a function of the sample-covariance averaging interval for $K = 10$, 20 for receiver spans of one ($M = 1$) and three symbol intervals ($M = 3$) in a two-path fading channel at a SNR of 20 dB.

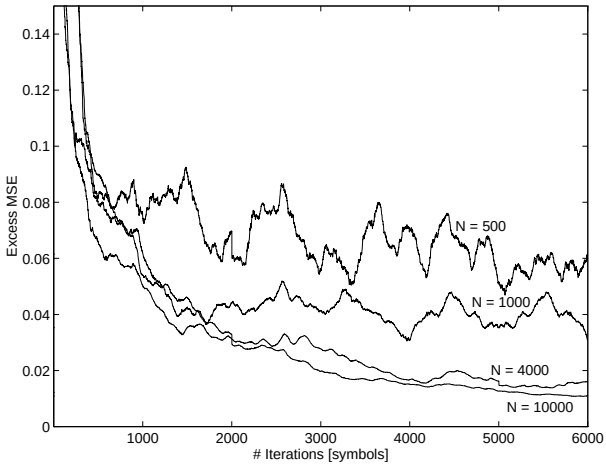

Fig. 4.10. Excess mean squared error as a function of the number of iterations for the blind adaptive LS receiver of span three symbol intervals ($M = 3$) with different forgetting factors ($1 - 2/N$) in a 10-user case at a SNR of 20 dB and vehicle speeds of 40 km/h.

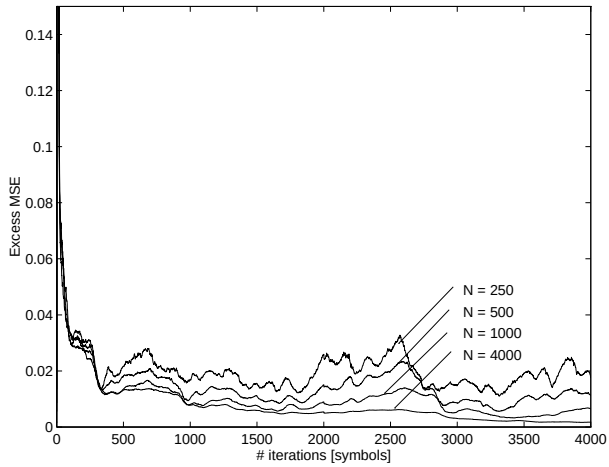

Fig. 4.11. Excess mean squared error as a function of the number of iterations for the blind adaptive LS receiver of span one symbol interval ($M = 1$) with different forgetting factors ($1 - 2/N$) in a 10-user case at a SNR of 20 dB and vehicle speeds of 40 km/h.

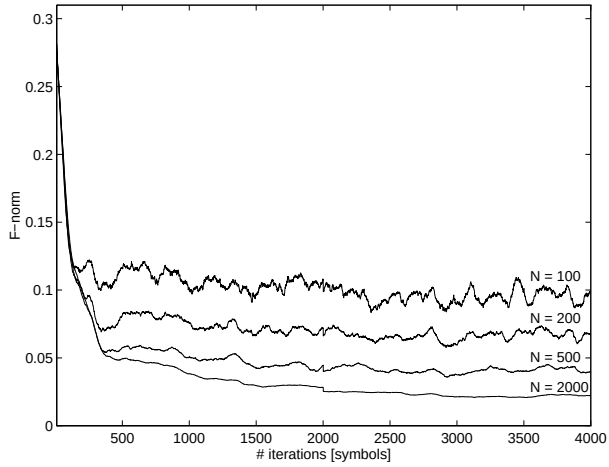

Fig. 4.12. Frobenius norm for the iterative inverse updating algorithm in a 10-user case at a SNR of 20 dB and vehicle speeds of 40 km/h.

Table 4.1. The BERs of different blind adaptive receivers at a SNR of 20 dB in a two-path Rayleigh fading channel at vehicle speeds of 40 km/h. The acronyms used are: adaptive LMMSE-RAKE (LR), adaptive MOE (MOE), Griffiths' algorithm (GRA), constant modulus algorithm with instantaneous channel tap powers (CMA), constant modulus algorithm with average channel tap powers (CMA2), constrained adaptive LMMSE-RAKE (C-LR), constrained constant modulus algorithm with instantaneous channel tap powers (C-CMA), constrained Griffiths' algorithm (C-GRA), constrained constant modulus algorithm with average channel tap powers (C-CMA2) and conventional RAKE (RAKE).

Adaptive receiver	$K = 30$		$K = 15$		
	μ=100^{-1}	μ=10^{-1}	μ=100^{-1}	μ=10^{-1}	μ=2^{-1}
LR	$4.5{\cdot}10^{-2}$	$3.9{\cdot}10^{-1}$	$6.3{\cdot}10^{-4}$	$7.2{\cdot}10^{-4}$	$3.0{\cdot}10^{-2}$
MOE	$2.8{\cdot}10^{-2}$	$4.2{\cdot}10^{-2}$	$6.0{\cdot}10^{-4}$	$2.1{\cdot}10^{-3}$	$9.1{\cdot}10^{-2}$
GRA	$2.8{\cdot}10^{-2}$	$4.7{\cdot}10^{-2}$	$6.4{\cdot}10^{-4}$	$3.3{\cdot}10^{-3}$	$1.2{\cdot}10^{-1}$
CMA	$3.9{\cdot}10^{-2}$	$4.0{\cdot}10^{-1}$	$1.2{\cdot}10^{-3}$	$2.1{\cdot}10^{-2}$	$5.0{\cdot}10^{-1}$
CMA2	$3.3{\cdot}10^{-2}$	$4.0{\cdot}10^{-1}$	$1.8{\cdot}10^{-3}$	$2.1{\cdot}10^{-2}$	$5.0{\cdot}10^{-1}$
C-LR	$3.2{\cdot}10^{-2}$	$4.2{\cdot}10^{-2}$	$6.3{\cdot}10^{-4}$	$6.4{\cdot}10^{-4}$	$1.9{\cdot}10^{-3}$
C-CMA	$3.3{\cdot}10^{-2}$	$5.0{\cdot}10^{-1}$	$6.1{\cdot}10^{-4}$	$3.8{\cdot}10^{-1}$	$5.0{\cdot}10^{-1}$
C-GRA	$2.8{\cdot}10^{-2}$	$4.2{\cdot}10^{-2}$	$6.1{\cdot}10^{-4}$	$2.3{\cdot}10^{-3}$	$9.7{\cdot}10^{-2}$
C-CMA2	$2.9{\cdot}10^{-2}$	$5.0{\cdot}10^{-1}$	$7.7{\cdot}10^{-4}$	$2.7{\cdot}10^{-1}$	$5.0{\cdot}10^{-1}$
RAKE	$3.1{\cdot}10^{-2}$	$3.1{\cdot}10^{-2}$	$7.1{\cdot}10^{-3}$	$7.1{\cdot}10^{-3}$	$7.1{\cdot}10^{-3}$

4.1.3. Adaptive LMMSE-RAKE with adaptive branch switching

The adaptive LMMSE-RAKE receivers have the fastest convergence among the blind adaptive receivers studied in the previous section. The basic algorithm results in slightly worse performance than the algorithm with the orthogonality constraint. At low SNRs or high system loads the conventional RAKE receiver can outperform the basic adaptive LMMSE-RAKE receiver. This is due to the fact that an imperfect reference signal was used in adaptation. In some circumstances all blind adaptive receivers may confront convergence problems and the performance may be significantly degraded. To avoid this problem, the adaptive filter should be switched off during the periods when the conventional RAKE receiver would give better performance. This may be useful in applications when there is a high risk that the adaptation can fail for some reason. The two possibilities for the adaptive filter branch switching studied are the MSE and the correlation based methods.

The steady-state MSE can be approximated as $J_{k,l}^{(\infty)} \approx J_{[opt]k,l} = \mathrm{E}\big[|c_{k,l}|^2\big] - \boldsymbol{\Sigma}_{\bar{\mathbf{r}}d_{k,l}}^{\mathrm{H}} \boldsymbol{\Sigma}_{\bar{\mathbf{r}}}^{-1} \boldsymbol{\Sigma}_{\bar{\mathbf{r}}d_{k,l}}$. This can be also written as

$$J_{k,l}^{(\infty)} = \mathrm{E}\big[|c_{k,l}|^2\big]\big(1 - \mathrm{E}\big[|c_{k,l}|^2\big]\bar{\mathbf{s}}_{k,l}^{\mathrm{T}} \boldsymbol{\Sigma}_{\bar{\mathbf{r}}}^{-1} \bar{\mathbf{s}}_{k,l}\big). \tag{4.35}$$

The actual MSE value after training over a finite number symbols also includes the excess MSE term (4.15), but assuming that the step-size is small, it can be neglected. The steady-state MSEs as a function of the number of users for different SNRs in a two-path Rayleigh fading channel with multipath components of equal energy is depicted in Figure 4.15. As the number of users increases or the SNR gets lower, the MSE increases. Therefore, the MSE can be used as an indicator for the low SNR or high system load, which are the cases when the conventional RAKE has slightly better performance than the adaptive LMMSE-RAKE receiver. The MSE can be estimated in practical receivers as

$$J_{k,l}^{(n)} = \frac{1}{W} \sum_{i=n-W-1}^{n} |e^{(i)}|^2, \tag{4.36}$$

where W is the averaging interval. The block diagram of the adaptive LMMSE-RAKE receiver with the MSE based branch switching is given in Figure 4.13.

Another switching method is based on the correlation between the adaptive interference suppression filter and the signature sequence of the desired user. The justification for this approach is given in the following. The optimum filter coefficients are given as

$$\begin{aligned} \mathbf{w}_{k,l} &= \mathrm{E}\big[|c_{k,l}|^2\big] \boldsymbol{\Sigma}_{\bar{\mathbf{r}}}^{-1} \bar{\mathbf{s}}_{k,l} \\ &= \Big(\mathrm{E}\big[|c_{k,l}|^2\big] \boldsymbol{\Sigma}_{\bar{\mathbf{r}}}^{-1} - \mathbf{I}\Big) \bar{\mathbf{s}}_{k,l} + \bar{\mathbf{s}}_{k,l} \\ &= \mathbf{x}_{k,l} + \bar{\mathbf{s}}_{k,l}. \end{aligned} \tag{4.37}$$

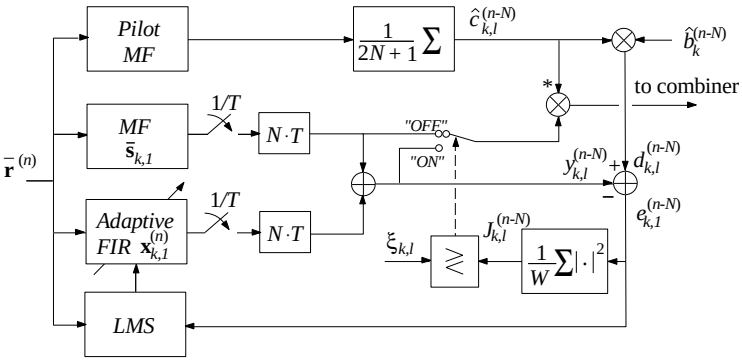

Fig. 4.13. Block diagram of one receiver branch in the adaptive LMMSE-RAKE receiver with automatic adaptive branch switching based on the MSE.

The orthogonality condition for the fixed and adaptive filter components is $\bar{\mathbf{s}}_{k,l}^{\mathrm{T}}\mathbf{x}_{k,l} = 0$, which in this case can be written as

$$\begin{aligned}\bar{\mathbf{s}}_{k,l}^{\mathrm{T}}\mathbf{x}_{k,l} &= \bar{\mathbf{s}}_{k,l}^{\mathrm{T}}\left(\mathrm{E}\left[|c_{k,l}|^2\right]\boldsymbol{\Sigma}_{\bar{\mathbf{r}}}^{-1} - \mathbf{I}\right)\bar{\mathbf{s}}_{k,l} \\ &= \mathrm{E}\left[|c_{k,l}|^2\right]\bar{\mathbf{s}}_{k,l}^{\mathrm{T}}\boldsymbol{\Sigma}_{\bar{\mathbf{r}}}^{-1}\bar{\mathbf{s}}_{k,l} - 1, \end{aligned} \tag{4.38}$$

which is zero only in the single-user single-path noiseless case, when $\bar{\mathbf{s}}_{k,l}^{\mathrm{T}}\boldsymbol{\Sigma}_{\bar{\mathbf{r}}}^{-1}\bar{\mathbf{s}}_{k,l} = \mathrm{E}\left[|c_{k,l}|^2\right]^{-1}$. The optimum normalization coefficient $\mathcal{N}$ in the adaptive filter decomposition is found from

$$\bar{\mathbf{s}}_{k,l}^{\mathrm{T}}\left(\mathcal{N}\,\boldsymbol{\Sigma}_{\bar{\mathbf{r}}}^{-1} - \mathbf{I}\right)\bar{\mathbf{s}}_{k,l} = 0 \tag{4.39}$$

to be $\mathcal{N} = \left(\bar{\mathbf{s}}_{k,l}^{\mathrm{T}}\boldsymbol{\Sigma}_{\bar{\mathbf{r}}}^{-1}\bar{\mathbf{s}}_{k,l}\right)^{-1}$, which is the same as for the MOE receivers. Hence, only the MOE criterion leads to the optimum filter decomposition, as could be expected.

With the adaptive LMMSE-RAKE receiver the adaptive and the fixed filter components are allowed to correlate. The correlation is small if the number of users is low and the SNR high. At low SNRs or high system loads, the correlation becomes more significant. This is depicted in Figure 4.16 for various number of users and SNRs. Therefore, the correlation can be used as an indicator in the adaptive filter branch switching. The filtered squared correlation can be expressed as

$$J_{k,l}^{(n)} = \frac{1}{W}\sum_{i=n-W-1}^{n}|\mathbf{x}_{k,l}^{\mathrm{H}(i)}\bar{\mathbf{s}}_{k,l}|^2. \tag{4.40}$$

The block diagram of the adaptive LMMSE-RAKE receiver with the correlation based branch switching is given in Figure 4.14.

When $J_{k,l}^{(n)}$ exceeds a predetermined threshold ($\xi_{k,l}$), the adaptive part is switched off and only the conventional (MF) receiver branch is used in RAKE combining

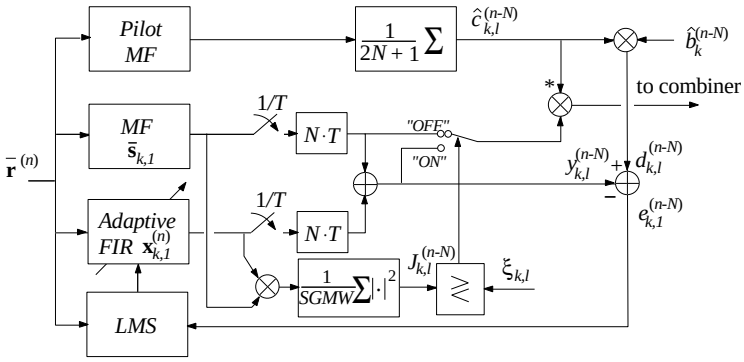

Fig. 4.14. Block diagram of one receiver branch in the adaptive LMMSE-RAKE receiver with automatic adaptive branch switching based on the correlation method.

(see Figures 4.13 and 4.14). The adaptive part is switched on again when $J_{k,l}^{(n)}$ is smaller than the threshold:

$$\mathbf{w}_{k,l}^{(n)} = \begin{cases} \bar{\mathbf{s}}_{k,l}, & J_{k,l}^{(n)} \geq \xi_{k,l} \\ \bar{\mathbf{s}}_{k,l} + \mathbf{x}_{k,l}^{(n)}, & J_{k,l}^{(n)} < \xi_{k,l}. \end{cases} \tag{4.41}$$

The adaptive interference suppression filter is updated continuously regardless of whether it is switched on or off in the multipath combining. The threshold $\xi_{k,l}$ is set based on the switching criterion used as will be discussed in the next section.

4.1.3.1. Numerical examples

The BER simulations were carried out in a two-path fading channel with the maximum delay spread of 10 chip intervals and vehicle speed of 40 km/h which results in the maximum normalized Doppler shift of $4.63 \cdot 10^{-3}$. The other parameters used in the simulations are the same as in Section 4.1.1.1

As can be seen from Figure 4.4, the conventional RAKE receiver has better BER than the basic adaptive LMMSE-RAKE receiver at low SNRs and high system loads. The adaptive receiver branch switching is used to overcome this so that either the conventional RAKE or the adaptive LMMSE-RAKE is used depending on the SNR and system load. Only the basic adaptive LMMSE-RAKE receiver was studied. First, the MSE based method (4.36) was studied. Based on the steady-state MSE for different SNRs and number of users (Figure 4.16), the threshold $\xi_{k,l}$ was set to 0.5 in simulations. As can be seen, this threshold value limits the use of the LMMSE-RAKE receiver to the case of 15 active users at the SNR of 5 dB. The averaging window size W was set to 500 in the simulations. The BER simulation

results are presented in Figure 4.17. At first glance, the receiver seems to perform as desired. In the case when $K = 20$ (not shown in the figure) the MSE criterion always switched the receiver to the conventional RAKE mode. Hence, it is robust only in extreme cases when the interference level is either low or very high. The correlation based method, on the contrary, was robust in all cases studied. First, the squared correlation for different SNRs and system loads was evaluated (Figure 4.16). Based on these values the threshold $\xi_{k,l}$ was set to 0.2 in simulations, which limits the the use of the LMMSE-RAKE receiver to the case of 10 active users at the SNR of 5 dB. The averaging window size W was set to 500 symbol intervals. The BER results with the correlation based switching criterion (4.40) are given in Figure 4.18. According to the results, the correlation based switching is robust. With the orthogonality constraint, the correlation is forced towards zero and the correlation based method cannot be used.

4.1.4. Discussion

A novel blind adaptive single-user receiver was developed in this section. The numerical examples show that the conventional RAKE receiver can be used to train the adaptive LMMSE-RAKE receiver. The convergence of the receiver is much better in comparison to the other known blind adaptive receivers based on the LMS algorithms. When the number of users is not too high, i.e., when the conventional RAKE receiver has good enough performance to provide reliable reference signal to adaptive filter training, the performance is also superior to other known blind adaptive LMS based receivers.

The performance of the blind adaptive least squares receiver was also studied in a frequency-selective fading channel. It converges faster with narrow processing windows than the blind adaptive receivers using LMS algorithms. The BER performance is somewhat similar to the LMS based algorithms. The sample-covariance inverse required in the blind adaptive LS receiver can be utilized in receiver timing acquisition phase also, which makes this approach quite interesting.

The basic adaptive LMMSE-RAKE receiver can have worse performance than the conventional RAKE receiver in some cases. To overcome this problem either an additional orthogonality constraint can be used in adaptation or the adaptive filter branch can be switched off when the adaptation has failed. The latter approach may provide additional robustness to the receiver operation in general. The correlation based switching criterion was proven to be reliable in cases studied.

In cases when the training is based on a training sequence, the final MSE can be used in the postcombining LMMSE receiver as a quality indicator to be used in automatic repeat request (ARQ) protocols [91] or antenna diversity combining [90] in determining whether the training has been succesful or not. In the next section, the adaptive postcombining receivers operating in fading channels will be discussed.

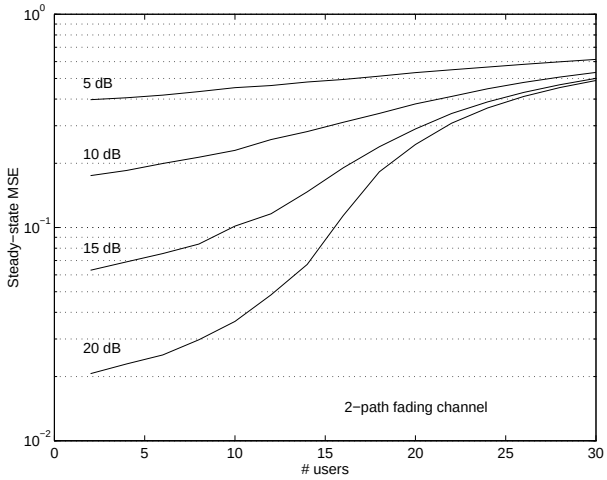

Fig. 4.15. The steady-state MSEs as a function of the number of users for different average SNRs in a two-path fading channel.

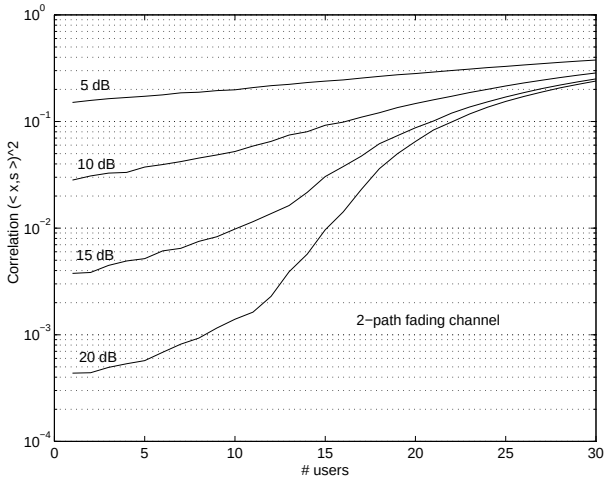

Fig. 4.16. The squared correlations between the adaptive filter weights and the fixed signature sequence as a function of the number of users for different average SNRs in a two-path fading channel.

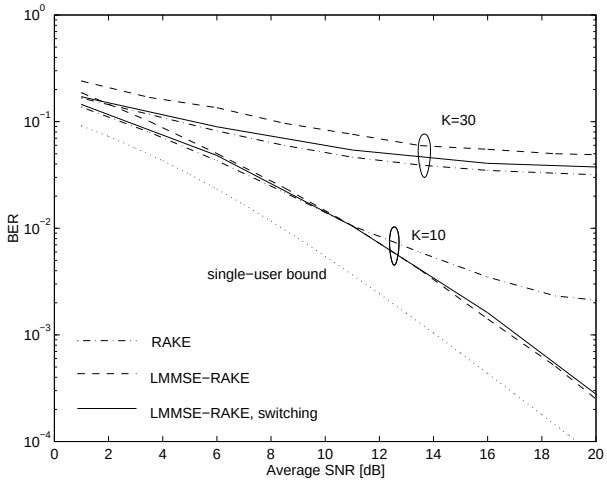

Fig. 4.17. Simulated BERs for the conventional RAKE, adaptive LMMSE-RAKE (no switching) and adaptive LMMSE-RAKE with the MSE based switching in a two-path fading channel for vehichle speeds of 40 km/h with different numbers of users.

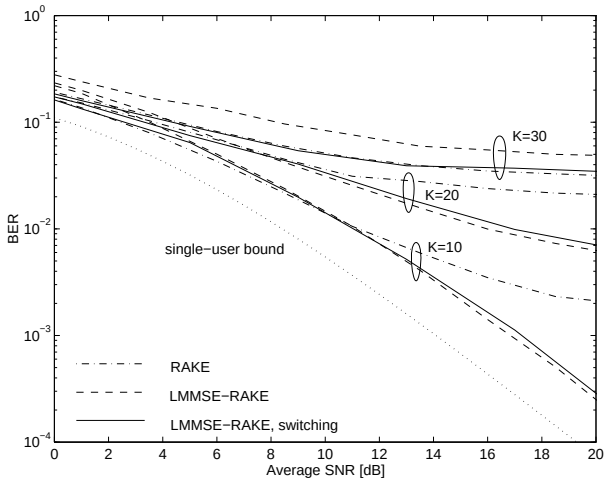

Fig. 4.18. Simulated BERs for the conventional RAKE, adaptive LMMSE-RAKE (no switching) and adaptive LMMSE-RAKE with the correlation based switching in a two-path fading channel for vehichle speeds of 40 km/h with different numbers of users.

4.2. Adaptive postcombining LMMSE receivers

The major difference between the precombining and the postcombining LMMSE receivers is the order of multipath combining and interference suppression. This influences the number of interference suppression filters in practical implementations. Only one adaptive filter is needed with the postcombining LMMSE receivers, whereas, the precombining LMMSE receiver needs an interference suppression filter for each RAKE finger. Another difference in the practical adaptive implementations of the precombining LMMSE receivers (or the blind receivers in general) and the postcombining LMMSE receivers is that the precombining LMMSE receivers require the delays for multipath components to be known. Fractionally spaced equalizers (FSE) [22] are commonly used to relax the timing requirements in equalizers. In fact, when taking samples at the Nyquist rate, only a rough timing for the training sequence is required with the postcombining LMMSE receivers.

Packet data applications will become important in the future, in particular for high data rate applications. Usually each data packet starts with a preamble which is used for packet detection and receiver synchronization. It can be also used for adaptive receiver training provided that the preamble is long enough. Although the preamble should be few hundred symbols to guarantee convergence, its relative portion of the whole packet is quite small in high data rate applications. It can be anticipated that the capacity of the systems supporting the use of the adaptive LMMSE receiver is much higher than with systems based on the conventional RAKE receivers.

In this section, the issues related to adaptive postcombining LMMSE receivers in fading channels are studied. The basic structure of the adaptive postcombining LMMSE receiver is presented in Section 4.2.1. The general convergence analysis is carried out in Section 4.2.2 in order to evaluate the usefulness of the adaptive postcombining LMMSE receivers in fading channels. The performance results with RAKE based training presented in Section 4.2.3 are used to demonstrate the feasibility of the adaptive receiver concept based on the training by using the conventional RAKE receiver.

4.2.1. Fractionally spaced adaptive LMMSE receiver

Let the input sample vector during the nth symbol over $M = 2D+1$ symbol intervals be $\bar{\mathbf{r}}^{(n)} = \left[\mathbf{r}^{\mathrm{T}(n-D)}, \ldots, \mathbf{r}^{\mathrm{T}(n)}, \ldots, \mathbf{r}^{\mathrm{T}(n+D)}\right]^{\mathrm{T}}$. The received signal vectors are fed to linear filters with impulse response: $\mathbf{w}_k^{(n)} = \left[w_k^{(n)}(0), \ldots, w_k^{(n)}(MSG-1)\right]^{\mathrm{T}}$. The output of the receiver can be written as $y_k^{(n)} = \mathbf{w}_k^{\mathrm{H}(n)} \bar{\mathbf{r}}^{(n)}$. The error functions, $e_k^{(n)} = d_k^{(n)} - y_k^{(n)}$, produced by the difference between the reference signals and the filter outputs, are used to update the filter weights. The block diagram of the adaptive LMMSE receiver is given in Figure 4.19.

The filter coefficients are derived using the MSE criterion ($\mathrm{E}[|e_k^{(n)}|^2]$), which leads to the optimal filter coefficients [21] $\mathbf{w}_{[opt]k} = \mathbf{\Sigma}_{\bar{\mathbf{r}}}^{-1} \mathbf{\Sigma}_{\bar{\mathbf{r}} d_k}$, where $\mathbf{\Sigma}_{\bar{\mathbf{r}}}$ is the

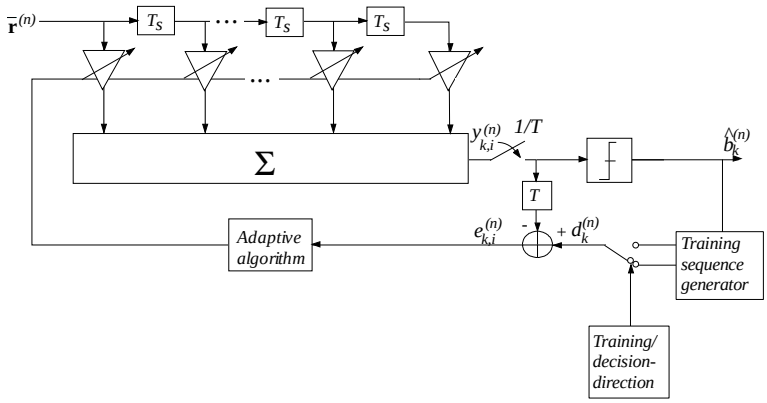

Fig. 4.19. Fractionally spaced adaptive LMMSE receiver.

covariance matrix of $\bar{\mathbf{r}}$ and $\mathbf{\Sigma}_{\bar{\mathbf{r}}d_k}$ is the cross-correlation vector between $\bar{\mathbf{r}}$ and d_k. For the optimum filter coefficients the minimum MSE becomes $J_{[opt]k} = 1 - \mathbf{\Sigma}_{\bar{\mathbf{r}}d_k}^{\mathrm{H}} \mathbf{w}_{[opt]k}$ for unit symbol energy.

The filter weights can be calculated iteratively by using the LMS algorithm:

$$\mathbf{w}_k^{(n+1)} = \mathbf{w}_k^{(n)} + \mu^{(n)} e_k^{*(n)} \bar{\mathbf{r}}^{(n)}. \tag{4.42}$$

As was pointed out in Chapter 3, the convergence is crucial for the adaptive postcombining LMMSE receivers operating in fading channels. From the LMS algorithm point of view, the step-size μ should be as large as possible to obtain the fastest possible convergence in time-varying channels. To guarantee the stability of the LMS algorithm the step-size should be bounded $0 < \mu < \frac{2}{\lambda_{max}}$, where λ_{max} is the largest eigenvalue of the matrix $\mathbf{\Sigma}_{\bar{\mathbf{r}}}$. In time-varying systems, the largest eigenvalue may change significantly, and hence, the step-size should be adapted to obtain optimum convergence speed and to ensure algorithm stability. The stability criterion is satisfied also when $0 < \mu < \frac{2}{\sum \lambda_i}$, where $\sum \lambda_i = \mathrm{tr}(\mathbf{\Sigma}_{\bar{\mathbf{r}}}) = \mathcal{P}$ is the input signal power. In the normalized LMS algorithm, the step-size is selected according to $\mu_{[NLMS]}^{(n)} = \mu / \hat{\mathcal{P}}$ with $\hat{\mathcal{P}} = \bar{\mathbf{r}}^{\mathrm{H}(n)} \bar{\mathbf{r}}^{(n)}$.

Even if the step-size can be chosen optimally, the optimum weights are not achieved in practice with the LMS algorithm due to filter misadjustment caused by the noise[7]. Also the finite training period that must be used in practice sets some constraints on the minimum MSE value. In fact, after a training period of n symbols, the MSE is given by

$$J_k^{(n)} = J_{[opt]k} + J_{[ex]k}^{(n)}, \tag{4.43}$$

where $J_{[ex]k}^{(n)} = \mathrm{tr}\big[\mathbf{\Sigma}_{\bar{\mathbf{r}}} \mathbf{\Gamma}^{(n)}\big]$ and $\mathbf{\Gamma}^{(n)} = \mathrm{E}\big[(\mathbf{w}_{[opt]k} - \mathbf{w}_k^{(n)})(\mathbf{w}_{[opt]k} - \mathbf{w}_k^{(n)})^{\mathrm{H}}\big]$ is the

[7]The optimum weights are obtained only when $\mu \to 0$ [21].

tap weight error covariance matrix at iteration n. The final steady state MSE achieved is given by [21]

$$J_k^{(\infty)} = \frac{J_{[opt]k}}{1 - \sum_{j=1}^{(2D+1)SG} \mu\lambda_j/(2-\mu\lambda_j)}. \tag{4.44}$$

The convergence rate is also crucial for other adaptive algorithms, such as the RLS algorithm. In the following section a general analysis for the adaptive algorithm convergence requirements in fading channels is developed.

4.2.2. General convergence analysis

In order to evaluate the usefulness of the adaptive versions of the postcombining LMMSE receivers in fading channels, the receiver outage probability will be analyzed with different rates of fading. The analysis of the outage probability for a practical LMMSE receiver requires the fixing of several parameters which are functions of the propagation channel and the system load. The convergence time of the adaptive LMMSE receiver depends on the relative time delays between the users, their channel realizations, signal-to-noise ratios, spreading sequences, number of users and propagation paths. Moreover, the convergence time depends on the adaptive algorithm itself and the parameters used therein. For the aforementioned reasons, the receiver outage probability analysis is simplified to keep it as general as possible. No parameters on the active users or on the adaptive algorithm need to be fixed. In the analysis, a certain convergence time will be assumed for a given maximum Doppler shift. The outage probability is evaluated for different thresholds R which determine the *bad channel state*. The bad channel state for the adaptive LMMSE receiver occurs when the envelope of any of the multipath components of the desired user goes below a predetermined threshold R.

The results give an impression of the convergence time requirements for the adaptive versions of the postcombining LMMSE receivers for different rates of fading. The analysis gives only an upper bound for the convergence time, since it is assumed that the bad convergence takes place if the power of any of the multipath components goes below the pre-determined threshold R. However, in some circumstances the adaptive LMMSE receiver may converge close to the correct LMMSE solution even if some of the multipath components fall into a deep fade. Such is the case if the number of multipath components is relatively high and the multipath intensity profile is not flat. The convergence time is analyzed with relatively small number of multipath components with a flat multipath profile, and hence, the analysis is applicable.

Assuming Rayleigh distributions

$$p(|c_{k,l}|) = \frac{|c_{k,l}|}{\mathrm{E}[|c_{k,l}|^2]/2}\, e^{-\frac{|c_{k,l}|^2}{\mathrm{E}[|c_{k,l}|^2]}} \tag{4.45}$$

for the envelopes of the multipath components, the probability for the bad channel

state is

$$Pr\left\{\text{bad channel state}\right\} = Pr\left\{|c_{k,l}| < R\right\} = 1 - e^{-\frac{R^2}{\mathrm{E}[|c_{k,l}|^2]}}. \tag{4.46}$$

The probability for the *good channel state* is naturally $1 - Pr\{\text{bad channel state}\}$, and in the following it will be assumed that during the good channel state, the channel is fixed. The *probability for bad convergence* in an L path channel with equal average energies ($\mathrm{E}[|c_{k,l}|^2] = 1/L$) is

$$Pr\left\{\text{bad convergence}\right\} = L\left(1 - e^{-\frac{R^2}{\mathrm{E}[|c_{k,l}|^2]}}\right). \tag{4.47}$$

If a certain adaptive algorithm has a convergence time t_{conv} in a good channel state, and if we assume that during the bad channel state the convergence time is the duration of the bad channel state plus the convergence time in the good channel state, the *average convergence time* can be determined as

$$\begin{aligned} \bar{t}_{conv} &= \left(1 - Pr\left\{\text{bad convergence}\right\}\right) t_{conv} \\ &+ Pr\left\{\text{bad convergence}\right\} \left(t_{conv} + \bar{t}_{fade}\right) \\ &= t_{conv} + Pr\left\{\text{bad convergence}\right\} \bar{t}_{fade}, \end{aligned} \tag{4.48}$$

where $\bar{t}_{fade}$ is the average fade duration defined as [172]

$$\bar{t}_{fade} = \sqrt{\frac{\mathrm{E}[|c_{k,l}|^2]/2}{\pi}}\ \frac{e^{-\frac{R^2}{\mathrm{E}[|c_{k,l}|^2]}} - 1}{Rf_d}, \tag{4.49}$$

where f_d is the maximum Doppler shift. The average convergence time becomes then

$$\bar{t}_{conv} = t_{conv} + L\left(1 - e^{-\frac{R^2}{\mathrm{E}[|c_{k,l}|^2]}}\right)\sqrt{\frac{\mathrm{E}[|c_{k,l}|^2]/2}{\pi}}\ \frac{e^{-\frac{R^2}{\mathrm{E}[|c_{k,l}|^2]}} - 1}{Rf_d}. \tag{4.50}$$

Finally, the outage probability can be defined as the relative portion between the times when the receiver is in training mode and when it is not. The average total time between two bad channel stages is defined as an inverse of the *average level crossing rate* [172]

$$N_R = L\sqrt{\frac{\pi}{\mathrm{E}[|c_{k,l}|^2]/2}} R f_d e^{-\frac{R^2}{\mathrm{E}[|c_{k,l}|^2]}}. \tag{4.51}$$

The outage probability is then given by

$$Pr\left\{\text{outage}\right\} = \bar{t}_{conv} N_R. \tag{4.52}$$

4.2.3. Numerical examples

Convergence analysis

An important question with the postcombining LMMSE detectors is the convergence rate required for the adaptive algorithm given a certain rate of fading. This can be analyzed by examining the outage probability analysis[8] results (Figures 4.20 – 4.22) carried out according to the analysis presented in Section 4.2.2. The results with different convergence times, normalized maximum Doppler shifts and bad channel state thresholds are presented in Figure 4.20.

The following discussion is based on the assumption that the bad channel threshold is -10 dB. Below this value, a faded multipath component leads to problems in receiver convergence. With the maximum normalized Doppler shift of 10^{-4}, a convergence time of the order of 100 symbol intervals is required. Similarly, for the normalized Doppler of 10^{-5}, the required convergence time is around 1000 symbol intervals. For high data rates in an indoor environment, the maximum normalized Doppler shifts are very low and even the LMS algorithms could be used to adapt the receiver. In vehicular environments, the standard LMS algorithms converge too slowly for adapting the postcombining LMMSE receivers. In future CDMA systems, the highest data rates are expected to be used mainly in indoor environments, and thus, the normalized Doppler shifts will be relatively high in vehicular environment. In Figure 4.23, the maximum normalized Doppler shifts for various vehicle speeds and data rates are presented. The curves have been generated by using (2.28). Using the convergence rate requirements results of Figures 4.20 – 4.22 and the curves of Figure 4.23, it is possible to estimate the data rates required to make the relative fading rates sufficiently slow for a certain algorithm or type of receiver.

By using the general convergence analysis, similar evaluations can be made for different parameters of interest. In Figure 4.21, the outage probability in multipath channels as a function of the bad channel state threshold are presented for the maximum normalized Doppler shift of 10^{-4}. The maximum tolerable Doppler shifts as a function of the convergence times with different outage probabilities and bad channel thresholds are presented in Figure 4.22. Conclusions similar to the ones drawn above can be easily made from those results as well.

BER simulations for the RAKE based training

In the BER analysis with imperfect training (Section 4.1.1), it was assumed that the optimal LMMSE receiver was used. In reality, an adaptive LMS algorithm is used to iteratively approximate the optimum LMMSE receiver. As was pointed out earlier, the step-size must be small enough so that the impact of errors can be sufficiently averaged out. This is illustrated by two examples in Figures 4.24

[8]Actually, 1 - outage probability denoted by $\overline{\text{outage}}$ has been evaluated.

and 4.25. As we can see, the squared error increases rapidly after every reference symbol error. In order to minimize the impact of reference symbol errors, the step-size must be chosen accordingly. If the reference BER is low (Figure 4.24), a larger step-size could be used. When the reference BER increases (Figure 4.25), the step-size must be decreased. This will in turn slow down the convergence.

The impact of the incorrect reference signal on the BER performance of the adaptive postcombining LMMSE detector was studied through simulation. The decisions made by the conventional RAKE receiver have been used to train the LMMSE receiver of length 3 symbol intervals. The receiver sampling rate was one sample per chip. The step-size parameter in the NLMS algorithm was $\mu = 10^{-1}$. Gold codes of length 31 chips and BPSK modulation was used. The BER results are presented in Figure 4.26 in a two-path fixed channel. The results indicate that the erroneous reference signal does not have a dramatic impact on the BER performance if the number of users is not too high. The conventional RAKE receiver can therefore also be used to train the adaptive postcombining LMMSE receiver in the event that there is not a training sequence available.

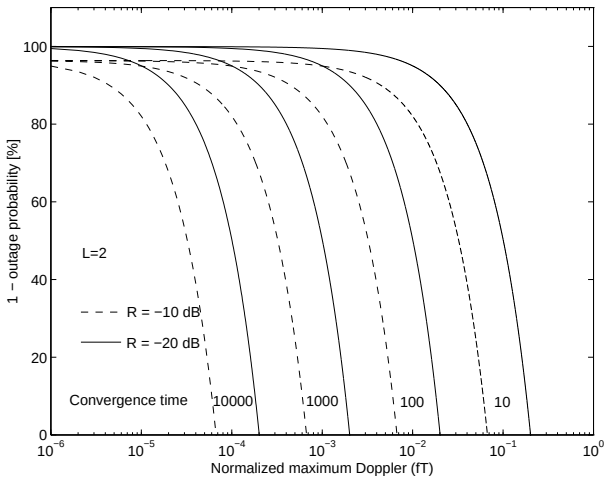

Fig. 4.20. $\overline{\text{Outage}}$ probability as a function of the maximum Doppler shift for different convergence rates and bad channel state thresholds in a two-path fading channel.

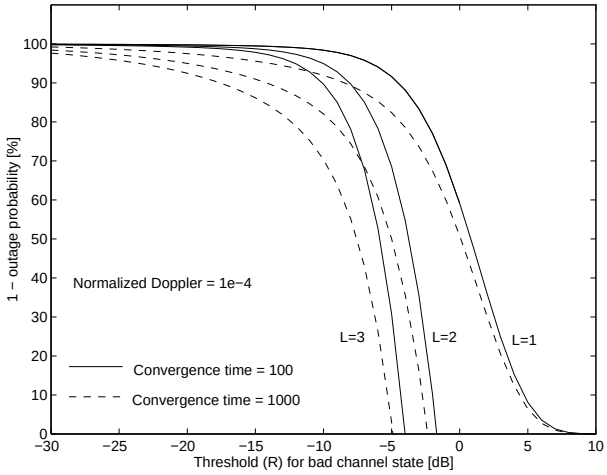

Fig. 4.21. $\overline{\text{Outage}}$ **probability as a function of bad channel state threshold with different numbers of propagation paths for the maximum normalized Dopper shift of** 10^{-4}**.**

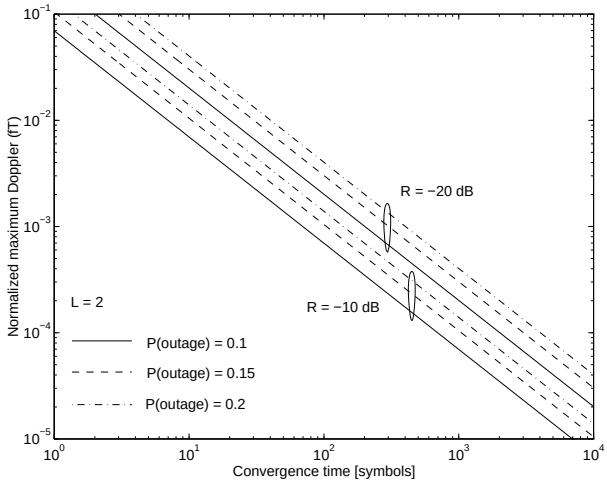

Fig. 4.22. Maximum Doppler shift as a function of convergence time for different outage probabilities and bad channel state thresholds in a two-path channel.

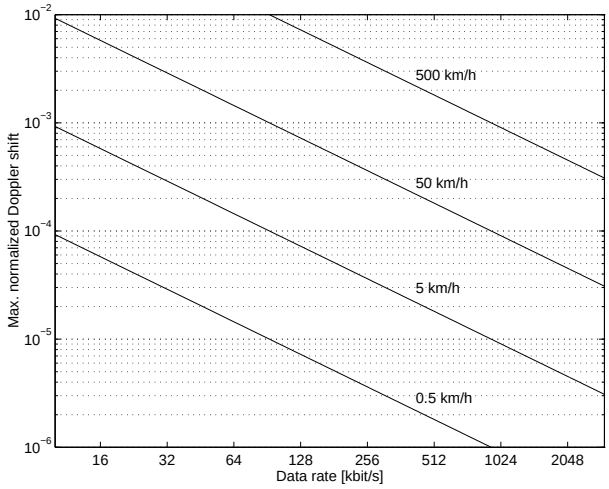

Fig. 4.23. Maximum Doppler shifts versus data rates for various vehicle speeds at the carrier frequency of 2.0 GHz.

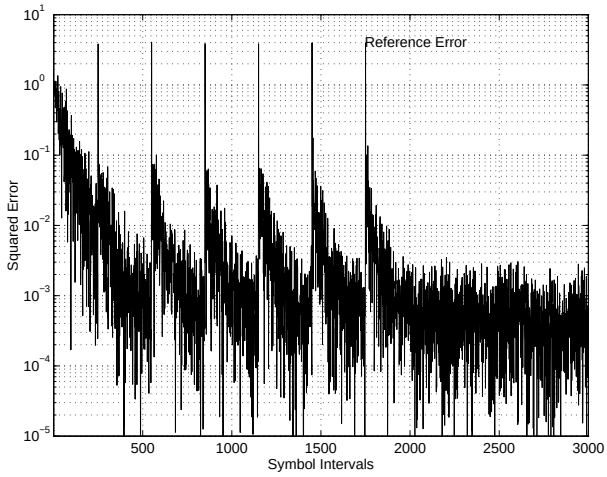

Fig. 4.24. The mean squared error for the postcombining LMMSE receiver using the NLMS algorithm in an AWGN channel with $K = 10$, $\mu = 2^{-1}$, reference BER $= 3 \cdot 10^{-3}$, processing gain 31.

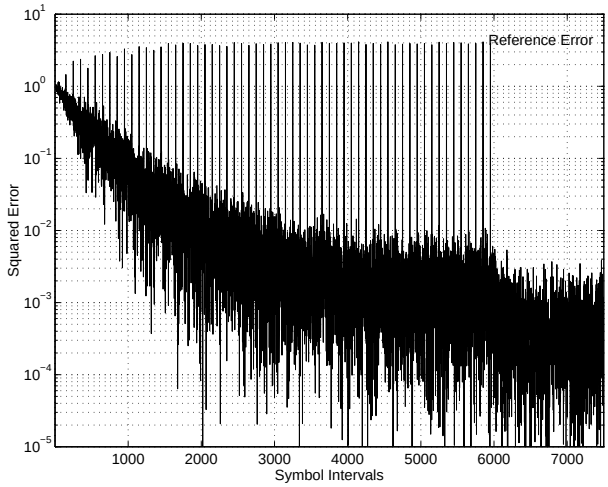

Fig. 4.25. The mean squared error for the postcombining LMMSE receiver using the NLMS algorithm in an AWGN channel with $K = 10$, $\mu = 20^{-1}$, reference BER $= 1 \cdot 10^{-2}$, processing gain 31.

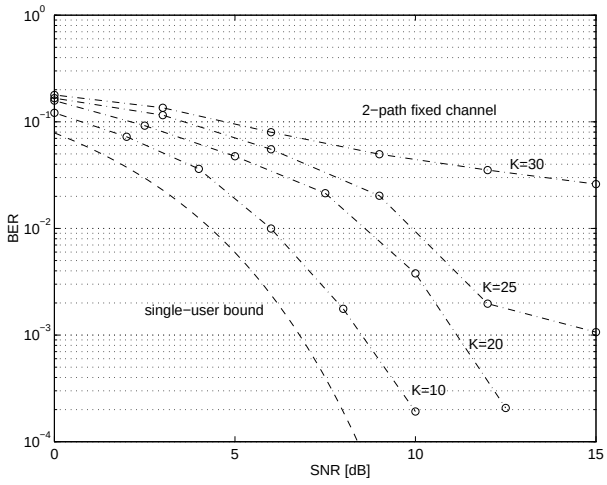

Fig. 4.26. Simulated bit error rates as a function of the average SNR for the adaptive postcombining LMMSE receiver using the NLMS algorithm in a two-path fixed channel with maximum delay spread of 10 chips for different numbers of users and processing gain of 31. The decisions made by the conventional RAKE receiver are used in training.

4.2.4. Discussion

According to the numerical results, the postcombining LMMSE receiver can be used when the maximum normalized Doppler shift is rather low. In practice, the postcombining LMMSE receivers can be used with the highest data rates with rather low spreading factors. The maximum feasible spreading factor depends on the length, i.e., the span of the receiver. The limiting factor is the number of FIR filter taps. In present GSM tranceivers the number of equalizer taps is less than few tens of taps. It can therefore be assumed that the maximum number of LMMSE filter taps is around one hundred in near future CDMA applications. Hence, the maximum spreading factor could be well below one hundred with the receiver span of 3 symbols and 2 samples per chip. By using some dimension reduction techniques [195] the length of the input signal vector can be made smaller without sacrificing performance significantly. As a consequence, longer effective input data vectors can be processed without increasing the length of the receiver.

Based on both the general convergence analysis, it may be concluded that the adaptive postcombining LMMSE receivers are well suited to packet data systems operating in an indoor environment. In [91], an adaptive postcombining LMMSE receiver based on a multiple step-size LMS algorithm was studied in a general packet data system operating in an indoor environment. The basic idea behind the multiple step-size LMS algorithm is that the same data block is processed in parallel with several step-sizes of the LMS algorithm. Furthermore, the receiver is allowed to iterate several times over the same input data block to improve the convergence. It was shown in [91] that both the BER and the packet error rates are significantly improved in comparison to the receiver using the basic NLMS algorithm. The MSE indicator after receiver training used for packet rejection can be used for ARQ.

An imperfect training signal can be used to train the postcombining LMMSE receivers. The drawback of using the data decisions of the conventional RAKE receiver is the lower convergence rate due to small step-size necessary for proper adaptation. Nevertheless, the results show that although the system does not provide a training sequence, the adaptive postcombining LMMSE receivers can be used. Since the decisions made by the conventional RAKE receiver can be used to train both the precombining and the postcombining LMMSE receivers, a receiver concept which combines these receivers and dynamically switches between them is possible. The switching between the conventional RAKE receiver and the adaptive receivers must be based on the success of the adaptation. With the postcombining LMMSE receivers, this is determined by the rate of fading. The switching with the precombining LMMSE receivers can be based on the correlation between the adaptive and fixed filter components.

4.3. Summary

In this chapter, adaptive LMMSE receivers were studied. Both numerical analysis and computer simulations were used to evaluate the performance and the applicability of the LMMSE receivers in fading channels. It can be concluded that the postcombining LMMSE receiver has potentially higher capacity than the precombining LMMSE receiver. Based on the general convergence analysis, the postcombining LMMSE receivers can only be applied with the highest data rates when the normalized rate of fading is sufficiently small for practical adaptive algorithms. Furthermore, since the adaptive implementations require training sequences, the postcombining LMMSE receivers are mainly suited to such packet data applications where data packets start with a preamble. The precombining LMMSE receivers do not have such convergence requirements and there are in principle no constraints for their use in fading channels.

It was shown by analysis and simulations that the conventional RAKE receiver is often sufficient for training the adaptive LMMSE receivers. The convergence with the adaptive LMMSE-RAKE receiver is faster than with other known blind adaptive receivers based on LMS algorithms. However, when the BER of the conventional RAKE receiver is too high, the adaptation may fail. In those cases, the BER of the basic adaptive LMMSE-RAKE is worse than with the conventional RAKE receivers. In order to avoid the performance degradation in comparison to the conventional RAKE receivers, the adaptive filter branch should be switched off during the periods when the adaptation has failed. The correlation based switching criterion proved to be a robust method for switching dynamically between the conventional RAKE and the adaptive precombining LMMSE receivers. If an additional orthogonality constraint is used in adapting the LMMSE-RAKE receiver, the performance is never worse than with the conventional RAKE receivers. In that case the adaptive filter branch need not and cannot be switched on and off dynamically by using the correlation based switching criterion.

The adaptive LMMSE receivers require relatively short spreading sequences so that multiple-access interference retains cyclo-stationarity which is required in practical adaptive algorithms. It is also necessary that the spreading factor is not too high in order to keep the number of adaptive filter taps low. These requirements are met in the FMA2 concept, where the spreading factor is in the range of $4 - 256$ and the length of the spreading sequence is 256. The lowest spreading factors are used for high data rate services. Hence, a reconfigurable adaptive RAKE receiver, which switches dynamically between the adaptive LMMSE-RAKE, the adaptive postcombining LMMSE and the conventional RAKE receiver is feasible in the FMA2 concept.

Both the postcombining and the precombining LMMSE receivers require timing synchronization. The postcombining LMMSE receivers need only rough symbol synchronization in FSE implementations. The precombining LMMSE receivers, on the other hand, require synchronization at the chip level. Synchronization issues in the precombining LMMSE receivers are discussed in the following chapter.

5. Delay estimation in precombining LMMSE receivers

The research of multiuser detection has also stimulated the studies of near-far resistant channel parameter estimators. Delay estimation in particular has been found to be one of the most demanding problems. The maximum likelihood type delay estimators for multiuser CDMA systems are very complex [57, 181, 196]. One popular research topic in recent years has been subspace based delay estimators [195, 197, 198, 199] derived originally for spectrum estimation [200, 201]. However, it has been shown that the subspace based delay estimators are not efficient in highly loaded CDMA systems [202]. The blind least squares single-user receivers can be used for delay acquisition as was discussed in Section 4.1.2.2. By using the minimum variance principle in deriving the delay estimator, the resulting estimator is of the same form as the blind MOE receiver [107].

This section is organized as follows. The mean acquisition times are analyzed numerically for the noncoherent and coherent matched filter acquisition, the minimum variance method based delay acquisition and subspace based delay estimators in Section 5.1. The inverse of the sample-covariance matrix needed in the minimum variance based acquisition and blind LS receivers will be also utilized in the non-coherent delay-locked loops in Section 5.2 to improve their tracking performance.

5.1. Delay acquisition

Delay acquisition in the precombining LMMSE receivers in multipath fading channels is studied in this section. Delay acquisition in multipath channels is defined to be the case when the delay of at least one multipath component has been found. After that the data reception can begin and the receiver is switched to the tracking mode.

Coherent integration, i.e., integration or summation over several symbol intervals prior to squaring can be used to suppress interference in delay estimation in

systems with a pilot channel in the downlink [31, 203] provided that the frequency error, e.g., due to fading is not too large. In cases when there is no pilot channel available, noncoherent delay estimators may be used. Another possibility is to use decision-directed delay estimators [39]. Near-far resistant delay estimators have better performance than the conventional methods in multiuser CDMA systems. Usually different methods are compared based on the probability of acquisition only. However, a more interesting figure of merit is the mean acquisition time which describes the average time which elapses from the beginning to the end of acquisition. In this section the mean acquisition times are analyzed numerically for different delay estimators suitable to single-user CDMA receivers.

5.1.1. Minimum variance delay estimator

In Section 4.1.2 several blind adaptive receivers were briefly reviewed. Most of the blind adaptive receivers are based on the constrained optimization of the receiver output energy. The principle for solving the constrained optimization problems was not discussed. The usual approach to solve such problems is based on the Lagrange multipliers, which converts the constrained problem into an equivalent unconstrained one. Given the optimization problem

$$\min_{\mathbf{w}_{k,l}} \left\{ \mathbf{w}_{k,l}^{\mathrm{T}} \mathbf{\Sigma}_{\bar{\mathbf{r}}} \mathbf{w}_{k,l} \right\} \qquad \text{subject to } \mathbf{w}_{k,l}^{\mathrm{T}} \bar{\mathbf{s}}_{k,l} = 1, \tag{5.1}$$

where $\mathbf{w}_{k,l}^{\mathrm{T}} \mathbf{\Sigma}_{\bar{\mathbf{r}}} \mathbf{w}_{k,l} = \mathrm{E}\left[|y_{k,l}|^2\right]$ is the minimum output energy of the linear receiver $\mathbf{w}_{k,l}$ for the kth user's lth path with spreading waveform $\bar{\mathbf{s}}_{k,l}$, the Lagrangian is

$$L(\mathbf{w}_{k,l}, \eta) = \mathbf{w}_{k,l}^{\mathrm{T}} \mathbf{\Sigma}_{\bar{\mathbf{r}}} \mathbf{w}_{k,l} + \eta(\mathbf{w}_{k,l}^{\mathrm{T}} \bar{\mathbf{s}}_{k,l} - 1), \tag{5.2}$$

where η is a real number called the Lagrange multiplier. To remove the constraint, the gradient of the Lagrangian is set to zero and the equation is solved for $\mathbf{w}_{k,l}$. In this case the gradient is $2\mathbf{\Sigma}_{\bar{\mathbf{r}}} \mathbf{w}_{k,l} + \eta \bar{\mathbf{s}}_{k,l}$. Setting this to zero gives

$$\mathbf{w}_{k,l} = -\frac{\eta}{2} \mathbf{\Sigma}_{\bar{\mathbf{r}}}^{-1} \bar{\mathbf{s}}_{k,l}, \tag{5.3}$$

which must satisfy the constraint $\mathbf{w}_{k,l}^{\mathrm{T}} \bar{\mathbf{s}}_{k,l} = 1$. Hence, $-(\eta/2) \bar{\mathbf{s}}_{k,l}^{\mathrm{T}} \mathbf{\Sigma}_{\bar{\mathbf{r}}}^{-1} \bar{\mathbf{s}}_{k,l} = 1$ and $\eta = -2\left(\bar{\mathbf{s}}_{k,l}^{\mathrm{T}} \mathbf{\Sigma}_{\bar{\mathbf{r}}}^{-1} \bar{\mathbf{s}}_{k,l}\right)^{-1}$. Using this in (5.3) results in the solution

$$\mathbf{w}_{k,l} = \frac{\mathbf{\Sigma}_{\bar{\mathbf{r}}}^{-1} \bar{\mathbf{s}}_{k,l}}{\bar{\mathbf{s}}_{k,l}^{\mathrm{T}} \mathbf{\Sigma}_{\bar{\mathbf{r}}}^{-1} \bar{\mathbf{s}}_{k,l}}, \tag{5.4}$$

which is the well known form for the minimum variance (MV) beamforming [191] and the MOE receivers [96]. The average output power of the minimum variance or the minimum output energy receiver is given by

$$\mathcal{P}_{[MV]}(\bar{\mathbf{s}}_{k,l}) \quad = \quad \mathrm{E}\left[(\mathbf{w}_{k,l}^{\mathrm{T}} \bar{\mathbf{r}})^2\right] = \mathbf{w}_{k,l}^{\mathrm{T}} \mathbf{\Sigma}_{\bar{\mathbf{r}}} \mathbf{w}_{k,l}$$

$$= \frac{\bar{\mathbf{s}}_{k,l}^{\mathrm{T}}\boldsymbol{\Sigma}_{\bar{\mathbf{r}}}^{-1}}{\bar{\mathbf{s}}_{k,l}^{\mathrm{T}}\boldsymbol{\Sigma}_{\bar{\mathbf{r}}}^{-1}\bar{\mathbf{s}}_{k,l}} \cdot \boldsymbol{\Sigma}_{\bar{\mathbf{r}}} \cdot \frac{\boldsymbol{\Sigma}_{\bar{\mathbf{r}}}^{-1}\bar{\mathbf{s}}_{k,l}}{\bar{\mathbf{s}}_{k,l}^{\mathrm{T}}\boldsymbol{\Sigma}_{\bar{\mathbf{r}}}^{-1}\bar{\mathbf{s}}_{k,l}}$$

$$= (\bar{\mathbf{s}}_{k,l}^{\mathrm{T}}\boldsymbol{\Sigma}_{\bar{\mathbf{r}}}^{-1}\bar{\mathbf{s}}_{k,l})^{-1}. \tag{5.5}$$

The output power is a function of the sampling instant of both the input signal vector and the receiver spreading code. This can be utilized in single-user delay acquisition in several ways as will be explained in the sequel.

In systems utilizing a pilot channel the received signal can be sampled at any timing offset. Given a user with the sampled spreading sequence $\bar{\mathbf{s}}_k$, find the delay for the sequence that maximizes the receiver output power. More formally,

$$\hat{\tau}_{k,l} = \arg\max_{\tau_{k,l}} \mathcal{P}_{[MV]}\big(\bar{\mathbf{s}}_k(\tau_{k,l})\big), \tag{5.6}$$

where $\bar{\mathbf{s}}_{k,l}(\tau_{k,l}) = \bar{\mathbf{s}}_k = [\mathbf{0}_{DSG+\tau_{k,l}}^{\mathrm{T}}, \mathbf{s}_k^{\mathrm{T}}, \mathbf{0}_{DSG-\tau_{k,l}}^{\mathrm{T}}]^{\mathrm{T}}$ and $\tau_{k,l}$ is time-discretized delay in samples. In practice, the covariance matrix $\boldsymbol{\Sigma}_{\bar{\mathbf{r}}}$ is not known and it must be estimated, as was discussed in Section 4.1.2.2.

It was pointed out in Section 4.1.2.3 that the sample-covariance estimation interval for the receiver processing windows larger than one symbol must be rather long to obtain small enough steady-state error. It is therefore beneficial to use as small receiver processing window size as possible. For a processing window size of one symbol interval, the minimum variance delay estimator must be defined in a different way to the case when there is no pilot channel available, i.e., the signal for the desired user contains data modulation. In such a case, the signature sequence must be split into two parts corresponding to two different symbol intervals such that the upper portion of the sequence is

$$\mathbf{s}_{[u]k}(\tilde{\tau}_{k,l}) = \big[s_k(T_s), \ldots, s_k(T_s\tilde{\tau}_{k,l}),\ \mathbf{0}_{(SG-\tilde{\tau}_{k,l})\times 1}^{\mathrm{T}}\big]^{\mathrm{T}}, \tag{5.7}$$

and the lower part is

$$\mathbf{s}_{[l]k}(\tilde{\tau}_{k,l}) = \big[\mathbf{0}_{(\tilde{\tau}_{k,l})\times 1}^{\mathrm{T}},\ s_k(T_s(\tilde{\tau}_{k,l}+1)), \ldots, s_k(T_sSG)\big]^{\mathrm{T}}. \tag{5.8}$$

The minimum-variance delay estimator will be then

$$\hat{\tau}_{k,l} = \arg\max_{\tilde{\tau}_{k,l}} \Big(\mathbf{s}_{[u]k}(\tilde{\tau}_{k,l})^{\mathrm{T}}\hat{\boldsymbol{\Sigma}}_{\bar{\mathbf{r}}}^{-1}\mathbf{s}_{[u]k}(\tilde{\tau}_{k,l}) + \mathbf{s}_{[l]k}(\tilde{\tau}_{k,l})^{\mathrm{T}}\hat{\boldsymbol{\Sigma}}_{\bar{\mathbf{r}}}^{-1}\mathbf{s}_{[l]k}(\tilde{\tau}_{k,l})\Big)^{-1}. \tag{5.9}$$

If the receiver processing window is large enough, the scheme (5.6) can be used even if there is no pilot channel available. In fact, the sufficient conditions for using this scheme in delay acquisition is that the receiver processing window is two symbol intervals long. This guarantees that at least one full symbol is inside the processing window. Another possibility would be to estimate the covariance matrix over one symbol interval with all trial delays while keeping the sampled spreading sequence fixed. This approach, however, is computationally demanding and impractical.

5.1.2. Subspace based delay estimators

Subspace based estimators have been proposed for single-user delay delay estimation in CDMA systems in [195, 197, 198, 199]. In this Section, a non-traditional interpretation of subspace based delay estimators is given and the connection to the minimum variance based method is presented. The minimum variance based delay estimator will also be compared to the subspace based delay estimators by some numerical examples.

The subspace delay estimators [197] are based on the eigenvalue decomposition of the covariance matrix [21, p. 166]: $\mathbf{\Sigma}_{\bar{\mathbf{r}}} = \mathbf{U}\mathbf{\Lambda}\mathbf{U}^{\mathrm{H}}$, where $\mathbf{U} = \left[\mathbf{u}_1, \ldots, \mathbf{u}_{SGM}\right] \in \mathbb{C}^{SGM}$ is a matrix of the eigenvectors ($\mathbf{u}_i$, $i \in \{1, \ldots, SGM\}$) and $\mathbf{\Lambda} = \mathrm{diag}(\lambda_i) \in \mathbb{R}^{SGM}$ is a diagonal matrix of the eigenvalues ($\lambda_i, i \in \{1, \ldots, SGM\}$) of the covariance matrix. The connection between the minimum variance, MUSIC (multiple signal classification [201]) and the eigenvector (EV) based estimators can be explained by different estimators for the inverse of the sample-covariance matrix. The inverse of the covariance matrix can be presented by using the eigenvectors and the corresponding eigenvalues [21]. By doing so, the inverse of the covariance matrix for the minimum variance delay estimator can be written as

$$\mathbf{\Sigma}_{\bar{\mathbf{r}}}^{-1} = \mathbf{U}\mathbf{\Lambda}^{-1}\mathbf{U}^{\mathrm{H}} = \sum_{i=1}^{SGM} \lambda_i^{-1}\mathbf{u}_i\mathbf{u}_i^{\mathrm{H}}. \tag{5.10}$$

The differences between the minimum variance and subspace based methods may be interpreted as follows: the first one takes advantage of all eigenvalues and corresponding eigenvectors, whereas subspace based schemes use only a subset of those in estimating the inverse of the sample-covariance matrix.

The eigenvector based method [191, 204] uses only the $SGM - KL$ smallest eigenvalues and corresponding eigenvectors, which span the noise subspace. Hence, the inverse of the covariance matrix is estimated as

$$\hat{\mathbf{\Sigma}}_{\bar{\mathbf{r}}[EV,n]}^{-1} = \sum_{i=KL+1}^{SGM} \lambda_i^{-1}\mathbf{u}_i\mathbf{u}_i^{\mathrm{H}}, \tag{5.11}$$

where $\lambda_i \geq \lambda_j, \forall i < j$. The MUSIC algorithm [201] neglects the weights for the eigenvectors, i.e., all eigenvalues are set to unity. The inverse of the covariance matrix with the MUSIC algorithm is approximated as

$$\hat{\mathbf{\Sigma}}_{\bar{\mathbf{r}}[MUSIC,n]}^{-1} = \sum_{i=KL+1}^{SGM} \mathbf{u}_i\mathbf{u}_i^{\mathrm{H}}. \tag{5.12}$$

It is also possible to use the signal-plus-noise subspace [191, p. 377] (referred to as the signal subspace in the reminder of the thesis), which results in the covariance matrix inverse estimates as

$$\hat{\mathbf{\Sigma}}_{\bar{\mathbf{r}}[MUSIC,s]}^{-1} = \sum_{i=1}^{KL} \mathbf{u}_i\mathbf{u}_i^{\mathrm{H}}. \tag{5.13}$$

Due to the fact that [21, p. 166] $\mathbf{U}\mathbf{U}^{\mathrm{H}} = \mathbf{I}$ and

$$\begin{aligned}
\max\left(\mathcal{P}_{[MUSIC,n]}\right) &= \max\left(\bar{\mathbf{s}}_{k,l}^{\mathrm{T}} \sum_{i=KL+1}^{SGM} \mathbf{u}_i \mathbf{u}_i^{\mathrm{H}} \bar{\mathbf{s}}_{k,l}\right)^{-1} \\
&= \max\left(\bar{\mathbf{s}}_{k,l}^{\mathrm{T}} \left(\mathbf{I} - \sum_{i=1}^{KL} \mathbf{u}_i \mathbf{u}_i^{\mathrm{H}}\right) \bar{\mathbf{s}}_{k,l}\right)^{-1} \\
&= \min\left(\bar{\mathbf{s}}_{k,l}^{\mathrm{T}} \sum_{i=1}^{KL} \mathbf{u}_i \mathbf{u}_i^{\mathrm{H}} \bar{\mathbf{s}}_{k,l}\right)^{-1} \\
&= \min\left(\mathcal{P}_{[MUSIC,s]}\right), \qquad (5.14)
\end{aligned}$$

the output power must be minimized when using the signal subspace.

5.1.3. Conventional delay estimators

The conventional non-coherent delay estimator is simply obtained by setting $\mathbf{w}_{k,l} = \bar{\mathbf{s}}_{k,l}$. The output power of the conventional matched filter is then

$$\mathcal{P}_{[MF]}(\bar{\mathbf{s}}_{k,l}) = \mathrm{E}\left[(\bar{\mathbf{s}}_{k,l}^{\mathrm{T}} \bar{\mathbf{r}})^2\right] = \bar{\mathbf{s}}_{k,l}^{\mathrm{T}} \boldsymbol{\Sigma}_{\bar{\mathbf{r}}} \bar{\mathbf{s}}_{k,l}. \qquad (5.15)$$

The conventional delay estimator with extended despreading interval is obtained by modifying the sampled signature sequence so that the sequence is repeated several times, i.e.,

$$\begin{aligned}
\bar{\mathbf{s}}_{k,l} &= \Big[\left[s_k(T_s(SG - \tau_{k,l} + 1), \ldots, s_k(T_s SG)\right], \left[\mathbf{1}_{(M_{ext}-1)} \otimes \mathbf{s}_k\right]^{\mathrm{T}}, \\
&\qquad \left[s_k(T_s), \ldots, s_k(T_s(SG - \tau_{k,l}))\right]\Big]^{\mathrm{T}} \in \mathbb{R}^{M_{ext}SG}, \qquad (5.16)
\end{aligned}$$

where M_{ext} is the so-called coherent (or extended) integration time in symbols[1]. Hence, by multiplying an input vector $\bar{\mathbf{r}}$ of length M_{ext} symbol intervals by the extended sequence $\bar{\mathbf{s}}_{k,l}$ the despreading interval prior to squaring is M_{ext} symbols.

There are several strategies for spreading code timing acquisition. For examples, see [32] and references therein. In this thesis, only the matched filter type acquisition based on the maximum selection is considered. The mean acquisition time for such acquisition schemes in fading multipath channels is presented in the next section.

[1] $\mathbf{Z} = \mathbf{X} \otimes \mathbf{Y} \in \mathbb{C}^{x_1 y_1 \times x_2 y_2}$ denotes the Kronecker product between matrices $\mathbf{X} \in \mathbb{C}^{x_1 \times x_2}$ and $\mathbf{Y} \in \mathbb{C}^{y_1 \times y_2}$, i.e., all components of the matrix $\mathbf{X}$ are multiplied by the matrix $\mathbf{Y}$.

5.1.4. Acquisition time analysis

The acquisition scheme considered here is based on the maximum selection of the matched filter output, either by using the conventional techniques or the covariance matrix inverse based schemes. The mean acquisition time analysis is based on the unified theory of the timing acquisition presented in [34, 205, 206]. The analysis starts with the acquisition process state diagram, presented in Figure 5.1.

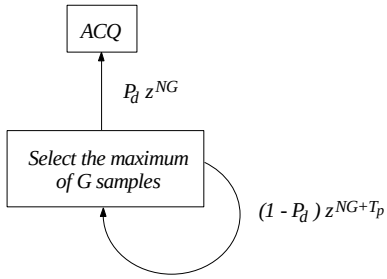

Fig. 5.1. State diagram for the acquisition process.

For the acquisition process of Figure 5.1, the so-called acquisition state (ACQ) generating function [34] is

$$P_{[ACQ]}(z) = \frac{P_d z^{NG}}{1-(1-P_d)z^{NG+T_P}}, \tag{5.17}$$

where P_d is the probability for detecting the correct delay (or probability of acquisition within the observation interval), G is the processing gain, N is the observation interval in symbols, T_P is the so-called false alarm penalty time in chip intervals, and z is the unit chip delay operator. The penalty time is the time which is consumed after a false acquisition. The probability of detection is defined in multipath channels as the probability of finding one of the L multipath components. The mean acquisition time can be determined as [34]

$$T_{MA} = \left(\frac{\partial}{\partial z} P_{[ACQ]}(z)\big|_{z=1} \right) T_c = \frac{NG + T_P(1-P_d)}{P_d} T_c, \tag{5.18}$$

where T_c is the chip interval. Given the probability of acquisition and the false alarm penalty time, the mean acquisition time can be easily determined.

5.1.5. Numerical examples

A semi-analytic approach is used in determining the mean acquisition time for the conventional non-coherent, conventional non-coherent with extended despreading interval, and the minimum variance method based matched filter delay acquisition schemes. The probability of acquisition was simulated with the following parameters: carrier frequency 2.0 GHz, symbol rate 16 kbits/s, 31 chip Gold code, and rectangular chip shape. A synchronous downlink case with equal energy two-path ($L = 2$) Rayleigh fading channel with vehicle speeds of 40 km/h (which results in the maximum normalized Doppler shift of $4.63 \cdot 10^{-3}$) was studied and the maximum delay spread was 10 μs. The number of users was 5 – 30 and the average SNR 10 dB. The receiver processing window of size one symbol ($M = 1$) and one sample per chip ($S = 1$) was used. An unmodulated pilot channel was used in all cases for delay acquisition of the form (5.6). The observation intervals considered in delay acquisition were between 10 – 500 symbol intervals. After averaging over the observation interval, the maximum values of the delay estimator output are searched. The correct code acquisition is declared if one of the multipath components is found. The false alarm penalty time (T_P) used in the mean acquisition time analysis was 500 symbol intervals.

The probabilities of acquisition for the schemes studied are presented in Figure 5.2 as a function of the number of users with the observation interval of 200 symbols. The results indicate that the minimum variance based method improves the acquisition performance in comparison to the conventional non-coherent acquisition. With larger system loads both methods give relatively poor acquisition performance, whereas the conventional acquisition scheme with the extended despreading interval also performs well in those cases. The subspace based delay estimators give good performance when the number of users is relatively low. According to these results, the maximum number of users in the two-path channels is between 10 and 20 to obtain acceptable performance. After the number of signal components exceeds the dimensions of the sample-covariance matrix, the subspace based delay estimators are not defined. Similar results have been reported in [202]. It can be also seen from Figure 5.2 that the iterative sample-covariance updating method (4.34) results in almost the same acquisition performance as the direct inversion method.

The mean acquisition times as a function of the observation intervals for the different methods are presented in Figures 5.3 – 5.5. Based on the results it has been possible to select the optimum observation interval for each scheme for a given number of users. Using the optimum observation intervals, the mean acquisition times of the different schemes are shown in Figure 5.6 as a function of the number of users. With relatively small system loads, the conventional non-coherent acquisition scheme results in a shorter mean acquisition time than the minimum variance based method. This is due to the fact that reliable sample-covariance estimation requires close to one hundred symbol intervals. When the number of users increases, more averaging is required with the conventional scheme and it is beneficial to use the minimum variance based delay acquision method. As we can see, the iterative implementation of the minimum variance method

according to (4.34) impairs the performance only slightly.

Assuming the bit rate of 16 kbit/s, the mean acquisition times in a 30-user case for different schemes are: conventional MF 0.63 s, minimum variance method 0.38 s, conventional MF with extended despreading interval 1 ms. Assuming the same probabilities for detection also with higher spreading factors under the same relative system load, the corresponding numbers with spreading factor of 256 would be roughly: 5 s for the conventional MF, 3 s for the minimum variance method and 8 ms for the conventional MF with extended despreading interval. The difference in the mean acquisition times for the conventional MF and the minimum variance methods is large enough to seriously consider the use of the minimum variance method based acquisition in practical systems.

5.1.6. Discussion

Code acquisition performance of the CDMA downlink receivers with several methods in a frequency-selective fading channel was studied in this section. The conventional acquisition scheme with an extended despreading interval clearly gives the best performance amongst the schemes studied. Unfortunately the scheme cannot be used in all CDMA systems. The extended integration requires either an unmodulated pilot channel or a control channel with a low data rate. The first approach has been used in the IS-95 system. The latter approach would be suitable for systems where pilot symbols of lower rate are used for channel estimation. This is the case in the WCDMA and FMA2 concepts, where the control channel containing pilot symbols always has the data rate of 16 kbit/s, whereas, the data channel has a varying data rate up to 2 Mbit/s.

The iterative minimum variance based delay acquisition can be used to improve the acquisition performance of the conventional non-coherent method. Based on the results, the minimum variance method gives the best performance among the advanced acquisition schemes studied. The practical iterative version of the scheme also performs well and seems to result in reasonable mean acquisition times.

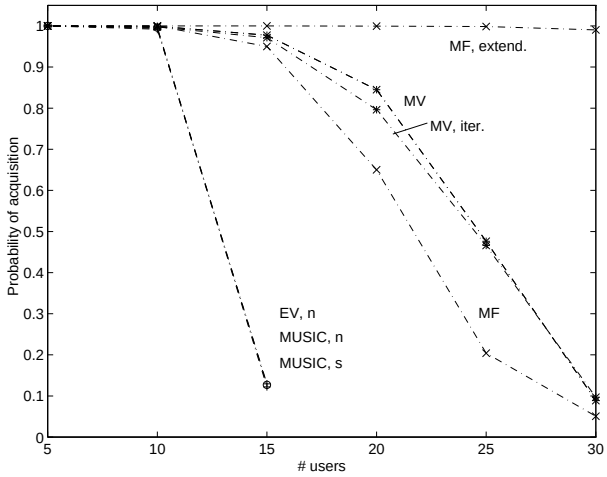

Fig. 5.2. Probability of acquisition for different delay acquisition schemes as a function of the number of users in a two-path Rayleigh fading channel with vehicle speeds of 40 km/h, average SNR of 10 dB, and observation intervals of 200 symbols.

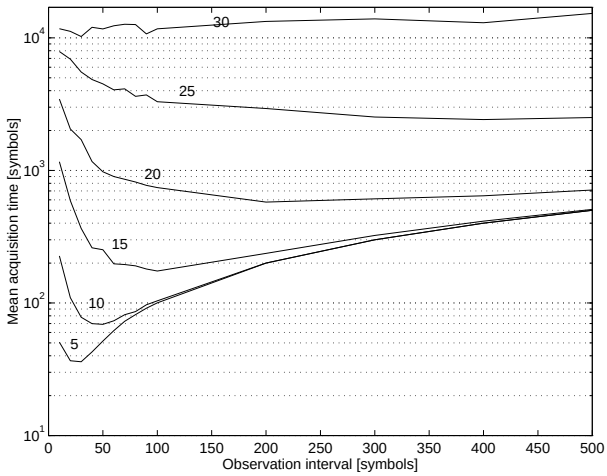

Fig. 5.3. Mean acquisition times for the conventional non-coherent delay acquisition as a function of the observation interval in a two-path Rayleigh fading channel with vehicle speeds of 40 km/h, average SNR of 10 dB, and 5, 10, 15, 20, 25 and 30 users.

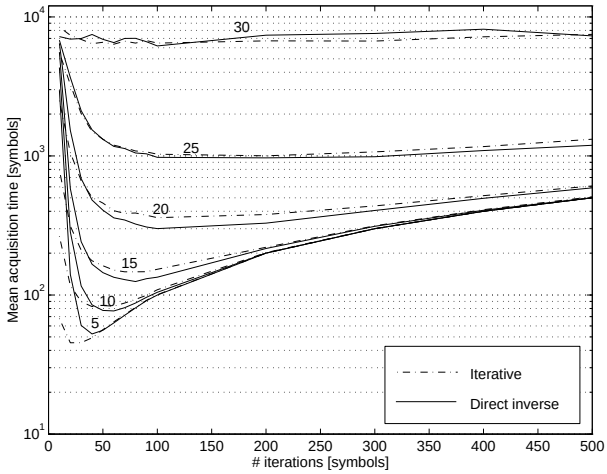

Fig. 5.4. Mean acquisition times for the minimum variance method based delay acquisition schemes with direct and iterative sample-covariance inverse computation as a function of the observation interval in a two-path Rayleigh fading channel with vehicle speeds of 40 km/h, average SNR of 10 dB, and 5, 10, 15, 20, 25 and 30 users.

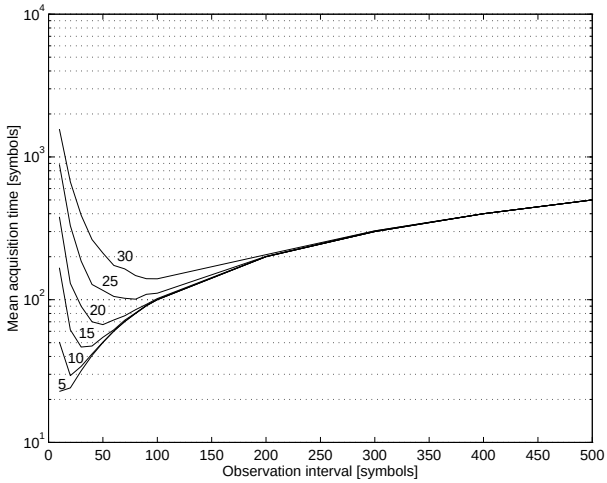

Fig. 5.5. Mean acquisition times for the conventional non-coherent delay acquisition with extended despreading interval as a function of the observation interval in a two-path Rayleigh fading channel with vehicle speeds of 40 km/h, average SNR of 10 dB, and 5, 10, 15, 20, 25 and 30 users.

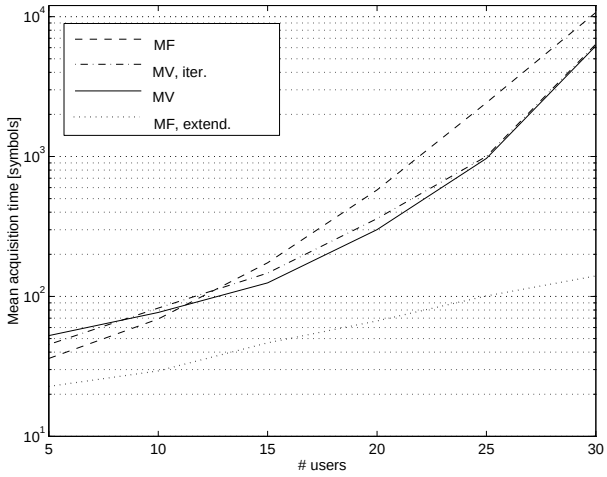

Fig. 5.6. Mean acquisition times for the conventional non-coherent scheme, the conventional non-coherent scheme with extended despreading interval, the minimum variance method with direct and the iterative sample-covariance inverse computation based delay acquisition scheme with the optimum observation interval as a function of the number of users in a two-path Rayleigh fading channel with vehicle speeds of 40 km/h, and average SNR of 10 dB.

5.2. Delay tracking

The adaptive LMMSE-RAKE receivers, as well as other blind adaptive receivers, require continuous delay tracking. The fixed portion in the filter weight vector must be updated according to the channel delay. Without the decomposition of the filter weights into fixed and adaptive components, the delay tracking could be omitted. Nevertheless, the reference signal cannot be provided by the conventional RAKE without the knowledge of the delays.

The BER sensitivity of the precombining LMMSE receivers to the delay errors is examined in Section 5.2.1. The minimum variance method is then developed in Section 5.2.2 for delay tracking in the blind adaptive LS receivers.

5.2.1. BER sensitivity to delay estimation errors

Linear receivers are known to be rather sensitive to delay estimation errors. It was shown in [63] that delay errors of as little as 0.1 of a chip interval can degrade

the performance of the decorrelating receiver so as to render the receiver useless. The reason for the sensitivity of the linear receivers to delay estimation errors is intuitively clear. The usual way to define the LMMSE receiver is based on the form $\mathbf{w}_{k,l} = \left(\mathbf{S}(\mathbf{R} + \sigma^2/(\mathbf{A}^{\mathrm{T}}\mathbf{A}))^{-1}\right)_{k,l}$, where $(\cdot)_{k,l}$ denotes the column corresponding to the kth user's lth path receiver vector. In the case of delay estimation errors, the cross-correlation matrix $\mathbf{R}$ has mismatch, which will be amplified in matrix inversion. By using the other form of the precombining LMMSE receivers, namely $\mathbf{w}_{k,l} = \mathbf{\Sigma}_{\bar{\mathbf{r}}}^{-1}\bar{\mathbf{s}}_{k,l}$, the mismatch due to timing errors does not influence the inverse and the performance degradation is less severe given that the vector $\bar{\mathbf{s}}_{k,l}$ spans at least one symbol interval plus the multipath spread (see p. 106). Therefore, the latter way of computing the precombining LMMSE receivers is more robust against delay estimation errors. The blind LS receivers (Section 4.1.2.2) are explicitely of the latter form, and should be more robust against timing errors.

The sensitivity to timing errors was studied by using the bit error probability analysis presented in Section 3.1.1. For curiosity, both the Gaussian approximation and the exact analysis were used. The parameters in the analysis were the same as in Section 3.1.3. It should be emphasized that the rectangular chip waveform was used and hence, the results are slightly pessimistic. Both multipath components had the same fixed absolute delay error. The results are presented in Figure 5.7.

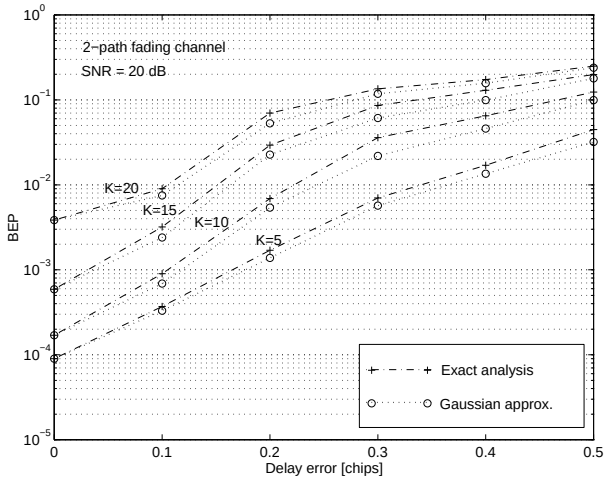

Fig. 5.7. Bit error probabilities (BEP) as a function of the delay error for the precombining LMMSE receiver for both the exact analysis and with the Gaussian approximation in two-path fading channels with vehicle speeds of 40 km/h and average SNRs of 20 dB.

Firstly, the Gaussian approximation is quite accurate for the precombining LMMSE receivers with delay errors at least without near-far problem. The re-

sults indicate that the timing accuracy requirements are of the order of 0.1 chips in order to not degrade performance too much in a system with power control. In the next section, delay tracking for the blind LS receivers is studied.

5.2.2. Delay tracking in blind LS receivers

The minimum variance delay estimator presented in Section 5.1.1 and the blind LS receiver of Section 4.1.2.2 will be extended to consider delay tracking in this section. The motivation is, of course, to improve the tracking performance of the conventional non-coherent DLLs. It is assumed that the receiver has estimated the covariance matrix $\mathbf{\Sigma}_{\bar{\mathbf{r}}}$ and the inverse is available for delay tracking.

In delay acquisition, the received signal is used to construct an estimate of the covariance matrix. Once the inverse of the covariance matrix exists, the delay can be acquired by finding the maximum output power for the MOE based receiver. In delay tracking the inverse of the covariance matrix already exists and it is updated as the channel changes. The approach taken in delay tracking is to pre-process the received signal by multiplying it by the inverse of the sample-covariance matrix in order to suppress interference due to other users. After the pre-processing, the received signal is despread and a delay-locked loop (DLL) is used to track the best timing position [2]. Since the early and the late phased sequences do not match the best timing position (on-time) some of the near-far resistance will be lost[2]. However, if the early-late difference is not very large, the loss should be tolerable. This can also be seen from Figure 5.7. With 0.5 chip timing offset, the BER is degraded significantly, whereas, an offset of $0.1 - 0.2$ chip intervals results in rather good BER performance.

The signal at the output of the despreading device during the nth symbol interval is

$$y_{k,l}^{(n)}(\hat{\tau}_{k,l}^{(n)}) = \bar{\mathbf{s}}_{k,l}^{\mathrm{T}}(\hat{\tau}_{k,l}^{(n)})\hat{\mathbf{\Sigma}}_{\bar{\mathbf{r}}}^{-1}\bar{\mathbf{r}}^{(n)}, \tag{5.19}$$

where $\hat{\tau}_{k,l}^{(n)}$ is the time-discretized delay estimate during the nth symbol interval. The delay estimator with an observation interval $\mathcal{T}$ symbols maximizes the function

$$\hat{\tau}_{k,l}^{(n)} = \arg\max_{\tau_{k,l}} \sum_{j=n-\mathcal{T}+1}^{n} \left(y_{k,l}^{(j)}(\tau_{k,l})\right)^2. \tag{5.20}$$

Instead of direct maximization, (5.20) can be solved by setting the derivative to zero. The DLLs are based on the approximation of the derivative by the early and late difference. In practice the received signal is despread with early and late phased sequences and the difference produced by them is driven towards zero in the feedback loop [2]. By applying the early-late approximation for the derivative results in the timing error signal

$$e_{k,l}^{(n)} = \left(\bar{\mathbf{s}}_{k,l}^{\mathrm{T}}(\hat{\tau}_{k,l}^{(n)} + \Delta)\hat{\mathbf{\Sigma}}_{\bar{\mathbf{r}}}^{-1}\bar{\mathbf{r}}^{(n)}\right)^2 - \left(\bar{\mathbf{s}}_{k,l}^{\mathrm{T}}(\hat{\tau}_{k,l}^{(n)} - \Delta)\hat{\mathbf{\Sigma}}_{\bar{\mathbf{r}}}^{-1}\bar{\mathbf{r}}^{(n)}\right)^2$$

[2]The sample-covariance is estimated for the on-time code phase.

$$= \left(y_{k,l}^{(n)}(\hat{\tau}_{k,l}^{(n)} + \Delta)\right)^2 - \left(y_{k,l}^{(n)}(\hat{\tau}_{k,l}^{(n)} - \Delta)\right)^2, \tag{5.21}$$

where 2Δ is the early-late difference in chip intervals. Due to the squaring, the resulting DLL is non-coherent. The block diagram of the proposed improved DLL is given in Figure 5.8.

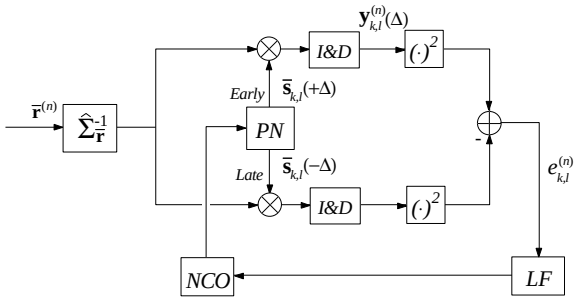

Fig. 5.8. The block diagram of the improved DLL suitable for the blind LS receivers.

5.2.3. Tracking error analysis

The exact analysis of the feedback loops leads to difficult mathematical problems [33]. In particular, the dependence of the loop noise power spectral density on the estimated parameter value causes problems in the analysis. To simplify the analysis, the so-called linear analysis methods are used [17], where the loop noise power spectrum is evaluated at the equilibrium point, i.e., $e_{k,l} = 0$. Furthermore, if the loop bandwidth [207] is narrow, the loop noise power spectrum can be assumed to be constant within the loop band in many cases. With these assumptions, the code tracking error variance can be presented as [17, 33, 35, 208]

$$\mathrm{var}(\hat{\tau}) = \frac{1}{[s'(0)]^2}\frac{\sigma^2}{E_b}\left(1 + \zeta\frac{\sigma^2}{E_b}\right)2B_L T, \tag{5.22}$$

where $s'(0)$ is the slope of the s-curve at the origin, ζ is the squaring-loss obtained from the pulse shape after pre-processing and $2B_L T$ is the normalized two-sided loop bandwidth.

Using this simplified analysis, the aim is to show that the tracking error variance can be made smaller by pre-processing the received signal by multiplying the received signal vector by the inverse of the covariance matrix prior to squaring. The analysis will be carried out in a two path fading channel assuming that the multipath components are distinguishable and do not cause any distortion to the s-curves. This assumption means that the fading processes are uncorrelated and

the loop filter is sufficiently narrow to average the fading, i.e., the s-curves are completely stable (see Section 6.2.2.2). For more accurate analysis in fading multipath channels, the methods presented in [36] could be used. It is also assumed that the loop noise is white and Gaussian. Therefore, the multiple-access interference is modelled as additional white Gaussian noise. Applying the Gaussian approximation presented in Section 3.1.2, the noise variance in a multipath channel with equal energy paths for the improved DLL can be written as

$$\begin{aligned}\sigma^2 &= \sum_{k'=1,k'\neq k}^{K} \frac{A_{k'}^2}{A_k^2} \sum_{l'=1}^{L} \bar{\mathbf{s}}_{k',l'}^{\mathrm{T}} \boldsymbol{\Sigma}_{\bar{\mathbf{r}}}^{-1} \bar{\mathbf{s}}_{k,l}(\Delta) \\ &+ \sum_{l'=1,l'\neq l}^{L} \left(\bar{\mathbf{s}}_{k,l'}^{\mathrm{T}} \boldsymbol{\Sigma}_{\bar{\mathbf{r}}}^{-1} \bar{\mathbf{s}}_{k,l}(\Delta)\right)^2 + \sigma^2 \left(\boldsymbol{\Sigma}_{\bar{\mathbf{r}}}^{-1} \bar{\mathbf{s}}_{k,l}(\Delta)\right)^2. \qquad (5.23)\end{aligned}$$

For the conventional DLL, $\boldsymbol{\Sigma}_{\bar{\mathbf{r}}}^{-1} = \mathbf{I}$. The Gaussian approximation is degraded slightly due to the timing offset of the spreading sequence of the desired component $\bar{\mathbf{s}}_{k,l}(\Delta)$ (see Figure 5.7). The Gaussian approximation is also less accurate for the conventional DLL (see Figure 3.2).

5.2.4. Numerical examples

The DLL parameters used in the code tracking variance analysis are presented in Table 5.1. The other parameters user were: root raised cosine filtering with roll-off 0.5, 31 chip Gold sequences, two-path fading channels with vehicle speed of 40 km/h (which results in the maximum normalized Doppler shift of $4.63 \cdot 10^{-3}$), 2.0 GHz carrier frequency, and two-sided normalized loop bandwidth $2B_LT = 0.04$. The slope of the s-curve at the origin is larger and the squaring loss smaller for the MV-DLL when the early-late difference is smaller. The smaller the early-late difference, the more efficiently interference can be suppressed. Hence, it can be expected that the tracking performance can be improved with small early-late differences by using the pre-processing described earlier. The tracking error analysis results are presented in Figure 5.9 for the SNR of 10 dB and in Figure 5.10 for the SNR of 20 dB. According to the results, the pre-processing is useful with small early-late differences, as expected. The improved tracking performance with smaller early-late differences has the cost of decreased mean-time-to-lose-lock (MTLL), which is proportional to the s-curve area [209]. However, in mobile communications, the MTLL is not as important a parameter as the tracking variance due to fast changes in channel multipath profile.

Table 5.1. The s-curve slope and the squaring loss for the conventional and the improved non-coherent DLLs with various early-late differences (2Δ).

	Conv. DLL		MV-DLL	
2Δ	$s'(0)$	ζ	$s'(0)$	ζ
1.0	3.94	2.66	2.38	5.42
0.75	4.19	1.56	3.86	2.63
0.50	2.70	1.16	4.68	1.53

5.2.5. Discussion

The tracking performance of the conventional and an improved non-coherent DLLs was studied. It was noticed that due to mismatch in the sample-covariance inverse for the early and late phased spreading codes, the method improves the performance of the non-coherent DLLs only with small early-late differences, i.e., when the mismatch is small. If the inverse for the sample-covariance is separately available for the early and late phased correlators, the performance of the improved DLLs would always be better than with the conventional non-coherent DLLs. In such a case the early-late correlator outputs would be computed according to $y_{k,l}^{(n)}(\pm\Delta) = \bar{\mathbf{s}}_{k,l}^{\mathrm{T}}(\pm\Delta)\mathbf{\Sigma}_{\bar{\mathbf{r}}(\pm\Delta)}^{-1}\bar{\mathbf{r}}^{(n)}$. The computation of the early-late inverse sample-covariance matrices $\mathbf{\Sigma}_{\bar{\mathbf{r}}(\pm\Delta)}^{-1}$ would increase the blind LS receiver complexity.

It is worth noting that with the sample-correlate-choose-largest (SCCL) [210] loops, the difference between the advanced and retarded correlators is usually one sample, and the pre-processing with the sample-covariance matrix is well suited to those loops. The SCCL loops will be studied in Section 6.2.2.3 with interference cancellation receivers. Another issue to be mentioned is the small early-late differences required in multipath channels to diminish s-curve distortions caused by nonideal signature sequence autocorrelation properties. Therefore, the improved delay tracking scheme studied in this section can be applied in spread-spectrum receivers operating in multipath channels.

5.3. Summary

The timing synchronization aspects of the adaptive precombining LMMSE receivers were considered in this section. The minimum variance method based delay acquisition method and the improved delay tracking method are well suited to the blind adaptive LS receivers. Also, the classic subspace based delay estimator principles were presented. The mean acquisition time analysis showed that the acquisition performance of the conventional non-coherent matched filter scheme can be improved by using the minimum variance method. Similarly, the track-

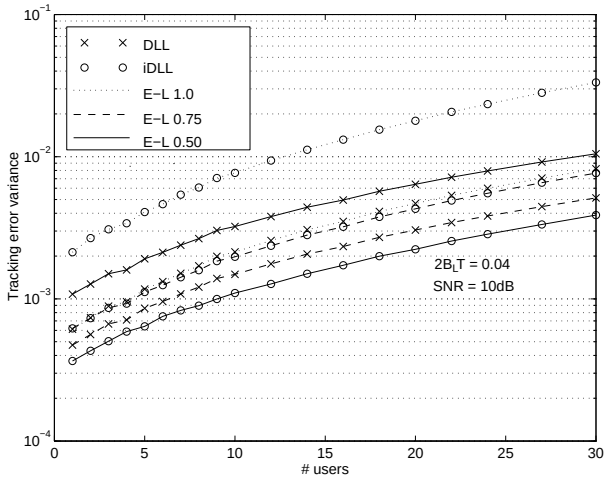

Fig. 5.9. Tracking error variances as a function of the number of users for the conventional (DLL) and the improved (iDLL) non-coherent DLLs with $2\Delta = 1.0$, 0.75 and 0.50 at the SNR of 10 dB and loop bandwidth $2B_LT = 0.04$.

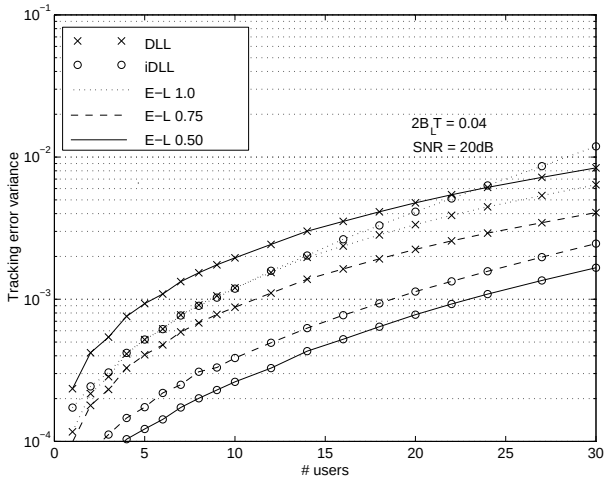

Fig. 5.10. Tracking error variances as a function of the number of users for the conventional (DLL) and the improved (iDLL) non-coherent DLLs with $2\Delta = 1.0$, 0.75 and 0.50 at the SNR of 20 dB and loop bandwidth $2B_LT = 0.04$.

ing performance of the non-coherent DLLs can be improved by pre-processing the received signal by the inverse of the sample-covariance matrix. However, if the system provides an unmodulated pilot channel, the conventional MF based delay estimation with extended despreading interval was shown to result in good delay acquisition performance.

6. Parallel interference cancellation based multiuser receivers

The optimal multiuser MLSD receiver makes the data decisions based on the whole received data block according to

$$\hat{\mathbf{b}} = \arg \max_{\mathbf{b} \in \Xi^{N_b K}} p(\mathbf{y}|\mathbf{b}), \tag{6.1}$$

where $p(\mathbf{y}|\mathbf{b})$ is the Gaussian probability density function of the matched filter bank output vector $\mathbf{y} \in \mathbb{C}^{KLN_b}$ conditioned on the data vector $\mathbf{b}$. The optimal MLSD receiver is decoupled into an estimator which estimates the received noiseless signal and a correlator, which correlates the received signal with this estimate. The multiuser estimator-correlator receiver [13] for frequency-selective Rayleigh fading channels has the forms [25]

$$\begin{aligned} \hat{\mathbf{b}} &= \arg \min_{\mathbf{b} \in \Xi^{N_b K}} \mathbf{y}^{\mathrm{H}} \boldsymbol{\Sigma}_{\mathbf{y}|\mathbf{b}}^{-1} \mathbf{y} \\ &= \arg \max_{\mathbf{b} \in \Xi^{N_b K}} \hat{\mathbf{h}}_{[MMSE]}^{\mathrm{H}} \mathbf{y}, \end{aligned} \tag{6.2}$$

where $\boldsymbol{\Sigma}_{\mathbf{y}|\mathbf{b}}$ is the MF bank output covariance matrix conditioned on the data vector and $\hat{\mathbf{h}}_{[MMSE]} = \left(\mathbf{R} + \sigma^2 \boldsymbol{\Sigma}_{\mathbf{h}|\mathbf{b}}\right)^{-1} \mathbf{y}$ is the MMSE estimate of the product vector between the channel coefficients and data, conditioned on the data vector. The estimation and correlation must be performed for all possible data sequences, and thus, the MLSD receiver is very complex. Moreover, the optimal multiuser receiver for multipath fading channels consists of multi-dimensional joint channel estimation and detection problems, and thus, the optimal multiuser receiver for fading channels is even more complex than the optimal receiver for AWGN channels. For that reason, several suboptimal multiuser detectors have been proposed, see e.g., [4, 5, 6, 25] and references therein. Suboptimal multiuser receivers based on parallel interference cancellation are considered in the reminder of the thesis. Data detection, channel estimation, delay acquisition, delay tracking, inter-cell interference suppression and array processing in the PIC receivers are studied.

6.1. PIC receivers in frequency-selective fading channels

The most usual way to approximate the optimal MLSD receiver is to separate the data detection and channel estimation problems. In Chapter 3, it was pointed out that the precombining interference suppression type receivers have the property that the multiuser interference suppression filter is independent of the channel coefficients. Hence a natural way to decompose the data detection and channel estimation problems is to estimate the channel at the output of the multiuser interference suppression or cancellation device by applying the conventional single-user channel estimation techniques. This type of multiuser receivers have been found to result in good performance in both linear and non-linear multiuser receivers operating in fading channels [25, 174] and are also studied in this thesis.

If LMMSE receivers are the most promising for the single-user downlink receivers, parallel interference cancellation receivers are for the multiuser uplink receivers. The capacity and the performance of the PIC receivers has been found to result in superior performance in comparison to other practical multiuser receivers in frequency-selective fading channels [25]. The parallel interference cancellation receivers are relatively simple to implement at the base stations which demodulate the signals of all users. The PIC method can be applied to data detection as well as to channel parameter estimation [40]. In data detection, parallel interference cancellation is used in the multistage algorithm [114] at each cancellation stage. The PIC based delay tracker [40] is quite similar to the expectation maximization delay estimator presented in [146]. The EM algorithm has been used in [116] for estimating the complex channel coefficients in a multistage receiver. The recursive algorithm developed in [116] is equivalent to the PIC based channel estimator [40]. The direction-of-arrival estimation problem is similar to that of delay estimation, and hence the space alternating generalized EM algorithm for joint demodulation in antenna array receivers in multiuser CDMA systems proposed in [144] can also be presented in the PIC framework.

There are two possibilities to implement PIC receivers in practice. Interference cancellation can take place either before or after matched filtering. The block diagrams of the two options are given in Figures 6.1(a) and 6.1(b). The receivers are mathematically equivalent and have the same performance. However, the receiver structure of Figure 6.1(b) enables the use of near-far resistant delay estimators without additional complexity if the delay estimator uses the signal after interference cancellation. The algorithm derivations given in the reminder of the thesis are based mainly on the receiver structure of Figure 6.1(a) to keep notations as simple as possible. Nevertheless the receiver algorithms can be applied to both receivers regardless of the notations used.

The parallel interference cancellation receivers are based on the optimal ML receiver which minimizes the squared Euclidean norm $\|\mathbf{r} - \mathbf{SCAb}\|^2$ with respect to all unknown, but deterministic parameters. The approach is suboptimal in time-varying channels but is found to result in practical receiver algorithms [17] even in the case when the joint estimation problem is decoupled. In PIC receivers, the optimal ML receiver is approximated further so that when estimating the parameters of the kth user's lth path, it is assumed that the other users parameters

are known. The contribution of the other users in the decision statistics is taken into account by subtracting an estimate of the multiple access interference before data detection. The parallel interference cancellation principle is derived in the sequel.

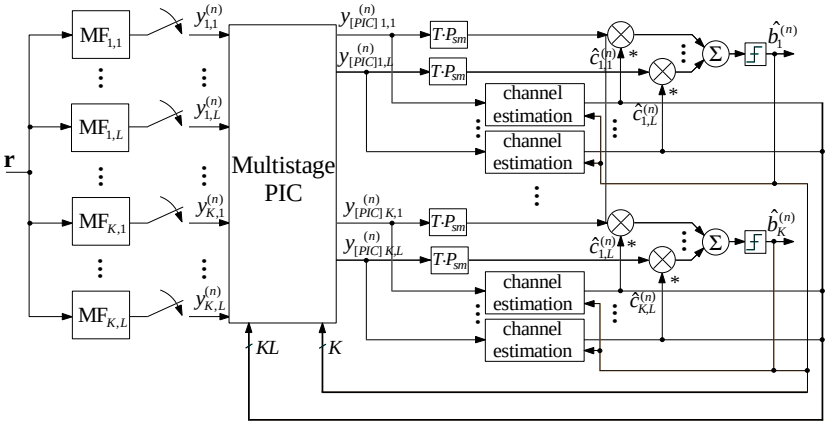

(a) Interference cancellation after matched filtering.

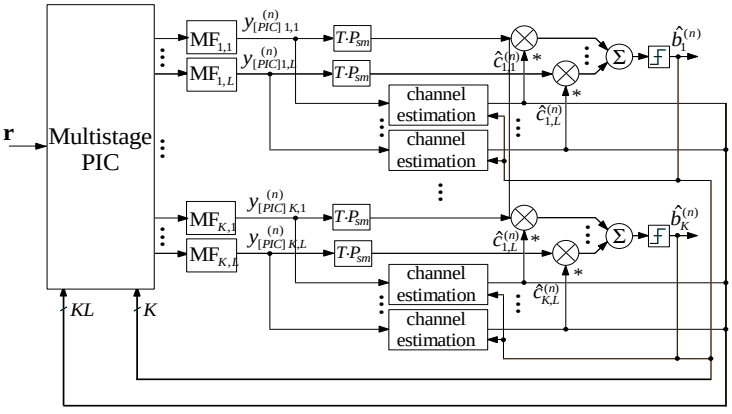

(b) Interference cancellation before matched filtering.

Fig. 6.1. Parallel interference cancellation receivers.

The following changes will be made to simplify the notations: $\mathbf{A} = \mathbf{I}$, i.e., the user energies are included in the diagonal channel coefficient matrix $\mathbf{C} \in \mathbb{C}^{KLN_b \times KLN_b}$. The two versions of the linear system model will be used interchangebly: $\mathbf{r} = \mathbf{SCb} + \mathbf{n} = \mathbf{SBc} + \mathbf{n}$, with $\mathbf{C} = \mathrm{diag}(\mathbf{c})$ and $\mathbf{B} = \mathrm{diag}(\mathbf{b})$, where $\mathrm{diag}(\cdot)$ denotes a diagonal matrix formed from a vector. By doing so, the data vector $\mathbf{b} \in \Xi^{KLN_b}$ is different from the one used for single-user receivers, i.e., each data bit is repeated for each multipath component in the system model: $\mathbf{b} = \left[\mathbf{b}^{\mathrm{T}(0)}, \ldots, \mathbf{b}^{\mathrm{T}(N_b-1)}\right]^{\mathrm{T}}$, where $\mathbf{b}^{(n)} = \left[\mathbf{1}_L^{\mathrm{T}} \cdot b_1^{(n)}, \ldots, \mathbf{1}_L^{\mathrm{T}} \cdot b_K^{(n)}\right]^{\mathrm{T}}$.

The received signal is first passed through the matched filter bank (see Figure 6.1(a)). The output of the bank of matched filters can be written as

$$\begin{aligned} \mathbf{y} &= \mathbf{S}^{\mathrm{T}}\mathbf{r} = \mathbf{S}^{\mathrm{T}}\mathbf{SCAb} + \mathbf{S}^{\mathrm{T}}\mathbf{n} \\ &= \mathbf{RCAb} + \tilde{\mathbf{n}} = (\mathbf{R} - \mathbf{I}_{KLN_b} + \mathbf{I}_{KLN_b})\mathbf{CAb} + \tilde{\mathbf{n}} \\ &= \mathbf{CAb} + (\mathbf{R} - \mathbf{I}_{KLN_b})\,\mathbf{CAb} + \tilde{\mathbf{n}} = \mathbf{CAb} + \boldsymbol{\Psi} + \tilde{\mathbf{n}}, \end{aligned} \tag{6.3}$$

where $\mathbf{y} = \left[\mathbf{y}^{\mathrm{T}(0)}, \ldots, \mathbf{y}^{\mathrm{T}(N_b-1)}\right]^{\mathrm{T}} \in \mathbb{C}^{KLN_b}$ is the matched filter bank output vector, $(\mathbf{R})_{i,i} = 1$, and $\boldsymbol{\Psi} = \left[\boldsymbol{\Psi}^{\mathrm{T}(0)}, \ldots, \boldsymbol{\Psi}^{\mathrm{T}(N_b-1)}\right]^{\mathrm{T}} \in \mathbb{C}^{KLN_b}$ is the multiple-access interference vector. The matched filter outputs during the nth symbol interval can be written as

$$\begin{aligned} \mathbf{y}^{(n)} &= \mathbf{C}^{(n)}\mathbf{b}^{(n)} + \boldsymbol{\Psi}^{(n)} + \tilde{\mathbf{n}}^{(n)} \\ &= \mathbf{C}^{(n)}\mathbf{b}^{(n)} + \sum_{i=-D}^{D} \left(\mathbf{R}^{(n,n+i)} - \delta_{i,0}\mathbf{I}_{KL}\right) \mathbf{C}^{(n+i)}\mathbf{b}^{(n+i)} + \mathbf{n}^{(n)}, \end{aligned} \tag{6.4}$$

where $D = \left\lceil \frac{T+T_m}{T} \right\rceil$, T_m is the maximum delay spread of all users' channels, $\delta_{i,0}$ is the Kronecker delta, $\mathbf{R}^{(n)}$, $\mathbf{C}^{(n)}$, $\mathbf{b}^{(n)}$ are all-zeros $\forall\ n \notin \{0, 1, \ldots, N_b - 1\}$, $\mathbf{y}^{(n)} = \left[y_{1,1}^{(n)}, \ldots, y_{1,L}^{(n)}, \ldots, y_{K,L}^{(n)}\right]^{\mathrm{T}}$ with

$$y_{k,l}^{(n)} = \sum_{j=SGn+\tau_{k,l}}^{SG(n+1)-1+\tau_{k,l}} s_k\big(T_s(j - \tau_{k,l} - SGn)\big)\, r(T_s j) = \mathbf{s}_{k,l}^{\mathrm{T}(n)}\mathbf{r}, \tag{6.5}$$

where $r(T_s j)$ is one received sample and $s_k(T_s j)$ is one sample from the spreading sequence. A simple way to deal with MAI is to estimate and subtract it from the matched filter outputs before synchronization and data detection, which results in interference cancellation based algorithms. PIC is a special case where the interference is cancelled similarly for all users in parallel.

There are two possibilities for the MAI estimation in PIC receivers. The first approach is to use the soft-decisions in MAI estimation, which results in the so-called SD-PIC receivers [133, 135, 140, 141, 211, 212]

$$\hat{\boldsymbol{\Psi}}^{(n)} = \sum_{i=-D}^{D} \left(\mathbf{R}^{(n,n+i)} - \delta_{i,0}\mathbf{I}\right) \widehat{\mathbf{Cb}}^{(n+i)}. \tag{6.6}$$

The SD-PIC receivers use channel coefficient data symbol products in MAI estimation. Hence, the channel coefficients are not estimated in the receiver, which

usually are differentially coherent. It was shown in [140] that the SD-PIC receiver with the infinite number of cancellation stages is actually a decorrelating receiver. In order to obtain performance improvement with respect to the optimum SD-PIC receiver with infinite number of stages, which has the same performance as the decorrelator [140], some nonlinearities are required in interference cancellation. The nonlinearities are also needed to reduce the bias of the MAI estimates [141, 142].

The third generation WCDMA systems will use coherent receivers at the base stations, hence the channel coefficients need to be estimated. Estimated channel coefficients can be used to improve the efficiency of interference cancellation due to more accurate MAI estimates. The MAI estimates in the so-called hard-decision PIC (HD-PIC) receivers [25, 39, 40, 125, 129, 130, 131, 213] can be expressed as

$$\hat{\mathbf{\Psi}}^{(n)} = \sum_{i=-D}^{D} \left(\mathbf{R}^{(n,n+i)} - \delta_{i,0}\mathbf{I} \right) \hat{\mathbf{C}}^{(n+i)} \hat{\mathbf{b}}^{(n+i)}. \tag{6.7}$$

HD-PIC receiver is a natural choice for nonlinear MAI estimation and cancellation, i.e., bias reduction in PIC receivers. The performance of the HD-PIC based algorithms depends on the quality of the MAI estimates, which can be degraded by inaccurate channel coefficient estimates, data estimates, delay estimates or incomplete system model. The data detection is discussed in Section 6.1.1, channel coefficient estimation in Section 6.1.2, delay estimation in Section 6.2 and unknown users causing inaccuracies to the system model in Section 6.3.

6.1.1. Multistage data detection

The PIC based data detectors and channel estimators require tentative data decisions to form the MAI estimates. Tentative decisions are obtained from the earlier stages of the multistage detector [114]. The multistage detector improves the MAI estimates iteratively, i.e., by using several receiver stages. The data decisions in the case of BPSK modulation at the pth receiver stage can be written as

$$\begin{aligned} \hat{\mathbf{b}}^{(n)}(p) &= \operatorname{sgn}\Big[\operatorname{Re}\big\{ \mathcal{C}\hat{\mathbf{C}}^{\mathrm{H}(n)}(p) \big(\mathbf{y}^{(n)} - \hat{\mathbf{\Psi}}^{(n)}(p) \big) \big\} \Big] \\ &= \operatorname{sgn}\Big[\operatorname{Re}\big\{ \mathcal{C}\hat{\mathbf{C}}^{\mathrm{H}(n)}(p) \mathbf{y}^{(n)}_{[PIC]}(p) \big\} \Big] \end{aligned} \tag{6.8}$$

where $\mathcal{C} = \mathbf{I}_K \otimes \mathbf{1}_L^{\mathrm{T}}$ is the multipath combining matrix, and

$$\hat{\mathbf{\Psi}}^{(n)}(p) = \sum_{i=-D}^{D} \left(\mathbf{R}^{(n,n+i)} - \delta_{i,0}\mathbf{I} \right) \hat{\mathbf{C}}^{(n+i)}(p) \, \hat{\mathbf{b}}^{(n+i)}(p). \tag{6.9}$$

Depending on the channel estimation and multistage schemes, the data estimates and channel estimates can be obtained either from the previous stage or the following stages. In the original multistage detector [114], only the tentative data

decisions from the previous stage are used at the next stage when estimating MAI. This is depicted in Figure 6.2 for a receiver with two cancellation stages and the maximum delay spread of one symbol interval ($D = 2$).

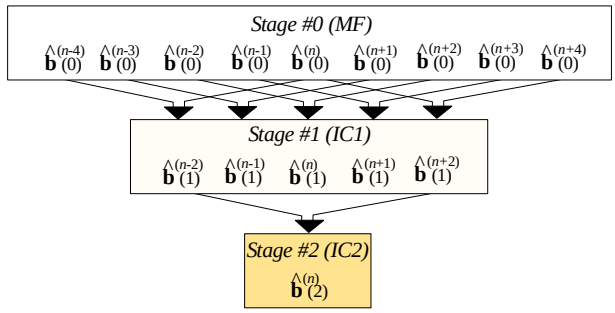

Fig. 6.2. The flow diagram of the basic multistage algorithm with two cancellation stages.

To make a decision for one data symbol requires nine tentative decisions from the MF stage and five tentative decisions from the first cancellation stage. Another possibility would be to use the old tentative decisions at every stage for the D past time intervals, since those decisions are already of better quality than the ones produced by the previous stage. The third option, which is used here, is to feed back the decisions of the last stage to all other stages, and always to use the latest decisions which should be of the best quality. This is illustrated in Figure 6.3. Now, only five symbols from the MF stage and three from the first cancellation stage are used. The others are obtained by feeding them back from the second cancellation stage, which results in improved MAI estimates and more reliable interference cancellation.

The multistage receiver structure also depends on the channel estimation strategy. The last receiver stage usually has the most accurate estimates of MAI and channel coefficients. It would therefore be beneficial to estimate the channel coefficients only at the last stage and to feed them back to the earlier stages. If the channel is changing very rapidly, the channel estimates from the last receiver stage cannot be used at the previous stages, and there is no feedback between stages. The maximum delay spread influences the processing delay in multistage receivers and hence the feedback issue also depends on the system parameters and the propagation environment.

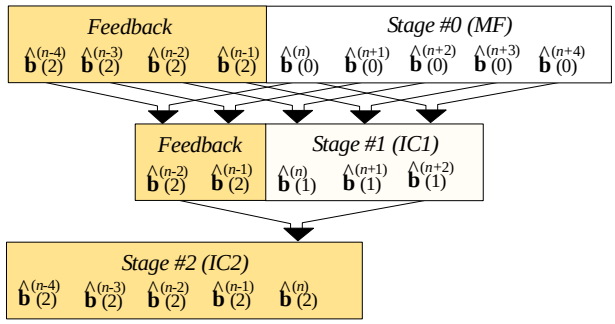

Fig. 6.3. The flow diagram of the decision-feedback multistage algorithm with two cancellation stages.

6.1.2. Channel coefficient estimation

The principle behind the PIC based channel estimators is simple. The rough channel estimates are found by subtracting the MAI estimates from the matched filter outputs and by multiplying the remainder by the conjugate of the symbol estimate. Assuming perfect data symbol and MAI estimates, the rough channel estimates can be written as

$$\begin{aligned}\tilde{\mathbf{c}}^{(n)} &= \mathbf{B}^{\mathrm{H}(n)}\left(\mathbf{y}^{(n)} - \boldsymbol{\Psi}^{(n)}\right)\\ &= \mathbf{B}^{\mathrm{H}(n)}\left[\mathbf{B}^{(n)}\mathbf{c}^{(n)} + \boldsymbol{\Psi}^{(n)} + \tilde{\mathbf{n}}^{(n)} - \boldsymbol{\Psi}^{(n)}\right]\\ &= \mathbf{c}^{(n)} + \check{\mathbf{n}}^{(n)},\end{aligned} \tag{6.10}$$

where $\tilde{\mathbf{c}}^{(n)} = \left[\tilde{c}_{1,1}^{(n)}, \ldots, \tilde{c}_{1,L}^{(n)}, \ldots, \tilde{c}_{K,L}^{(n)}\right]^{\mathrm{T}}$ is called the rough channel estimate vector and $\check{\mathbf{n}}^{(n)}$ is the noise vector.

The PIC based channel estimator can also be derived starting from the maximum likelihood principles. Given that the delays and the data bits for all users are known, the channel coefficients are obtained from

$$\begin{aligned}\hat{\mathbf{c}} &= \arg\max_{\mathbf{c}} \boldsymbol{\Lambda}(\mathbf{c}) = \arg\min_{\mathbf{c}} \left\{||\mathbf{r} - \mathbf{S}\mathbf{B}\mathbf{c}||^{\mathbf{2}}\right\}\\ &= \arg\min_{\mathbf{c}} \left\{\mathbf{c}^{\mathrm{H}}\mathbf{B}^{\mathrm{H}}\mathbf{R}\mathbf{B}\mathbf{c} - 2\,\mathrm{Re}\left\{\mathbf{c}^{\mathrm{H}}\mathbf{B}^{\mathrm{H}}\mathbf{y}\right\}\right\}.\end{aligned} \tag{6.11}$$

Taking the derivative of (6.11) with respect to $\mathbf{c}$ and setting the derivative to zero results in

$$\begin{aligned}\partial\boldsymbol{\Lambda}(\mathbf{c})/\partial\mathbf{c} &= \mathbf{B}^{\mathrm{H}}\left(\mathbf{y} - \mathbf{R}\mathbf{B}\mathbf{c}\right) = \mathbf{0}\\ \Leftrightarrow \quad \mathbf{c} &= \mathbf{B}^{\mathrm{H}}\left(\mathbf{y} - \mathbf{R}\mathbf{B}\mathbf{c}\right) + \mathbf{c}\\ \mathbf{c} &= \mathbf{B}^{\mathrm{H}}\left(\mathbf{y} - \mathbf{R}\mathbf{B}\mathbf{c} + \mathbf{B}\mathbf{c}\right)\\ \mathbf{c} &= \mathbf{B}^{\mathrm{H}}\left(\mathbf{y} - (\mathbf{R} - \mathbf{I})\mathbf{B}\mathbf{c}\right)\\ \mathbf{c} &= \mathbf{B}^{\mathrm{H}}\left(\mathbf{y} - \boldsymbol{\Psi}\right) = \mathbf{B}^{\mathrm{H}}\left(\mathbf{y} - \boldsymbol{\Psi}(\mathbf{c})\right).\end{aligned} \tag{6.12}$$

The closed form solution does not exist, since $\mathbf{\Psi}(\mathbf{c})$ depends on the channel coefficients $\mathbf{c}$. The channel coefficients are solved iteratively in PIC based multistage receiver by using the latest channel coefficient estimates in forming $\mathbf{\Psi}(\mathbf{c})$. By looking at (6.12), we can see that the impact of data modulation must be removed in channel estimation. Equation (6.12) does not imply, however, that the channel estimates can and must be filtered in order to utilize the correlation, i.e., the memory of the channel.

The two main techniques to remove the impact of data modulation in channel estimation are the data-aided (DA) and decision-directed (DD) methods [17]. The WCDMA proposal [10] uses pilot symbols in channel estimation. However, since the maximum pilot symbol rate is only 1.6 kHz, it means that for 90% of the time there is no pilot symbol available. For more efficient channel estimation, DA and DD methods are combined in the PIC receiver studied in this section. The combination of the DA and DD methods causes additional problems that must be dealt with. Specifically, the decision-directed algorithms may experience the so-called cycle-slips or hang-ups [17, 33] due to decision errors. If a cycle-slip or hang-up takes place, the phase of the channel estimate has a constant error of 180 degrees in the case of BPSK data modulation. In such a situation, all decisions are erroneous with coherent receivers in the noiseless case.

In single-user systems, a usual way to deal with hang-up is to use known pilot symbols in channel estimation to remove phase ambiquity. Typically about 10% of the received symbols are pilot symbols in mobile communications with speech services [30]. The rate of pilot symbols can be reduced remarkably if the optimum interpolators in the LMMSE sense [214, 215] are used to interpolate channel estimates for time instants when there is no pilot symbol available. In [25, 129] the optimum Wiener interpolators were used in multiuser receivers for channel estimation. In the sequel only filters, predictors and smoothers[1] without interpolation are considered.

In the PIC based multistage detector, pilot symbols are used to detect false tentative decisions which may be due to hang-up. If the tentative decision is different from the pilot symbol, an error counter associated with the hang-up detector for the receiver which made the error is incremented. Similarly, it is decremented when the decision and the pilot symbol are equal, unless the error counter content is already zero. When the error counter contents exceeds a predetermined threshold, a hang-up state decision is made and corrected by multiplying the contents of the predictor and smoother in Figure 6.4 by -1 in the case of BPSK data modulation.

The tentative decision and channel estimation errors degrade the MAI estimates of all users and the performance can be degraded remarkably without precautions. In the HD-PIC based multistage detector, the detector itself may cause situations similar to hang-up in highly loaded cases due to inaccurate MAI estimate causing error propagation to all other stages. A simple way to overcome error propagation is to reject corrupted rough channel estimates in the channel estimator. This can

[1]Filters utilize the past and the present samples, smoothers the past and the future samples and predictors only the past samples to estimate the present parameter value. Prediction and smoothing require data delaying to retain causality.

be carried out by hard-limiting the rough channel coefficient values prior to channel estimation filtering.

6.1.2.1. Channel estimation filtering

After the MAI estimates have been subtracted and the effect of data has been removed, the channel estimation problem can be separated into KL filtering tasks. If the rough channel estimates of all users are all filtered similarly, the filtered estimates can be expressed by

$$\hat{\mathbf{c}}^{(n)} = \mathbf{v}^{\mathrm{T}} \mathbf{\Omega}^{(n)}, \tag{6.13}$$

where $\mathbf{v} = [v(1), \ldots, v(P_{pr} + P_{sm} + 1)]^{\mathrm{T}} \in \mathbb{R}^{P_{pr}+P_{sm}+1}$ is a linear channel estimation filter, P_{pr} and P_{sm} are the integers defining the type of channel estimator, $\mathbf{\Omega}^{(n)} = [\bar{\mathbf{c}}_{1,1}^{(n)}, \ldots, \bar{\mathbf{c}}_{K,L}^{(n)}] \in \mathbb{C}^{(P_{pr}+P_{sm}+1)\times KL}$ is the input matrix that contains the rough channel estimates over the past $P_{pr} + P_{sm} + 1$ symbol intervals with $\bar{\mathbf{c}}_{k,l}^{(n)} = \left[\tilde{c}_{k,l}^{(n-P_{pr})}, \ldots, \tilde{c}_{k,l}^{(n+P_{sm})}\right]^{\mathrm{T}}$ and P_{sm} defines the type of estimator:

filter	$P_{sm} = 0$,
smoother	$P_{sm} > 0$,
predictor	$P_{sm} < 0$.

Quite often the filter tap weights for all users and paths are chosen to be $1/(P_{pr}+P_{sm}+1)$ which results in the so-called moving average (MA) estimator with uniform weighting (termed moving average estimator in this thesis). The moving average estimator is by no means optimal, unless the SNR and the rate of fading are low. The optimal choice of the tap weights $\mathbf{v}$ depends on the signal-to-noise ratio and the rate of fading, which are different for every user and path. The optimal single-user MMSE [175] channel estimator for the kth user's lth path is linear and is given by

$$\hat{c}_{k,l}^{(n)} = \mathbf{v}_{[opt]k,l}^{\mathrm{T}} \bar{\mathbf{c}}_{k,l}^{(n)} = (\mathbf{\Sigma}_{\bar{\mathbf{c}}_{k,l}}^{-1} \mathbf{\Sigma}_{\bar{\mathbf{c}}_{k,l} c_{k,l}})^{\mathrm{T}} \bar{\mathbf{c}}_{k,l}^{(n)}, \tag{6.14}$$

where $\mathbf{\Sigma}_{\bar{\mathbf{c}}_{k,l}}$ denotes the covariance matrix of $\bar{\mathbf{c}}_{k,l}$ and $\mathbf{\Sigma}_{\bar{\mathbf{c}}_{k,l} c_{k,l}}$ is the cross-correlation between $\bar{\mathbf{c}}_{k,l}$ and $c_{k,l}$.

A technique to apply smoother type channel estimation filters in DD channel estimation has been proposed for single-user communications in [170]. A similar technique was developed for the multistage detector in [25, 129]. The scheme combines the data-aided and decision-directed channel estimators. Pilot symbols are used when they are available, otherwise decision-direction is used. The channel estimator consist of a predictor and a smoother (see Figure 6.4). The predictor provides channel estimates to be used for making the tentative data decisions, which are needed to remove the effect of data modulation when there is no pilot symbol available. The channel estimates produced by the predictor are also fed back to the previous receiver stages for MAI estimation. The channel estimates obtained from the smoother are applied in a maximal ratio combiner, and the

final data decisions $\hat{b}_k^{(n-P_{sm})}(sm)$ are made. The use of the smoother improves the channel estimation performance in comparison to the use of the predictor alone, since the memory of the fading channel can be utilized more efficiently. If there is no feedback in the receiver, each receiver stage can have a separate smoother for channel estimation. This would increase the processing delay in the receiver. If the channel estimates from the last stage are fed back to all previous stages, the delay or the lag-error in the channel estimates should be minimized. The LMMSE predictors at the last stage are therefore used to produce the channel estimates for each receiver stage and the smoother is used only at the last stage.

The optimization of the predictor coefficients is crucial in the receiver structure which feeds back the predicted channel coefficients to all cancellation stages for MAI estimation. The optimal LMMSE predictor weights depend on the SNR and the rate of fading, both of which are changing over time. The weights could be optimized for the presumed operation point but the channel estimation would be impaired for other SNRs or rates of fading. In the next section some alternatives for adaptively calculating the predictor weights are considered.

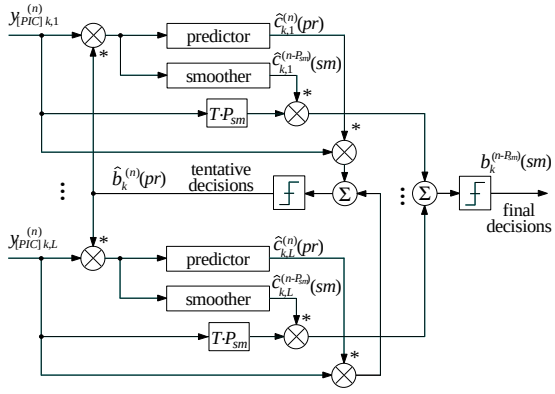

Fig. 6.4. Two-stage DD channel estimator structure.

6.1.2.2. Adaptive channel estimation filtering

The LMMSE filters lend themselves to adaptive implementations. In fact, the channel estimation filter can be made adaptive by using adaptive predictors [170, 215]. The optimum predictor, which would require knowledge of the channel correlation function, can be approximated by using iterative gradient based algorithms. It should be noted that the optimum LMMSE predictor in the PIC based receiver

is different from the single-user LMMSE predictor (6.14) due to the imperfect interference cancellation. Thus, the adaptive predictors may sometimes yield better performance than the optimum single-user LMMSE predictor. In the following sections, finite impulse response (FIR) and infinite impulse response (IIR) type predictors based on the LMS algorithm are presented.

Linear FIR predictor

The output of the linear FIR predictor is given by $\hat{c}_{k,l}^{(n)} = \mathbf{v}_{k,l}^{\mathrm{T}(n)} \bar{\mathbf{c}}_{k,l}^{(n)}$. In an LMS predictor, the error signal can be formed as $e_{k,l}^{(n)} = \tilde{c}_{k,l}^{(n-1)} - \hat{c}_{k,l}^{(n)}$ (see Figure 6.5). The stochastic estimate for the gradient vector is $\nabla_{k,l} = -2e_{k,l}^{(n)} \bar{\mathbf{c}}_{k,l}^{*(n)}$ and the LMS algorithm for updating the coefficients $\mathbf{v}_{k,l}^{(n)}$ can be written as [21]

$$\mathbf{v}_{k,l}^{(n+1)} = \mathbf{v}_{k,l}^{(n)} + 2\mu_{k,l} e_{k,l}^{(n)} \bar{\mathbf{c}}_{k,l}^{*(n)}. \tag{6.15}$$

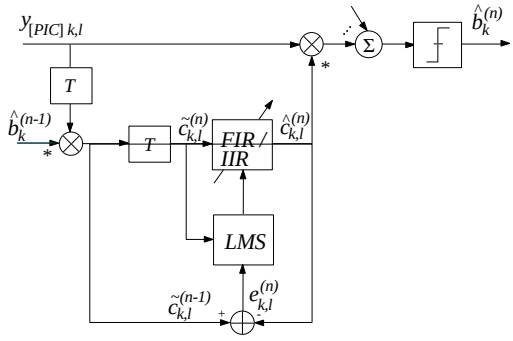

Fig. 6.5. Adaptive predictor.

Recursive IIR predictor

First order IIR filters are often used as channel estimation filters in RAKE receivers [216]. With filter weights α and $1-\alpha$, the filter is called a recursive integrator or an alpha tracker [216]. A general Nth order adaptive IIR filter has been presented in [217], where the adaptive IIR filter is structured as two adaptive FIR filters in cascade. Therefore, the adaptive IIR filter can be seen as controlling two adaptive FIR filters simultaneously. Let the first order IIR filter weights be $v_{k,l}^{(n)}$ (feedforward

coefficient) and $q_{k,l}^{(n)}$ (feedback coefficient). The IIR predictor output can then be written as

$$\hat{c}_{k,l}^{(n)} = v_{k,l}^{(n)} \tilde{c}_{k,l}^{(n)} + q_{k,l}^{(n)} \hat{c}_{k,l}^{(n-1)}, \tag{6.16}$$

where $\tilde{c}_{k,l}^{(n)}$ is the rough channel estimate. The gradient vector with respect to the filter weights with the stochastic approximation is $\nabla_{k,l} = -2e_{k,l}^{(n)} [\tilde{c}_{k,l}^{(n)}, \hat{c}_{k,l}^{(n-1)}]^{\mathrm{H}}$ and the LMS algorithm for updating the coefficients $v_{k,l}$ and $q_{k,l}$ can be expressed as [217]

$$\begin{bmatrix} v_{k,l}^{(n+1)} \\ q_{k,l}^{(n+1)} \end{bmatrix} = \begin{bmatrix} v_{k,l}^{(n)} \\ q_{k,l}^{(n)} \end{bmatrix} + 2\mu_{k,l} e_{k,l}^{(n)} \begin{bmatrix} \tilde{c}_{k,l}^{*(n)} \\ \hat{c}_{k,l}^{*(n-1)} \end{bmatrix}. \tag{6.17}$$

The filter is not restricted to be an alpha tracker; the weights $v_{k,l}^{(n)}$ and $q_{k,l}^{(n)}$ are adjusted independently. The filter weights should be constrained during the adaptation process due to stability problems of adaptive IIR filters. Proper stability constraints for the first order IIR filters are simply: $0 < |v_{k,l}| < 1$ and $0 < |q_{k,l}| < 1$. Another possibility would be to estimate the gradient only with respect to one filter weight and then apply the constraints: $0 < |v_{k,l}| \leq 1$ and $q_{k,l} = 1 - v_{k,l}$. This constrains the filter to be the alpha tracker [216].

6.1.3. Numerical examples

First, the simulation results for the channel estimation filtering are presented. The channel model used was a single-path Rayleigh fading channel with the vehicle speed of 80 km/h and carrier frequency of 2.0 GHz. Relatively high rate fading was used to make the channel estimation more difficult and challenging. The data rate is assumed to be 16 kbit/s (which results in the maximum normalized Doppler shift of $9.26 \cdot 10^{-3}$). Gold codes of length 31 chips were used and the receiver sampling rate was 1 sample per chip.

A simple moving average estimator performs well if the length of the estimator can be adjusted. The optimum length of the estimator depends on the rate of fading (or vehicle speed) and the signal-to-noise ratio. The complex channel coefficient mean squared errors for different SNRs at vehicle speeds of 80 km/h as a function of the MA estimator length are presented in Figure 6.6. The same curves have also been produced for different vehicle speeds at 0 dB which are shown in Figure 6.7. The simulations were performed with the assumption that the data is known. As can be seen, there is always an optimum value for the MA estimator length depending on the SNR and the Doppler spread. Thus, there is a need for adaptive channel estimators. The most reasonable values in mobile applications for speech services for the MA estimator length is between 5 and 15 symbol intervals.

The alpha tracker (or recursive integrator) approximates the moving average estimator. The optimum values for the filter parameters also depend on the rate of fading and the SNR (Figures 6.8 and 6.9). In mobile applications with speech services, the filter feedback coefficient should be between 0.7 and 0.9.

Although the convergence rate is not of the greatest importance in channel estimation filtering due to slow changes in channel statistics, they will be briefly discussed below. The parameters used are: single-path uncorrelated Rayleigh fading channels for different users with vehicle speeds of 80 km/h, a symbol rate of 16 kbit/s (which results in the maximum normalized Doppler shift of $9.26 \cdot 10^{-3}$), a carrier frequency of 2.0 GHz, the number of users 30, 10 users have 10 dB higher power, the SNR of the users with lower power was 10 dB. Only one cancellation stage was used with perfect knowledge of data symbols of all users for simplicity.

The rate of convergence of the adaptive LMS predictors depends on the users' energies and the initial predictor weights. The stronger the user, the faster the convergence, and the more carefully the stepsize μ has to be chosen to avoid stability problems. The convergence rate of the LMS FIR predictor for the users with 10 dB higher power was roughly 500 symbol intervals when the initial weights corresponded to an MA estimator of length 20 symbols and $\mu = 5 \cdot 10^{-6}$. The convergence time for the weak users with equal power was roughly 5000. With a stepsize greater than 10^{-5}, the LMS FIR algorithm becomes unstable in the presence of strong interference.

The convergence of the LMS IIR predictor was more sensitive to the selection of μ and the initial filter weights than the LMS FIR predictor. With $\mu = 5 \cdot 10^{-4}$ and initial filter weights $v_{k,l}^{(0)} = 0.8$ and $q_{k,l}^{(0)} = 0.2$, the convergence time was about 1000 symbol intervals for the stronger users and more than 10000 symbols for the weak users. The instability of the LMS IIR predictor can be avoided by constraining the filter weights. The constraints used in the simulations were $0.01 \leq v_{k,l} \leq 0.5$ and $0.5 \leq q_{k,l} \leq 0.99$. Interestingly, the filter weights corresponded to the recursive integrator in the steady-state regardless of the initial conditions satisfying the constraints.

The channel estimation MSEs for the LMS FIR, LMS IIR and MA estimators are given in Figure 6.10. Based on the results, the LMS FIR predictor of length 20 symbols has the best performance of the three. The MSE of the MA estimator of length 10 symbols saturates around 20 dB. The LMS IIR predictor also performs better than the MA estimator, but its performance is worse than with the LMS FIR predictor. The results indicate that the adaptive channel estimation filters can significantly improve the channel estimation performance.

Another issue that was studied by simulations is the impact of the channel estimate and the data decision feedback in the HD-PIC multistage receivers. The parameters used are summarized in Table 6.1. The channel estimation filters used in the simulations were the optimum single-user LMMSE filters (see (6.14)) to simplify the simulations. The multistage receiver used was as presented in Figure 6.3 and the channel estimator structure was the same as in Figure 6.4.

Simulation results for channel estimation with and without feedback are given in Figure 6.11. As we can see, feeding back the channel estimates gives better BER performance than independent estimators at every stage (with two cancellation stages) with the simulation parameters given in Table 6.1. Increasing the number of stages to three does not degrade the performance from the channel estimation point of view, as can bee seen from Figure 6.12. It can also be seen from Figure 6.12 that increasing the number of cancellation stages from 2 to 3 yields only minimal

performance improvement. The difference to the ideal channel case and to the single-user bound is 3.5 dB at the BER level of 10^{-2}. The difference between ideal and estimated channel BERs is due to the channel estimation errors caused by the feedback and the inaccuracy of the final channel estimate.

In the PIC based multistage detectors, the decision and the channel estimation errors propagate to the MAI estimates of all users and the performance can be degraded remarkably without precautions. There are several ways to prevent error-propagation due to poor channel estimates in the PIC based multistage receivers. In Figure 6.13, two different options have been compared in terms of the resulting BER. The first one is based on the hang-up detection and correction alone. The second one includes hard-limitation of the rough channel estimates in addition to the hang-up correction. As can be seen, the hang-up correction alone is not sufficient when the number of users is high. By rejecting the corrupted rough channel estimates in channel estimation, the performance can be improved. The rough channel estimates are compared to a threshold of three times the average envelope of the channel ($3\overline{|c_{k,l}|}$), which was assumed to be known. If the threshold is exceeded, the rough channel estimate for that user is set to zero. The performance of such a rough channel estimate control scheme is presented in Figure 6.13 as the solid lines. As we can see, the receiver no longer collapses with a large number of users. The scheme does not degrade the performance with lower number of users either.

Table 6.1. Parameters used in BER simulations.

Parameter	Value
Gold code length	$G = 31$
Number of users	$K = 8 - 32$
Number of paths	$L = 2$
Maximum delay spread	$T_m = T/2$
Channel profile	second path -6 dB
Pilot symbol density	10%
Vehicle speeds	80 km/h
Symbol rates	16 kbits/s
PIC stages	1 – 3
Predictor parameters	P_{sm} = -1 P_{pr} = 10
Smoother parameters	P_{sm} = 10 P_{pr} = 10
Hang-up detection threshold	2 symbols

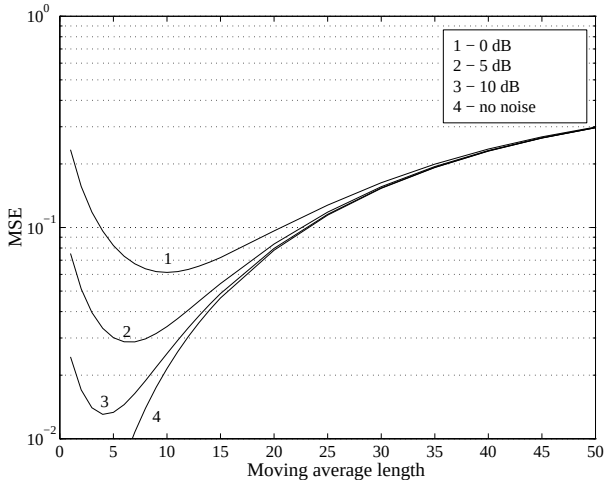

Fig. 6.6. Channel estimation MSEs as a function of the moving averaging interval with vehicle speeds of 80 km/h and various average SNRs, single-user case.

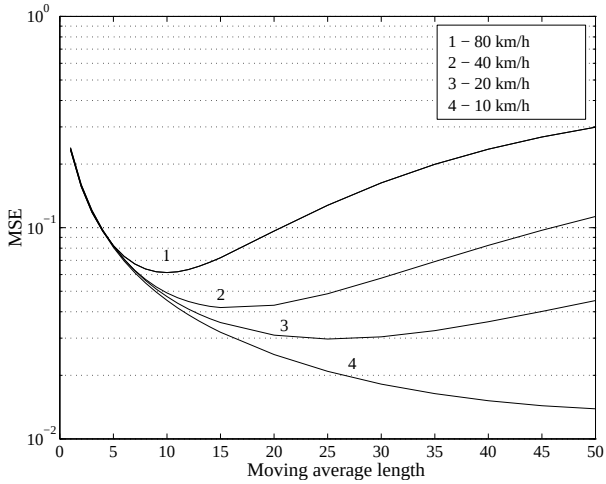

Fig. 6.7. Channel estimation MSE as a function of the moving averaging interval with SNR of 0 dB and various vehicle speeds, single-user case.

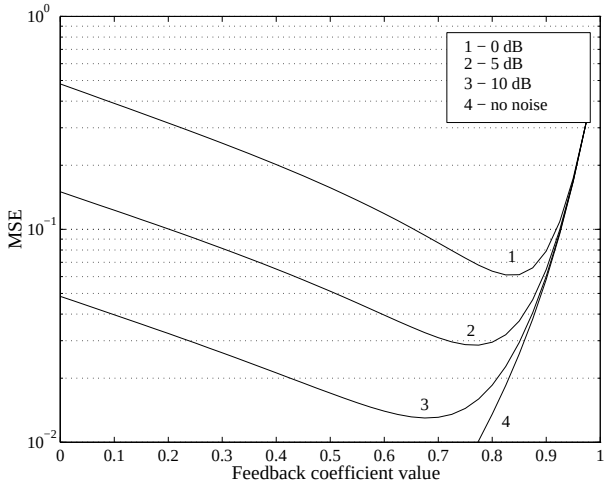

Fig. 6.8. Channel estimation MSEs as a function of the feedback coefficient of the recursive integrator with vehicle speeds of 80 km/h and various average SNRs, single-user case.

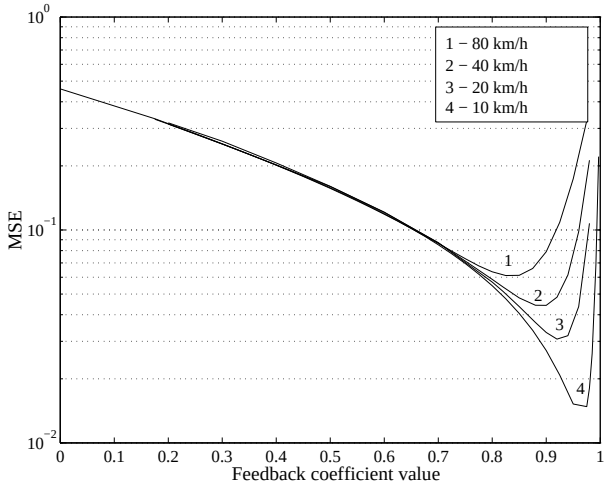

Fig. 6.9. Channel estimation MSE as a function of the feedback coefficient of the recursive integrator with SNR of 0 dB and various vehicle speeds, single-user case.

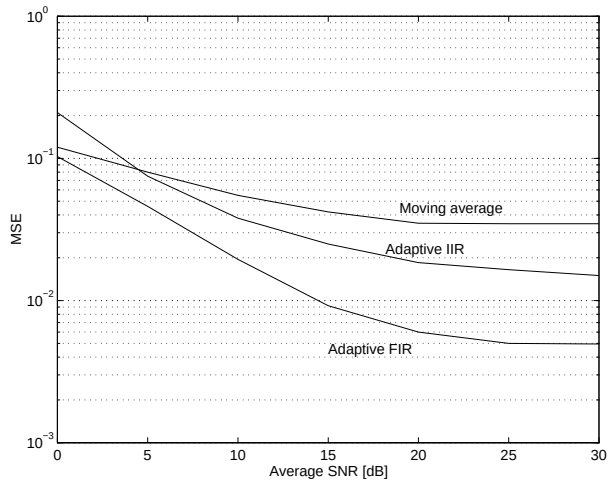

Fig. 6.10. Channel estimation MSEs for the adaptive FIR (filter length 20 symbols, $\mu = 5 \cdot 10^{-6}$) and IIR ($\mu = 5 \cdot 10^{-4}$) predictors and for the moving average estimator (length 10 symbols) in a 30-user case in a one-path fading channel with vehicle speeds of 80 km/h, 10 users of 10 dB higher power.

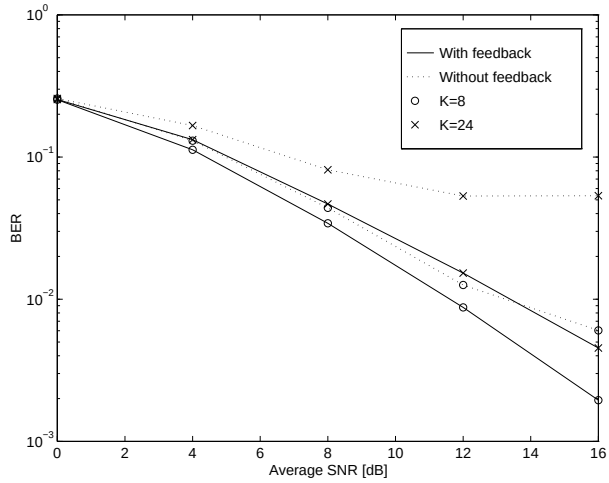

Fig. 6.11. Impact of the channel estimate feedback on the BER, with $K = 8$ and $K = 24$ users in a two-path channel (second path 6 dB weaker) with two cancellation stages.

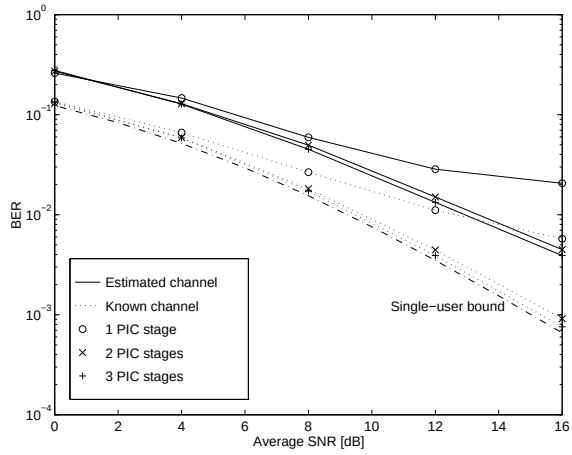

Fig. 6.12. BER with different numbers of cancellation stages for the known and estimated channels, with $K = 24$ users in two-path fading channels (second path 6 dB weaker).

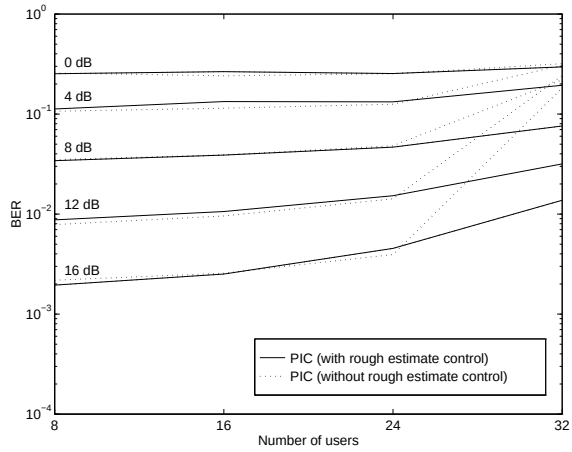

Fig. 6.13. BER with and without rough channel estimate control, with average SNRs of 0, 4, 8, 12, and 16 dB in two-path channels (second path 6 dB weaker) with two cancellation stages.

6.1.4. Discussion

Multistage HD-PIC receivers in fading channels were studied in this section. The main emphasis was on channel estimation filtering and studying the impacts of the channel estimate and data decision feedback on the receiver performance. The numerical results showed possible gains when using adaptive channel estimation filters. Feeding back the channel estimates from the last receiver stage results in satisfactory performance if the fading is not too fast. It was noticed that the hang-up detection is crucial in the PIC based multistage detectors using decision-directed channel estimation due to the error propagation into MAI estimates of all users. It was seen that rejecting excessively large rough channel estimate values in channel estimation is one possible solution to circumvent detrimental error propagation in the PIC receiver.

6.2. Delay estimation in PIC receivers

The main problem to be solved regarding the delay estimation in multiuser CDMA receivers is to decompose the multidimensional optimization problem to several problems of fewer dimensions. One possibility to split the KL dimensional problem to the KL separate delay estimation problems is to use the expectation maximization [146] or the space alternating generalized EM [144] methods. The PIC based delay estimators and the EM or SAGE algorithms result in very similar algorithms [40]. The parallel interference cancellation method can be used both in delay acquisition and delay tracking in multiuser receivers. In the sequel, the PIC based delay estimator is developed.

For the known channel coefficients and data, the maximum likelihood estimates for the delays for all users are obtained from

$$\hat{\boldsymbol{\tau}} = \arg\min_{\boldsymbol{\tau}} \left\{ ||\mathbf{r} - \mathbf{SBc}||^2 \right\}. \tag{6.18}$$

In the PIC based delay estimators, (6.18) is solved separately for each user and path assuming that the other user and path parameters are known. By defining a complement code matrix for the kth user's lth path $\bar{\mathbf{S}}_{k,l} = \mathbf{S} - \mathbf{S}_{k,l}$ with $\mathbf{S}_{k,l} = \left[\mathbf{S}_{k,l}^{(0)}, \ldots, \mathbf{S}_{k,l}^{(N_b-1)}\right]$ and $\mathbf{S}_{k,l}^{(n)} = \left[\mathbf{0}, \ldots, \mathbf{0}, \mathbf{s}_{k,l}^{(n)}, \mathbf{0}, \ldots, \mathbf{0}\right] \in \mathbb{R}^{SGN_b \times KL}$, the delay estimate for the kth user's lth path can be expressed as

$$\begin{aligned} \hat{\tau}_{k,l} &= \arg\min_{\tau_{k,l}} \left\{ ||\mathbf{r} - (\mathbf{S}_{k,l} + \bar{\mathbf{S}}_{k,l})\mathbf{Bc}||^2 \right\} \\ &= \arg\min_{\tau_{k,l}} \left\{ ||\mathbf{r} - \mathbf{S}_{k,l}\mathbf{Bc}||^2 - 2\mathrm{Re}\left\{ \mathbf{c}^{\mathrm{H}}\mathbf{B}^{\mathrm{H}}\bar{\mathbf{S}}_{k,l}^{\mathrm{T}}(\mathbf{r} - \mathbf{S}_{k,l}\mathbf{Bc}) \right\} \right\}, \end{aligned} \tag{6.19}$$

where the constant $||\bar{\mathbf{S}}_{k,l}\mathbf{Bc}||^2$ not having an impact on the minimization of (6.19) has been dropped. Furthermore, due to the normalization of the signature sequence energies $\mathbf{S}_{k,l}^{\mathrm{T}}\mathbf{S}_{k,l} = \mathbf{I}$, (6.19) can be written as

$$\hat{\tau}_{k,l} = \arg\min_{\tau_{k,l}} \left\{ -2\mathrm{Re}\left\{ \mathbf{c}^{\mathrm{H}}\mathbf{B}^{\mathrm{H}}\mathbf{S}_{k,l}^{\mathrm{T}}\mathbf{r} \right\} - 2\mathrm{Re}\left\{ \mathbf{c}^{\mathrm{H}}\mathbf{B}^{\mathrm{H}}\bar{\mathbf{S}}_{k,l}^{\mathrm{T}}(\mathbf{r} - \mathbf{S}_{k,l}\mathbf{Bc}) \right\} \right\}$$

$$
\begin{aligned}
&= \arg\min_{\tau_{k,l}} \left\{ -2\mathrm{Re}\left\{ \mathbf{c}^{\mathrm{H}}\mathbf{B}^{\mathrm{H}}\left(\mathbf{S}_{k,l}^{\mathrm{T}}\mathbf{r} + \bar{\mathbf{S}}_{k,l}^{\mathrm{T}}\mathbf{r} - \bar{\mathbf{S}}_{k,l}^{\mathrm{T}}\mathbf{S}_{k,l}\mathbf{B}\mathbf{c} \right) \right\} \right\} \\
&= \arg\max_{\tau_{k,l}} \left\{ \mathrm{Re}\left\{ \mathbf{c}^{\mathrm{H}}\mathbf{B}^{\mathrm{H}}\left((\mathbf{S}_{k,l}^{\mathrm{T}} + \bar{\mathbf{S}}_{k,l}^{\mathrm{T}})\mathbf{r} - \bar{\mathbf{S}}_{k,l}^{\mathrm{T}}\mathbf{S}_{k,l}\mathbf{B}\mathbf{c} \right) \right\} \right\} \\
&= \arg\max_{\tau_{k,l}} \left\{ \mathrm{Re}\left\{ \mathbf{c}^{\mathrm{H}}\mathbf{B}^{\mathrm{H}}\left(\mathbf{S}_{k,l}^{\mathrm{T}}\mathbf{r} - \bar{\mathbf{S}}_{k,l}^{\mathrm{T}}\mathbf{S}_{k,l}\mathbf{B}\mathbf{c} \right) \right\} \right\}, \qquad (6.20)
\end{aligned}
$$

which can be also written as

$$
\begin{aligned}
\hat{\tau}_{k,l} &= \arg\max_{\tau_{k,l}} \left\{ \mathrm{Re}\left\{ \mathbf{c}^{\mathrm{H}}\mathbf{B}^{\mathrm{H}}\left(\mathbf{S}_{k,l}^{\mathrm{T}}\mathbf{r} - (\mathbf{S}^{\mathrm{T}} - \mathbf{S}_{k,l}^{\mathrm{T}})\mathbf{S}_{k,l}\mathbf{B}\mathbf{c} \right) \right\} \right\} \\
&= \arg\max_{\tau_{k,l}} \left\{ \mathrm{Re}\left\{ \mathbf{c}^{\mathrm{H}}\mathbf{B}^{\mathrm{H}}\left(\mathbf{y}_{k,l} - (\mathbf{S}^{\mathrm{T}}\mathbf{S}_{k,l} - \mathbf{I})\mathbf{B}\mathbf{c} \right) + \mathbf{c}^{\mathrm{H}}\mathbf{c} \right\} \right\} \\
&= \arg\max_{\tau_{k,l}} \left\{ \mathrm{Re}\left\{ \mathbf{c}^{\mathrm{H}}\mathbf{B}^{\mathrm{H}}\left(\mathbf{y}_{k,l} - \boldsymbol{\Psi}_{k,l} \right) \right\} \right\}, \qquad (6.21)
\end{aligned}
$$

where the MF output vector for the kth user's lth path has the components $\mathbf{y}_{k,l} = \left[\mathbf{y}_{k,l}^{(0)}, \ldots, \mathbf{y}_{k,l}^{(N_b-1)}\right]^{\mathrm{T}} \in \mathbb{C}^{KLN_b}$ with $\mathbf{y}_{k,l}^{(n)} = \left[0, \ldots, 0, y_{k,l}^{(n)}, 0, \ldots, 0\right] \in \mathbb{C}^{KL}$, and the interference vector for the kth user's lth path $\boldsymbol{\Psi}_{k,l} = \left[\boldsymbol{\Psi}_{k,l}^{(0)}, \ldots, \boldsymbol{\Psi}_{k,l}^{(N_b-1)}\right]^{\mathrm{T}} \in \mathbb{C}^{KLN_b}$ with $\boldsymbol{\Psi}_{k,l}^{(n)} = \left[0, \ldots, 0, \Psi_{k,l}^{(n)}, 0, \ldots, 0\right] \in \mathbb{C}^{KL}$. Finally, (6.21) reduces to

$$
\hat{\tau}_{k,l}^{(n+1)} = \arg\max_{\tilde{\tau}_{k,l}} \left\{ \mathrm{Re} \sum_{i=n-\mathcal{T}+1}^{n} \left\{ \hat{c}_{k,l}^{*(i)} \hat{b}_{k}^{*(i)} \left[y_{k,l}^{(i)}(\tilde{\tau}_{k,l}) - \hat{\Psi}_{k,l}^{(i)}(\tilde{\tau}_{k,l}) \right] \right\} \right\}. \qquad (6.22)
$$

for each user and path with an observation interval $\mathcal{T}$ symbols.

6.2.1. Delay acquisition

There are two approaches to delay acquisition in PIC based receivers. The first one is to assume that there is only one user to be acquired at a time. The other one is to acquire all user delays jointly. The first option is more practical and simple to implement in PIC receivers. The latter leads to quite impractical acquisition schemes for the PIC receivers, but is theoretically interesting [181].

A new user of a CDMA system can be acquired by using the conventional single-user delay acquisition methods [32] if the known interference is cancelled from the sampled wideband signal, i.e., prior to matched filtering (see Figure 6.1(b)). MAI is estimated for those users and propagation paths that are being received already. The wideband signal after interference cancellation for the kth user's lth path at the pth cancellation stage is given by

$$
\bar{\mathbf{r}}_{[PIC]k,l}^{(n)}(p) = \bar{\mathbf{r}}^{(n)} - \hat{\boldsymbol{\Psi}}_{[\mathbf{r}]k,l}^{(n)}(p), \qquad (6.23)
$$

where $\hat{\boldsymbol{\Psi}}_{[\mathbf{r}]k,l}^{(n)}$ is the wideband MAI estimate for the kth user's lth path. For the

definition of the wideband interference term, a sub-matrix of $\mathbf{S}$ (2.8) is needed:

$$\mathbf{S}_{[D]}^{(n)} = \begin{pmatrix} \mathbf{S}^{(n-2)}(2) & \mathbf{S}^{(n-1)}(1) & \mathbf{S}^{(n)}(0) & \mathbf{0} & \mathbf{0} \\ \mathbf{0} & \mathbf{S}^{(n-1)}(2) & \mathbf{S}^{(n)}(1) & \mathbf{S}^{(n+1)}(0) & \mathbf{0} \\ \mathbf{0} & \mathbf{0} & \mathbf{S}^{(n)}(2) & \mathbf{S}^{(n+1)}(1) & \mathbf{S}^{(n+2)}(0) \end{pmatrix}, \in \mathbb{R}^{3SG \times 5KL} \tag{6.24}$$

where it is assumed that $D = 2$ for notational simplicity[2]. The channel coefficient matrix over the window of $2D + 1$ symbol intervals is defined as

$$\mathbf{C}_{[D]}^{(n)} = \mathrm{diag}\left[\mathbf{c}^{\mathrm{T}(n-D)}, \ldots, \mathbf{c}^{\mathrm{T}(n)}, \ldots, \mathbf{c}^{\mathrm{T}(n+D)}\right] \tag{6.25}$$

and the data vector as

$$\mathbf{b}_{[D]}^{(n)} = \left[\mathbf{b}^{\mathrm{T}(n-D)}, \ldots, \mathbf{b}^{\mathrm{T}(n)}, \ldots, \mathbf{b}^{\mathrm{T}(n+D)}\right]^{\mathrm{T}}. \tag{6.26}$$

Furthermore, the complement matrix for the windowed spreading sequence matrix is defined as

$$\bar{\mathbf{S}}_{[D]k,l}^{(n)} = \mathbf{S}_{[D]}^{(n)} - \mathbf{S}_{[D]k,l}^{(n)}, \tag{6.27}$$

where $\mathbf{S}_{[D]k,l}^{(n)}$ contains only the kth user's lth path components and other components are set to zero (similar to as in Section 6.2). Now, the wideband MAI estimate for the kth user's lth path can be expressed as

$$\hat{\mathbf{\Psi}}_{[\mathbf{r}]k,l}^{(n)}(p) = \bar{\mathbf{S}}_{[D]k,l}^{(n)} \hat{\mathbf{C}}_{[D]}^{(n)}(p) \hat{\mathbf{b}}_{[D]}^{(n)}(p). \tag{6.28}$$

In delay acqusition, the new users and paths being acquired are not included in the spreading code matrix and thus, $\bar{\mathbf{S}}_{[D]k,l}^{(n)} = \mathbf{S}_{[D]k,l}^{(n)}$. Since the delays are changing slowly, the delay estimator should operate on the last receiver stage signals. The delay acquisition problem for the new user with index $K + 1$ can be expressed as

$$\hat{\tau}_{K+1}^{(n+1)} = \arg\max_{\tilde{\tau}} \sum_{i=n-\mathcal{T}+1}^{n} \left\{ \left| \bar{\mathbf{s}}_{K+1}^{\mathrm{T}}(\tilde{\tau}) \bar{\mathbf{r}}_{[PIC]K+1}^{(i)}(P) \right|^2 \right\}, \tag{6.29}$$

where P is the number of cancellation stages. The propagation path index is dropped due to the definition of delay acquisition in multipath channels (p. 104).

[2]More generally, the dimensions of the matrix are $(D + 1)SG \times (2D + 1)KL$.

6.2.1.1. Numerical examples

A semi-analytic approach is used to evaluate the mean acquisition times for the conventional and PIC based delay acquisition schemes. The probabilities of acquisition within a given observation interval are simulated and then the mean acquisition time is computed according to (5.18). It will be assumed that there is only one new user to be acquired and the definition for the delay acquisition is the case when the delay of at least one multipath component has been found. The main parameters used in the simulations were: two-path Rayleigh fading channel with equal energy taps, vehicle speeds of 80 km/h and a carrier frequency of 2.0 GHz. The data rate was assumed to be 16 kbit/s. Gold codes of length 31 chips were used, the receiver sampling rate was 1 sample per chip. The observation interval in the delay acquisition was between 10 – 100 symbol intervals, the number of known or synchronized users was between 8 – 32 and their SNR was 10 dB. The new user being acquired had the SNR of 0, 10 or 20 dB (the power offset with respect to the synhronized users was -10, 0 or 10 dB). The PIC based acquisition scheme was based on the receiver structure described earlier in Section 6.1.1, i.e., two cancellation stages were used and the channel estimation was carried out at the last cancellation stage. The false alarm penalty time (T_p) used in the mean acquisition time analysis has been 500 symbol intervals.

The probability of acquisition as a function of the number of users for the observation intervals of 10 and 100 symbols both for the MF and PIC based acquisition schemes are presented in Figure 6.14. The SNR of the new user was 10 dB (power offset 0 dB). Clearly, the PIC based acquisition scheme is more reliable than the conventional MF based acquisition scheme in all cases studied.

The mean acquisition times in chip intervals as a function of the observation interval for both the conventional and the PIC based acquisition schemes in the case of 24 synchronized users are illustrated in Figure 6.15 for different unsynchronized user power offsets. As we can see, the observation interval of 10 symbols results in the shortest delay acquisition time and it is therefore used in the sequel.

The mean acquisition times as a function of the unsynchronized user power offset for different numbers of synchronized users are shown in Figure 6.16 for the conventional MF based acquisition and in Figure 6.17 for the PIC based acquisition. The results indicate that it is beneficial to use a higher power for the new user from the conventional MF acquisition point of view. Increasing the power from 0 dB offset does not lead to much benefit in the PIC based acquisition unless the number of users is very large. In fact, allowing the new user to transmit at a higher power than the synchronized users is detrimental to the PIC based data detection as will be shown in Section 6.3. By comparing the acquisition time analysis results of the conventional and the PIC based schemes at the SNR of 10 dB (0 dB offset) for the new unsynchronized user, we can see that the PIC based acquisition results in at least two times shorter delay acquisition times when the number of users is at most 24. When the number of users is very large, the unsynchronized user is more harmful to the PIC receiver which operates close to its capacity limit. In such a case, cancellation fails more easily and the conventional MF based acquisition results in almost the same acquisition performance.

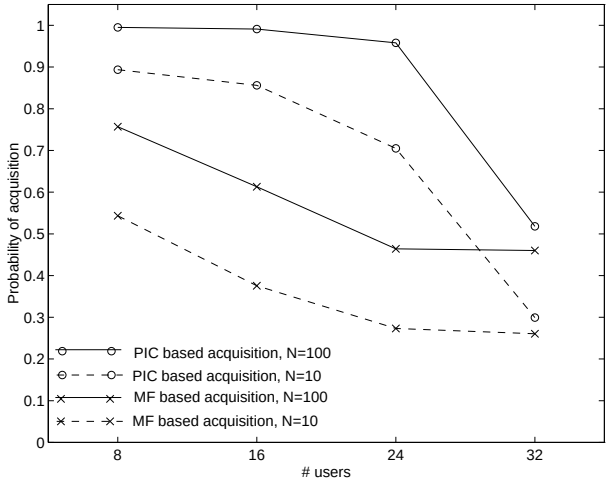

Fig. 6.14. Probability of acquisition for the PIC and MF based acquisition as a function of the number of users in a two-path Rayleigh fading channel with vehicle speeds of 80 km/h, observation intervals 10 and 100 symbols and the unsynchronized user power offset of 0 dB (SNR 10 dB).

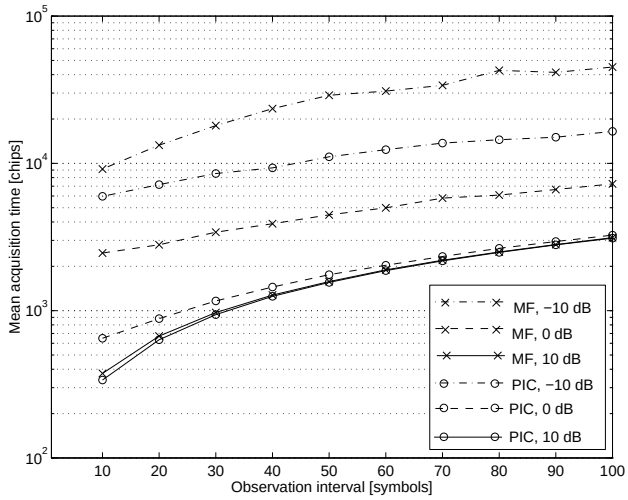

Fig. 6.15. Mean acquisition times for the PIC and MF based acquisition as a function of the observation interval in a two-path Rayleigh fading channel with vehicle speeds of 80 km/h, 24 synchronized users and the unsynchronized user power offset -10, 0 or 10 dB (SNR 0, 10, 20 dB).

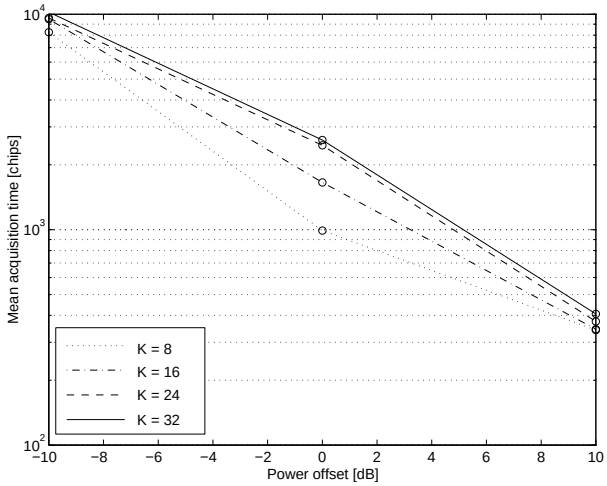

Fig. 6.16. Mean acquisition times for the MF based acquisition as a function of the unknown user power offset in a two-path Rayleigh fading channel with vehicle speeds of 80 km/h for different numbers of users with the observation interval of 10 symbols (SNR 0 − 20 dB).

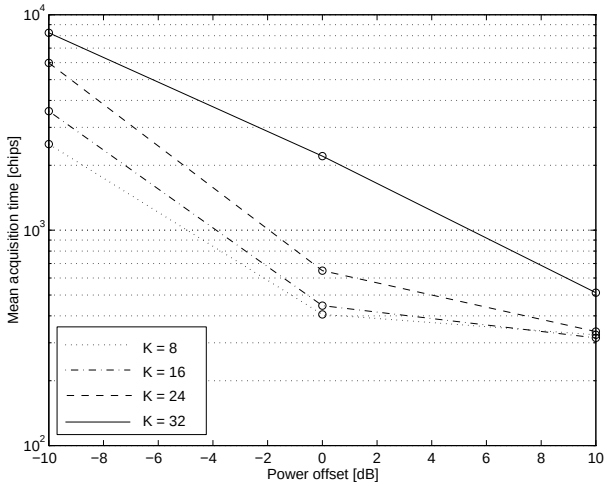

Fig. 6.17. Mean acquisition times for the PIC based acquisition as a function of the unknown user power offset in a two-path Rayleigh fading channel with vehicle speeds of 80 km/h for different numbers of users with the observation interval of 10 symbols (SNR 0 − 20 dB).

6.2.1.2. Discussion

Delay acquisition in PIC receivers was studied in this section. Based on the mean acquisition time analysis, it can be concluded that the PIC based acquisition results in significantly shorter acquisition times than the conventional MF acquisition if the number of users is less than the processing gain. In highly loaded cases, the PIC receiver is already operating at the upper limit of its capabilities and the new unsynchronized user may cause significantly worse cancellation efficiency to existing users. In such a case, the advantage of using the PIC method in delay acquisition does not lead to significant benefit in comparison to the conventional MF based acquisition.

6.2.2. Delay tracking

In this section, the PIC method is used in deriving delay trackers. Using the principles of the delay-locked loop techniques together with the lead-lag phase-locked loops [218], two alternative DLL implementations for fading channels will be introduced.

The operation of the feedback control loops is determined by the s-curve, which presents the error signal as a function of the reference parameter error. If the amplitude of the input signal is fluctuating, the s-curve will fluctuate respectively [33]. Quite often perfect automatic gain control (AGC) is assumed which results in a steady s-curve. In a DS-CDMA receiver, the AGC is twofold: the wideband radio frequency (RF) signal level is controlled by the so-called pre-synch AGC, and the amplitude of the despread narrowband signal is controlled by the post-synch AGC [219]. The most reasonable way to deal with the post-synch AGC is to integrate it into the synchronization algorithms, which results in adaptive loop gain control algorithms for normalizing the s-curve. In this section, proper means are derived for adaptively adjusting the loop gain in the PIC based DLLs.

6.2.2.1. BER sensitivity to delay estimation errors

In order to get some understanding on the timing accuracy requirements, the BER sensitivity of the multistage HD-PIC receivers to delay estimation errors was simulated in fading channels. The receiver and the channel estimator structure used is as in Sections 6.1.1 and 6.1.2 and the parameters used in the simulations are the same as presented in Table 6.1 with the exception that the chip shaping filter was a raised cosine with roll-off 0.75 and that the propagation paths were of equal power. The number of users was 16 and Gold codes of length 31 have been used. The delay errors are assumed to follow the zero-mean Gaussian distribution limited to the range of $\pm$ 1.0 chips.

The BERs for various delay error standard deviations (normalized to the chip

interval) without a near-far problem are presented in Figure 6.18 in a known channel case and in Figure 6.20 with channel estimation. According to the results, the delay error standard deviation should be less than 0.1 chips in order to not degrade the performance significantly. In the case of a near-far problem (5 users have 10 dB higher power), the delay estimation accuracy requirements are more stringent, as can be seen from Figures 6.19 and 6.21. With the standard deviation value of 0.1 chips, the BER degradation is relatively high in the case of estimated channel. Based on the results, it may be concluded that the delay error standard deviation should be around 0.05 chips in practice.

6.2.2.2. Quasi-coherent DLL

The PIC based delay-locked loops are found by taking the derivative of the argument in (6.22) and setting the derivative to zero. The timing error signal can be written as

$$\begin{aligned}
\epsilon_{k,l}^{(n)} &= \frac{\partial}{\partial \tilde{\tau}_{k,l}} \mathrm{Re}\left\{ \hat{c}_{k,l}^{*(n)} \hat{b}_k^{(n)} \left[y_{k,l}^{(n)}(\tilde{\tau}_{k,l}) - \hat{\Psi}_{k,l}^{(n)}(\tilde{\tau}_{k,l}) \right] \right\} \\
&= \mathrm{Re}\left\{ \hat{c}_{k,l}^{*(n)} \hat{b}_k^{(n)} \left[\frac{\partial}{\partial \tilde{\tau}_{k,l}} y_{k,l}^{(n)}(\tilde{\tau}_{k,l}) - \frac{\partial}{\partial \tilde{\tau}_{k,l}} \hat{\Psi}_{k,l}^{(n)}(\tilde{\tau}_{k,l}) \right] \right\} \\
&\approx \mathrm{Re}\left\{ \hat{c}_{k,l}^{*(n)} \hat{b}_k^{(n)} \left[\left(y_{k,l}^{(n)}(\hat{\tau}_{k,l}^{(n-1)} + \Delta) - y_{k,l}^{(n)}(\hat{\tau}_{k,l}^{(n-1)} - \Delta) \right) \right.\right. \\
&\quad \left.\left. - \left(\hat{\Psi}_{k,l}^{(n)}(\hat{\tau}_{k,l}^{(n-1)} + \Delta) - \hat{\Psi}_{k,l}^{(n)}(\hat{\tau}_{k,l}^{(n-1)} - \Delta) \right) \right] \right\}, \qquad (6.30)
\end{aligned}$$

where the derivative is approximated by the early-late difference (2Δ). Assuming ideal channel coefficient and data estimates, the timing error signal has the form

$$\begin{aligned}
\epsilon_{k,l}^{(n)} &= \mathrm{Re}\left\{ c_{k,l}^{*(n)} b_k^{(n)} \left[c_{k,l}^{(n)} b_k^{(n)} \left(R_{kl,kl}^{(n,n)}(\hat{\tau}_{k,l}^{(n-1)} + \Delta) - R_{kl,kl}^{(n,n)}(\hat{\tau}_{k,l}^{(n-1)} - \Delta) \right) \right.\right. \\
&\quad + \left(\Psi_{k,l}^{(n)}(\hat{\tau}_{k,l}^{(n-1)} + \Delta) - \Psi_{k,l}^{(n)}(\hat{\tau}_{k,l}^{(n-1)} - \Delta) \right) \\
&\quad \left.\left. - \left(\hat{\Psi}_{k,l}^{(n)}(\hat{\tau}_{k,l}^{(n-1)} + \Delta) - \hat{\Psi}_{k,l}^{(n)}(\hat{\tau}_{k,l}^{(n-1)} - \Delta) \right) + \bar{n}^{(n)} \right] \right\} \\
&= |c_{k,l}^{(n)}|^2 e_{k,l}^{(n)} + \check{n}^{(n)}, \qquad (6.31)
\end{aligned}$$

where $\check{n}^{(n)}$ is the noise term containing MAI estimation errors, $e_{k,l}^{(n)}$ is the ideal timing error signal in the absence of fading, noise and interference, and $R_{kl,kl}^{(n,n)}(\cdot)$ is the autocorrelation value with the given delay. If a moving average filter is used as the loop filter[3], the output of the loop filter in fading channels can be written

[3]The moving average filter is used here only to simplify the notations. Depending on the closed-loop transfer function [33] this type of loop filter may lead to an unstable feedback circuit and hence it cannot be used as a loop filter in all cases.

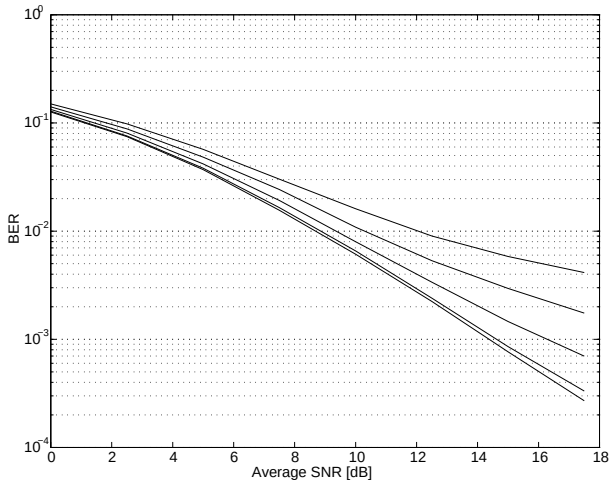

Fig. 6.18. The BER of the two-stage HD-PIC receiver in a two-path fading channel as a function of the average SNR with various delay estimation error standard deviations (σ_τ = 0, 0.05, 0.1, 0.15, 0.2 from down to up) with $K = 16$, no near-far problem, known channel gains.

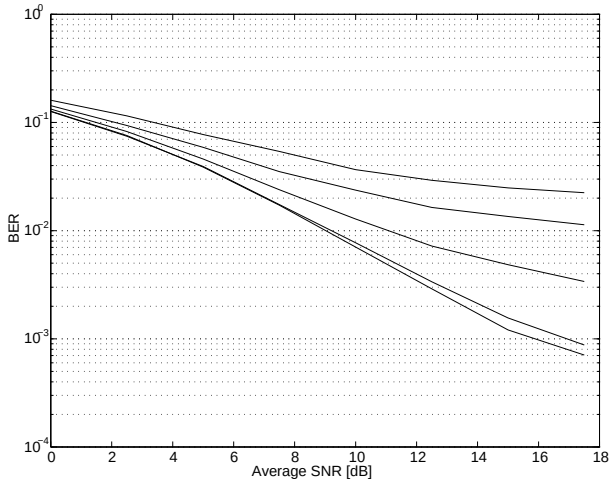

Fig. 6.19. The BER of the two-stage HD-PIC receiver in a two-path fading channel as a function of the average SNR with various delay estimation error standard deviations (σ_τ = 0, 0.05, 0.1, 0.15, 0.2 from down to up) with $K = 16$, 5 users have 10 dB higher power, known channel gains.

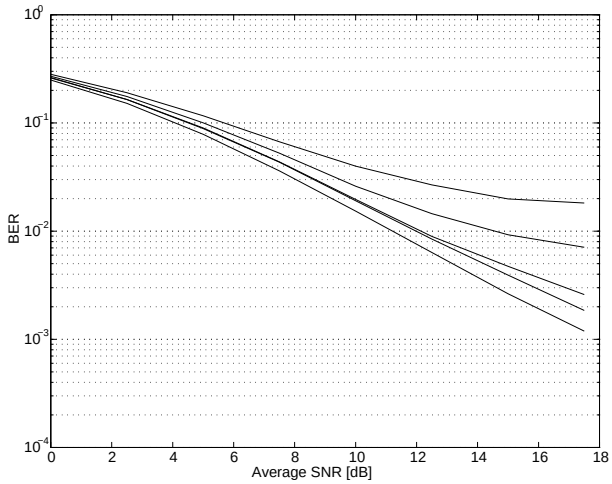

Fig. 6.20. The BER of the two-stage HD-PIC receiver in a two-path fading channel as a function of the average SNR with various delay estimation error standard deviations (σ_τ = 0, 0.05, 0.1, 0.15, 0.2 from down to up) with $K = 16$, no near-far problem, estimated channel.

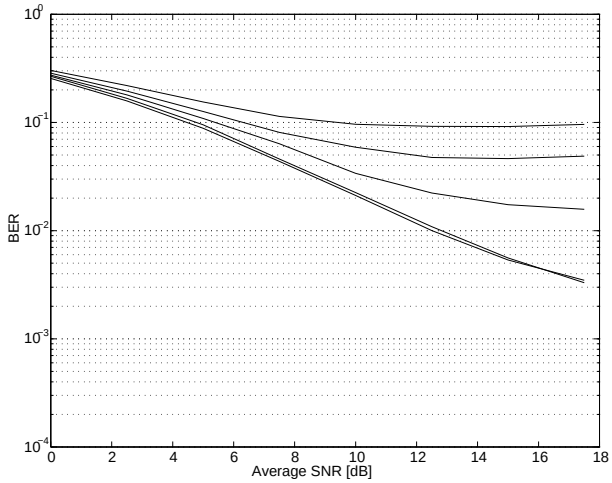

Fig. 6.21. The BER of the two-stage HD-PIC receiver in a two-path fading channel as a function of the average SNR with various delay estimation error standard deviations (σ_τ = 0, 0.05, 0.1, 0.15, 0.2 from down to up) with $K = 16$, 5 users have 10 dB higher power, estimated channel.

as

$$\begin{aligned}\tilde{c}_{k,l}^{(n)} &= \frac{1}{\mathcal{T}} \sum_{i=n-\mathcal{T}+1}^{n} \left(\left| c_{k,l}^{(i)} \right|^2 e_{k,l}^{(i)} + \check{n}^{(i)} \right) \\ &= \tilde{\mathcal{A}}_{k,l}^{2(n)} e_{k,l}^{(n)} + \tilde{n}^{(n)}, \end{aligned} \tag{6.32}$$

where $\mathcal{T}$ is the effective loop filter integration time in symbol intervals, $\tilde{\mathcal{A}}_{k,l}^{(n)}$ is the filtered amplitude component and the delay is assumed to be fixed within the observation interval $\mathcal{T}$, i.e., $e_{k,l}^{(i)} = e_{k,l},\ \forall i \in \{n - \mathcal{T} + 1, \ldots, n\}$.

In the case of time-discretized delay tracking, the post-synch AGC has to normalize the s-curve in such a way that only the term $e_{k,l}^{(n)}$ is left after normalization of (6.32). In other words, the term $\tilde{\mathcal{A}}_{k,l}^{2(n)}$ needs to be compensated for to guarantee the stability of the loop. A multiuser receiver is an alternative to conventional receivers which require accurate power control. Thus the average signal level in multiuser receivers is allowed to vary. The residual amplitude estimation is therefore crucial for the DLLs in multiuser receivers. In digital DLLs with a limited number of possible timing positions, the s-curve is quantized. In such cases, the post-synch AGC is needed to keep the timing error signal within the dynamic range of the s-curve.

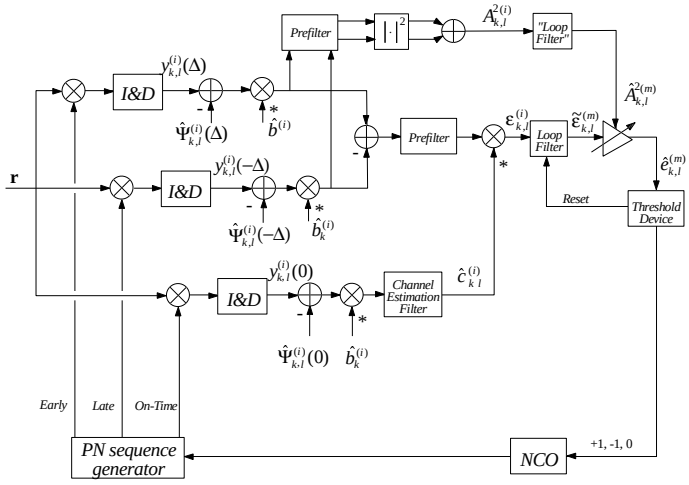

Fig. 6.22. Quasi-coherent DLL.

The structure of the quasi-coherent DLL (QC-DLL) is presented in Figure 6.22. The residual amplitude estimation consists of taking the absolute value of the filtered complex channel coefficient and squaring, which both are nonlinear operations. The noise will cause some bias to the estimate due to nonlinearities.

Some prefiltering is therefore needed to suppress noise before the nonlinearities. The prefilter should be selected in a similar manner as the channel estimation filters. After prefiltering and nonlinearities, the resulting rough amplitude estimate should be filtered by the equivalent of the loop filter. The filters do not need to be alike, only the effective integration times should be equal. This guarantees that the estimate corresponds to the residual amplitude component at the output of the loop filter. The residual amplitude estimate can now be written as

$$\begin{aligned}\hat{\mathcal{A}}_{k,l}^{2(n)} &= \frac{1}{\mathcal{T}}\left[\sum_{i=n-\mathcal{T}+1}^{n}\left(\left|\sum_{j=1}^{J} v_{k,l}^{(n)}(j) y_{[PIC]k,l}^{(i-j+1)}(\hat{\tau}_{k,l}^{(i-1)}+\Delta)\right|^2\right)\right. \\ &+ \left.\sum_{i=n-\mathcal{T}+1}^{n}\left(\left|\sum_{j=1}^{J} v_{k,l}^{(n)}(j) y_{[PIC]k,l}^{(i-j+1)}(\hat{\tau}_{k,l}^{(i-1)}-\Delta)\right|^2\right)\right], \qquad (6.33)\end{aligned}$$

where $v_{k,l}^{(n)}(j)$ are the prefilter weights for the FIR type filter which can be adapted according to (6.15) and $y_{[PIC]}$ is the matched filter output after interference cancellation.

A close examination of the loop filter output (6.32) and the residual amplitude estimate (6.33) reveals that they do not coincide exactly in time. The reason for this is the prefiltering used in the residual amplitude estimation. In fact, the timing error signal should also be prefiltered, before complex coefficient weighting and loop filtering (see Fig. 6.22). The effect of data modulation must be removed before the prefiltering. The resulting timing error detector is one kind of smoother where the extra delay inherent in smoothers is implemented by the prefilter. The timing error signal with prefiltering is

$$\begin{aligned}\tilde{\epsilon}_{k,l}^{(n)} &= \frac{1}{\mathcal{T}}\sum_{i=n-\mathcal{T}+1}^{n}\hat{c}_{k,l}^{*(i)}\left(\sum_{j=1}^{J} v_{k,l}^{(n)}(j)\right. \\ &\left.\cdot\hat{b}_{k}^{(i-j+1)}\left(y_{[PIC]k,l}^{(i-j+1)}(\hat{\tau}_{k,l}^{(i-j)}+\Delta)-y_{[PIC]k,l}^{(i-j+1)}(\hat{\tau}_{k,l}^{(i-j)}-\Delta)\right)\right). \qquad (6.34)\end{aligned}$$

The normalized timing error signal is finally obtained by dividing (6.34) by (6.33):

$$\hat{e}_{k,l}^{(n)} = \frac{\tilde{\epsilon}_{k,l}^{(n)}}{\hat{\mathcal{A}}_{k,l}^{2(n)}}. \qquad (6.35)$$

The normalized timing error signal $\hat{e}_{k,l}^{(n)}$ is used to control the phase of the local reference code generator. In a digital receiver, the minimum shift of the local sampled sequence is one sample interval. Usually four samples per chip results in satisfactory performance. In [220, 221], a lead-lag phase-locked loop (PLL) [218] has been used to achieve robust phase control of the reference signal. The local reference is either advanced or retarded by one sample according to the sign of the timing error signal. Actually, the timing error signal is applied to a threshold

device which outputs either ± 1 or 0, accordingly. The threshold level is usually set to the middle of the s-curve origin and the first non-zero point.

Nonlinear loop filters [222] are well suited for the lead-lag loops. In [218], a sequential filter (or a random walk filter) was used. Here, a dynamic integrate-and-dump (DI&D) filter [223] will be used. The DI&D filter consists of a recursive integrator followed by a threshold device. The difference between the usual I&D and DI&D filters is that the first one is reset regularly and the DI&D filter is reset only after a timing correction.

6.2.2.3. SCCL loop

In [224] a reduced range search was introduced for single-user symbol synchronization. The authors called the scheme sample-correlate-choose-largest (SCCL) symbol synchronizer. It is based on three parallel correlators, which are spaced one sample apart. The correlator outputs are filtered over $\mathcal{T}$ symbol intervals in an integrate-and-dump filter. The outputs of the I&D filters are then passed to a nonlinear device, which selects the maximum correlation value to be the timing estimate for the next $\mathcal{T}$ symbol intervals. The timing correction principle of the SCCL loop is the same as in lead-lag phase-locked loops [218]. In comparison to the standard early-late DLLs, the SCCL loop is more robust, since it does not require the so-called post-synch AGC for s-curve amplitude normalization prior to timing control as will be explained in the sequel.

The structure of a PIC based SCCL delay tracker is presented in Figure 6.23. The effect of the data modulation is removed after interference cancellation. Then the correlator outputs are prefiltered and weighted by the conjugate of the channel coefficient estimates. By using similar filters in prefiltering and channel estimation filtering, the delay error (or lag-error) in the channel coefficient estimates becomes negligible. In fact, this results in the similar structure as in non-coherent DLLs with the exception that the signals are filtered prior to squaring, i.e., the despreading interval is implicitely extended (see Section 5.1.3). The signals at the output of the FIR prefilters can be written as

$$\bar{y}_{k,l}^{(i)}(\tilde{\tau}_{k,l}) = \sum_{j=1}^{J} v_{k,l}^{(i)}(j)\check{y}_{k,l}^{(i-j+1)}(\tilde{\tau}_{k,l}), \tag{6.36}$$

and for the IIR prefilters as

$$\bar{y}_{k,l}^{(i)}(\tilde{\tau}_{k,l}) = v_{k,l}^{(i)}\check{y}_{k,l}^{(i)}(\tilde{\tau}_{k,l}) + q_{k,l}^{(i)}\bar{y}_{k,l}^{(i-1)}(\tilde{\tau}_{k,l}), \tag{6.37}$$

where

$$\check{y}_{k,l}^{(i)}(\tilde{\tau}_{k,l}) = \hat{b}_k^{*(i)}\left(y_{k,l}^{(i)}(\tilde{\tau}_{k,l}) - \hat{\Psi}_{k,l}^{(i)}(\tilde{\tau}_{k,l})\right) = \hat{b}_k^{*(i)} y_{[PIC]k,l}^{(i)}(\tilde{\tau}_{k,l}) \tag{6.38}$$

is the MAI "free" and weighted correlator output with trial delay $\tilde{\tau}_{k,l} = \hat{\tau}_{k,l}^{(n')} + \Delta_u$, $\Delta_u \in \{-1, 0, +1\}$, $n' = \lfloor \frac{n}{\mathcal{T}} \rfloor$ [4], and $v_{k,l}^{(i)}$, $q_{k,l}^{(i)}$ are the prefilter weights. The delay

[4] $\lfloor x \rfloor$ denotes the largest integer less than or equal to x, i.e., the floor function.

estimate for the next $\mathcal{T}$ symbols is

$$\begin{aligned}\hat{\tau}_{k,l}^{(n'+1)} &= \arg \max_{\hat{\tau}_{k,l}^{(n')}+\Delta_u} \left(\mathrm{Re}\left\{\hat{y}_{k,l}^{(n'+1)}(\hat{\tau}_{k,l}^{(n')}+\Delta_u)\right\}\right) \\ &= \hat{\tau}_{k,l}^{(n')} + \arg \max_{\Delta_u} \left(\mathrm{Re}\left\{\hat{y}_{k,l}^{(n'+1)}(\hat{\tau}_{k,l}^{(n')}+\Delta_u)\right\}\right), \end{aligned} \tag{6.39}$$

where

$$\hat{y}_{k,l}^{(n'+1)} = \frac{1}{\mathcal{T}} \sum_{i=n-\mathcal{T}+1}^{n} \tilde{y}_{k,l}^{(i)} = \frac{1}{\mathcal{T}} \sum_{i=n-\mathcal{T}+1}^{n} \hat{c}_{k,l}^{*(i)} \bar{y}_{k,l}^{(i)}. \tag{6.40}$$

The timing error correction in the SCCL loop is not based on the exact values of the s-curve, but rather on the selection of the maximum of the three trials. Since the amplitude component is roughly the same for every trial value, residual amplitude components need not to be compensated for.

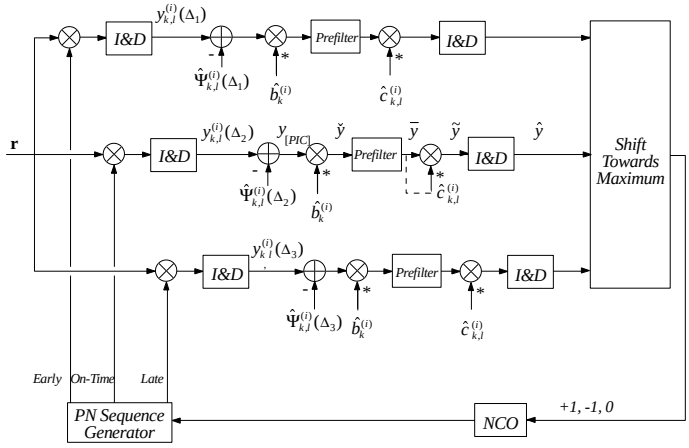

Fig. 6.23. SCCL delay tracking loop.

6.2.2.4. Numerical examples

The main parameters used in the simulations were: carrier frequency 2.0 GHz, symbol rate 16 kbits/s, 31 chip Gold codes, the number of users 1 – 30, the number of samples per chip was eight, and one-path Rayleigh fading channels with vehicle speeds of 80 km/h (which results in the maximum normalized Doppler shift of $9.26 \cdot 10^{-3}$) were used. Perfect data detection was assumed, so only one

cancellation stage was used. Only one near-far situation was studied in the 30-user case (10 users have 10 dB higher power). The observation interval was $\mathcal{T} = 70$, and an adaptive LMS FIR predictor of length 20 symbols was used for the channel coefficient estimation. The normalized root mean squared error (RMSE) averaged over the desired users of equal energy (RMSE $= \frac{1}{20}\sum_{k,l=1}^{20} T_c^{-1}\sqrt{E|\hat{\tau}_{k,l} - \tau_{k,l}|^2}$,) was used as the performance measure in delay tracking.

The performance of the quasi-coherent DLL and the SCCL loops are presented in Figure 6.24. The SCCL has 5 – 6 dB better tracking performance than the QC-DLL in the single-user case. The comparison of the loops is not fair, since the loop bandwidths may differ and are difficult to determine analytically for the loops studied. However, the transient responses of the loops have been adjusted to be similar and the comparison is justified. The PIC based QC-DLL has remarkably worse performance in the 30-user case than the SCCL loop. About 20 – 30 % of the users had a bias of ± 1 sample, which causes a bias in the average RMSE. This is caused by inaccurate MAI estimates, which will cause biased residual amplitude estimates and biased normalized timing error signals. Therefore, the average RMSE is saturated to the level of 0.06 – 0.07.

The root mean squared (RMS) code tracking error for the conventional SCCL loop in the presence of MAI is presented also in Figure 6.24. The RMSE saturates around 10 dB SNR with the conventional SCCL loop. The RMSE of the PIC based algorithm does not saturate at the SNRs of practical interest. It can be expected that the saturation level of the PIC based algorithms is quite low; with ideal MAI estimates the asymptotic RMSE approaches zero. Nevertheless, the performance was slightly worse than with the conventional algorithm at low SNRs. In these examples, only one cancellation stage was used for simplicity. It is clear that the performance of the PIC based DLLs is improved remarkably when taking into account the fact that the PIC based receivers perform cancellation several times in the multistage receivers and that the delay trackers can be placed in the last receiver stage. On the other hand, the performance will be degraded when there are errors in the data decisions. In section 6.2.2.1, the delay estimation requirements for PIC receivers were estimated. By comparing the results of Figure 6.24 to these requirements we can see that the PIC based SCCL loop satisfies the requirements.

The BER performance of the multistage HD-PIC detector with the PIC based SCCL loop based delay tracking was also simulated. The results are presented in Figure 6.25. The observation interval in the SCCL loop was 50 symbols. The chip shaping filter used was the root raised cosine filter with roll-off 0.75. Four samples per chip were taken at the receiver. The timing accuracy of the receiver was eight samples, i.e., the filtered PN sequence of the receiver has been sampled eight times per chip. Four of those are selected for despreading according to the SCCL based timing control. The BER was simulated both with and without the near-far case (5 users have 10 dB higher power) with 16 users. It is obvious that the practical delay tracking algorithms in PIC based receivers do not degrade the BER performance significantly at the SNRs of practical interest. Hence the delay tracking performance is not the limiting factor when applying the PIC receivers to practical systems.

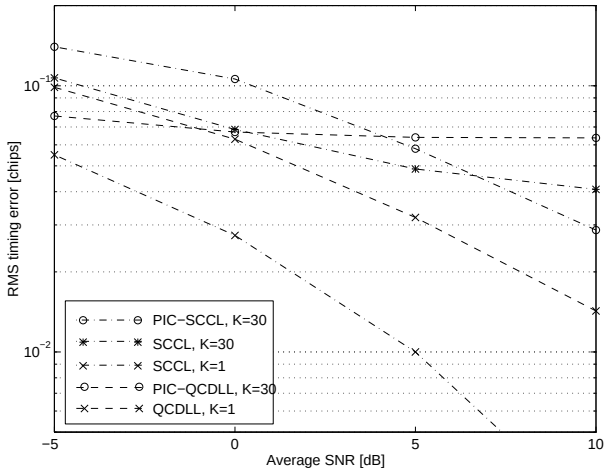

Fig. 6.24. RMS delay errors for the PIC based and the conventional SCCL and QC-DLL loops in Rayleigh fading channels in single-user and 30-user cases. The observation interval was 70 symbols.

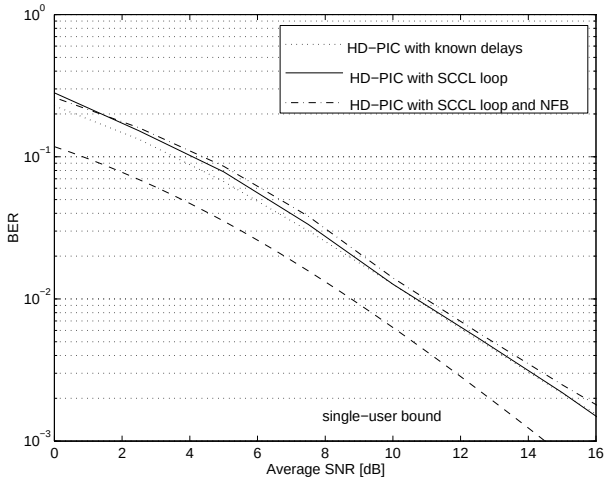

Fig. 6.25. Bit error rate of the two-stage HD-PIC receiver using an SCCL loop for delay tracking in a two-path fading channel with vehicle speeds of 80 km/h and $K = 16$.

6.2.2.5. Discussion

Delay tracking in the PIC receivers was studied in this section. The performance of the PIC based and the conventional delay trackers was investigated in an asynchronous CDMA system. A PIC based receiver for estimating the channel coefficients and data was used in conjunction with the delay trackers. According to the results, the DLLs which require adaptive loop gain control result in biased delay trackers in multiuser environment. Only the SCCL loop resulted in unbiased delay trackers. The SCCL loop was studied both with and without interference cancellation. The results indicate that the PIC based SCCLs have better performance than the conventional SCCLs at high SNRs, whereas the conventional SCCLs had better performance at low SNRs. It was observed that the BER is not degraded much in practical HD-PIC receivers utilizing the PIC based SCCL loops in delay tracking.

6.3. Residual interference suppression in PIC receivers

The parallel interference cancellation relies on the knowledge of the number of users and propagation paths. In practice the number is not known exactly, e.g., due to inter-cell interference, unknown propagation paths or new users trying to connect to the base station. As a result, there will be some residual interference even with perfect cancellation of the known signal components. In many cases the inter-cell interference can be large enough to degrade the performance of the PIC receivers significantly. For that reason residual interference suppression is crucial to guarantee that the PIC receivers can operate reliably. In this chapter, one possibility for residual interference suppression in PIC receivers is considered. The approach taken is to combine the precombining LMMSE and PIC receivers.

6.3.1. Hybrid LMMSE-PIC receiver

Let us consider the receiver structure of Figure 6.1(b). The received signal vector after interference cancellation at the pth stage for the desired signal component is given by (see p. 142)

$$\bar{\mathbf{r}}^{(n)}_{[PIC]k,l}(p) = \bar{\mathbf{r}}^{(n)} - \hat{\bar{\mathbf{\Psi}}}^{(n)}_{[\mathbf{r}]k,l}. \tag{6.41}$$

In the standard PIC receiver, the signal is despread by matched filtering

$$y^{(n)}_{[PIC]k,l}(p) = \bar{\mathbf{s}}^{\mathrm{T}}_{k,l}\bar{\mathbf{r}}^{(n)}_{[PIC]k,l}(p). \tag{6.42}$$

The matched filters can be replaced with the precombining LMMSE filters studied in Chapters 3 and 4. The resulting hybrid LMMSE-PIC receiver processes each multipath component according to

$$y^{(n)}_{[L-PIC]k,l}(p) = \bar{\mathbf{s}}^{\mathrm{T}}_{k,l}\mathbf{\Sigma}^{-1}_{\bar{\mathbf{r}}_{[PIC]k,l}(p)}\bar{\mathbf{r}}^{(n)}_{[PIC]k,l}(p) = \mathbf{w}^{\mathrm{T}}_{[PIC]k,l}(p)\bar{\mathbf{r}}^{(n)}_{[PIC]k,l}(p). \tag{6.43}$$

The techniques studied in Chapter 4 can be used to iteratively calculate the residual interference suppression filters $\mathbf{w}_{[PIC]k,l}(p)$ for every cancellation stage.

The matched filters can be replaced by the LMMSE filters at any receiver stage. When the LMMSE filters are also used to produce the rough channel estimates, attention must be paid to the normalization of the LMMSE receiver coefficients. Large filter gains increase absolute values of MAI estimates and a small gain decreases the MAI terms. Hence, a unit filter gain for the desired signal component would be desirable. In fact, the normalization according to the MOE criterion which results in the filter coefficient vector $\mathbf{w}_{[MOE]k,l} = \frac{\mathbf{\Sigma}_{\tilde{\mathbf{r}}}^{-1}\bar{\mathbf{s}}_{k,l}}{\bar{\mathbf{s}}_{k,l}^{\mathrm{T}}\mathbf{\Sigma}_{\tilde{\mathbf{r}}}^{-1}\bar{\mathbf{s}}_{k,l}}$, gives the unit filter gain to the desired signal component ($\bar{\mathbf{s}}_{k,l}^{\mathrm{T}}\mathbf{w}_{[MOE]k,l} = 1$). In the numerical examples, normalization according to the MOE criterion will be used.

6.3.2. Numerical examples

The channel model used was a two-path equal energy Rayleigh fading channel with vehicle speeds of 80 km/h and a carrier frequency of 2.0 GHz. The data rate was assumed to be 16 kbit/s (which results in the maximum normalized Doppler shift of $9.26 \cdot 10^{-3}$) and the maximum delay spread was one symbol interval. Gold codes of length 31 chips were used, the receiver sampling rate was 1 sample per chip. There were 16 known users at the SNR of 15 dB and one unknown user. The power of the unknown user was between -20 – 20 dB in comparison to the other users. The blind LS receiver described in Section 4.1.2.2 was used in the HD-PIC receiver to suppress residual interference due to unknown signal components. The sample-covariance was estimated recursively by using a forgetting factor value $\gamma = 0.999$. Direct inversion of the sample-covariance matrix was performed once per hundred data symbols to speed up simulations.

The BER results for the basic HD-PIC receiver are presented in Figure 6.26 for the average SNRs of 5, 10 and 15 dB as a function of the unknown user power difference with respect to the synchronized users. The results reveal that the BER is degraded significantly with an unknown user with a 10 dB higher power. At SNRs higher than 10 dB, an unknown user with the same power as the synchronized known users is sufficient to cause a significant performance degradation.

The BER results for the hybrid LMMSE-PIC receiver are presented in Figure 6.27 for the average SNRs of 15 dB as a function of the unknown user power difference with respect to the synchronized users. If the blind LS receiver is used instead of the matched filter at the last receiver stage ("IC2" in the figure), which produces the channel estimates for all receiver stages (see Section 6.1.2), the BER degradation is significantly smaller. When the blind interference suppression filter is used both at the matched filter stage and the last cancellation stage ("MF & IC2" in the figure), the performance improvement is marginal compared with the "IC2" case. The blind LS receiver at the first stage alone did not improve the performance of the basic HD-PIC receiver due to relatively poor channel estimates. The best performance was obtained when the blind LS receiver is used at every

receiver stage ("MF & IC1 & IC2" in the figure). In fact, the performance with a blind adaptive LS receiver with span of three symbol intervals ($M = 3$) is almost insensitive to the unknown user in the cases studied. The difference between the receivers of span one and three is quite small in the case when all receiver stages include blind interference suppression with $K = 16$.

The BER results as a function of the number of users at the SNR of 15 dB and unknown user power offset of 10 dB are presented in Figure 6.28. The basic HD-PIC receiver has untolerable high BER in all cases studied. The BERs of the LMMSE-PIC receivers with span one and three are almost the same up to 16 active users. Increasing the number of users up to 32 reveals that the receiver with span three has significantly lower BER than the receiver with span one symbol interval. In fact, the BER of the LMMSE-PIC with span one is almost as high as with the basic HD-PIC with 32 active users. In the case of 28 active users, the BER of the receiver with span one is significantly smaller than with the basic HD-PIC receiver. Hence, the hybrid LMMSE-PIC receiver with blind interference suppression filters of span one symbol interval at every receiver stage can be used to achieve robustnes against unsynchronized users. The performance gains with it are significant when the number of active users is less than the processing gain of the system.

6.3.3. Discussion

The performance of the PIC receivers is sensitive to the unknown signal components that cannot be cancelled. If the power of the unknown components is high, the performance is degraded significantly. The performance degradation is due to the biased MAI estimates. Some methods to make the bias smaller have been reported in [141, 142]. The previously known methods for bias reduction are based on some form of partial interference cancellation [142] where only a fraction of the MAI estimate is subtracted at each cancellation stage. In this chapter, a more effective method was presented; the residual interference is suppressed with a linear filter rather than partial cancellation with a single weight.

It was observed in Section 6.2.1 that the PIC based delay acquisition method does not always improve the performance of the conventional MF method when the number of users is high or the power of the new user being acquired is high. It was shown that the BER performance of the PIC receivers is significantly degraded due to unsynchronized users. Taking advantage of the hybrid LMMSE-PIC receiver in the acquisition of the new users, it can be anticipated that the acquisition performance can be further improved. It is also possible to apply the minimum variance based acquisition (see Section 5.1.1) for the new user.

In future CDMA systems, the data rates of different users can vary significantly. The simplest technique to change the data rate is to change the spreading factor. The users with a higher data rate may cause significant interference to the lower data rate users. In the case when base station diversity is not used, the high data rate users from the other cells may degrade the performance of the PIC receivers significantly. The combination of the blind adaptive and PIC receivers solves the

bias problem due to unknown signal components of high power. Hence the hybrid LMMSE-PIC receiver is seen as one of the most promising alternatives for base station receivers in the future CDMA systems. Further studies are still needed to provide more insight about their applicability to practical systems.

In a mixed data rate system, the PIC receiver with cancellation prior to despreading can be used without any additional difficulties. Since the MAI estimate is formed for the wideband signal for each user and path, the actual data rate does not have a major impact on the MAI estimation and interference cancellation. When applying the proposed residual interference suppression method in PIC receivers operating in a variable spreading factor system, the basic linear interference suppression filter should be modified. Most linear interference suppression algorithms require the interference to be cyclo-stationary (see Section 3.2.2). In order to retain cyclo-stationarity, the linear interference suppression filter taps must be cyclically shifted from one symbol interval to another. Effectively, the receiver uses the lowest spreading factor for all users in despreading (and blind interference suppression). The sub-symbols produced by the linear interference suppression filters are then combined for the low data rate users. Although not studied in this thesis, the application of the hybrid LMMSE-PIC receivers in mixed data rate systems seems to be possible in WCDMA type systems.

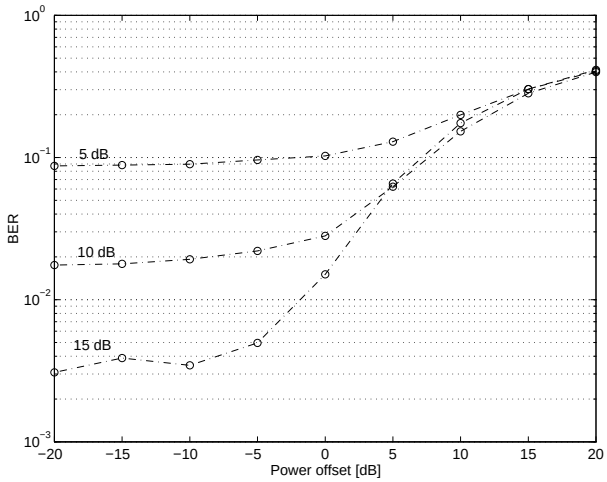

Fig. 6.26. BER for the HD-PIC receiver in two-path fading channels with different SNRs (5, 10, 15 dB) as a function of the unknown user power offset with respect to the known users, $K = 16 + 1$.

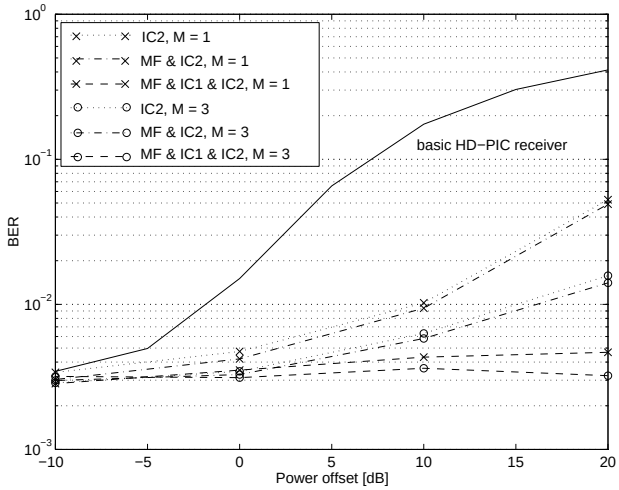

Fig. 6.27. BER for the LMMSE-PIC receivers with span one ($M = 1$) and three ($M = 3$) symbol intervals in two-path fading channels at the SNR of 15 dB as a function of the unknown user power offset with respect to the known users, $K = 16 + 1$.

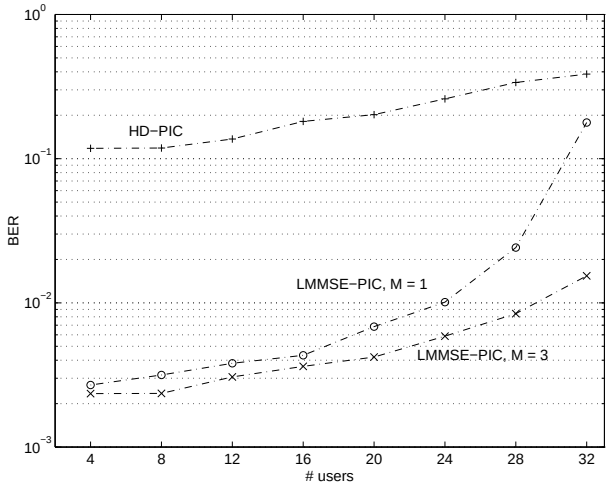

Fig. 6.28. BER for the HD-PIC and LMMSE-PIC receivers with span one ($M = 1$) and three ($M = 3$) symbol intervals in two-path fading channels at SNR of 15 dB as a function of the number of users with one unknown user of 10 dB higher power.

6.4. Spatial signal processing in PIC receivers

The PIC receivers can be extended to the spatial domain in a similar fashion as the LMMSE receivers (Section 3.3). The most practical versions of the PIC receivers perform interference suppression prior to matched filtering and multipath combining. In that receiver configuration, the best performance is obtained if the spatial domain processing precedes interference suppression. The PIC receiver with such spatial domain processing is derived in Appendix 5.

The spatial-temporal PIC receiver is a straightforward extension of the basic PIC receivers. However, neither simulations nor analysis for the spatial-temporal multistage PIC will be made in this thesis. In [144] some studies for the spatial-temporal HD-PIC receiver have been made. The performance of the receiver was shown to be very good in the cases studied.

Once the delays and the direction-of-arrivals are estimated (see Appendix 5) the PIC based multistage detection can be carried out. The spatial-temporal multistage PIC makes the decisions at the pth stage according to

$$\begin{aligned}\hat{\mathbf{b}}^{(n)}(p) &= \operatorname{sgn}\Big[\operatorname{Re}\big\{\mathcal{C}\hat{\mathbf{C}}^{\mathrm{H}(n)}(p)\big(\mathbf{Y}^{(n)} - \hat{\tilde{\mathbf{\Psi}}}^{(n)}(p)\big)\big\}\Big] \\ &= \operatorname{sgn}\Big[\operatorname{Re}\big\{\mathcal{C}\hat{\mathbf{C}}^{\mathrm{H}(n)}(p)\mathbf{y}^{(n)}_{[PIC]}(p)\big\}\Big] \qquad (6.44)\end{aligned}$$

where $\mathcal{C} = \mathbf{I}_K \otimes \mathbf{1}_L^{\mathrm{T}}$ is the multipath combining matrix, $\mathbf{Y}^{(n)} = \sum_{k=1}^{K}\sum_{l=1}^{L}\mathbf{Y}^{(n)}_{k,l} \in \mathbb{C}^{KL}$ is the spatially combined matched filter output vector and $\hat{\tilde{\mathbf{\Psi}}}^{(n)}(p) = \sum_{k=1}^{K}\sum_{l=1}^{L}\hat{\tilde{\mathbf{\Psi}}}^{(n)}_{k,l}(p) \in \mathbb{C}^{KL}$ is the corresponding MAI vector (see Appendix 5 for more details).

6.5. Summary

Data detection, channel estimation, delay acquisition, delay tracking, residual interference suppression and array processing in PIC receivers was studied in this chapter. In fading channels the channel estimation filtering is crucial to obtain good performance. Adaptive channel estimation filters were derived and analyzed by simulations. Their performance is significantly better than with the non-adaptive filters. It was also found that the channel estimates needed in MAI estimation should be fed back from the last receiver stage to all other stages. The bit error rate simulations showed that the proposed receiver configuration results in good performance in highly loaded systems.

The PIC method was also applied to delay estimation at the base station receivers. Based on the mean acquisition time analysis, it can be concluded that the PIC based acquisition results in significantly shorter acquisition times with respect to the conventional MF acquisition in most cases. The PIC method was also shown to improve the tracking performance of the conventional DLLs. It was observed that the BER is not degraded significantly in the practical HD-PIC re-

ceivers utilizing PIC based SCCL loops in delay tracking. Hence, the PIC based timing synchronization is a preferable choice for the PIC receivers.

The blind adaptive receivers derived in Chapter 4 were combined to the PIC receivers in order to suppress residual interference, e.g., due to other cells. The hybrid LMMSE-PIC receiver was shown to give superior performance in comparison to the plain multistage HD-PIC receivers in the presence of the unknown signal components. This property is important in multi-cell environment when inter-cell interference can be significant. The hybrid LMMSE-PIC receiver is therefore seen very promising for the base station receivers in future CDMA systems.

The PIC receivers were extended to the spatial domain. The PIC based joint delay-DOA estimator was derived. A PIC receiver with spatial combining was also presented. No performance analysis was performed, however.

7. Summary and conclusions

Advanced receivers capable of suppressing multiple-access interference in wideband CDMA systems operating in frequency-selective fading channels were considered in this thesis. The introductory chapter included a literature review related to the topic under consideration. In Chapter 2 linear system models were derived for the purposes of the thesis. As a motivation for the rest of the thesis, some weak points related to conventional RAKE receivers in future CDMA systems were pointed out. In particular, the small spreading factors to be used with high data rate services were shown to create inter-path-interference problem with the conventional RAKE receivers.

Linear minimum mean squared error receivers for frequency-selective fading channels were derived in Chapter 3. The postcombining LMMSE receiver performs first multipath combining and subsequently interference suppression. The order of multipath combining and interference suppression is the opposite in the precombining LMMSE receivers. The receiver convergence problems caused by channel fading can be avoided by using the precombining LMMSE receivers. Based on the developed bit error probability analysis, it was shown that the postcombining LMMSE receivers potentially have a larger capacity than the precombining LMMSE receivers. The fading channel analysis also showed that the precombining LMMSE receivers offer significant performance and capacity improvements in comparison to the conventional RAKE receivers. The fading channel analysis was also performed for the FRAMES WCDMA concept. Based on the analysis, it can be anticipated that the conventional RAKE receivers cannot provide the quality required for the services specified for the UMTS. The downlink power control and mixed services with different QoS requirements also cause a severe near-far problem in the downlink. To support the use of adaptive equalizers in the WCDMA downlink, the signal structure should be modified, i.e., short scrambling codes should be used instead of the long ones. The LMMSE receiver principles were also extended to the spatial domain. It was shown that several alternative combinations of the spatial-temporal LMMSE receivers are possible.

Adaptive versions of the LMMSE receivers were studied in Chapter 4. The precombining LMMSE receiver results in separate interference suppression filters for each RAKE finger, hence it is called the LMMSE-RAKE receiver. Since the

receiver adaptation is based on the decisions and the channel estimates obtained from a conventional RAKE receiver, no training sequences are needed. Based on the convergence studies, the adaptive LMMSE-RAKE receiver can provide significant improvements in receiver convergence in comparison to other known blind adaptive receivers using LMS algorithms. If even faster convergence is required, one possibility is to use blind adaptive LS receivers, which were shown to yield good performance with relatively short observation intervals for sample-covariance matrix estimation. The general convergence analysis for the postcombining LMMSE receivers revealed that it is possible to use the postcombining LMMSE receivers with the highest data rates when the normalized rate of fading is low. It was also shown that it is possible to train the postcombining LMMSE receiver by using the decisions of the conventional RAKE receiver.

In Chapter 5, delay estimation in the precombining LMMSE receivers was studied. The minimum variance method suitable for the blind adaptive LS receivers was shown to improve the performance of the conventional delay acquisition schemes in CDMA systems. The BER sensitivity of the precombining LMMSE receivers to the delay estimation errors showed that the timing requirements to the blind adaptive receiver can be met with practical delay estimators. The inverse of the sample-covariance matrix needed in blind adaptive LS receivers was also utilized to derive an improved delay tracking algorithm. The analysis showed improvements in comparison to the standard delay-locked loop techniques.

Parallel interference cancellation based multiuser receivers were studied in Chapter 6. Data detection, channel estimation, delay acquisition, delay tracking, other cell interference suppression and array processing in PIC receivers were considered. In fading channels, the channel estimation filtering is crucial for obtaining good performance. Adaptive channel estimation filters were derived and analysed through simulations. Their performance is significantly better than with the non-adaptive filters. It was also determined that the channel estimates needed in MAI estimation should be fed back from the last receiver stage to all other stages. The bit error rate simulations showed that the proposed receiver configuration results in good performance in highly loaded systems. The PIC method in delay acquisition improves the acquisition performance in comparison to the conventional MF based method in most cases. The PIC method was also shown to improve the tracking performance of the conventional DLLs. Hence, the PIC based timing synchronization is a preferable choice for the PIC receivers. The blind adaptive receiver concepts derived in Chapter 4 were combined with the PIC receivers in order to suppress the residual interference, e.g., due to other cells. The hybrid LMMSE-PIC receiver was shown to give superior performance in comparison to the plain multistage PIC receiver in the presence of the unknown signal components. This property is important in a multi-cell environment when inter-cell interference can be relatively high. The hybrid LMMSE-PIC receiver is seen as one of the most promising alternatives for the base station receivers in future CDMA systems. The PIC receivers were extended to the spatial domain. The PIC based direction-of-arrival estimator was derived. No performance analysis was performed, however.

The results of this thesis indicate that the WCDMA system without interference cancellation or suppression results in significant performance and capacity

losses, since the performance of the conventional RAKE receivers degrades when increasing the data rate. Techniques for interference suppression in the downlink receivers and interference cancellation in the uplink were developed in this thesis. Although it is obvious that these techniques could give the expected capacity and the performance of the UMTS, the present WCDMA proposals in Japan and Europe support the use of these techniques only in the uplink direction.

At the base station receivers, most of the known interference suppression and cancellation techniques can be used and the uplink receiver performance can be improved significantly in comparison to the conventional RAKE receivers. The possibilities for improved downlink performance and capacity are quite limited. The present WCDMA proposal supports only the interference cancellation at mobile terminals due to the use of long scrambling codes. Since the data rate is allowed to vary frame-by-frame, interference may change dramatically for each frame. This will further complicate interference suppression and cancellation at mobile terminals since the rate information must be acquired from each user's data sequence. Hence, all users' data must first be demodulated to obtain the tentative decisions for interference cancellation and then decoded to obtain the rate information. The so-called blind rate detection schemes could be used also, but the practical implementations would require matched filters for all possible data rates for all data channels at the mobile terminals. Interference suppression and cancellation would be easier to implement if the data rate would change less often and if the network could provide explicit information of other user's data rates.

The mixed data rate issues were not addressed in detail in this thesis. In the case of mixed services, the received signal should be processed in blocks corresponding to the smallest spreading factor in linear interference suppression schemes. Otherwise, interference due to users with smaller spreading factor cannot be suppressed. The PIC based receiver with cancellation prior to matched filtering is well suited to mixed service systems, since the wideband interference term can be estimated and cancelled in a similar fashion as in a single data rate system without extra complexity or difficulty. However, the performance analysis for the conventional RAKE receivers revealed that the service mix cannot be very extensive, i.e., the spreading factors should not differ too much to limit the interference level. In practice, the set of data rates could be a cell specific or a carrier frequency specific parameter. The limited set of data rates would simplify the implementations of the blind rate detection schemes.

Interpath interference degrades the performance with small spreading factors due to correlated diversity branches. One possibility for improved downlink performance is to decorrelate the propagation paths to obtain the maximum diversity gain. Another possible solution would be to use adaptive channel impulse response matched filters prior to signal despreading. After such a channel matched filter the channel caused distortion is compensated and only one correlator is needed for despreading. Adaptive channel matched filters can also be used in the systems with long spreading codes and hence they may be applied to WCDMA downlink terminals.

In order to provide a further proof of the usefulness of the advanced receiver concepts studied in this thesis, they should be validated in more realistic scenar-

ios. When studying interference reduction methods, the single-cell environment can be used to obtain only indicative results. Power control in particular which is known to be one of the major problems in IS-95 system and will also be one of the problems in the WCDMA system, requires a multi-cell environment for receiver algorithm research. This would require hardware demonstrators due to the high computing power required. Mixed services with power control and channel coding in multi-cell environment should be studied together with interference suppression or cancellation based receivers. Unfortunately, the time schedule of the standardization process is extremely tight and there is little opportunity left for serious hardware trials. It is possible that the UMTS will not comprehensively support the use of multiuser receiver techniques. Nevertheless, some of the schemes studied in this thesis can be utilized in the forthcoming UMTS, at least in base station receivers. Another application area for these receiver techniques is in the unlicenced ISM (industrial, scientific and medical) band applications. The wireless local loops (WLL), cordless phones and wireless local area networks (WLAN) are the applications where they can and will be used to improve the performance, capacity and reliability of existing systems.

References

1. Steele R (1992) Mobile Radio Communications. Pentech Press, London.
2. Simon MK, Omura JK, Scholtz RA & Levitt BK (1994) Spread Spectrum Communications Handbook. McGraw-Hill, New York, USA.
3. Price R & Green PE (1958) A communication technique for multipath channels. Proceedings of the IRE 46: 555–570.
4. Duel-Hallen A, Holtzman J & Zvonar Z (1995) Multiuser detection for CDMA systems. IEEE/ACM Personal Communications 2(2): 46–58.
5. Juntti M & Glisic S (1997) Advanced CDMA for wireless communications. In: Glisic SG & Leppänen PA (eds), Wireless Communications: TDMA Versus CDMA, Kluwer, 4: 447–490.
6. Moshavi S (1996) Multi-user detection for DS-CDMA communications. IEEE Communications Magazine 34(10): 124–137.
7. Ojanperä T & Prasad R (1998) Wideband CDMA for Third Generation Mobile Communications. Artech House.
8. Ovesjö F, Dahlman E, Ojanperä T, Toskala A & Klein A (1997) FRAMES multiple access mode 2 — wideband CDMA. In: Proc. IEEE International Symposium on Personal, Indoor, and Mobile Radio Communications (PIMRC), Helsinki, Finland, 1: 42–46.
9. Adachi F, Sawahashi M, Dohi T & Ohno K (1996) Coherent DS-CDMA: Promising multiple access for wireless multimedia mobile communications. In: Proc. IEEE International Symposium on Spread Spectrum Techniques and Applications (ISSSTA), Mainz, Germany, 1: 351–358.
10. Toskala A, Castro J, Dahlman E, Latva-aho M & Ojanperä T (1998) FRAMES FMA2 wideband-CDMA for UMTS. European Transaction on Telecommunications, to appear.
11. Schwartz M, Bennett WR & Stein S (1966) Communication Systems and Techniques. McGraw-Hill, Inc., New York, USA.
12. Bello PA (1963) Charcterization of randomly time-variant linear channels. IEEE Transactions on Communication Systems 11(4): 360–393.
13. Kailath T (1960) Correlation detection of signals perturbed by a random channel. IRE Transactions on Information Theory 6(3): 361–366.
14. Verdú S (1984) Optimum multiuser signal detection. Ph.D. Thesis, University of Illinois, Urbana-Champaign, IL, USA.

15. Verdú S (1986) Optimum multiuser asymptotic efficiency. IEEE Transactions on Communications 34(9): 890–897.

16. Schneider KS (1979) Optimum detection of code division multiplexed signals. IEEE Transactions on Aerospace and Electronic Systems 15(1): 181–185.

17. Meyr H, Moeneclaey M & Fechtel SA (1998) Digital Communication Receivers, Synchronization, Channel Estimation and Signal Processing. John Wiley and Sons, New York, USA.

18. Trees HLV (1968) Detection, Estimation, and Modulation Theory, Part I. John Wiley, New York, USA.

19. Trees HLV (1971) Detection, Estimation, and Modulation Theory, Part III. John Wiley, New York, USA.

20. Laster JD & Reed JH (1997) Interference rejection in digital wireless communications. IEEE Signal Processing Magazine 14(3): 37–62.

21. Haykin S (1996) Adaptive Filter Theory. Prentice Hall, Upper Saddle River, NJ, USA, 3rd edn.

22. Proakis JG (1995) Digital Communications. McGraw-Hill, Inc., New York, USA, 3rd edn.

23. Lin S & Costello D (1983) Error Control Coding. Prentice-Hall, Englewood Cliffs, NJ, USA.

24. Tanenbaum A (1996) Computer Networks. Prentice-Hall, Englewood Cliffs, NJ, 3rd edn.

25. Juntti M (1997) Multiuser Demodulation for DS-CDMA Systems in Fading Channels. Acta Univ Oul C106.

26. Klein A (1996) Multi-user detection of CDMA signals – algorithms and their application to cellular mobile radio. Ph.D. Thesis, University of Kaiserslautern, Kaiserslautern, Germany.

27. Verdú S (1997) Demodulation in the presence of multiuser interference: Progress and misconceptions. In: Docampo D, Figueiras-Vidal A & Perez-Gonzalez F (eds), Intelligent Methods in Signal Processing and Communications, Birkhauser, Boston, MA, USA, 15–44.

28. Mämmelä A (1995) Diversity Receivers in a Fast Fading Multipath Channel. VTT Publications 253.

29. Haeb R & Meyr H (1989) A systematic approach to carrier recovery and detection of digitally phase modulated signals on fading channels. IEEE Transactions on Communications 37(7): 748–754.

30. European Telecommunications Standards Institute (1998) UMTS terrestrial radio access concept evaluation. ETSI UMTS 30.06.

31. Qualcomm, Inc., San Diego, CA (1992) An Overview of the Application of Code Division Multiple Access (CDMA) to Digital Cellular Systems and Personal Cellular Networks.

32. Iinatti J (1997) Matched Filter Code Acquisition Employing a Median Filter in Direct Sequence Spread-Spectrum Systems with Jamming. Acta Univ Oul C102.

33. Meyr H & Ascheid G (1990) Synchronization in Digital Communications, Volume 1, Phase-, Frequency-Locked Loops and Amplitude Control. John Wiley and Sons, New York, USA.

34. Polydoros A (1982) On the synchronization aspects of direct-sequence spread-spectrum systems. Ph.D. Thesis, University of Southern California, Los Angeles, CA, USA.

35. de Gaudenzi R, Luise M & Viola R (1993) A digital chip timing recovery loop for band-limited direct-sequence spread-spectrum signals. IEEE Transactions on Communications 41(11): 1760–1769.

36. Sheen WH & Stüber G (1994) Effects of multipath fading on delay-locked loops for spread spectrum systems. IEEE Transactions on Communications 42(2/3/4): 1947–1956.

37. van Nee RDJ (1992) The multipath estimating delay lock loop. In: Proc. IEEE International Symposium on Spread Spectrum Techniques and Applications (ISSSTA), Yokohama, Japan, 39–42.

38. Latva-aho M & Vallström J (1996) Quasi-coherent delay-locked loops for fading channels. In: Proc. IEEE International Symposium on Spread Spectrum Techniques and Applications (ISSSTA), Mainz, Germany, 1: 455–459.

39. Latva-aho M & Lilleberg J (1996) Delay trackers for multiuser CDMA receivers. In: Proc. IEEE International Conference on Universal Personal Communications (ICUPC), Boston, MA, USA, 1: 326–330.

40. Latva-aho M & Lilleberg J (1998) Parallel interference cancellation in multiuser CDMA channel estimation. Wireless Personal Communications 7(2/3): 171–195.

41. Gardner FM (1990) Demodulator reference recovery techniques suited for digital implementation. ESTEC Contract no. 6847/86/NL/DG, European Space Agency.

42. Verdú S (1993) Multiuser detection. In: Advances in Statistical Signal Processing, JAI Press Inc., Greenwich, CT, 2: 369–409.

43. Taylor DP, Vitetta GM, Hart BD & Mämmelä A (1998) Wireless channel equalization. European Transactions on Telecommunications 9(2): 117–143.

44. Klein A & Baier PW (1993) Linear unbiased data estimation in mobile radio systems applying CDMA. IEEE Journal on Selected Areas in Communications 11(7): 1058–1066.

45. Lupas R & Verdú S (1989) Linear multiuser detectors for synchronous code-division multiple-access channels. IEEE Transactions on Information Theory 34(1): 123–136.

46. Lupas R & Verdú S (1990) Near-far resistance of multiuser detectors in asynchronous channels. IEEE Transactions on Communications 38(4): 496–508.

47. Varanasi MK (1993) Noncoherent detection in asynchronous multiuser channels. IEEE Transactions on Information Theory 39(1): 157–176.

48. Varanasi MK & Aazhang B (1991) Optimally near-far resistant multiuser detection in differentially coherent synchronous channels. IEEE Transactions on Information Theory 37(4): 1006–1018.

49. Zvonar Z & Brady D (1995) Differenially coherent multiuser detection in asynchronous CDMA flat Rayleigh fading channels. IEEE Transactions on Communications 43(2/3/4): 1252–1255.

50. Zvonar Z (1996) Multiuser detection in asynchronous CDMA frequency-selective fading channels. Wireless Personal Communications 3(3–4): 373–392.

51. Zvonar Z & Brady D (1994) Multiuser detection in single-path fading channels. IEEE Transactions on Communications 42(2/3/4): 1729–1739.

52. Zvonar Z & Brady D (1995) Suboptimal multiuser detector for frequency-selective Rayleigh fading synchronous CDMA channels. IEEE Transactions on Communications 43(2/3/4): 154–157.

53. Brown T & Kaveh M (1995) A decorrelating detector for use with antenna arrays. International Journal of Wireless Information Networks 2(4): 239–246.

54. Huang HC (1996) Combined multipath processing, array processing, and multiuser detection for DS-CDMA channels. Ph.D. Thesis, Princeton University, Princeton, NJ, USA.

55. Jung P & Blanz J (1995) Joint detection with coherent receiver antenna diversity in CDMA mobile radio systems. IEEE Transactions on Vehicular Technology 44(1): 76–88.

56. Jung P, Blanz J, Nasshan M & Baier PW (1994) Simulation of the uplink of JD-CDMA mobile radio systems with coherent receiver antenna diversity. Wireless Personal Communications 1(2): 61–89.

57. Miller SY (1989) Detection and estimation in multiple-access channels. Ph.D. Thesis, Princeton University, Princeton, NJ, USA.

58. Miller SY & Schwartz SC (1995) Integrated spatial-temporal detectors for asynchronous Gaussian multiple-access channels. IEEE Transactions on Communications 43(2/3/4): 396–411.

59. Zvonar Z (1996) Combined multiuser detection and diversity reception for wireless CDMA systems. IEEE Transactions on Vehicular Technology 45(1): 205–211.

60. Juntti MJ & Lilleberg JO (1997) Linear FIR multiuser detection for multiple data rate CDMA systems. In: Proc. IEEE Vehicular Technology Conference (VTC), Phoenix, AZ, USA, 2: 455–459.

61. Saquib M, Yates R & Mandayam N (1996) Decorrelating detectors for a dual rate synchronous DS/CDMA system. In: Proc. IEEE Vehicular Technology Conference (VTC), Atlanta, GA, USA, 1: 377–381.

62. Iltis RA & Mailaender L (1996) Multiuser detection of quasisynchronous CDMA signals using linear decorrelators. IEEE Transactions on Communications 44(11): 1561–1571.

63. Parkvall S, Ström E & Ottersten B (1996) The impact of timing errors on the performance of linear DS-CDMA receivers. IEEE Journal on Selected Areas in Communications 14(8): 1660–1668.

64. Zheng FC & Barton SK (1995) On the performance of near-far resistant CDMA detectors in the presence of synchronization errors. IEEE Transactions on Communications 43(12): 3037–3045.

65. Juntti MJ & Aazhang B (1997) Finite memory-length linear multiuser detection for asynchronous CDMA communications. IEEE Transactions on Communications 45(5): 611–622.

66. Tsatsanis MK & Giannakis GB (1996) Optimal decorrelating receivers for DS-CDMA systems: A signal processing framework. IEEE Transactions on Signal Processing 44(12): 3044–3055.

67. Wijayasuriya SSH, Norton GH & McGeehan JP (1996) A sliding window decorrelating receiver for multiuser DS-CDMA mobile radio networks. IEEE Transactions on Vehicular Technology 45(3): 503–521.

68. Madhow U & Honig ML (1994) MMSE interference suppression for direct-sequence spread-spectrum CDMA. IEEE Transactions on Communications 42(12): 3178–3188.

69. Xie Z, Short RT & Rushforth CK (1990) A family of suboptimum detectors for coherent multiuser communications. IEEE Journal on Selected Areas in Communications 8(4): 683–690.

70. Klein A, Kaleh GK & Baier PW (1996) Zero forcing and minimum mean-square-error equalization for multiuser detection in code-division multiple access channels. IEEE Transactions on Vehicular Technology 45(2): 276–287.

71. Wu WC & Chen KC (1996) Linear multiuser detectors for synchronous CDMA communication over Rayleigh fading channels. In: Proc. IEEE International Symposium on Personal, Indoor, and Mobile Radio Communications (PIMRC), Taipei, Taiwan, 2: 578–582.

72. Bernstein X & Haimovich AM (1996) Space-time optimum combining for CDMA communications. Wireless Personal Communications 3(1-2): 73–89.

73. Gray SD, Preisig JC & Brady D (1997) Multiuser detection in a horizontal underwater acoustic channel using array observations. IEEE Transactions on Signal Processing 45(1): 148–160.

74. Honig M & Veerakachen W (1996) Performance variability of linear multiuser detection for DS/CDMA. In: Proc. IEEE Vehicular Technology Conference (VTC), Atlanta, GA, USA, 1: 372–376.

75. Poor HV & Verdú S (1997) Probability of error in MMSE multiuser detection. IEEE Transactions on Information Theory 43(3): 858–871.

76. Barbosa AN & Miller SL (1998) Adaptive detection of DS/CDMA signals in fading channels. IEEE Transactions on Communications 46(1): 115–124.

77. Latva-aho M (1998) Bit error probability analysis for FRAMES W-CDMA downlink receivers. IEEE Transactions on Vehicular Technology, to appear.

78. Ulukus S & Yates RD (199x) Adaptive power control and MMSE interference suppression. International Journal of Wireless Information Networks, to appear.

79. Esmailzadeh R & Nagakawa M (1993) Pre-rake diversity combination for direct sequence spread spectrum mobile communications systems. IEICE Transactions on Communications E76-B(8): 1008–1015.

80. Rapajic PB & Vucetic BS (1995) Linear adaptive transmitter-receiver structures for asynchronous CDMA systems. European Transactions on Telecommunications 6(1): 21–27.

81. Miller SL (1995) An adaptive direct-sequence code-division multiple-access receiver for multiuser interference rejection. IEEE Transactions on Communications 43(2/3/4): 1746–1755.

82. Rapajic PB & Vucetic BS (1994) Adaptive receiver structures for asynchronous CDMA systems. IEEE Journal on Selected Areas in Communications 12(4): 685–697.

83. Lee KB (1996) Orthogonalization based adaptive interference suppression for direct-sequence code-division multiple-access systems. IEEE Transactions on Communications 44(9): 1082–1085.

84. Miller SL (1996) Training analysis of adaptive interference suppression for direct-sequence code-division multiple-access systems. IEEE Transactions on Communications 44(4): 488–495.

85. Oppermann I (1997) CDMA system aspects and capacity. Ph.D. Thesis, Sydney University, Sydney, Australia.

86. Woodward G, Rapajic P & Vucetic BS (1996) Adaptive algorithms for asynchronous DS-CDMA receivers. In: Proc. IEEE International Symposium on Personal, Indoor, and Mobile Radio Communications (PIMRC), Taipei, Taiwan, 2: 583–587.

87. Latva-aho M & Juntti M (1997) Modified adaptive LMMSE receiver for DS-CDMA systems in fading channels. In: Proc. IEEE International Symposium on Personal, Indoor, and Mobile Radio Communications (PIMRC), Helsinki, Finland, 2: 554–558.

88. Latva-aho M & Juntti M (199x) LMMSE detection for DS-CDMA systems in fading channels. IEEE Transactions on Communications, submitted.

89. Latva-aho M, Juntti M & Oppermann I (199x) Reconfigurable adaptive RAKE receiver for wideband CDMA systems. European Transactions on Telecommunications, submitted.

90. Latva-aho M & Oppermann I (199x) A packetized wideband CDMA system based on adaptive LMMSE receivers with antenna diversity. IEEE Transactions on Vehicular Technology, submitted.

91. Oppermann I & Latva-aho M (1997) Adaptive LMMSE receiver for wideband CDMA systems. In: Proc. Communication Theory Mini-Conference (CTMC) in conjunction with IEEE Global Telecommunication Conference (GLOBECOM), Phoenix, AZ, USA, 133–138.

92. Oppermann I & Vucetic BS (1996) Capacity of a coded direct sequence spread spectrum system over fading satellite channels using an adaptive LMS-MMSE receiver. IEICE Transactions on Fundamentals of Electronics Communications and Computer Sciences E79-A(12): 2043–2049.

93. Honig M (1998) Adaptive linear interference suppression for packet DS-CDMA. European Transactions on Telecommunications 9(2): 173–181.

94. Chu LC & Mitra U (1996) Improved MMSE-based multi-user detectors for mismatched delay channels. In: Proc. Conference on Information Sciences and Systems (CISS), Princeton University, Princeton, NJ, USA, 1: 326–331.

95. de Gaudenzi R, Giannetti F & Luise M (1998) Design of a low-complexity adaptive interference-mitigating detector for DS/SS receivers in CDMA radio networks. IEEE Transactions on Communications 46(1): 125–134.

96. Honig M, Madhow U & Verdú S (1995) Blind adaptive multiuser detection. IEEE Transactions on Information Theory 41(3): 944–960.

97. Park SC & Doherty JF (1997) Generalized projection algorithm for blind interference suppression in DS/CDMA communications. IEEE Transactions on Circuits and Systems Part II Analog and Digital Signal Processing 44(6): 453–460.

98. Schodorf JB & Williams DB (1997) A constrained optimization approach to multiuser detection. IEEE Transactions on Signal Processing 45(1): 258–262.

99. Tsatsanis MK (1997) Inverse filtering criteria for CDMA systems. IEEE Transactions on Signal Processing 45(1): 102–112.

100. Zečević N & Reed J (1997) Blind adaptation algorithms for direct-sequence spread-spectrum CDMA single-user detection. In: Proc. IEEE Vehicular Technology Conference (VTC), Phoenix, AZ, USA, 3: 2133–2137.

101. Honig M, Shensa M, Miller S & Milstein L (1997) Performance of adaptive linear interference suppression for DS-CDMA in the presence of flat Rayleigh fading. In: Proc. IEEE Vehicular Technology Conference (VTC), Phoenix, AZ, USA, 3: 2191–2195.

102. Wang X & Poor HV (1998) Blind equalization and multiuser detection in dispersive CDMA channels. IEEE Transactions on Communications 46(1): 91–103.

103. Mangalvedhe NR & Reed JH (1997) Blind CDMA interference rejection in multipath channels. In: Proc. IEEE Vehicular Technology Conference (VTC), Phoenix, AZ, USA, 1: 21–25.

104. Ge H (1997) Adaptive schemes of implementing the LMMSE multiuser detector for CDMA. In: Proc. IEEE International Conference on Communications (ICC), Montreal, Canada.

105. Honig M (1996) Performance of adaptive interference suppression for DS-CDMA with a time-varying user population. In: Proc. IEEE International Symposium on Spread Spectrum Techniques and Applications (ISSSTA), Mainz, Germany, 1: 267–271.

106. Iltis RA (1998) Performance of constrained and unconstrained adaptive multiuser detectors for quasi-synchronous CDMA. IEEE Transactions on Communications 46(1): 135–143.

107. Madhow U (1997) Blind adaptive interference suppression for the near-far resistant acquisition and demodulation of direct-sequence CDMA. IEEE Transactions on Signal Processing 45(1): 124–136.

108. Honig M, Miller S, Shensa M & Milstein L (199x) Performance of adaptive linear interference suppression in the presence of dynamic fading. IEEE Transactions on Communications, submitted.

109. Abrams BS, Zeger AE & Jones TE (1995) Efficiently structured CDMA receiver with near-far immunity. IEEE Transactions on Vehicular Technology 44(1): 1–13.

110. Mowbray RS, Pringle RD & Grant PM (1992) Increased CDMA system capacity through adaptive cochannel interference regeneration and cancellation. IEE Proceedings I 139(5): 515–524.

111. Sanada Y & Wang Q (1996) A co-channel interference cancellation technique using orthogonal convolutional codes. IEEE Transactions on Communications 44(5): 549–556.

112. Tachikawa S (1992) Characteristics of M-ary/spread spectrum multiple access communication systems using co-channel interference cancellation techniques. IEICE Transactions on Communications E76-B(8): 941–946.

113. Varanasi MK (1989) Multiuser detection in code-division multiple-access communications. Ph.D. Thesis, Rice University, Houston, TX, USA.

114. Varanasi MK & Aazhang B (1990) Multistage detection in asynchronous code-division multiple-access communications. IEEE Transactions on Communications 38(4): 509–519.

115. Varanasi MK & Aazhang B (1991) Near-optimum detection in synchronous code-division multiple-access systems. IEEE Transactions on Communications 39(5): 725–736.

116. Fawer U & Aazhang B (1995) A multiuser receiver for code division multiple access communications over multipath channels. IEEE Transactions on Communications 43(2/3/4): 1556–1565.

117. Kohno R, Imai H, Hatori M & Pasupathy S (1990) Combination of an adaptive array antenna and a canceller of interference for direct-sequence spread-spectrum multiple-access system. IEEE Journal on Selected Areas in Communications 8(4): 675–682.

118. Saifuddin A & Kohno R (1995) Performance evaluation of near-far resistant receiver DS/CDMA cellular system over fading multipath channel. IEICE Transactions on Communications E78-B(8): 1136–1144.

119. Saifuddin A, Kohno R & Imai H (1995) Integrated receiver structures of staged decoder and CCI canceller for CDMA with multilevel coded modulation. European Transactions on Telecommunications 6(1): 9–19.

120. Sanada Y & Wang Q (1997) A co-channel interference cancellation technique using orthogonal convolutional codes on multipath Rayleigh fading channel. IEEE Transactions on Vehicular Technology 46(1): 114–128.

121. Yoon YC, Kohno R & Imai H (1993) Cascaded co-channel interference cancellating and diversity combining for spread-spectrum multi-access system over multipath fading channels. IEICE Transactions on Communications E76-B(2): 163–168.

122. Yoon YC, Kohno R & Imai H (1993) A spread-spectrum multiaccess system with cochannel interference cancellation for multipath fading channels. IEEE Journal on Selected Areas in Communications 11(7): 1067–1075.

123. Holma H, Toskala A & Hottinen A (1996) Performance of CDMA multiuser detection with antenna diversity and closed loop power control. In: Proc. IEEE Vehicular Technology Conference (VTC), Atlanta, GA, USA, 1: 362–366.

124. Hottinen A, Holma H & Toskala A (1995) Performance of multistage multiuser detection in a fading multipath channel. In: Proc. IEEE International Symposium on Personal, Indoor, and Mobile Radio Communications (PIMRC), Toronto, Canada, 3: 960–964.

125. Latva-aho M & Lilleberg J (1996) Parallel interference cancellation in multiuser detection. In: Proc. IEEE International Symposium on Spread Spectrum Techniques and Applications (ISSSTA), Mainz, Germany, 3: 1151–1155.

126. Saifuddin A & Kohno R (1996) Performance evaluation of DS/CDMA scheme with diversity coding and MUI cancellation over fading multipath channel. IEICE Transactions on Fundamentals of Electronics Communications and Computer Sciences E79-A(12): 1994–2001.

127. Hottinen A, Holma H & Toskala A (1996) Multiuser detection for multirate CDMA communications. In: Proc. IEEE International Conference on Communications (ICC), Dallas, TX, USA.

128. Fawer U & Aazhang B (1996) Multiuser receivers for code-division multiple-access systems with trellis-based modulation. IEEE Journal on Selected Areas in Communications 14(8): 1602–1609.

129. Juntti MJ & Latva-aho M (199x) Multiuser receivers for CDMA systems in Rayleigh fading channels. IEEE Transactions on Vehicular Technology, submitted.

130. Juntti MJ, Latva-aho M & Heikkilä M (1997) Performance comparison of PIC and decorrelating multiuser receivers in fading channels. In: Proc. IEEE Global Telecommunication Conference (GLOBECOM), Phoenix, AZ, USA, 2: 609–613.

131. Latva-aho M & Lilleberg J (1996) Parallel interference cancellation based delay tracker for CDMA receivers. In: Proc. Conference on Information Sciences and Systems (CISS), Princeton, NJ, USA, 2: 852–857.

132. Gray SD, Kocic M & Brady D (1995) Multiuser detection in mismatched multiple-access channels. IEEE Transactions on Communications 43(12): 3080–3089.

133. Buehrer RM, Kaul A, Striglis S & Woerner BD (1996) Analysis of DS-CDMA parallel interference cancellation with phase and timing errors. IEEE Journal on Selected Areas in Communications 14(8): 1522–1535.

134. Orten P & Ottosson T (1997) Robustness of DS-CDMA multiuser detectors. In: Proc. Communication Theory Mini-Conference (CTMC) in conjunction with IEEE Global Telecommunication Conference (GLOBECOM), Phoenix, AZ, USA.

135. Buehrer RM, Correal NS & Woerner BD (1996) A comparison of multiuser receivers for cellular CDMA. In: Proc. IEEE Global Telecommunication Conference (GLOBECOM), London, U.K., 3: 1571–1577.

136. Agashe P & Woerner B (1996) Interference cancellation for a multicellular CDMA environment. Wireless Personal Communications 3(1-2): 1–15.

137. Bar-Ness Y & Sezgin N (1995) Adaptive threshold setting for multiuser CDMA signal separators with soft tentative decisions. In: Proc. Conference on Information Sciences and Systems (CISS), The John Hopkins University, Baltimore, MD, USA, 174–179.

138. Chen DW, Siveski Z & Bar-Ness Y (1994) Synchronous multiuser CDMA detector with soft decision adaptive canceler. In: Proc. Conference on Information Sciences and Systems (CISS), Princeton University, Princeton, NJ, USA, 1: 139–143.

139. Vanghi V & Vojcic B (1996) Soft interference cancellation in multiuser communications. Wireless Personal Communications 3(1-2): 111–128.

140. Buehrer RM & Woerner BD (1997) The asymptotic multiuser efficiency of M-stage interference cancellation receivers. In: Proc. IEEE International Symposium on Personal, Indoor, and Mobile Radio Communications (PIMRC), Helsinki, Finland, 2: 570–574.

141. Correal NS, Buehrer RM & Woerner BD (1997) Improved CDMA performance through bias reduction for parallel interference cancellation. In: Proc. IEEE International Symposium on Personal, Indoor, and Mobile Radio Communications (PIMRC), Helsinki, Finland, 2: 565–569.

142. Divsalar D, Simon MK & Raphaeli D (1998) Improved parallel interference cancellation for CDMA. IEEE Transactions on Communications 46(2): 258–268.

143. Dahlhaus D, Fleury H & Radović A (1998) A sequential algorithm for joint parameter estimation and multiuser detection in DS/CDMA systems with multipath propagation. Wireless Personal Communications, to appear.

144. Dahlhaus D, Jarosch A, Fleury H & Heddergott R (1997) Joint demodulation in DS/CDMA systems exploiting the space and time diversity of the mobile radio channel. In: Proc. IEEE International Symposium on Personal, Indoor, and Mobile Radio Communications (PIMRC), Helsinki, Finland, 1: 47–52.

145. Nelson LB & Poor HV (1996) Iterative multiuser receivers for CDMA channels: An EM-based approach. IEEE Transactions on Communications 44(12): 1700–1710.

146. Radović A & Aazhang B (1993) Iterative algorithms for joint data detection and delay estimation for code division multiple access communication systems. In: Proc. Annual Allerton Conference on Communications, Control, and Computing, Allerton House, Monticello, IL, USA.

147. Dempster AP, Laird NM & Rubin DB (1977) Maximum likelihood from incomplete data via the EM algorithm. Journal of Royal Statistical Society 39(1): 1–38.

148. Fessler J & Hero A (1994) Space-alternating generalized expectation-maximization algorithm. IEEE Transactions on Signal Processing 42(10): 2664–2677.

149. Patel P & Holtzman J (1994) Analysis of a simple successive interference cancellation scheme in a DS/CDMA system. IEEE Journal on Selected Areas in Communications 12(10): 796–807.

150. Soong ACK & Krzymien WA (1995) Performance of a reference symbol assisted multistage successive interference cancelling receiver in a multi-cell CDMA wireless systems. In: Proc. IEEE Global Telecommunication Conference (GLOBECOM), Singapore, 1: 152–156.

151. Hui A & Letaief K (1998) Multiuser asynchronous DS/CDMA detectors in multipath fading links. IEEE Transactions on Communications 46(3): 384–391.

152. Nesper O & Ho P (1996) A pilot symbol assisted interference cancellation scheme for an asynchronous DS/CDMA system. In: Proc. IEEE Global Telecommunication Conference (GLOBECOM), London, U.K., 3: 1447–1451.

153. Nesper O & Ho P (1996) A reference symbol assisted interference cancelling hybrid receiver for an asynchronous DS/CDMA system. In: Proc. IEEE International Symposium on Personal, Indoor, and Mobile Radio Communications (PIMRC), Taipei, Taiwan, 1: 108–112.

154. Soong ACK & Krzymien WA (1996) A novel CDMA multiuser interference cancellation receiver with reference symbol aided estimation of channel parameters. IEEE Journal on Selected Areas in Communications 14(8): 1536–1547.

155. Soong ACK & Krzymien WA (1997) Performance of a reference symbol assisted multi-stage successive interference cancelling receiver with quadriphase spreading. In: Proc. IEEE Vehicular Technology Conference (VTC), Phoenix, AZ, USA, 2: 460–464.

156. Viterbi AJ (1990) Very low rate convolutional codes for maximum theoretical performance of spread-spectrum multiple-access channels. IEEE Journal on Selected Areas in Communications 8(4): 641–649.

157. Johansson AL & Svensson A (1995) Successive interference cancellation in multiple data rate DS/CDMA systems. In: Proc. IEEE Vehicular Technology Conference (VTC), Chicago, IL, USA, 704–708.

158. Johansson AL & Svensson A (1996) Multistage interference cancellation in multirate DS/CDMA on a mobile radio channel. In: Proc. IEEE Vehicular Technology Conference (VTC), Atlanta, GA, USA, 2: 666–670.

159. Cheng FC & Holtzman JM (1994) Effect of tracking error on DS/CDMA successive interference cancellation. Tech Rep WINLAB-TR-90, WINLAB, Rutgers University, Piscataway, NJ, USA.

160. Soong ACK & Krzymien WA (1996) Robustness of the reference symbol assisted multistage successive interference cancelling receiver with imperfect parameter estimates. In: Proc. IEEE Vehicular Technology Conference (VTC), Atlanta, GA, USA, 2: 676–680.

161. Oon TB, Steele R & Li Y (1997) Performance of an adaptive successive serial-parallel CDMA cancellation scheme in flat Rayleigh fading channels. In: Proc. IEEE Vehicular Technology Conference (VTC), Phoenix, AZ, USA, 1: 193–197.

162. van der Wijk F, Janssen GMJ & Prasad R (1995) Groupwise successive interference cancellation in a DS/CDMA system. In: Proc. IEEE International Symposium on Personal, Indoor, and Mobile Radio Communications (PIMRC), Toronto, Canada, 2: 742–746.

163. Alexander PD, Rasmussen LK & Schlegel C (1997) A linear receiver for coded multiuser CDMA. IEEE Transactions on Communications 45(5): 605–610.

164. Haifeng W, Lilleberg J & Rikkinen K (1997) A new sub-optimal multiuser detection approach for CDMA systems in Rayleigh fading channel. In: Proc. Conference on Information Sciences and Systems (CISS), The Johns Hopkins University, Baltimore, MD, USA, 1: 276–280.

165. Juntti MJ (199x) Performance of multiuser detection in multirate CDMA systems. Wireless Personal Communications, submitted.

166. Juntti MJ (1998) Multiuser detector performance comparisons in multirate CDMA systems. In: Proc. IEEE Vehicular Technology Conference (VTC), Ottawa, Canada, 1: 36–40.

167. Varanasi MK (1995) Group detection in synchronous Gaussian code-division multiple-access channels. IEEE Transactions on Information Theory 41(3): 1083–1096.

168. Varanasi MK (1996) Parallel group detection for synchronous CDMA communication over frequency-selective Rayleigh fading channels. IEEE Transactions on Information Theory 42(1): 116–128.

169. Divsalar D & Simon M (1995) Improved CDMA performance using parallel interference cancellation. Tech rep, Jet Propulsion Laboratory, California Institute of Technology, Pasadena, CA.

170. Liu Y & Blostein SD (1995) Identification of frequency non-selective fading channels using decision feedback and adaptive linear prediction. IEEE Transactions on Communications 43(2/3/4): 1484–1492.

171. Bellanger MG (1987) Adaptive Digital Filters and Signal Analysis. Marcel Dekker, Inc., New York.

172. Parsons JD (1992) The Mobile Radio Propagation Channel. Pentech Press, London.

173. Verdú S (1986) Minimum probability of error for asynchronous Gaussian multiple-access channels. IEEE Transactions on Information Theory 32(1): 85–96.

174. Zvonar Z (1993) Multiuser detection for Rayleigh fading channels. Ph.D. Thesis, Northeastern University, Boston, MA, USA.

175. Kay S (1993) Fundamentals of Statistical Signal Processing: Estimation Theory. Prentice-Hall, Englewood Cliffs, NJ, USA.

176. Barrett MJ (1987) Error probability for optimal and suboptimal quadratic receivers in rapid Rayleigh fading channels. IEEE Journal on Selected Areas in Communications 5(2): 302–304.

177. Juntti MJ (1997) Performance of decorrelating multiuser receiver with data-aided channel estimation. In: Proc. Communication Theory Mini-Conference (CTMC) in conjunction with IEEE Global Telecommunication Conference (GLOBECOM), Phoenix, AZ, USA, 123–127.

178. Ottosson T (1998) Coding, modulation and multiuser decoding for DS-CDMA systems. Ph.D. Thesis, Chalmers University of Technology, Göteborg, Sweden.

179. European Telecommunications Standards Institute (1997) Concept group alpha - wideband direct-sequence cdma (WCDMA). Tdoc SMG2 UMTS 111/97.

180. Juntti MJ, Aazhang B & Lilleberg JO (1998) Iterative implementation of linear multiuser detection for asynchronous CDMA systems. IEEE Transactions on Communications 46(4): 503–508.

181. Lilleberg J, Nieminen E & Latva-aho M (1996) Blind iterative multiuser delay estimator for CDMA. In: Proc. IEEE International Symposium on Personal, Indoor, and Mobile Radio Communications (PIMRC), Taipei, Taiwan, 2: 565–568.

182. Krim H & Viberg M (1996) Two decades of array signal processing research – the parametric approach. IEEE Signal Processing Magazine 13(3): 67–94.

183. Paulraj A & Papadias C (1997) Space-time processing for wireless communications. IEEE Signal Processing Magazine 14(6): 49–83.

184. Naguib AF, Paulraj A & Kailath T (1994) Capacity improvement with base-station antenna arrays in cellular CDMA. IEEE Transactions on Vehicular Technology 43(3): 691–698.

185. Kohno R (1998) Spatial and temporal communication theory using adaptive antenna array. IEEE/ACM Personal Communications 5(1): 28–35.

186. Paulraj AJ & Ng BN (1998) Space-time modems for wireless personal communications. IEEE/ACM Personal Communications 5(1): 36–48.

187. Oppermann I & Latva-aho M (1998) Capacity of a packetised wideband LMMSE CDMA system with antenna diversity. In: Proc. IEEE International Symposium on Spread Spectrum Techniques and Applications (ISSSTA), Sun City, South Africa, 3: 786–791.

188. Miller SL & Barbosa AN (1996) A modified MMSE receiver for detection of DS-CDMA signals in fading channels. In: Proc. IEEE Military Communications Conference (MILCOM), Reston, VA, USA, 898–902.

189. Tsatsanis MK (1995) Time-varying system identification and channel equalization using wavelets and higher-order statistics. In: Leondes CT (ed), Control and Dynamic Systems: Advances in Theory and Applications, Academic Press, San Diego, CA, USA, 68: 333–394.

190. Martone M (1995) Blind multichannel deconvolution in multiple access spread spectrum communications using higher order statistics. In: Proc. IEEE International Conference on Communications (ICC), Seattle, WA, USA, 1: 49–53.

191. Johnson DH & Dudgeon DE (1993) Array Signal Processing: Concepts and Techniques. Prentice Hall, Englewood Cliffs, NJ, USA.

192. Treichler JR, Johnson CR & Larimore MG (1987) Theory and Design of Adaptive Filters. John Wiley and Sons, New York, USA.

193. Wang X & Poor HV (1998) Blind multiuser detection: A subspace approach. IEEE Transactions on Information Theory 44(2): 677–690.

194. Scharf LL (1991) Statistical Signal Processing: Detection, Estimation, and Time Series Analysis. Addison-Wesley, Reading, MA, USA.

195. Ström E (1994) Direct-sequence code-division multiple access systems: Near-far resistant parameter estimation and detection. Ph.D. Thesis, University of Florida, Gainesville, FL, USA.

196. Iltis RA & Mailaender L (1994) An adaptive multiuser detector with joint amplitude and delay estimation. IEEE Journal on Selected Areas in Communications 12(5): 774–785.

197. Bensley SE & Aazhang B (1996) Subspace-based channel estimation for code division multiple access communication systems. IEEE Transactions on Communications 44(8): 1009–1019.

198. Parkvall S (1996) Near-far resistant DS-CDMA systems: Parameter estimation and data detection. Ph.D. Thesis, Royal Institute of Technology, Stockholm, Sweden.

199. Ström EG, Parkvall S, Miller SL & Ottersen BE (1996) Propagation delay estimation in asynchronous direct-sequence code-division multiple access systems. IEEE Transactions on Communications 44(1): 84–93.

200. Kay SM & Marple SL (Nov 1981) Spectrum analysis - a modern perspective. Proceedings of the IEEE 64: 1380–1419.

201. Schmidt RO (1981) A signal subspace approach to multiple emitter location and spectral estimation. Ph.D. Thesis, Stanford University, Stanford, CA, USA.

202. Zheng D, Li J, Miller SL & Ström EG (1997) An efficient code-timing estimator for DS-CDMA signals. IEEE Transactions on Signal Processing 45(1): 82–89.

203. Viterbi AJ (1995) CDMA: Principles of Spread Spectrum Communication. Addison-Wesley Wireless Communications Series, Addison-Wesley, Reading, MA, USA.

204. Johnson D & DeGraaf S (1982) Improving the resolution of bearing in passive sonar arrays by eigenvalue analysis. IEEE Transactions on Acoustics Speech and Signal Processing 30(4): 638–647.

205. Polydoros A & Weber C (1984) A unified approach to serial search spread-spectrum code acquisition – part I: General theory. IEEE Transactions on Communications 32(5): 542–549.

206. Polydoros A & Weber C (1984) A unified approach to serial search spread-spectrum code acquisition – part II: A matched-filter receiver. IEEE Transactions on Communications 32(5): 550–560.

207. Gardner FM (1979) Phaselock Techniques, 2nd edn. John Wiley and Sons.

208. Moeneclaey M & Jonghe GD (1991) Tracking performance of digital chip synchronization algorithms for bandlimited direct-sequence spread-spectrum communication. IEE Electronic Letters 27(13): 1147–1149.

209. Bernhard U (1995) Nichtkohärenter delay-locked loop mit optimalem systemverhalten für übertragungssysteme mit bandspreizung. Ph.D. Thesis, Eidgenössichen Technischen Hochschule Zürich, Switzerland.

210. Chen KC & Davisson LD (1994) Analysis of SCCL as a PN-code tracking loop. IEEE Transactions on Communications 42(11): 2942–2946.

211. Buehrer RM (1996) The application of multiuser detection to cellular CDMA. Ph.D. Thesis, Faculty of the Virginia Polytechnic Institute and State University, Blacksburg, VA, USA.

212. Cameron R (1997) Fixed-point implementation of a multistage receiver. Ph.D. Thesis, Virginia Polytechnic Institute, Blacksburg, VA, USA.

213. Latva-aho M, Juntti M & Heikkilä M (1997) Parallel interference cancellation receiver for DS-CDMA systems in fading channels. In: Proc. IEEE International Symposium on Personal, Indoor, and Mobile Radio Communications (PIMRC), Helsinki, Finland, 2: 559–564.

214. Fechtel SA & Meyr H (1994) Optimal parametric feedforward estimation of frequency-selective fading radio channels. IEEE Transactions on Communications 42(2/3/4): 1639–1650.

215. Mämmelä A & Kaasila VP (1997) Smoothing and interpolation in a pilot symbol assisted diversity system. International Journal of Wireless Information Networks 4(3): 205–214.

216. Grant PM, Povey GJR & Pringle RD (1992) Performance of a spread spectrum RAKE receiver design. In: Proc. IEEE International Symposium on Spread Spectrum Techniques and Applications (ISSSTA), Yokohama, Japan, 71–74.

217. Lindquist CS (1989) Adaptive & Digital Signal Processing with Digital Filtering Applications. Steward & Sons, Miami, FL, USA.

218. Lindsey WC & Chie CM (1981) A survey of digital phase-locked loops. Proceedings of the IEEE 69(4): 410–431.

219. Welti AL & Bobrovsky BZ (1994) On optimal AGC structure for direct sequence spread spectrum PN-code tracking. IEEE Transactions on Communications 42(2/3/4): 680–688.

220. Cessna JR & Levy JDM (1972) Phase noise and transient times for a binary quantized digital phase-locked loop in white Gaussian noise. IEEE Transactions on Communications 20(4): 94–104.

221. Yamamoto H & Mori S (1978) Performance of a binary quantized all digital phase-locked loop with a new class of sequential filter. IEEE Transactions on Communications 26(1): 35–45.

222. Williamson D (1979) Improved phase-locked loop performance via nonlinear loop filters. IEEE Transactions on Communications 27(3): 542–556.

223. Latva-aho M (1996) Method and arrangement for controlling a loop filter. U.S. patent No. 5,589,795, Nokia Mobile Phones Ltd. Salo, Finland.

224. Chen KC & Davisson LD (1992) Analysis of a new bit tracking loop - SCCL. IEEE Transactions on Communications 40(1): 199–209.

List of symbols and abbreviations

$\mathbf{A}$	diagonal matrix of the received amplitudes of all users over a data block of N_b symbols ($KN_b \times KN_b$)
$\mathbf{A}^{(n)}$	diagonal matrix of the received amplitudes of all users over one symbol interval ($K \times K$)
A_k	received amplitude of the kth user
A_p	amplitude of the pilot channel
$\mathcal{A}_{k,l}^{(n)}$	residual amplitude component in the timing error signal at the nth symbol interval
$\tilde{\mathcal{A}}_{k,l}^{(n)}$	filtered residual amplitude component
$\mathbf{b}$	vector of data symbols of all users over N_b symbol intervals ($N_bK \times 1$); vector of data symbols of all users over N_b symbol intervals in uplink receivers ($N_bKL \times 1$)
$\mathbf{b}^{(n)}$	vector of data symbols of all users over one symbol interval ($K \times 1$)
$\mathbf{b}_{[D]}^{(n)}$	windowed data vector ($(2D+1)KL \times 1$)
$b_k^{(n)}$	data symbol of the kth user at the nth symbol interval
$\mathbf{B}$	vector of data symbols of all users over N_b symbol intervals in uplink receivers ($N_bKL \times N_bKL$)
B_L	DLL loop bandwidth
$\mathbf{c}$	vector of the channel coefficients of all users over N_b symbol intervals ($N_bKL \times 1$)
$\mathbf{c}^{(n)}$	vector of the channel coefficients of all users at nth symbol interval ($KL \times 1$)
$\mathbf{c}_k^{(n)}$	vector of the channel coefficients of the kth user at nth symbol interval ($L \times 1$)
$\bar{\mathbf{c}}_{k,l}^{(n)}$	rough channel coefficient estimate vector for kth user's lth path ($(P_{pr}+P_{sm}+1) \times 1$)

$\tilde{\mathbf{c}}^{(n)}$	rough channel estimate vector at the nth symbol interval ($KL \times 1$)
$\tilde{c}_{k,l}^{(n)}$	rough channel estimate for the kth user's lth path
$c_k(t)$	channel impulse response of the kth user
$c_{k,i}(t)$	channel impulse response of the kth user at the ith antenna
$c_k^{(n)}(t)$	channel impulse response of the kth user at the nth symbol interval
$c_{k,l}^{(n)}$	channel complex coeffcient of lth multipath component for the kth user at the nth symbol interval
$c_{k,l,i}^{(n)}$	channel complex coefficient of the kth user's lth multipath component at the ith antenna during the nth symbol interval
c_{light}	speed of light
$\mathbf{C}$	matrix of channel coefficient vectors of all users over N_b symbol intervals ($KLN_b \times KN_b$); matrix of channel coefficient vectors of all users over N_b symbol intervals in uplink receivers ($KLN_b \times KLN_b$)
$\mathbf{C}_i$	matrix of channel coefficient vectors of all users over N_b symbol intervals at the ith antenna ($KLN_b \times KN_b$); matrix of channel coefficient vectors of all users over N_b symbol intervals at the ith antenna in uplink receivers ($KLN_b \times KLN_b$)
$\mathbf{C}^{(n)}$	matrix of channel coefficient vectors of all users at the nth symbol interval ($KL \times K$)
$\mathbf{C}_{[D]}^{(n)}$	windowed channel coefficient matrix ($(2D+1)KL \times (2D+1)KL$)
$\mathbf{C}_i^{(n)}$	matrix of channel coefficient vectors of all users at the nth symbol interval at the ith antenna ($KL \times K$)
$\mathcal{C}$	multipath combining matrix ($K \times KL$)
$\mathcal{C}_k$	channel capacity of the kth user
$\mathbb{C}$	set of complex numbers
$d_k^{(n)}$	desired response for the kth user at the nth symbol interval
$d_{k,l}$	desired response for the kth user's lth path
$d_{k,l}^{(n)}$	desired response for the kth user's lth path at the nth symbol interval
$\mathbf{D}_i$	product of the spreading code matrix and the channel matrix for the ith antenna
$\bar{\mathbf{D}}_{k,l,i}$	product of the spreading code matrix and the channel matrix, components of the kth user's lth path are zeros
$\mathbf{D}_{k,l,i}$	product of the spreading code matrix and the channel matrix, only the components of the kth user's lth path are non-zeros
D	"half" of the processing window length; maximum delay spread

	in symbol intervals
$e(\phi_{k,l})$	unit vector pointing to the direction $\phi_{k,l}$
$e_k^{(n)}$	error signal in adaptive algorithms for the kth user at the nth symbol interval
$e_{k,l}^{(n)}$	error signal in adaptive algorithms for the kth user's lth path at the nth symbol interval
$\hat{e}_{k,l}^{(n)}$	normalized timing error signal for the kth user's lth path at the nth symbol interval
E_b	bit energy
E_k	transmitted energy of the kth user
f_c	carrier frequency
f_d	maximum Doppler shift
$\mathbf{F}_{k,l}$	matrix of the spreading sequence of the kth user's lth path over M symbol intervals ($MSG \times M$)
G	processing gain
G_{max}	largest processing gain in a mixed data rate system
G_{min}	smallest processing gain in a mixed data rate system
$\mathbf{h}$	vector consisting of the product of channel coefficients, data symbols and amplitude of all users
$\hat{\mathbf{h}}_{[MMSE]}$	MMSE estimate of vector $\mathbf{h}$
i	summation index; antenna index
$\mathbf{I}$	identity matrix
$\mathbf{I}_L$	identity matrix ($L \times L$)
I	number of antennas
j	summation index; index for chips of spreading sequences
J_k	cost function (MSE) for the kth user
$J_{k,l}$	cost function (MSE) for the kth user's lth path
$J_{k,l}^{(n)}$	MSE for the kth user's lth path at the nth symbol interval
$J_{k,l}^{(\infty)}$	MSE for the kth user's lth path in steady-state
$J_{[ex]k,l}^{(n)}$	excess MSE for the kth user's lth path at the nth symbol interval
$J_{[LS]k,l}$	least squares cost function for the kth user's lth path
$J_{[opt]k,l}$	MSE for the kth user's lth path with an optimum LMMSE filter
$\mathcal{J}_0$	zero-order Bessel function of the first kind
k	user index
K	number of active users
l	propagation path index
$\mathbf{L}_{[post]}$	postcombining LMMSE detector ($SGN_b \times KN_b$)

$\mathbf{L}_{[pre]}$	precombining LMMSE detector ($SGN_b \times KLN_b$)
L	number of propagation paths
L_k	number of propagation paths for the kth user
M	processing window size in symbol intervals
M_{ext}	length of the extended despreading interval in symbols
$\mathbf{n}$	noise vector over N_b symbol intervals ($SGN_b \times 1$)
$\mathbf{n}_i$	noise vector over N_b symbols at the ith antenna ($SGN_b \times 1$)
$\mathbf{n}^{(n)}$	noise vector during the nth symbol interval ($SG \times 1$)
$\tilde{\mathbf{n}}$	matched filter output noise vector over N_b symbols ($KLN_b \times 1$)
$\tilde{\mathbf{n}}^{(n)}$	matched filter output noise vector at the nth symbol interval ($KL \times 1$)
$\check{\mathbf{n}}^{(n)}$	noise vector at the nth symbol interval ($KL \times 1$)
n	discrete symbol interval index
$n(t)$	complex envelope of the noise process
$n_i(t)$	complex envelope of the noise process at the ith antenna
$\check{n}^{(n)}, \bar{n}^{(n)}, \tilde{n}^{(n)}$	noise components in DLLs
N	observation interval, smoothing delay
N_b	number of symbols in a data packet
N_R	average level crossing rate
$\mathcal{N}$	normalization coefficient
$\mathcal{O}$	relative portion of the information bits in a frame
$p(t)$	chip waveform
$p(\cdot)$	probability density function of the argument
P	scrambling code length in WCDMA; number of IC stages in PIC receivers
P_d	probability of detecting the correct code phase
P_e	probability of bit error
P_k	probability of bit error for the kth user
P_{pr}	number of coefficients in the prediction part of the channel estimation filter
Pr	probability
P_{sm}	number of coefficients in the smoothing part of the channel estimation filter
$P_{[ACQ]}(z)$	acquisition state generating function
$\mathcal{P}_{[EV,n]}$	output power of the eigenvector based estimator using noise subspace
$\mathcal{P}$	input signal power
$\mathcal{P}_{[MF]}$	output power for the matched filter estimator

$\mathcal{P}_{[MUSIC,n]}$	output power for the MUSIC estimator using noise subspace
$\mathcal{P}_{[MUSIC,s+n]}$	output power for the MUSIC estimator using signal plus noise subspace
$\mathcal{P}_{[MV]}$	output power of the minimum variance estimator
$q_{k,l}^{(n)}$	feedback coefficient in the IIR channel estimation filter
$\mathbf{Q}$	"multipath combining" matrix in the BEP analysis
$r(t)$	complex envelope of the received continuous-time signal
$r_i(t)$	complex envelope of the received continuous-time signal at the ith antenna
$r(nT_s)$	nth sample of received signal
$r_i(nT_s)$	nth sample of received signal at the ith antenna
$\mathbf{r}$	received signal vector over N_b symbol intervals ($SGN_b \times 1$)
$\mathbf{r}_i$	received signal vector over N_b symbol intervals at the ith antenna ($SGN_b \times 1$)
$\mathbf{r}^{(n)}$	received signal vector at the nth symbol interval ($SG \times 1$)
$\mathbf{r}_i^{(n)}$	received signal vector at the nth symbol interval at the ith antenna ($SG \times 1$)
$\bar{\mathbf{r}}^{(n)}$	received signal vector over a processing window of M symbol intervals ($SGM \times 1$)
$\bar{\mathbf{r}}_i^{(n)}$	received signal vector over a processing window of M symbol intervals at the nth symbol interval at the ith antenna ($SGM \times 1$)
$\bar{\mathbf{r}}_{[PIC]}^{(n)}$	received signal vector over M symbol intervals after MAI cancellation ($SGM \times 1$)
$\mathbf{R}$	correlation matrix over N_b symbol intervals ($KLN_b \times KLN_b$)
$\mathbf{R}^{(n,n')}$	elements of correlation matrix ($KL \times KL$)
$\mathbf{R}_{k,k'}^{(n,n')}$	elements of correlation matrix ($L \times L$)
R	threshold determining the bad channel state
$R_{kl,k'l'}^{(n,n')}$	cross-correlation between users k and k' for their lth and l'th path
$R_{kl,k'l'}^{(n,n')}(\tilde{\tau}_{k,l})$	cross-correlation with a trial delay $\tilde{\tau}_{k,l}$
$\mathbb{R}$	set of real numbers
$\mathbf{s}_k$	sampled signature sequence of the kth user ($SG \times 1$)
$\mathbf{s}_{k,l}^{(n)}$	sampled signature sequence corresponding to the kth user's lth path in the code matrix $\mathbf{S}$ ($SGN_b \times 1$)
$\bar{\mathbf{s}}_{k,l}$	sampled signature sequence of the kth user's lth path over the receiver processing window of M symbols ($SGM \times 1$)
$\bar{\mathbf{s}}_{p,l}$	sampled signature sequence of the pilot channel's lth path over the receiver processing window of M symbols ($SGM \times 1$)

$\mathbf{s}_{[l]k}$	lower part of the kth user's spreading sequence
$\mathbf{s}_{[u]k}$	upper part of the kth user's spreading sequence
$\bar{\mathbf{s}}_{[MRC]k}$	multipath combined signature sequence for the kth user over the receiver processing window of M symbols ($SGM \times 1$)
$s'(0)$	s-curve slope at the origin
$s_k(t)$	signature waveform of the kth user
$s_k(j)$	chip j of the kth user
$s_{[s]}$	scrambling code
$s_{[w]k}$	Walsh code of the kth user
$\mathbf{S}$	matrix of the sampled signature waveforms over N_b symbol intervals ($SGN_b \times KLN_b$)
$\mathbf{S}_i$	matrix of the sampled signature waveforms over N_b symbol intervals at the ith antenna ($SGN_b \times KLN_b$)
$\mathbf{S}_{k,l}$	matrix of the sampled signature waveforms over N_b symbol intervals, only the components of the kth user's lth path are non-zeros ($SGN_b \times KLN_b$)
$\bar{\mathbf{S}}_{k,l}$	matrix of the sampled signature waveforms over N_b symbol intervals, the components of the kth user's lth path are zeros ($SGN_b \times KLN_b$)
$\mathbf{S}^{(n)}$	matrix of the sampled signature waveforms over one symbol interval ($SGN_b \times KL$)
$\mathbf{S}^{(n)}(0)$	matrix of the samples of signature waveforms ($SG \times KL$)
$\mathbf{S}^{(n)}_{[D]}$	windowed spreading code matrix ($(D+1)SG \times (2D+1)KL$)
$\mathbf{S}^{(n)}_{[D]k,l}$	windowed spreading code matrix containing only the kth user's lth path components ($(D+1)SG \times (2D+1)KL$)
$\bar{\mathbf{S}}^{(n)}_{[D]k,l}$	windowed spreading code matrix, the components of the kth user's lth path are zeros ($(D+1)SG \times (2D+1)KL$)
S	number of samples per chip
t	continuous-time index
t_{conv}	convergence time
$\bar{t}_{conv}$	average convergence time
$\bar{t}_{fade}$	average fade duration
T	length of a symbol period
T_m	delay spread
T_c	length of a chip period
T_{coh}	channel coherence time
T_P	false alarm penalty time
T_s	sample interval

$\mathcal{T}$	estimator observation interval in symbols
T_{MA}	mean acquisition time
$\mathbf{u}_i$	ith eigenvector
$\mathbf{U}$	column matrix of eigenvectors ($SGM \times SGM$)
$\mathbf{v}$	FIR channel estimation filter coefficients ($(P_{pr} + P_{sm} + 1) \times 1$)
$\mathbf{v}_{k,l}$	FIR channel estimation filter coefficients for the kth user lth path ($(P_{pr} + P_{sm} + 1) \times 1$)
$v_{k,l}^{(n)}$	feedforward coefficient in IIR channel estimation filter
$\mathbf{w}_k^{(n)}$	adaptive receiver filter coefficients at the nth symbol interval for the kth user
$\mathbf{w}_{k,l}$	receiver filter coefficients for the kth user's lth path
$\mathbf{w}_{k,l}^{(n)}$	adaptive receiver filter coefficients at the nth symbol interval for the kth user's lth path
$\mathbf{w}_{[MOE]k,l}$	optimum MOE receiver filter coefficients for the kth user's lth path
$\mathbf{w}_{[MSE]k,l}$	optimum LMMSE receiver filter coefficients for the kth user's lth path
$w_{k,l}^{(n)}(j)$	jth coefficient of adaptive receiver filter for the kth user's lth path at the nth symbol interval
$\mathbf{w}_{[PIC]k,l}(p)$	residual interference suppression filter coefficients at the pth stage of the PIC receiver for the kth user's lth path
W	averaging interval
$\mathbf{x}_{k,l}^{(n)}$	adaptive filter component of the kth user's lth path at the nth symbol interval
$\mathbf{y}$	vector of matched filter outputs of all users over N_b symbol intervals ($N_b KL \times 1$)
$\mathbf{y}_{k,l}$	vector of matched filter outputs for the kth user's lth path (other user components are zeros) ($KLN_b \times 1$)
$\mathbf{y}^{(n)}$	vector of matched filter outputs of all users at the nth symbol interval ($KL \times 1$)
$\mathbf{y}_{k,l}^{(n)}$	vector of matched filter outputs for the kth user's lth path (other user components are zeros) at the nth symbol interval ($KL \times 1$)
$\mathbf{y}_{[post]}$	output vector of the postcombining LMMSE receiver
$\mathbf{y}_{[pre]}$	output vector of the precombining LMMSE receiver
$\mathbf{y}_{[PIC]}^{(n)}$	PIC output vector at the nth symbol interval ($KL \times 1$)
$y_k^{(n)}$	adaptive filter output of the kth user at the nth symbol interval
$y_{k,l}^{(n)}$	adaptive filter or matched filter output of the kth user's lth multipath component at the nth symbol interval

$y_{k,l}^{(n)}(\tilde{\tau}_{k,l})$	matched filter output of the kth user's lth multipath component at the nth symbol interval with a trial delay $\tilde{\tau}_{k,l}$
$y_{[PIC]k,l}^{(n)}$	PIC output for the kth user's lth component at nth symbol interval
$\mathbf{Y}$	spatially combined matched filter output for all users over N_b symbol intervals ($KLN_b \times 1$)
$\mathbf{Y}_{k,l}$	spatially combined matched filter output for the kth user's lth path (other user components are zeros) over N_b symbol intervals ($KLN_b \times 1$)
$\mathbf{Y}_{k,l}^{(n)}$	spatially combined matched filter output for the kth user's lth path (other user components are zeros) at the nth symbol interval ($KL \times 1$)
$Y_{k,l}^{(n)}$	spatially combined matched filter output for the kth user's lth path at the nth symbol interval
z^{-1}	unit delay operator
$z_k^{(n)}$	decision variable for the kth user's nth symbol
$\mathbf{0}_L$	zero matrix ($L \times L$)
$\mathbf{1}_L$	vector of all ones ($L \times 1$)
α	recursive channel estimation filter weight
$\delta_{k,k'}$	Kronecker delta function
$\delta(t)$	Dirac's delta function
Δ	half of the early-late difference
Δ_u	time-discretized trial delay
$\Delta\tau_{k,l}$	delay error of the kth user's lth path
$\epsilon_{k,l}^{(n)}$	rough timing error signal for the kth user's lth path
$\tilde{\epsilon}_{k,l}^{(n)}$	filtered timing error signal for the kth user's lth path
η	Lagrange multiplier
$\phi_{k,l}$	direction-of-arrival for the kth user's lth path
$\boldsymbol{\phi}$	direction vector of all users ($KL \times 1$)
$\boldsymbol{\phi}_k$	direction vectors of the kth user ($L \times 1$)
$\boldsymbol{\phi}_i$	steering vector at the ith antenna ($KL \times 1$)
$\tilde{\boldsymbol{\phi}}_i$	matrix of steering vectors at the ith antenna ($KL \times K$)
$\boldsymbol{\Phi}_i$	matrix of steering vectors ($KLN_b \times KN_b$)
$\varphi_{k,l}(.)$	channel autocorrelation (autocovariance) function
γ	forgetting factor
$\boldsymbol{\Gamma}^{(n)}$	filter tap weight error covariance at the nth symbol interval
λ	carrier wavelength
λ_i	ith eigenvalue

λ_{max}	maximum eigenvalue
$\mathbf{\Lambda}(\cdot)$	log-likelihood function
$\mathbf{\Lambda}$	diagonal matrix of eigenvalues ($SGM \times SGM$)
μ	step-size parameter in LMS algorithms
$\mu_{k,l}$	step-size parameter for the kth user's lth path
$\boldsymbol{\nu}$	vector of decision variable elements ($2L \times 1$)
$\nabla_{k,l}$	gradient for the kth user's lth path
Ξ	modulation symbol alphabet
$\omega, \omega^{(n)}$	constant modulus
$\mathbf{\Omega}^{(n)}$	input matrix for the channel estimator ($(P_{pr} + P_{sm} + 1) \times KL$)
$\mathbf{\Psi}$	MAI vector over N_b symbol intervals ($KLN_b \times 1$)
$\mathbf{\Psi}^{(n)}$	MAI vector at the nth symbol interval ($KL \times 1$)
$\mathbf{\Psi}^{(n)}(p)$	MAI vector at the pth stage in a multistage receiver
$\hat{\mathbf{\Psi}}^{(n)}_{[\mathbf{r}]k,l}$	MAI estimate vector for the sampled signal $\bar{\mathbf{r}}^{(n)}$ for the kth user's lth path ($SGM \times 1$)
$\Psi^{(n)}_{k,l}$	MAI for the kth user's lth path
$\Psi^{(n)}_{k,l}(\tilde{\tau}_{k,l})$	MAI for the kth user's lth path with a trial delay $\tilde{\tau}_{k,l}$
$\hat{\mathbf{\Psi}}$	multiple-access interference estimate
$\mathbf{\Psi}_{k,l}$	multiple-access interference vector for the kth user's lth path (other components are zeros) ($KLN_b \times 1$)
$\mathbf{\Psi}^{(n)}_{k,l}$	multiple-access interference vector for the kth user's lth path (other components are zeros) at the nth symbol interval ($KL \times 1$)
$\Psi^{(n)}_{k,l}$	multiple-access interference term for the kth user's lth path at the nth symbol interval
$\bar{\mathbf{\Psi}}$	spatially combined multiple-access interference vector for all users ($KLN_b \times 1$)
$\bar{\mathbf{\Psi}}_{k,l}$	spatially combined multiple-access interference vector for the kth user's lth path (other components are zeros) ($KLN_b \times 1$)
$\bar{\mathbf{\Psi}}^{(n)}_{k,l}$	spatially combined multiple-access interference vector for the kth user's lth path (other components are zeros) at the nth symbol interval ($KL \times 1$)
$\bar{\Psi}^{(n)}_{k,l}$	spatially combined multiple-access interference term for the kth user's lth path at the nth symbol interval
σ^2	two-sided power spectral density of noise process
σ_d^2	reference signal power
$\mathbf{\Sigma}_{\mathbf{a}}$	covariance matrix of vector $\mathbf{a}$
$\mathbf{\Sigma}_{\mathbf{c}}$	channel covariance matrix

$\mathbf{\Sigma}_{\mathbf{a}b}$	cross-correlation between $\mathbf{a}$ and b
$\tilde{\mathbf{\Sigma}}_{\bar{\mathbf{r}}d}$	cross-correlation between $\bar{\mathbf{r}}$ and d with imperfect reference signal
τ_k	delay of the kth user transmitted signal
$\tau_{k,l}$	delay of the kth user's lth multipath component
$\tau_{k,l,i}$	delay of the kth user's lth multipath component at the ith antenna
$\tau_{[max]}$	maximum delay difference between multipath components
$\tilde{\tau}_{k,l}$	trial delay value for the kth user's lth path
$\boldsymbol{\tau}$	a vector of all user's delays ($KL \times 1$)
ζ	squaring loss
ξ_i	position vector of the ith antenna with respect to some arbitrary reference point
$\xi_{k,l}$	branch switching threshold for the kth user's lth path

A/D	analog-to-digital
AGC	automatic gain control
ARQ	automatic repeat request
AWGN	additive white Gaussian noise
BEP	analytical bit error probability
BER	bit error rate
BPSK	binary phase shift keying
CDMA	code-division multiple-access
CM	constant modulus
DA	data-aided
DD	decision-directed
DI&D	dynamic integrate-and-dump
DLL	delay-locked loop
DOA	direction-of-arrival
DS	direct-sequence
EGC	equal gain combining
EM	expectation maximization
ETSI	European Telecommunications Standards Insitute
EV	eigenvector
FDD	frequency-division duplex
FDMA	frequency-division multiple-access
FH	frequency hopping
FIR	finite impulse response

FMA2	FRAMES multiple access mode 2
FRAMES	Future Radio Wideband Multiple Access Systems
FSE	fractionally spaced equalizer
GSC	generalized sidelobe canceller
GSM	Global System for Mobile Communications
HD	hard decision
IC	interference cancellation
IIR	infinite impulse response
ICI	inter-channel interference
IPI	inter-path interference
ISI	inter-symbol interference
ISM	industrial, scientific and medical
IS-95	Interim Standard 95
ITU	International Telecommunication Union
I&D	integrate-and-dump
LEO	low earth orbit
LF	loop filter
LMMSE	linear minimum mean squared error
LMS	least mean squares
LS	least squares
MA	moving average
MAI	multiple-access interference
MC	multicode
MF	matched filter
ML	maximum likelihood
MLSD	maximum likelihood sequence detection
MMSE	minimum mean squared error
MOE	minimum output energy
MPSK	M-ary phase shift keying
MRC	maximal ratio combining
MSE	mean squared error
MST	multiuser-spatial-temporal
MTLL	mean-time-to-lose-lock
MUD	multiuser demodulation
MUSIC	multiple signal classification
MV	minimum variance
NCO	numerically controlled oscillator

NFB	near-far problem
NLMS	normalized LMS
ODMA	opportunity driven multiple-access
OFDM	orthogonal frequency-division multiplex
PIC	parallel interference cancellation
PLL	phase-locked loop
PN	pseudo-random noise
PSK	phase shift keying
QC-DLL	quasi-coherent delay-locked loop
QoS	quality-of-service
QPSK	quatenary phase shift keying
RF	radio frequency
RLS	recursive least squares
RMS	root mean squared
RMSE	root mean squared error
SAGE	space alternating generalized expectation maximization
SCCL	sample-correlate-choose-largest
SIC	successive (or serial) interference cancellation
SD	soft decision
SINR	signal-to-interference-plus-noise ratio
SMG2	Special Mobile Group 2
SMT	spatial-multiuser-temporal
SNR	signal-to-noise ratio
SS	spread-spectrum
STM	spatial-temporal-multiuser
TDD	time-division duplex
TDMA	time-division multiple-access
TMS	temporal-multiuser-spatial
UMTS	Universal Mobile Telephone System
US	uncorrelated scattering
UTRA	ETSI UMTS Terrestrial Radio Access
VSF	variable spreading factor
WLAN	wireless local area network
WLL	wireless local loop
WSS	wide-sense stationary
WSSUS	wide-sense stationary uncorrelated scattering
WCDMA	wideband code-division multiple-access

$*$	convolution
$(\cdot)^*$	complex conjugation
$(\cdot)_{[MRC]}$	maximal ratio combining applied to the argument
$(\cdot)_{max}$	maximum of the argument
$(\cdot)_{min}$	minimum of the argument
$(\cdot)^{(n)}$	value at the nth symbol interval
$(\cdot)_{[PIC]}$	hard decision parallel interference cancellation
$(\cdot)_{[L-PIC]}$	combined parallel interference cancellation and LMMSE receiver
$\hat{(\cdot)}$	estimate of the argument
$\bar{(\cdot)}$	a vector over the receiver processing window
arg	argument
$\mathbf{A}^{\mathrm{H}}$	conjugate transpose of $\mathbf{A}$
$\mathbf{A}^{-1}$	inverse of $\mathbf{A}$
$\mathbf{A}^{\mathrm{T}}$	transpose of $\mathbf{A}$
$\mathrm{diag}(\cdots)$	diagonal matrix with elements $\cdots$ on main diagonal
$\mathrm{E}(\cdot)$	expectation
$L(\cdot)$	Lagrangian
$\max(\cdot)$	maximum
$\min(\cdot)$	minimum
$\mathrm{Q}(.)$	normalized and scaled Gaussian complementary error function
$\mathrm{Re}(\cdot)$	real part
$\mathrm{sgn}(\cdot)$	signum function
$\mathrm{std}(\cdot)$	standard deviation
$\mathrm{var}(\cdot)$	variance
$\mathrm{tr}(\mathbf{A})$	trace of $\mathbf{A}$
$\lvert\cdot\rvert$	magnitude, absolute value
$\lVert\cdot\rVert$	Euclidean norm
$\lVert\cdot\rVert_F$	Frobenius norm
$\lfloor x \rfloor$	largest integer less than or equal to x
$\lceil x \rceil$	smallest integer larger than or equal to x
$(\mathbf{x})_n$	nth element of vector x
$(\mathbf{A})_{ij}$	element at the ith row and jth column of matrix $\mathbf{A}$
$\frac{\partial}{\partial \mathbf{x}}$	gradient vector with respect to $\mathbf{x}$
$< \cdot, \cdot >$	inner product
$\otimes$	Kronecker product $\left(\mathbf{Z} = \mathbf{X} \otimes \mathbf{Y}\right.$, i.e., all components of the matrix $\mathbf{X}$ are multiplied by the matrix $\left.\mathbf{Y}\right)$

$\odot$	Schur product $\left(\mathbf{Z} = \mathbf{X} \odot \mathbf{Y}\right.$, i.e., all components of the matrix $\mathbf{X}$ are multiplied by the components of matrix $\mathbf{Y}$ elementwise $\left.\right)$

Different forms of LMMSE estimators

It is well known [175, p. 391] that for a general discrete linear system described by

$$\mathbf{r} = \mathbf{H}\boldsymbol{\Theta} + \mathbf{n}, \tag{A2.1}$$

where $\mathbf{r} \in \mathbb{C}^{N\times 1}$ is input data vector, $\mathbf{H} \in \mathbb{C}^{N\times P}$ is the linear system generating matrix, $\boldsymbol{\Theta} \in \mathbb{C}^{P\times 1}$ is an unknown random parameter vector with zero mean and covariance $\boldsymbol{\Sigma}_{\boldsymbol{\Theta}}$, and $\mathbf{n} \in \mathbb{C}^{N\times 1}$ is a zero mean complex Gaussian noise vector with covariance $\sigma^2\mathbf{I}$, the LMMSE estimator for $\boldsymbol{\Theta}$ can be written as

$$\begin{aligned}
\hat{\boldsymbol{\Theta}} &= \boldsymbol{\Sigma}_{\boldsymbol{\Theta}}\mathbf{H}^{\mathrm{H}}\left(\mathbf{H}\boldsymbol{\Sigma}_{\boldsymbol{\Theta}}\mathbf{H}^{\mathrm{H}} + \sigma^2\mathbf{I}\right)^{-1}\mathbf{r} \\
&= \left(\boldsymbol{\Sigma}_{\boldsymbol{\Theta}}^{-1} + \mathbf{H}^{\mathrm{H}}\mathbf{H}/\sigma^2\right)^{-1}\mathbf{H}^{\mathrm{H}}/\sigma^2\mathbf{r} \\
&= \left(\mathbf{H}^{\mathrm{H}}\mathbf{H} + \sigma^2\boldsymbol{\Sigma}_{\boldsymbol{\Theta}}^{-1}\right)^{-1}\mathbf{H}^{\mathrm{H}}\mathbf{r}.
\end{aligned} \tag{A2.2}$$

The estimator consists of three components: matched filtering ($\mathbf{H}^{\mathrm{H}}\mathbf{r}$), correlation matrix for the matched filter ($\mathbf{H}^{\mathrm{H}}\mathbf{H}$) and matched filter output noise-to-"signal" term ($\sigma^2\boldsymbol{\Sigma}_{\boldsymbol{\Theta}}^{-1}$). Depending on the receiver construction, each of these three components can vary. For the postcombining LMMSE receiver, $\mathbf{H} = \mathbf{SCA}$ and the resulting LMMSE estimator for bits ($\boldsymbol{\Theta} = \mathbf{b}$) is

$$\mathbf{L} = \mathbf{SCA}\left(\mathbf{AC}^{\mathrm{H}}\mathbf{RCA} + \sigma^2\mathbf{I}\right)^{-1} \in \mathbb{C}^{SGN_b\times KN_b}, \tag{A2.3}$$

since $\boldsymbol{\Sigma}_{\mathbf{b}} = \mathrm{E}\left[\mathbf{b}\mathbf{b}^{\mathrm{H}}\right] = \mathbf{I}$. In the case of the precombining LMMSE receiver, $\mathbf{H} = \mathbf{S}$ and the LMMSE estimator for channel coefficient data product ($\boldsymbol{\Theta} = \mathbf{CAb} \hat{=} \mathbf{h}$) becomes

$$\mathbf{M} = \mathbf{S}\left(\mathbf{R} + \sigma^2\boldsymbol{\Sigma}_{\mathbf{h}}^{-1}\right)^{-1} \in \mathbb{R}^{SGN_b\times KLN_b}, \tag{A2.4}$$

since

$$\begin{aligned}
\boldsymbol{\Sigma}_{\mathbf{CAb}} &= \mathrm{E}\left[\mathbf{CAb}(\mathbf{CAb})^{\mathrm{H}}\right] \\
&= \mathrm{diag}\left[A_1^2\left(\mathrm{E}[|c_{1,1}|^2], \ldots, \mathrm{E}[|c_{1,L}|^2]\right), \ldots, A_K^2\left(\mathrm{E}[|c_{K,1}|^2], \ldots, \mathrm{E}[|c_{K,L}|^2]\right)\right] \\
&\hat{=} \boldsymbol{\Sigma}_{\mathbf{h}}.
\end{aligned} \tag{A2.5}$$

Impact of the imperfect channel estimates on the precombining LMMSE receiver adaptation

Assuming that the radio channel is estimated by using an unmodulated pilot channel (the pilot code will be denoted by $\bar{\mathbf{s}}_p$ and the pilot channel has power A_p^2) and a moving average smoother of length $2N+1$, the channel estimate can be written as

$$\hat{c}_{k,l}^{(n)} = \frac{1}{2N+1} \sum_{i=-N}^{N} \bar{\mathbf{s}}_{p,l}^{\mathrm{T}} \bar{\mathbf{r}}^{(n-i)}. \tag{A3.1}$$

To simplify notations, it will be first assumed that the receiver processing window is equal to one symbol interval ($M = 1$) and the number of propagation paths is one ($c_{k,l} \hat{=} c_k$, $\bar{\mathbf{s}}_{k,l} \hat{=} \bar{\mathbf{s}}_k$, $\bar{\mathbf{s}}_{p,l} \hat{=} \bar{\mathbf{s}}_p$). The received vector during the nth symbol interval in a synchronous downlink channel for user $k = 1$ can be written as

$$\bar{\mathbf{r}}^{(n)} = c_1^{(n)} \left(A_1 \bar{\mathbf{s}}_1 b_1^{(n)} + A_p \bar{\mathbf{s}}_p + \sum_{k=2}^{K} A_k \bar{\mathbf{s}}_k b_k^{(n)} \right) + \bar{\mathbf{n}}^{(n)}. \tag{A3.2}$$

The cross-correlation between the received signal and imperfect reference is analyzed by assuming perfect knowledge of data bits and using the channel estimator of (A3.1). The transposed complex conjugate of the cross-correlation has the form

$$\begin{aligned}
\boldsymbol{\Sigma}_{\bar{\mathbf{r}}d}^{\mathrm{H}} &= \mathrm{E}\left[d^{(n)} \bar{\mathbf{r}}^{\mathrm{H}(n)} \right] \\
&= \mathrm{E}\left[b_1^{(n)} \hat{c}_1^{(n)} \bar{\mathbf{r}}^{\mathrm{H}(n)} \right] \\
&= \mathrm{E}\left[b_1^{(n)} \frac{1}{2N+1} \sum_{i=-N}^{N} \bar{\mathbf{s}}_p^{\mathrm{T}} \bar{\mathbf{r}}^{(n-i)} \bar{\mathbf{r}}^{\mathrm{H}(n)} \right] \\
&= \frac{1}{2N+1} \sum_{i=-N}^{N} \bar{\mathbf{s}}_p^{\mathrm{T}} \mathrm{E}\left[b_1^{(n)} \bar{\mathbf{r}}^{(n-i)} \bar{\mathbf{r}}^{\mathrm{H}(n)} \right].
\end{aligned} \tag{A3.3}$$

The expectation can be expanded as

$$
\begin{aligned}
&\mathrm{E}\left[b_1^{(n)}\bar{\mathbf{r}}^{(n-i)}\bar{\mathbf{r}}^{\mathrm{H}(n)}\right] \\
&= \mathrm{E}\left[b_1^{(n)}\left(c_1^{(n-i)}\left(A_1\bar{\mathbf{s}}_1 b_1^{(n-i)} + A_p\bar{\mathbf{s}}_p + \sum_{k=2}^{K} A_k\bar{\mathbf{s}}_k b_k^{(n-i)}\right) + \bar{\mathbf{n}}^{(n-1)}\right)\right. \\
&\left.\cdot\left(c_1^{*(n)}\left(A_1\bar{\mathbf{s}}_1^{\mathrm{T}} b_1^{*(n)} + A_p\bar{\mathbf{s}}_p^{\mathrm{T}} + \sum_{k=2}^{K} A_k\bar{\mathbf{s}}_k^{\mathrm{T}} b_k^{*(n)}\right) + \bar{\mathbf{n}}^{\mathrm{H}(n)}\right)\right] \\
&= \mathrm{E}\left[b_1^{(n)}c_1^{(n-i)}c_1^{*(n)}\left(A_1\bar{\mathbf{s}}_1 b_1^{(n-i)}\left(A_1\bar{\mathbf{s}}_1^{\mathrm{T}} b_1^{*(n)} + A_p\bar{\mathbf{s}}_p^{\mathrm{T}} + \sum_{k=2}^{K} A_k\bar{\mathbf{s}}_k^{\mathrm{T}} b_k^{*(n)}\right)\right.\right. \\
&+A_p\bar{\mathbf{s}}_p\left(A_1\bar{\mathbf{s}}_1^{\mathrm{T}} b_1^{*(n)} + A_p\bar{\mathbf{s}}_p^{\mathrm{T}} + \sum_{k=2}^{K} A_k\bar{\mathbf{s}}_k^{\mathrm{T}} b_k^{*(n)}\right) \\
&\left.\left.+\sum_{k=2}^{K} A_k\bar{\mathbf{s}}_k b_k^{(n-i)}\left(A_1\bar{\mathbf{s}}_1^{\mathrm{T}} b_1^{*(n)} + A_p\bar{\mathbf{s}}_p^{\mathrm{T}} + \sum_{k=2}^{K} A_k\bar{\mathbf{s}}_k^{\mathrm{T}} b_k^{*(n)}\right)\right)\right] \\
= \;& \mathrm{E}\left[b_1^{(n)}c_1^{(n-i)}c_1^{*(n)}A_1\bar{\mathbf{s}}_1 b_1^{(n-i)}A_1\bar{\mathbf{s}}_1^{\mathrm{T}} b_1^{*(n)}\right] \qquad (=0) \\
&+\mathrm{E}\left[b_1^{(n)}c_1^{(n-i)}c_1^{*(n)}A_1\bar{\mathbf{s}}_1 b_1^{(n-i)}A_p\bar{\mathbf{s}}_p^{\mathrm{T}}\right] \qquad (=x_1) \\
&+\mathrm{E}\left[b_1^{(n)}c_1^{(n-i)}c_1^{*(n)}A_1\bar{\mathbf{s}}_1 b_1^{(n-i)}\sum_{k=2}^{K} A_k\bar{\mathbf{s}}_k^{\mathrm{T}} b_k^{*(n)}\right] \qquad (=0) \\
&+\mathrm{E}\left[b_1^{(n)}c_1^{(n-i)}c_1^{*(n)}A_p\bar{\mathbf{s}}_p A_1\bar{\mathbf{s}}_1^{\mathrm{T}} b_1^{*(n)}\right] \qquad (=x_2) \\
&+\mathrm{E}\left[b_1^{(n)}c_1^{(n-i)}c_1^{*(n)}A_p\bar{\mathbf{s}}_p A_p\bar{\mathbf{s}}_p^{\mathrm{T}}\right] \qquad (=0) \\
&+\mathrm{E}\left[b_1^{(n)}c_1^{(n-i)}c_1^{*(n)}A_p\bar{\mathbf{s}}_p\sum_{k=2}^{K} A_k\bar{\mathbf{s}}_k^{\mathrm{T}} b_k^{*(n)}\right] \qquad (=0) \\
&+\mathrm{E}\left[b_1^{(n)}c_1^{(n-i)}c_1^{*(n)}\sum_{k=2}^{K} A_k\bar{\mathbf{s}}_k b_k^{(n-i)}A_1\bar{\mathbf{s}}_1^{\mathrm{T}} b_1^{*(n)}\right] \qquad (=0) \\
&+\mathrm{E}\left[b_1^{(n)}c_1^{(n-i)}c_1^{*(n)}\sum_{k=2}^{K} A_k\bar{\mathbf{s}}_k b_k^{(n-i)}A_p\bar{\mathbf{s}}_p^{\mathrm{T}}\right] \qquad (=0) \\
&+\mathrm{E}\left[b_1^{(n)}c_1^{(n-i)}c_1^{*(n)}\sum_{k=2}^{K} A_k\bar{\mathbf{s}}_k b_k^{(n-i)}\sum_{k=2}^{K} A_k\bar{\mathbf{s}}_k^{\mathrm{T}} b_k^{*(n)}\right] \qquad (=0) \\
\hat{=}\;& x_1 + x_2, \qquad \text{(A3.4)}
\end{aligned}
$$

where

$$
\begin{aligned}
x_1 &= A_1A_p\mathrm{E}\left[c_1^{(n-i)}c_1^{*(n)}\right]\mathrm{E}\left[b_1^{(n)}b_1^{(n-i)}\right]\bar{\mathbf{s}}_1\bar{\mathbf{s}}_p^{\mathrm{T}} \\
&= \begin{cases} 0, & i \neq 0 \\ A_1A_p\mathrm{E}\left[c_1^{(n-i)}c_1^{*(n)}\right]\bar{\mathbf{s}}_1\bar{\mathbf{s}}_p^{\mathrm{T}}, & i = 0, \end{cases} \qquad \text{(A3.5)}
\end{aligned}
$$

and

$$x_2 \quad = \quad A_1 A_p \mathrm{E}\big[c_1^{(n-i)} c_1^{*(n)}\big] \bar{\mathbf{s}}_p \bar{\mathbf{s}}_1^{\mathrm{T}}. \tag{A3.6}$$

Finally, the cross-correlation term in the case of estimated channel can be expressed as

$$\begin{aligned}
\boldsymbol{\Sigma}_{\bar{\mathbf{r}}d}^{\mathrm{H}} &= \bar{\mathbf{s}}_p^{\mathrm{T}} \frac{A_1 A_p}{2N+1} \sum_{i=-N}^{N} \mathrm{E}\big[c_1^{(n-i)} c_1^{*(n)}\big] \left(\bar{\mathbf{s}}_p \bar{\mathbf{s}}_1^{\mathrm{T}} + \mathrm{E}\big[b_1^{(n)} b_1^{(n-i)}\big] \bar{\mathbf{s}}_1 \bar{\mathbf{s}}_p^{\mathrm{T}} \right) \\
&= \frac{A_1 A_p}{(2N+1)} \left(\sum_{i=-N}^{N} \varphi_1(i) \bar{\mathbf{s}}_1^{\mathrm{T}} + \varphi_1(0) \bar{\mathbf{s}}_p^{\mathrm{T}} \bar{\mathbf{s}}_1 \bar{\mathbf{s}}_p^{\mathrm{T}} \right) \\
&\approx \frac{A_1 A_p}{(2N+1)} \left(\sum_{i=-N}^{N} \varphi_1(i) \bar{\mathbf{s}}_1^{\mathrm{T}} \right),
\end{aligned} \tag{A3.7}$$

assuming that the pilot code and the user codes have relatively low cross-correlations with zero delay, i.e., $\bar{\mathbf{s}}_p^{\mathrm{T}} \bar{\mathbf{s}}_1 << 1$ and/or the channel is slowly fading such that $N >> 1$. In (A3.7), $\varphi_1(i) = \mathrm{E}\big[c_1^{(n)} c_1^{*(n+i)}\big]$ is the channel autocorrelation coefficient for delay of i symbols (see Section 2.2). The result is also valid in multipath channels assuming that there is no correlation between multipath components, i.e., $\mathrm{E}\big[c_l^{(n)} c_{l'}^{*(n+i)}\big] = 0, \forall l \neq l'$. With larger processing windows ($M > 1$), the consecutive data symbols do not correlate and the result is valid in that case as well.

System and channel models for multisensor receivers

The received signal at the ith reception point for a system with K users and L propagation paths can be written as [143]

$$r_i(t) = \sum_{n=0}^{N_b-1} \sum_{k=1}^{K} \sum_{l=1}^{L} A_k b_k^{(n)} c_{k,l,i}^{(n)} s_k(t - nT - \tau_{k,l,i}) + n_i(t), \tag{A4.1}$$

where N_b is the number of received symbols, K is the number of users, $A_k = \sqrt{E_k/T}$, E_k/T is the energy per symbol, $b_k^{(n)}$ is the nth transmitted data symbol, $s_k(t)$ is the kth user's signature sequence of length G chips per data symbol, T denotes the symbol interval, $n_i(t)$ is a complex zero mean additive white Gaussian noise process with two-sided power spectral density σ^2, $c_{k,l,i}^{(n)}$ is the complex attenuation factor of the kth user's lth path and $\tau_{k,l,i}$ is the propagation delay at the ith reception point. The received signal is time-discretized by anti-alias filtering and sampling $r_i(t)$ at the rate $T_s^{-1} = \frac{SG}{T}$, where S is the number of samples per chip. The received discrete-time signal over a data block of N_b symbols is

$$\mathbf{r}_i = \mathbf{S}_i \mathbf{C}_i \mathbf{A} \mathbf{b} + \mathbf{n}_i, \tag{A4.2}$$

where the vectors and matrices are formed as in the single-antenna case:

$$\mathbf{r}_i = \left[\mathbf{r}_i^{\mathrm{T}(0)}, \ldots, \mathbf{r}_i^{\mathrm{T}(N_b-1)}\right]^{\mathrm{T}} \in \mathbb{C}^{SGN_b},$$

$$\mathbf{r}_i^{\mathrm{T}(n)} = \left[r_i(T_s\,(nSG+1)), \ldots, r_i(T_s\,(n+1)SG)\right] \in \mathbb{C}^{SG},$$

$$\mathbf{S}_i = \left[\mathbf{S}_i^{(0)}, \ldots, \mathbf{S}_i^{(N_b-1)}\right] \in \mathbb{R}^{SGN_b \times KLN_b}$$

$$\mathbf{S}_i^{(n)} = \left[\mathbf{s}_{1,1,i}^{(n)}, \ldots, \mathbf{s}_{1,L,i}^{(n)}, \ldots, \mathbf{s}_{K,L,i}^{(n)}\right] \in \mathbb{R}^{SGN_b \times KL},$$

$$\mathbf{s}_{k,l,i}^{(n)} = \left[\mathbf{0}_{(nSG+\tau_{k,l,i})\times 1}^{\mathrm{T}},\ \mathbf{s}_k^{\mathrm{T}},\ \mathbf{0}_{((N_b-n-1)SG-\tau_{k,l,i})\times 1}^{\mathrm{T}}\right] \in \mathbb{R}^{SGN_b},$$

$$\mathbf{s}_k = \left[s_k(T_s), \ldots, s_k(T_s\,SG)\right]^{\mathrm{T}} \in \mathbb{R}^{SG}$$

$$\mathbf{C}_i = \mathrm{diag}\big[\mathbf{C}_i^{(0)}, \ldots, \mathbf{C}_i^{(N_b-1)}\big] \in \mathbb{C}^{KLN_b \times KN_b}$$
$$\mathbf{C}_i^{(n)} = \mathrm{diag}\big[\mathbf{c}_{1,i}^{(n)}, \ldots, \mathbf{c}_{K,i}^{(n)}\big] \in \mathbb{C}^{KL \times K},$$
$$\mathbf{c}_{k,i}^{(n)} = \big[c_{k,1,i}^{(n)}, \ldots, c_{k,L,i}^{(n)}\big]^{\mathrm{T}} \in \mathbb{C}^{L},$$
$$\mathbf{A} = \mathrm{diag}[\mathbf{A}^{(0)}, \ldots, \mathbf{A}^{(N_b-1)}\big] \in \mathbb{R}^{KN_b \times KN_b},$$
$$\mathbf{A}^{(n)} = \mathrm{diag}\big[A_1, \ldots, A_K\big] \in \mathbb{R}^{K \times K},$$
$$\mathbf{b} = \big[\mathbf{b}^{\mathrm{T}(0)}, \ldots, \mathbf{b}^{\mathrm{T}(N_b-1)}\big]^{\mathrm{T}} \in \Xi^{KN_b},$$
$$\mathbf{b}^{(n)} = \big[b_1^{(n)}, \ldots, b_K^{(n)}\big] \in \Xi^{K},$$
$$\mathbf{n}_i \in \mathbb{C}^{SGN_b}.$$

The channel impulse response for the kth user' s ith sensor can be written as [144]

$$c_{k,i}(t) = \sum_{l=1}^{L_k} c_{k,l}^{(n)} e^{j2\pi\lambda^{-1}\langle e(\phi_{k,l}),\xi_i\rangle} \delta(t - (\tau_{k,l,i} - c_{light}^{-1}\langle e(\phi_{k,l}), \xi_i\rangle)), \qquad \text{(A4.3)}$$

where L_k is the number of propagation paths (assumed to be the same for all users for simplicity; $L_k = L$, $\forall k$), $c_{k,l}^{(n)}$ is the complex attenuation factor of the kth user's lth path, $\tau_{k,l,i}$ is the propagation delay for the ith sensor, ξ_i is the position vector of the ith sensor with respect to some arbitrarily chosen reference point, c_{light} is the speed of light, λ is the wavelength of the carrier, $e(\phi_{k,l})$ is a unit vector pointing to direction $\phi_{k,l}$ (direction-of-arrival), and $\langle\cdot,\cdot\rangle$ indicates the inner product.

Assuming that the receiver sensors are within an area of a few wavelengths, the propagation delay over the receiver sensors can be neglected with the carrier frequencies and chip rates of the 3rd generation mobile phone systems, i.e., $\tau_{k,l,i} = \tau_{k,l}$, and $c_{light}^{-1}\langle e(\phi_{k,l}), \xi_i\rangle \approx 0$. Hence, the fading processes are the same at every antenna; only the phase of the received signal is different and it depends on the direction-of-arrival. Assuming also that the number of propagation paths is the same for all users, the channel impulse response can be written as

$$c_{k,i}(t) = \sum_{l=1}^{L} c_{k,l}^{(n)} e^{j2\pi\lambda^{-1}\langle e(\phi_{k,l}),\xi_i\rangle} \delta(t - \tau_{k,l}). \qquad \text{(A4.4)}$$

The channel matrix for the ith sensor consist of two components

$$\mathbf{C}_i = \mathbf{C} \odot \mathbf{\Phi}_i \in \mathbb{C}^{KLN_b \times KN_b}, \qquad \text{(A4.5)}$$

where $\mathbf{C}$ is the channel matrix defined in (2.13), $\odot$ is the Schur product[1] and $\mathbf{\Phi}_i = \mathrm{diag}\big(\tilde{\boldsymbol{\phi}}_i\big) \otimes \mathbf{I}_{N_b}$ with $\tilde{\boldsymbol{\phi}}_i = \mathrm{diag}\big(\boldsymbol{\phi}_1, \ldots, \boldsymbol{\phi}_K\big)$, $\boldsymbol{\phi}_k = \big[\phi_{k,1}, \ldots, \phi_{k,L}\big]^{\mathrm{T}}$ is the matrix of the direction vectors

$$\boldsymbol{\phi}_i = \Big[e^{j2\pi\lambda^{-1}<e(\phi_{1,1}),\xi_i>}, \ldots, e^{j2\pi\lambda^{-1}<e(\phi_{K,L}),\xi_i>}\Big]^{\mathrm{T}} \in \mathbb{C}^{KL}. \qquad \text{(A4.6)}$$

[1] $\mathbf{Z} = \mathbf{X} \odot \mathbf{Y} \in \mathbb{C}^{x \times y}$, i.e., all components of the matrix $\mathbf{X} \in \mathbb{C}^{x \times y}$ are multiplied elementwise by the matrix $\mathbf{Y} \in \mathbb{C}^{x \times y}$.

Derivation of the PIC based joint DOA and delay estimator

Let us start by modifying the linear model in the following manner:

$$\mathbf{r}_i = \mathbf{S}_i\mathbf{C}_i\mathbf{A}\mathbf{b} + \mathbf{n}_i = \mathbf{D}_i\mathbf{b} + \mathbf{n}_i, \tag{A5.1}$$

where $\mathbf{D}_i$ contains both the spatial and temporal information. By using similar notations as in Section 6.2 the following definition will be used: $\mathbf{D}_i = (\mathbf{D}_{k,l,i} + \bar{\mathbf{D}}_{k,l,i})$, where $\mathbf{D}_{k,l,i}$ contains only the elements for kth user's lth path and $\bar{\mathbf{D}}_{k,l,i}$ is a complement for that. The joint maximum likelihood estimator for delays and direction-of-arrivals is derived in the sequel by assuming that the data and the channel coefficients are known. The ML estimator for a receiver with I sensors can be written as

$$\begin{bmatrix} \hat{\boldsymbol{\tau}} \\ \hat{\boldsymbol{\phi}} \end{bmatrix} = \arg\min_{\boldsymbol{\tau},\boldsymbol{\phi}} \left\{ \sum_{i=1}^{I} ||\mathbf{r}_i - \mathbf{D}_i\mathbf{b}||^2 \right\}. \tag{A5.2}$$

In the PIC based estimators, this is solved separately for each user and path assuming the other user and path parameters known, i.e.,

$$\begin{aligned} \begin{bmatrix} \hat{\tau}_{k,l} \\ \hat{\phi}_{k,l} \end{bmatrix} &= \arg\min_{\tau_{k,l},\phi_{k,l}} \left\{ \sum_{i=1}^{I} ||\mathbf{r}_i - (\mathbf{D}_{k,l,i} + \bar{\mathbf{D}}_{k,l,i})\mathbf{b}||^2 \right\} \qquad \text{(A5.3)} \\ &= \arg\min_{\tau_{k,l},\phi_{k,l}} \left\{ \sum_{i=1}^{I} ||\mathbf{r}_i - \mathbf{D}_{k,l,i}\mathbf{b}||^2 \right. \\ &\quad \left. -2\mathrm{Re}\left\{ \sum_{i=1}^{I} \mathbf{b}^{\mathrm{H}}\bar{\mathbf{D}}_{k,l,i}^{\mathrm{H}}(\mathbf{r}_i - \mathbf{D}_{k,l,i}\mathbf{b}) \right\} \right\}. \end{aligned}$$

This can also be expressed as

$$\begin{bmatrix} \hat{\tau}_{k,l} \\ \hat{\phi}_{k,l} \end{bmatrix} = \arg\min_{\tau_{k,l},\phi_{k,l}} \left\{ -2\mathrm{Re}\left\{ \sum_{i=1}^{I} \mathbf{b}^{\mathrm{H}}\mathbf{D}_{k,l,i}^{\mathrm{H}}\mathbf{r}_i \right\} \right.$$

$$
\begin{aligned}
& - 2\mathrm{Re}\left\{\sum_{i=1}^{I} \mathbf{b}^{\mathrm{H}} \bar{\mathbf{D}}_{k,l,i}^{\mathrm{H}} (\mathbf{r}_i - \mathbf{D}_{k,l,i}\mathbf{b})\right\}\Bigg\} \\
= \; & \arg \min_{\tau_{k,l},\phi_{k,l}} \left\{ -2\mathrm{Re}\left\{\sum_{i=1}^{I} \mathbf{b}^{\mathrm{H}} \left(\mathbf{D}_{k,l,i}^{\mathrm{H}} \mathbf{r}_i + \bar{\mathbf{D}}_{k,l,i}^{\mathrm{H}} \mathbf{r}_i - \bar{\mathbf{D}}_{k,l,i}^{\mathrm{H}} \mathbf{D}_{k,l,i}\mathbf{b}\right)\right\}\right\} \\
= \; & \arg \max_{\tau_{k,l},\phi_{k,l}} \left\{ \mathrm{Re}\left\{\sum_{i=1}^{I} \mathbf{b}^{\mathrm{H}} \left((\mathbf{D}_{k,l,i}^{\mathrm{H}} + \bar{\mathbf{D}}_{k,l,i}^{\mathrm{H}})\mathbf{r}_i - \bar{\mathbf{D}}_{k,l,i}^{\mathrm{H}} \mathbf{D}_{k,l,i}\mathbf{b}\right)\right\}\right\} \\
= \; & \arg \max_{\tau_{k,l},\phi_{k,l}} \left\{ \mathrm{Re}\left\{\sum_{i=1}^{I} \mathbf{b}^{\mathrm{H}} \left(\mathbf{D}_{k,l,i}^{\mathrm{H}} \mathbf{r}_i - \bar{\mathbf{D}}_{k,l,i}^{\mathrm{H}} \mathbf{D}_{k,l,i}\mathbf{b}\right)\right\}\right\}, \qquad \text{(A5.4)}
\end{aligned}
$$

which can be also written as

$$
\begin{aligned}
\begin{bmatrix} \hat{\tau}_{k,l} \\ \hat{\phi}_{k,l} \end{bmatrix} = \; & \arg \max_{\tau_{k,l},\phi_{k,l}} \left\{ \mathrm{Re}\left\{\sum_{i=1}^{I} \mathbf{b}^{\mathrm{H}} \left(\mathbf{D}_{k,l,i}^{\mathrm{H}} \mathbf{r}_i - (\mathbf{D}_i^{\mathrm{H}} - \mathbf{D}_{k,l,i}^{\mathrm{H}})\mathbf{D}_{k,l,i}\mathbf{b}\right)\right\}\right\} \\
= \; & \arg \max_{\tau_{k,l},\phi_{k,l}} \left\{ \mathrm{Re}\left\{\sum_{i=1}^{I} \mathbf{b}^{\mathrm{H}} \left(\mathbf{C}_i^{\mathrm{H}} \mathbf{y}_{k,l,i} - (\mathbf{D}_i^{\mathrm{H}} \mathbf{D}_{k,l,i} - \mathbf{I})\mathbf{b}\right)\right\}\right\} \\
= \; & \arg \max_{\tau_{k,l},\phi_{k,l}} \left\{ \mathrm{Re}\left\{\sum_{i=1}^{I} \mathbf{b}^{\mathrm{H}} \mathbf{C}_i^{\mathrm{H}} \left(\mathbf{y}_{k,l,i} - \mathbf{\Psi}_{k,l,i}\right)\right\}\right\} \\
= \; & \arg \max_{\tau_{k,l},\phi_{k,l}} \left\{ \mathrm{Re}\left\{\mathbf{b}^{\mathrm{H}} \mathbf{C}^{\mathrm{H}} \left(\mathbf{Y}_{k,l} - \bar{\mathbf{\Psi}}_{k,l}\right)\right\}\right\}, \qquad \text{(A5.5)}
\end{aligned}
$$

where $\mathbf{Y}_{k,l} = \sum_{i=1}^{I} \mathbf{\Phi}_{k,l,i}^{\mathrm{H}} \mathbf{y}_{k,l,i} = \left[\mathbf{Y}_{k,l}^{(0)}, \ldots, \mathbf{Y}_{k,l}^{(N_b-1)}\right]^{\mathrm{T}} \in \mathbb{C}^{KLN_b}$ with $\mathbf{Y}_{k,l}^{(n)} = \left[0, \ldots, 0, Y_{k,l}^{(n)}, 0, \ldots, 0\right] \in \mathbb{C}^{KL}$ is the spatially combined matched filter output vector for the kth user's lth path with $Y_{k,l}^{(n)} = \sum_{i=1}^{I} \phi_{k,l,i}^{*} y_{k,l,i}^{(n)}$. The interference vector for the kth user's lth path is $\bar{\mathbf{\Psi}}_{k,l} = \left(\sum_{i=1}^{I} \mathbf{D}_i^{\mathrm{H}(n)} \mathbf{D}_{k,l,i}^{(n)} - \mathbf{I}\right)\mathbf{b} = \left[\bar{\mathbf{\Psi}}_{k,l}^{(0)}, \ldots, \bar{\mathbf{\Psi}}_{k,l}^{(N_b-1)}\right]^{\mathrm{T}} \in \mathbb{C}^{KLN_b}$ with $\bar{\mathbf{\Psi}}_{k,l}^{(n)} = \left[0, \ldots, 0, \bar{\Psi}_{k,l}^{(n)}, 0, \ldots, 0\right] \in \mathbb{C}^{KL}$. Equation (A5.5) reduces to

$$
\begin{aligned}
\begin{bmatrix} \hat{\tau}_{k,l} \\ \hat{\phi}_{k,l} \end{bmatrix} = \; & \arg \max_{\tau_{k,l},\phi_{k,l}} \left\{ \mathrm{Re} \sum_{j=m-\mathcal{T}+1}^{m} \sum_{i=1}^{I} \left\{ \hat{c}_{k,l,i}^{*(j)} \hat{b}_k^{*(j)} \left[y_{k,l,i}^{(j)}(\tilde{\tau}_{k,l}, \tilde{\phi}_{k,l}) \right.\right.\right. \\
& \left.\left.\left. - \; \hat{\Psi}_{k,l,i}^{(j)}(\tilde{\tau}_{k,l}, \tilde{\phi}_{k,l}) \right] \right\} \right\}. \qquad \text{(A5.6)}
\end{aligned}
$$

for each user and path in joint delay and direction-of-arrival estimators having an observation interval $\mathcal{T}$. The joint estimation problem can be decoupled by assuming the delays known when estimating the direction-of-arrivals and vice versa.